Theoretical Study of Phase Conjugation

Torsten Andersen

in Mesoscopic Interaction Volumes

Authors note to the electronic version

The author hereby grant you to redistribute and print this file for your own personal use, provided that no modifications are made. If you would like to cite any of the results published herein you are free to do so, but if it is possible please make your citation to one of the papers below:

Andersen, T. and O. Keller (1998a). Local-field theory for optical phase conjugation by degenerate four wave mixing in mesoscopic interaction volumes of condensed media. *Phys. Scr. 58*, 132–144.

Andersen, T. and O. Keller (1998b). Optical phase conjugation in a single-level metallic quantum well. *Phys. Rev. B 57*, 14793–14808.

Andersen, T. and O. Keller (1998c). Two-dimensional confinement of light in front of a single level quantum well phase conjugator. *Opt. Commun. 155*, 317–322.

Andersen, T. and O. Keller (1999). Local-field study of phase conjugation in nonmagnetic multi-level metallic quantum wells with probe fields of both propagating and evanescent character. *Phys. Rev. B*, (to be published).

The first of these articles contains most of Chapter 3 and Parts II and III. The second contains most of Chapters 10 and 11 and part of Appendix B. The third article consists of the results presented in Chapter 12. The last of the four articles is based on the analysis presented in Part V and Appendices B and C. It is, however, greatly expanded with numerical results.

If you plan to include some of this work (figures, tables, equations) into your own work, please contact the author. Current (as of October 1998) contact information is:

Dr. Torsten Andersen
Max-Planck-Institut für Mikrostrukturphysik
Weinberg 2
D–06120 Halle/Saale
Germany

e-mail: thor@mpi-halle.mpg.de
www: http://www.geocities.com/CapeCanaveral/Lab/9700/index.html

A limited number of printed copies of the thesis are available. Please contact the author or the publisher if you are interested.

Theoretical Study of Phase Conjugation in Mesoscopic Interaction Volumes

THEORETICAL STUDY OF PHASE CONJUGATION
IN MESOSCOPIC INTERACTION VOLUMES.

TEORETISK UNDERSØGELSE AF FASEKONJUGATION
I MESOSKOPISKE VEKSELVIRKNINGSRUMFANG.

Torsten Andersen

*Theoretical Study of Phase Conjugation
in Mesoscopic Interaction Volumes*

Preface

The present monograph describes results of my work carried out at the Institute of Physics at Aalborg University, Aalborg, Denmark in the period from February 1995 to May 1998 and at the Department of Physics and Astronomy at Mississippi State University, Starkville, Mississippi, United States of America in the period from August 1996 to January 1997. This monograph is submitted as a Ph.D. thesis to the Faculty of Engineering and Science at Aalborg University.

With this dissertation, I intend to describe in a unified fashion the work done in the time frame of the programme. It is my intention that the contents of this monograph should go deeper and broader into the material that has been processed for publishing in articles, and thus include results and comments on material not suitable for publication as parts of an article. The work is divided into six main parts, each consisting of some separate chapters. The outline of this monograph is presented in the following.

Outline of the dissertation

The motivation for carrying out the present study is given in Part I, divided into three separate chapters. In Chapter 1 a brief summary of the contributions to scientific progress within the last century, which I believe are the most important for my work, is presented. The historical summary includes remarks on nonlinear optics in general, optical phase conjugation in particular, near-field optics, and mesoscopic optics. Chapter 2 presents the theoretical model usually adopted in optical phase conjugation (standard theory). Chapter 3 consists of a discussion of the limitations of the standard theory as well as the requirements to a theoretical model that can be used when interaction takes place on small length scales and/or in the optical near-field region.

In Part II the task of developing a nonlocal theoretical description of phase conjugation of optical near-fields by degenerate four wave mixing is undertaken. It consists of three chapters. In Chapter 4 the basic working frame for the present treatment is established, starting from Maxwell's equations. Chapter 5 sets up the first and third order responses of an electron using the density matrix formalism starting from the Liouville equation of motion. In Chapter 6 the general conductivity response tensors for degenerate four-wave mixing excluding spin-effects are established, and their symmetries are discussed. Part II is concluded with a small discussion.

Part III discusses degenerate four-wave mixing in quantum-well structures on a somewhat general level. For this purpose, two chapters are written. In Chapter 8 the conductivity response tensors in the case where a system has broken translational invariance in one spatial direction are established and discussed, and Chapter 9 is devoted to a discussion of the consequences of scattering in a plane using polarized light.

In Part IV the optical phase conjugation response of a single-level quantum well is studied in four chapters. In Chapter 10 the theoretical considerations necessary to describe the phase conjugation response from a single-level quantum well are discussed, and in Chapter 11 the numerical results for the phase conjugated response from a copper quantum well are discussed. Chapter 12 consists of a discussion of two-dimensional confinement of light in front of the single-level quantum-well phase conjugator considered in Chapters 10 and 11. Chapter 13 concludes this part with a short discussion.

Part V takes a similar point of view as Part IV, but for the two-level quantum well. Theoretical considerations are presented in Chapter 14, while the numerical results are discussed in Chapter 15. A short discussion concludes this part in Chapter 16.

Part VI contains a concluding discussion on the developed theory and the numerical work followed by an outlook.

There are five Appendices included, consisting of calculations not suitable for the main text. Appendix A is a calculation of the linear and nonlinear conductivity tensors relevant for studying degenerate four-wave mixing in quantum well structures. Appendix B contains the principal analytic solutions to the integrals over the states parallel to the plane of translational invariance in the quantum well structures. In Appendix C, the absolute solution to the integrals over the states parallel to the plane of translational invariance in the quantum well structures are presented in terms of the principal solutions given in Appendix B. Appendix D contains a small calculation of the Fermi energy for a quantum well in the low-temperature limit and a calculation of the minimal and maximal values of the thickness of a quantum well given the desired number of occupied eigenstates across the quantum well. Appendix E contains some intermediate results in the calculation of the integrals over the source region in Chapter 14.

References used in this work are listed in the bibliography at the end of the dissertation according to the recommendations by the thirteenth edition of *The Chicago Manual of Style* with author(s), title, and publication data in alphabetic order after the first authors surname.

Notation

Footnotes are marked using a superscript number in the text, and the footnote itself is found at the bottom of the page. Citations to other people's work are made with reference to the authors surname(s) followed by the year of publication. The international system of units (SI) has been adopted throughout the work, except that the unit Ångström (Å) is used to denote certain distances ($1\text{Å} = 10^{-10}$m).

Vector quantities are denoted with a unidirectional arrow above them, i.e., $\vec{\kappa}$. Likewise, tensor quantities are denoted using a bidirectional arrow, i.e., $\overset{\leftrightarrow}{\sigma}$. Integrations over

vector quantities are denoted "$\int f(\vec{\kappa})d^n\kappa$", where n is the number of elements in the vector $\vec{\kappa}$, and $f(\vec{\kappa})$ is an arbitrary function of the integration variable $\vec{\kappa}$. Unit vectors are denoted $\vec{e}$ with an index indicating which direction is taken. The unit tensor is denoted by $\overline{\overline{\mathbb{1}}}$, and is usually a 3×3 tensor.

Latin indices $\{i, j, k, h\}$ generally refers to the three spatial coordinate labels $\{x, y, z\}$, and the latin indices $\{n, m, v, l\}$ generally refers to quantum states. Exceptions from this are (i) when the letter "i" appears in formulae and is not an index, it is the complex number $i^2 = -1$, (ii) when the letter "k" appears in formulae and is not an index, it is the wavenumber $k = |\vec{k}|$, (iii) the letter "m" with an index "e" is the electron mass. Summations over repeated indices are stated explicitly whenever it should be performed.

To avoid confusion regarding the placement of 2π's in the Fourier integral representation, the Fourier transform pair

$$\mathcal{F}(t) = \frac{1}{2\pi} \int \mathcal{F}(\omega) e^{-i\omega t} d\omega \qquad \Longleftrightarrow \qquad \mathcal{F}(\omega) = \int \mathcal{F}(t) e^{i\omega t} dt$$

is adopted between the time- and frequency domains, and thus to be consistent the transform pair

$$\mathcal{F}(\vec{r}) = \frac{1}{(2\pi)^3} \int \mathcal{F}(\vec{k}) e^{i\vec{k}\cdot\vec{r}} d^3k \qquad \Longleftrightarrow \qquad \mathcal{F}(\vec{k}) = \int \mathcal{F}(\vec{r}) e^{-i\vec{k}\cdot\vec{r}} d^3r$$

is adopted between real space and k-space, here shown in three dimensions.

Furthermore, the complex conjugate and the Hermitian adjoint of a quantity A are denoted A^* and $A^\dagger$, respectively. The phrases "+c.c." and "+H.a." at the end of an equation indicates the addition of the complex conjugate or the Hermitian adjoint of the foregoing terms. The phrase "+i.t." at the end of an equation denotes the addition of a term in which the wave-vector $\vec{k}$ is replaced by $-\vec{k}$. The Laplacian is denoted ∇^2. The Heaviside unit step function $\Theta(x)$ has the value $+1$ for $x > 0$ and 0 for $x < 0$, and the Kronecker delta δ_{ij} has the value $+1$ for $i = j$ and 0 for $i \neq j$. The Ludolphine number $3.14159265\ldots$ is denoted by the greek letter π.

Scientific papers and presentations based on this work

Parts of the work presented in this dissertation has been or will be published separately in the form of proceedings papers, articles, and letters. They are as follows:

Andersen, T. and O. Keller (1995a). Optical near-field phase conjugation: A nonlocal DFWM response tensor. In E. G. Bortchagovsky (Ed.), *Proceedings of the International Autumn School-Conference for Young Scientists "Solid State Physics: Fundamentals & Applications" (SSPFA'95)*, Kiev, pp. R5–R6. Institute of Semiconductor Physics of NASU. ISBN 5-7702-1199-7.

Andersen, T. and O. Keller (1996a). Phase Conjugation of Optical Near Fields: A new Nonlocal Microscopic Response Tensor. In O. Keller (Ed.), *Notions and Perspectives of Nonlinear Optics*, pp. 566–573. Singapore: World Scientific. ISBN 981-02-2627-6.

Andersen, T. and O. Keller (1998a). Local-field theory for optical phase conjugation by degenerate four wave mixing in mesoscopic interaction volumes of condensed media. *Phys. Scr. 58.* In press.

Andersen, T. and O. Keller (1998b). Optical phase conjugation in a single-level metallic quantum well. *Phys. Rev. B 57*, 14793–14808.

Andersen, T. and O. Keller (1998c). Two-dimensional confinement of light in front of a single level quantum well phase conjugator. *Opt. Commun.* Submitted.

Furthermore, an article on optical phase conjugation in a two-level (resonant) metallic quantum well is in preparation. In addition to the above-mentioned publications, presentations of abstracts has been given at conferences. They are:

Keller, O., M. Xiao and T. Andersen (1994). Phase conjugation and Near-Field Microscopy. Poster presented at the annual meeting of the Danish Optical Society, Lyngby, Denmark, November 24.

Andersen, T. and O. Keller (1995b) Random-phase-approximation study of the response function describing phase conjugation by degenerate four wave mixing. Poster presented at the annual meeting of the Danish Physical Society, Odense, Denmark, May 31–June 2.

Andersen, T. and O. Keller (1995c) Phase conjugation of optical near-fields: A new nonlocal response tensor allowing degenerate four wave mixing studies with probe beams strongly decaying in space. Talk given at the Third International Aalborg Summer School on Nonlinear Optics, Aalborg, Denmark, August 7–12.

Andersen, T. and O. Keller (1995d) Optical near-field phase conjugation: A nonlocal DFWM response tensor. Talk given at the International Autumn School-Conference for Young Scientists "Solid State Physics: Fundamentals & Applications" (SSPFA'95) in Uzhgorod, Ukraine, September 19–26.

Andersen, T. and O. Keller (1996b) Optical Phase Conjugation by Degenerate Four Wave Mixing in a Single Level Quantum Well. Poster presented at the annual meeting of the Danish Physical Society, Nyborg, Denmark, May 23–24.

Andersen, T. and O. Keller (1996c) Microscopic Description of Optical Near-Field Phase Conjugation. Talk given at the South Eastern Section Meeting of The American Physical Society, Atlanta-Decatur, Georgia (USA), November 14–16. *Bulletin of the American Physical Society 41*, p. 1660.

Andersen, T. and O. Keller (1997a) Optical Near-Field Phase Conjugation: A Microscopic Description. Poster presented at the Fourth International Conference on Near-Field Optics (NFO-4) Jerusalem, Israel, February 9–13.

Andersen, T. and O. Keller (1997b) Focusing of classical light beyond the diffraction limit. Poster presented at the annual meeting of the Danish Optical Society, Lyngby, Denmark, November 18–19.

The abstracts are printed in the relevant meeting programmes.

Software used in this project

Creation of the numerical results presented in this work has been done through development of computer programs, mainly in Fortran 90 (Metcalf and Reid 1996). The final set of programs consists of approximately 6000 lines of code developed by the present author. Because of the size I have chosen not to include a reprint of the code in this monograph. The presentation of the calculated data is done using gnuplot pre-3.6 with some 400 lines of code to generate the plots as encapsulated PostScript files. This dissertation has been typed entirely in LaTeX 2_ε (Goossens, Mittelbach, and Samarin 1994; Goossens, Rahtz, and Mittelbach 1997), an enhanced version of the typesetting program TeX, originally developed by Knuth (1984).

Acknowledgements

The topic of this work has been very fascinating to explore, and I would therefore like to thank professor, Dr. Scient. Ole Keller for introducing me to the world of mesoscopic physics, his huge support and the many inspiring discussions we have had throughout the period of this work. I would also like to thank professor, Dr. H. F. Arnoldus and the Department of Physics and Astronomy at Mississippi State University for kindly providing facilities and inspiration during my stay there. Additionally, I would like to thank the scientific staff at the Institute of Physics, Aalborg University for providing an inspiring atmosphere in general, and Dr. Brian Vohnsen in particular for many discussions on near-field optics and for reviewing parts of the text appearing in this dissertation.

My deepest thanks goes to my parents Maren and Agner Andersen for their moral and financial support, and to my brother Jens and my sisters Else, Karen, and Birgit. In addition, I would like to thank my friends around the globe who—together with my family—have enriched my life outside the academic world.

Finally, I wish to thank (i) the Faculty of Engineering and Science and the Institute of Physics at Aalborg University for providing the basic frame for my research work, (ii) the Mississippi Center for Supercomputing Research at the University of Mississippi, Jackson, Mississippi, for providing computer resources during my stay at Mississippi State University, and (iii) the people at Aalborg University Library for their excellent assistance in obtaining articles from far away in time and space.

Aalborg, Denmark, June 1998 **Torsten Andersen**

x

Contents

List of Figures

List of Tables

List of acronyms

DC	Direct current.
DFWM	Degenerate four-wave mixing.
ED	Electric dipole.
IB	Infinite barrier.
PCDFWM	Phase conjugation (by) degenerate four-wave mixing.
SVE	Slowly varying envelope.
SVEA	Slowly varying envelope approximation.
YAG	$Y_3Al_5O_{12}$ (Yariv and Yeh 1984).

Theoretical Study of Phase Conjugation in Mesoscopic Interaction Volumes

Part I

Motivation

Natura inest
in mentibus nostrum
insatiabilis quaedam
cupiditas veri videndi
(*Marcus Tullius Cicero*)

Chapter 1

Historical perspective

Indeed, as the great orator expressed it more than two millenia ago, nature has planted in our minds an insatiable longing to see the truth. This natural curiosity, I believe, has been the driving force behind scientific investigations in the history of mankind, and thus also behind the evolution of electromagnetic theory. But since the electrodynamic theory as we know it was initiated by Maxwell (1864, 1891), I will in the following historical remarks concentrate on the physics of the past century. Readers who want an overview of the evolution of electromagnetic theories before this century are referred to Born and Wolf (1980), and the comprehensive survey of Whittaker (1951).

The work described in the present dissertation is mainly concerned with a theoretical description of a nonlinear type of electromagnetic interactions called degenerate four-wave mixing (DFWM), particularly in the case where phase conjugation is obtained. The main interest behind this study is to model the behaviour of the DFWM interaction in mesoscopic volumes and in the optical near-field zone. Thus, in relation to established branches of modern optics, this work belongs to the fields of nonlinear optics (especially four-wave mixing), near-field optics, and mesoscopic systems. In the remaining of this chapter I therefore intend to describe briefly the contributions to scientific progress within the last century, which I believe are the most significant for the present study.

Although Einstein already in 1916 predicted the existence of stimulated emission (Einstein 1916, 1917), the main objective of optics remained linear observations until after the development of the maser in the early 1950's, where Townes and co-workers at Columbia University used stimulated emission for amplification of an electromagnetic field in combination with a resonator (Gordon, Zeiger, and Townes 1954, 1955). An application of the principles of the maser in the optical region of the electromagnetic spectrum was proposed in 1958 by Schawlow and Townes, and in 1960 Maiman constructed the first laser—a pulsed ruby laser. The first laser delivering a continous-wave output was constructed in 1961 using a mixture of Helium and Neon gasses (Javan, Jr., and Herriot 1961). The laser rapidly became of significant importance in optical physics, where the field of nonlinear optics was ignited by the successful observation by Franken, Hill, Peters, and Weinrich (1961) of radiation of light at the second harmonic frequency (with a wavelength λ of 3472Å) generated by a quartz crystal illuminated with light from a ruby laser ($\lambda = 6943$Å). Since then nonlinear optics has been of interest to many researchers around the globe exploring a large number of different nonlinear phenom-

ena, such as second-, third-, and higher order harmonic generation, optical rectification, sum and difference frequency generation, three-, four-, six-, and higher-number wave-mixing, laser cooling, laser induced atomic fusion, stimulated Raman- and Brillouin scattering, to mention a few [see, e.g., Bloembergen (1965), Boyd (1992), Mandel and Wolf (1995), Yariv and Yeh (1984), Shen (1984), Schubert and Wilhelmi (1986), and Mukamel (1995)].

The optical effect of interest in this work, optical phase conjugation, is nowadays usually produced by means of nonlinear optics, although the problem of reconstructing electromagnetic wavefronts started in the linear optical regime. The pioneering work on optical wavefront reconstruction (holography) was carried out several years before the invention of the laser by Gabor (1948, 1949) with the purpose of improving the re-solving power of the electron microscope [see also Bragg (1950)]. But only with the high intensities and with the degree of temporal and spatial coherence provided by the laser, holographic imaging became of practical importance. Such experiments were first reported by Leith and Upatnieks (1962, 1964). Soon thereafter Kogelnik (1965) used a hologram to correct static phase distortions introduced onto an optical wavefront. In this experiment a photosensitive film was used for holographic recording of an image, and the film had to be developed prior to its application for phase correction. This experiment of Kogelnik appears to be the first account on optical phase conjugation. However, since a new film has to be developed every time the phase distortion changes, this technique becomes rather cumbersome if the phase distortions changes frequently. A key discovery of Gerritsen (1967) made it possible to store holograms dynamically in crystals with an intensity-dependent refractive index, thereby extending the applicability domain of optical phase conjugation to cover descriptions where phase distortions are varying in time. Experimentally, the first real-time optical phase conjugation are cre-dited to Zel'dovich and co-workers (Zel'dovich, Popovichev, Ragul'skii, and Faizullov 1972; Nosach, Popovichev, Ragul'skii, and Faizullov 1972), in an experiment based on stimulated Brillouin scattering. In the late 1970's, Hellwarth (1977) suggested the use of a degenerate four-wave mixing process to produce the phase conjugated field. Im-mediately thereafter Yariv and Pepper (1977), and independently, Bloom and Bjorklund (1977), further analyzed the optical phase conjugation via DFWM, resulting in predic-tions of amplified reflection, coherent image amplification and oscillation. Over the past twentyfive years, thousands of scientific papers, several books and review articles de-scribing different aspects and applications of optical phase conjugation have been pub-lished, and phase conjugation in the form of DFWM is now an established discipline in modern experimental optics. The theoretical treatments of optical phase conjugation are usually based upon the work of Yariv (1978), using the phase conjugating system as a device in studies of other processes. A comprehensive and coherent introduction to the field of optical phase conjugation can be found in the books by Zel'dovich, Pilipet-sky, and Shkunov (1985) and Sakai (1992), while a more specialized introduction can be achieved through collections of review papers appearing in books by Fisher (1983) and Gower and Proch (1994), or separately, by Pepper (1982, 1985), Hellwarth (1982), and Knoester and Mukamel (1991). Other collections of papers can be found in, e.g.,

Goodman (1983), and Brueck (1989). Within the last few years, DFWM has been used for creation of optical phase conjugation in configurations where the probe field and the detector are within subwavelength distances from the phase-conjugating medium (Bozhevolnyi, Keller, and Smolyaninov 1994; Vohnsen 1997; Bozhevolnyi 1997).

The first account of attention to subwavelength (optical near-field) interaction of light with matter seems to be Synge (1928, 1932), who proposed an apparatus, in which a sample is illuminated through a small aperture in an opaque screen, the area of the aperture being substantially smaller than the diffraction limit of the light used for the illumination (of subwavelength size). The aperture should be moved in small increments (scanned) over the sample by use of a piezo-electric crystal. At every step of the scanning procedure the light transmitted through the sample should be collected and the intensity measured. The resolving power of such an instrument should be limited by the size of the aperture and the distance from the aperture to the sample rather than by the wavelength of the illuminating light. For whatever reason, the proposal of Synge was forgotten, and even though Bethe (1944) and Bouwkamp (1950a, 1950b) discussed the problem of diffraction by small holes, the idea of an optical near-field microscope remained forgotten until O'Keefe (1956) made the proposal, apparently without any knowledge of the instrument proposed by Synge. The first demonstration of an image obtained with scanning in the electromagnetic near-field zone was given by Ash and Nichols (1972), who used microwaves of wavelength of 3cm to resolve metallic gratings with linewidths down to 0.5mm, corresponding to 1/60-th of a wavelength. Another twelve years should pass before near-field electrodynamics was adressed again. Near-field optics evolved in the mid-eighties in the wake of the experimental works by the groups of Pohl, Lewis, and Fischer (Pohl, Denk, and Lanz 1984; Lewis, Isaacson, Harootunian, and Murray 1984; Fischer 1985; Fischer and Pohl 1989). The main efforts of this new branch of modern optics is concentrated on the original idea of subwavelength imaging [see, for example, the recently published book by Paesler and Moyer (1996), the proceedings of the first conference on near-field optics (Pohl and Courjon 1993), or proceedings from later conferences in near-field optics (Isaacson 1995; Paesler and van Hulst 1995; Nieto-Vesperinas and García 1996; van Hulst and Lewis 1998)].

The appearance of microscopes with subwavelength resolution inevitably poses the questions of the resolution limit and the degree of spatial confinement of light—two inseparable questions in near-field optics. Fundamentally, the spatial confinement problem is linked to the field-matter interaction in the vicinity of the source emitting the field and in the near-field region of the detector. In classical optics, near-field effects traditionally have played a minor role, and the possibilities for studying material properties on a small length scale usually are judged in relation to the diffraction limit criterion attributed to Ernst Abbe (1873) and the third baron Rayleigh (1896). The Rayleigh criterion, though mainly invoked in the context of spatial resolution, also sets the limit for the possibilities of light compression in far-field studies. As already emphasized by lord Rayleigh and later discussed, for instance, by Ronchi (1961), the resolution problem is not a simple one, even in classical optics. A recent survey of the resolution problem within the framework of classical optics has been given by den Dekker and van den Bos (1997).

When the interaction length of an electromagnetic field across the individual structures in a condensed matter system is on the order of an optical wavelength (typically a few atomic distances), the theoretical description of the field-matter interaction belongs to the field of mesoscopic electrodynamics. Within the last two decades studies of the optical properties of mesoscopic systems, such as quantum wells (single and multiple), -wires and -dots, surfaces, interfaces, and more exotic geometries have drawn the attention of many researchers. Because of the immediate potential for industrial application many of these studies have been concentrated on the properties of semiconductors (see, e.g., Weisbuch and Vinter (1991), and references herein). In recent years in particular investigations of the nonlinear electrodynamics have been in focus. Among the many nonlinear phenomena studies of second harmonic generation (Sipe and Stegeman 1982; Richmond, Robinson, and Shannon 1988; Heinz 1991; Reider and Heinz 1995; Liebsch 1995; Pedersen 1995), sum- and difference frequency generation (Reider and Heinz 1995; Bavli and Band 1991), photon drag (Keller 1993; Vasko 1996; Chen and Keller 1997; Keller and Wang 1997), DC-electric-field induced second harmonic generation (Aktsipetrov, Melnikov, Murzina, Nikulin, and Rubtsov 1995; Aktsipetrov, Fedyanin, and Downer 1996), the Kerr effect (Pustogowa, Hübner, and Bennemann 1994; Liu and Keller 1995; Rasing and Goerkamp 1995; Rasing 1996), electronic and vibrational surface Raman scattering (Nkoma 1989; Mishchenko and Fal'kovskii 1995; Garcia-Vidal and Pentry 1996), two-photon photoemission (Haight 1995; Fauster and Steinmann 1995; Georges 1995; Shalaev, Douketis, Haslett, Stuckless, and Moskovits 1996; Tergiman, Warda, Girardeau-Montaut, and Girardeau-Montaut 1997), and generation of higher harmonics (von der Linde 1996; Gavrila 1992) have played a prominent role. Among the more exotic phenomena, studies of the Aharonov-Bohm effect in mesoscopic rings (Wang 1997) and whispering-gallery modes in microspheres (Knight, Dubreuil, Sandoghdar, Hare, Lefèvre-Seguin, Raimond, and Haroche 1995) have also been carried out lately.

From a theoretical point of view the refractive index concept becomes meaningless for structures of mesoscopic size. Therefore, macroscopic approaches to describe the field-matter interaction have to be abandoned from the outset, and the theoretical analyses have to be based on the microscopic Maxwell equations combined with the Schrödinger equation. The Schrödinger equation describes the quantum state of the condensed matter system, and is a fundamental part of the quantum mechanics initiated in the beginning of the 20th century by such scientists as Planck, Einstein, Bohr, Heisenberg, Born, Jordan, de Broglie, Schrödinger and Dirac. Even an attempt to give a satisfactory historical survey of the development of quantum mechanics at this point will fail because of the almost universal status quantum mechanics has reached in the description of modern physics. Instead, for the history of quantum mechanics including a description of the mathematical foundation, please consult for example von Neumann (1932) or Bohm (1951). A modern and comprehensive description of quantum mechanics is given by Cohen-Tannoudji, Diu, and Laloë (1977), where also a comprehensive list of references to key papers can be found. An example of interesting papers is the series of articles by Schrödinger (1926a, 1926b).

Chapter 2

Standard theory of
optical phase conjugation by degenerate four-wave mixing

Optical phase conjugation is a nonlinear optical phenomenon, in which an incoming optical field is reflected in such a manner that the wavefronts of the reflected field coincide with the incoming field, hence also the name "wavefront inversion", frequently used in the literature. The principle of optical phase conjugation has gained widespread attention because of its ability to correct for distortions introduced in a path traversed by an optical signal. In principle, it works like this: An optical source is placed on one side of a distorting medium (crystal, waveguide, atmosphere, etc.). A system in which phase conjugation takes place (called the phase conjugator) is placed on the other side of the distorting medium. A field emitted from the source in the direction of the phase conjugator then travel through the distorting medium, and is reflected by the phase conjugator. The phase conjugator reverses the wavefront of the incoming (probe) field, and when the reflected light comes back through the distorting medium, the wavefront is (ideally) exactly reversed, compared to that originally emitted by the source. Since it is possible to see how the light was originally emitted by the source by looking at the phase conjugated replica, it is sometimes also given the somewhat misleading term "time reversal" (Yariv 1978). Several schemes exist to achieve phase conjugation, the most widely used called "degenerate four-wave mixing" (DFWM). Optical phase conjugation in the form of degenerate four-wave mixing (DFWM) is a nonlinear third order effect, where mixing of two counterpropagating "pump" fields and a "probe" (or "signal") field—all with the same frequency ω—results in, among other signals, a generated field (the "conjugate") with frequency $\omega = \omega + \omega - \omega$, which is counterpropagating to the probe field.

In the following, I present the theoretical model usually adopted in studies of optical phase conjugation by degenerate four-wave mixing, and consequently this chapter will consist mainly of textbook material. The treatment roughly follows that of Yariv and Fisher (1983) and of Boyd (1992). The DFWM geometry suggested by Yariv and Pepper (1977) is shown in Fig. 2.1. In this configuration, a lossless nonlinear optical medium is illuminated by two strong counterpropagating pump fields $\vec{E}_1$ and $\vec{E}_2$ and by a weak signal (probe) wave $\vec{E}_3$. The pump fields are usually taken to be plane waves, although they in principle are allowed to have any kind of wavefront as long as their amplitudes are complex conjugates of each other. The probe field can have a more complex wavefront. Resulting from the mixing process in the medium a conjugate field appears, propagating in the direction oppositely to the probe.
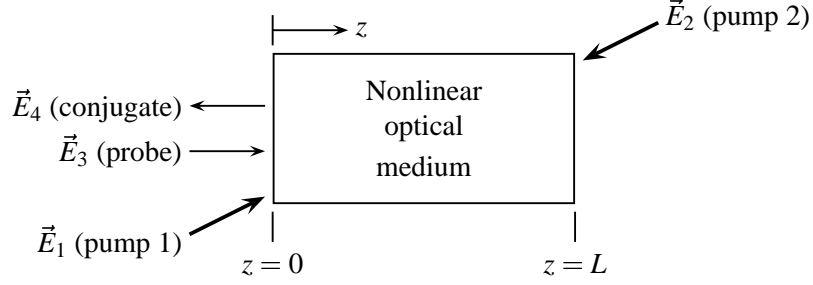
Figure 2.1: Geometry of phase conjugation by DFWM in the standard model.

In order to describe the electromagnetic field we first establish the wave equation for the interacting fields from the macroscopic Maxwell equations. It is thereafter reduced to its slowly varying envelope approximation (SVEA) form. The four macroscopic Maxwell equations are

$$\vec{\nabla} \times \vec{E}(\vec{r},t) = -\frac{\partial \vec{B}(\vec{r},t)}{\partial t}, \tag{2.1}$$

$$\vec{\nabla} \times \vec{H}(\vec{r},t) = \vec{J}(\vec{r},t) + \frac{\partial \vec{D}(\vec{r},t)}{\partial t}, \tag{2.2}$$

$$\vec{\nabla} \cdot \vec{D}(\vec{r},t) = \rho(\vec{r},t), \tag{2.3}$$

$$\vec{\nabla} \cdot \vec{B}(\vec{r},t) = 0. \tag{2.4}$$

We now assume that the material is homogeneous, nonmagnetic ($\vec{B} = \mu_0 \vec{H}$), and nonconducting ($\vec{J} = \vec{0}$) and that there are no free charges ($\rho = 0$). We write the displacement vector $\vec{D}(\vec{r},t)$ as

$$\vec{D}(\vec{r},t) = \varepsilon_0 \vec{E}(\vec{r},t) + \varepsilon_0 \vec{P}(\vec{r},t), \tag{2.5}$$

where $\vec{P}(\vec{r},t)$ is the polarization, which we split into its linear, $\vec{P}_{\mathrm{L}}$, and nonlinear, $\vec{P}_{\mathrm{NL}}$, components

$$\vec{P}(\vec{r},t) = \vec{P}_{\mathrm{L}}(\vec{r},t) + \vec{P}_{\mathrm{NL}}(\vec{r},t). \tag{2.6}$$

Above, the linear polarization describes the material response due to interaction with the field of first order. We thus define the linear susceptibility $\vec{\vec{\chi}}^{(1)}$ from the linear polarization in the manner $\vec{P}_{\mathrm{L}} = \vec{\vec{\chi}}^{(1)} \cdot \vec{E}$. The linear permittivity $\vec{\vec{\varepsilon}}_r$ is then found from the linear part of the displacement, giving $\vec{\vec{\varepsilon}}_r = \vec{\vec{1}} + \vec{\vec{\chi}}^{(1)}$. Taking the curl of Eq. (2.1) and inserting Eq. (2.2) into the resulting equation, we obtain (by use of the operator identity $\vec{\nabla} \times \vec{\nabla} \times = -\nabla^2 + \vec{\nabla}\vec{\nabla}\cdot$) the following wave equation

$$\left[\vec{\vec{1}} \nabla^2 - \frac{\vec{\vec{\varepsilon}}_r}{c^2} \frac{\partial^2}{\partial t^2} \right] \cdot \vec{E}(\vec{r},t) = \frac{1}{c^2} \frac{\partial^2 \vec{P}_{\mathrm{NL}}(\vec{r},t)}{\partial t^2}, \tag{2.7}$$

where we have assumed that the electric fields are perpendicular to their corresponding wavevector (transversality). The nonlinear polarization is usually described as a power series in the electric field,

$$\vec{P} = \vec{\chi}^{(1)} \cdot \vec{E} + \vec{\chi}^{(2)} : \vec{E}\vec{E} + \vec{\chi}^{(3)} \vdots \vec{E}\vec{E}\vec{E} + \ldots, \tag{2.8}$$

where $\vec{\chi}^{(1)}$ is the linear susceptibility, $\vec{\chi}^{(2)}$ is the second-order nonlinear susceptibility tensor, $\vec{\chi}^{(3)}$ is the third-order nonlinear susceptibility tensor, etc. This expansion is of course only of interest if we can assume that $\vec{P}^{(1)} \gg \vec{P}^{(2)} \gg \vec{P}^{(3)} \gg \cdots$ (the parametric approximation). Since we have assumed the medium to be lossless, the susceptibility tensors are real time-independent quantities, and hence also $\vec{\varepsilon}_r$ is a real quantity. The linear susceptibility tensor is included in the linear polarization ($\vec{P}_L$) above, and the lowest order nonlinear polarization of interest to DFWM is the third-order one, i.e.,

$$\vec{P}_{NL}(\vec{r},t) = \vec{\chi}^{(3)} \vdots \vec{E}(\vec{r},t)\vec{E}(\vec{r},t)\vec{E}(\vec{r},t). \tag{2.9}$$

Above, the sum-product operator "$\vdots$" is defined such that element i of the nonlinear polarization is

$$P_{NL,i}(\vec{r},t) = \sum_{jkh} \chi^{(3)}_{ijkh} E_h(\vec{r},t) E_k(\vec{r},t) E_j(\vec{r},t). \tag{2.10}$$

The total electric field is a sum of the four individual fields in the DFWM process,

$$\vec{E}(\vec{r},t) = \sum_{\alpha=1}^{4} \vec{E}_\alpha(\vec{r},t) = \frac{1}{2} \sum_{\alpha=1}^{4} \vec{E}_\alpha(\vec{r}) e^{i(\vec{k}_\alpha \cdot \vec{r} - \omega t)} + \text{c.c.}, \tag{2.11}$$

where $\vec{E}_\alpha(\vec{r})$ are slowly varying quantities, and the wavevector $\vec{k}_\alpha$ is real. Since we assumed that the pump fields $\vec{E}_1(\vec{r},t)$ and $\vec{E}_2(\vec{r},t)$ are counterpropagating, the sum of their wavevectors is zero, i.e., $\vec{k}_1 + \vec{k}_2 = \vec{0}$. Inserting Eq. (2.11) into Eq. (2.9), a large number of terms are generated. In the phase conjugation configuration we are particularly interested in the terms related to the first harmonic in the cyclic frequency ω. Among these terms are terms that can act as phase-matched source terms for the conjugate wave $\vec{E}_4(\vec{r},t)$ when the probe and conjugate fields are counterpropagating, i.e., when $\vec{k}_3 + \vec{k}_4 = \vec{0}$. Using these two properties of the wavevectors, terms with a spatial dependence of the form $e^{i\vec{k}_\alpha \cdot \vec{r}}$ are particularly important because they produce the phase-matched terms for the four interacting electric fields. The polarizations associated with these phase-matched contributions (at ω) become

$$\vec{P}_{NL}^{(1)}(\vec{r},t) = \frac{3}{8} \vec{\chi}^{(3)} \vdots \left[\vec{E}_1 \vec{E}_1 \vec{E}_1^* + 2 \sum_{\alpha \in \{2,3,4\}} \vec{E}_\alpha \vec{E}_1 \vec{E}_\alpha^* + 2\vec{E}_2^* \vec{E}_3 \vec{E}_4 \right] e^{i(\vec{k}_1 \cdot \vec{r} - \omega t)} + \text{c.c.}, \tag{2.12}$$

$$\vec{P}_{NL}^{(2)}(\vec{r},t) = \frac{3}{8} \vec{\chi}^{(3)} \vdots \left[\vec{E}_2 \vec{E}_2 \vec{E}_2^* + 2 \sum_{\alpha \in \{1,3,4\}} \vec{E}_\alpha \vec{E}_2 \vec{E}_\alpha^* + 2\vec{E}_1^* \vec{E}_3 \vec{E}_4 \right] e^{i(\vec{k}_2 \cdot \vec{r} - \omega t)} + \text{c.c.}, \tag{2.13}$$

$$\vec{P}_{\mathrm{NL}}^{(3)}(\vec{r},t) = \frac{3}{8}\vec{\chi}^{(3)}\!:\! \left[\vec{E}_3\vec{E}_3\vec{E}_3^* + 2\sum_{\alpha\in\{1,2,4\}}\vec{E}_\alpha\vec{E}_3\vec{E}_\alpha^* + 2\vec{E}_1\vec{E}_2\vec{E}_4^*\right] e^{i(\vec{k}_3\cdot\vec{r}-\omega t)} + \text{c.c.}, \quad (2.14)$$

$$\vec{P}_{\mathrm{NL}}^{(4)}(\vec{r},t) = \frac{3}{8}\vec{\chi}^{(3)}\!:\! \left[\vec{E}_4\vec{E}_4\vec{E}_4^* + 2\sum_{\alpha\in\{1,2,3\}}\vec{E}_\alpha\vec{E}_4\vec{E}_\alpha^* + 2\vec{E}_1\vec{E}_2\vec{E}_3^*\right] e^{i(\vec{k}_4\cdot\vec{r}-\omega t)} + \text{c.c.}, \quad (2.15)$$

in a short notation where $\vec{E} \equiv \vec{E}(\vec{r})$. With this splitting of the nonlinear polarization, the wave equation is satisfied, when each of the four fields and their related polarizations satisfy the wave equation separately. Next, assuming that the pump fields are much stronger than the probe and the conjugate fields, we can drop the terms in Eqs. (2.12)–(2.15) containing more than one weak-field component, thus obtaining

$$\vec{P}_{\mathrm{NL}}^{(1)}(\vec{r},t) = \frac{3}{8}\vec{\chi}^{(3)}\!:\! \left[\vec{E}_1\vec{E}_1\vec{E}_1^* + 2\vec{E}_2\vec{E}_1\vec{E}_2^*\right] e^{i(\vec{k}_1\cdot\vec{r}-\omega t)} + \text{c.c.}, \quad (2.16)$$

$$\vec{P}_{\mathrm{NL}}^{(2)}(\vec{r},t) = \frac{3}{8}\vec{\chi}^{(3)}\!:\! \left[\vec{E}_2\vec{E}_2\vec{E}_2^* + 2\vec{E}_1\vec{E}_2\vec{E}_1^*\right] e^{i(\vec{k}_2\cdot\vec{r}-\omega t)} + \text{c.c.}, \quad (2.17)$$

$$\vec{P}_{\mathrm{NL}}^{(3)}(\vec{r},t) = \frac{3}{4}\vec{\chi}^{(3)}\!:\! \left[\vec{E}_1\vec{E}_3\vec{E}_1^* + \vec{E}_2\vec{E}_3\vec{E}_2^* + \vec{E}_1\vec{E}_2\vec{E}_4^*\right] e^{i(\vec{k}_3\cdot\vec{r}-\omega t)} + \text{c.c.}, \quad (2.18)$$

$$\vec{P}_{\mathrm{NL}}^{(4)}(\vec{r},t) = \frac{3}{4}\vec{\chi}^{(3)}\!:\! \left[\vec{E}_1\vec{E}_4\vec{E}_1^* + \vec{E}_2\vec{E}_4\vec{E}_2^* + \vec{E}_1\vec{E}_2\vec{E}_3^*\right] e^{i(\vec{k}_4\cdot\vec{r}-\omega t)} + \text{c.c.}, \quad (2.19)$$

again in short notation. Note that by this approximation the polarizations associated with the pump fields have been decoupled from the probe and conjugate fields. Then we may first solve the wave equations for the pump fields, and thereafter insert the result into the wave equations for the probe and conjugate fields. Following this insertion, the probe and conjugate fields can be found. Since $\nabla^2\{\vec{E}(\vec{r})e^{i(\vec{k}\cdot\vec{r}-\omega t)}\} = \{(\nabla^2 + 2i[\vec{k}\cdot\vec{\nabla}] - k^2)\vec{E}(\vec{r})\}e^{i(\vec{k}\cdot\vec{r}-\omega t)}$, the wave equation for pump field 1 can be written

$$\left[\mathbb{1}\left(\nabla^2 + 2i[\vec{k}_1\cdot\vec{\nabla}] - k^2\right) + \frac{\omega^2}{c^2}\vec{\varepsilon}_r\right]\cdot\vec{E}_1 = -\frac{3\omega^2}{8c^2}\vec{\chi}^{(3)}\!:\! \left[\vec{E}_1\vec{E}_1\vec{E}_1^* + 2\vec{E}_2\vec{E}_1\vec{E}_2^*\right], \quad (2.20)$$

still in the short notation from above. Assuming now that we have an isotropic medium, the susceptibility tensors must be invariant to inversion and rotation around any axis in the chosen Cartesian coordinate system. The demand of inversion symmetry leaves all tensor elements with an odd number of x's, y's, or z's zero, and thus only diagonal elements survive in the linear susceptibility tensor, and only the 21 elements in the nonlinear susceptibility tensor of the form $\chi_{iijj}^{(3)}$, $\chi_{ijji}^{(3)}$, and $\chi_{ijij}^{(3)}$ are nonzero, i and j being any x, y, or z. The demand of invariance to rotational transformations results in the demand that the three remaining nonzero elements of the linear susceptibility tensor are equal, and thus we find that $\vec{\varepsilon}_r = \mathbb{1}\varepsilon_r$. In terms of the refractive index n of the medium, that is $\varepsilon_r = n^2$. For the nonlinear susceptibility tensor this demand implies that the nonzero elements can be written

$$\chi_{ijkh}^{(3)} = \chi_{xxyy}^{(3)}\delta_{ij}\delta_{kh} + \chi_{xyxy}^{(3)}\delta_{ik}\delta_{jh} + \chi_{xyyx}^{(3)}\delta_{ih}\delta_{jk}. \quad (2.21)$$

In the DFWM case, permutation symmetry between the two fields without the complex conjugation makes k and h interchangeable, and thus $\chi^{(3)}_{xyxy}$ is equal to $\chi^{(3)}_{xyyx}$, leaving the nonzero elements

$$\chi^{(3)}_{ijkh} = \chi^{(3)}_{xxyy}\delta_{ij}\delta_{kh} + \chi^{(3)}_{xyyx}(\delta_{ih}\delta_{jk} + \delta_{ik}\delta_{jh}) \tag{2.22}$$

in the nonlinear susceptibility tensor. Furthermore, inside the medium the modulus of the wavevectors are the same, $k_1 = k_2 = k_3 = k_4 = k = n\omega/c$. Under the above assumptions, Eq. (2.20) takes the form

$$\left(\nabla^2 + 2\mathrm{i}[\vec{k}_1 \cdot \vec{\nabla}]\right)\vec{E}_1(\vec{r}) = -\frac{3\omega^2}{8c^2}\left\{\chi^{(3)}_{xxyy}\left[[\vec{E}_1(\vec{r}) \cdot \vec{E}_1(\vec{r})]\vec{E}_1^*(\vec{r}) + 2[\vec{E}_2(\vec{r}) \cdot \vec{E}_1(\vec{r})]\vec{E}_2^*(\vec{r})\right]\right.$$
$$\left. + 2\chi^{(3)}_{xyyx}\left[\vec{E}_1(\vec{r})[\vec{E}_1(\vec{r}) \cdot \vec{E}_1^*(\vec{r})] + 2\vec{E}_2(\vec{r})[\vec{E}_1(\vec{r}) \cdot \vec{E}_2^*(\vec{r})]\right]\right\}. \tag{2.23}$$

Now the simplest assumption is that the four fields travel in a direction almost parallel to the z-axis (the paraxial approximation), that they have the same state of polarization, and that the pump waves have plane wavefronts (independent of x and y). Then instead of Eq. (2.23), Eq. (2.20) is rewritten into the form

$$\left(\frac{d^2}{dz^2} + 2\mathrm{i}k\frac{d}{dz}\right)E_1(z) = -\frac{3\omega^2}{8c^2}\chi^{(3)}_{xxxx}\left[|E_1(z)|^2 + 2|E_2(z)|^2\right]E_1(z), \tag{2.24}$$

still for an isotropic medium, and now having $k_1 = k_z$. Introducing into Eq. (2.24) the slowly varying envelope approximation (SVEA), in which it is assumed that $|k(dE/dz)| \gg |d^2E/dz^2|$, we obtain

$$\frac{dE_1(z)}{dz} = \frac{3\mathrm{i}\omega}{16nc}\chi^{(3)}_{xxxx}\left[|E_1(z)|^2 + 2|E_2(z)|^2\right]E_1(z) \equiv \mathrm{i}\kappa_1 E_1(z). \tag{2.25}$$

In a similar fashion we find that the pump field going in the negative z-direction is descibed by the equation

$$\frac{dE_2(z)}{dz} = -\frac{3\mathrm{i}\omega}{16nc}\chi^{(3)}_{xxxx}\left[|E_2(z)|^2 + 2|E_1(z)|^2\right]E_2(z) \equiv -\mathrm{i}\kappa_2 E_2(z), \tag{2.26}$$

since $k_2 = -k_z$. Since $\chi^{(3)}_{xxxx}$ and n are real quantities (from the assumption of a lossless medium), κ_1 and κ_2 are also real quantities. Eqs. (2.25) and (2.26) have solutions on the form $E_1(z) = E_1(0)e^{\mathrm{i}\kappa_1 z}$ and $E_2(z) = E_2(0)e^{-\mathrm{i}\kappa_2 z}$, respectively.

Next, we consider the probe and conjugate fields. If we assume that the incident probe wave can be decomposed into plane waves we can for simplicity consider only one of these at a time. Under this assumption, and keeping the approximations mentioned before, the wave equations for the probe and conjugate fields are

$$\frac{dE_3(z)}{dz} = \frac{3\mathrm{i}\omega}{8nc}\chi^{(3)}_{xxxx}\left\{\left[|E_1(0)|^2 + 2|E_2(0)|^2\right]E_3(z) + E_1(0)E_2(0)E_4^*(z)e^{\mathrm{i}(\kappa_1 - \kappa_2)z}\right\}$$
$$\equiv \mathrm{i}\kappa_3 E_3(z) + \mathrm{i}\kappa E_4^*(z), \tag{2.27}$$

$$\frac{dE_4(z)}{dz} = -\frac{3\mathrm{i}\omega}{8nc}\chi^{(3)}_{xxxx}\left\{\left[|E_1(0)|^2 + 2|E_2(0)|^2\right]E_4(z) + E_1(0)E_2(0)E_3^*(z)e^{\mathrm{i}(\kappa_1 - \kappa_2)z}\right\}$$
$$\equiv -\mathrm{i}\kappa_3 E_4(z) - \mathrm{i}\kappa E_3^*(z). \tag{2.28}$$

To achieve perfect phase matching between the probe and the conjugate field, κ has to be constant along z, requiring that $\kappa_1 = \kappa_2$, which means that the intensity of the two pump fields must be the same ($|E_1(z)|^2 = |E_2(z)|^2$). If we additionally introduce a change of variables by letting $E_3(z) = E_3'(z)e^{i\kappa_3 z}$ and $E_4(z) = E_4'(z)e^{-i\kappa_3 z}$, Eqs. (2.27) and (2.28) become

$$\frac{dE_3'(z)}{dz} = i\kappa E_4'^*(z), \tag{2.29}$$

$$\frac{dE_4'(z)}{dz} = -i\kappa E_3'^*(z), \tag{2.30}$$

and we notice in passing that the primed and the unprimed variables coincide in the input plane of the interaction region, i.e., at $z = 0$. Eqs. (2.29) and (2.30) shows why degenerate four-wave mixing leads to phase conjugation, since the generated field $E_4'(z)$ is driven only by the complex conjugate of the probe field amplitude. Differentiation of Eq. (2.29) and insertion of Eq. (2.30), an vice versa, we get

$$\frac{d^2E_3'(z)}{dz^2} + \kappa^2 E_3'(z) = 0, \tag{2.31}$$

$$\frac{d^2E_4'(z)}{dz^2} + \kappa^2 E_4'(z) = 0. \tag{2.32}$$

The characteristic equation is $\lambda^2 + \kappa^2 = 0$, which has solutions $\lambda = \pm i\kappa$. The general solution to Eqs. (2.31) and (2.32) is then

$$E_3'(z) = C_1 e^{i\kappa z} + C_2 e^{-i\kappa z}, \tag{2.33}$$
$$E_4'(z) = C_3 e^{i\kappa z} + C_4 e^{-i\kappa z}. \tag{2.34}$$

Assuming that we know the values $E_3'(0)$ and $E_4'(L)$, we can then find $E_3'(z)$ and $E_4'(z)$ as a function of these two boundary values. Then the solutions to the coupled differential equations, Eqs. (2.29) and (2.30), describing the electric field inside the phase conjugating medium, become

$$E_3'(z) = E_3'(0)\frac{\cos[\kappa(L-z)]}{\cos(\kappa L)} - iE_4'^*(L)\frac{\sin(\kappa z)}{\cos(\kappa L)}, \tag{2.35}$$

$$E_4'(z) = E_4'(L)\frac{\cos(\kappa z)}{\cos(\kappa L)} - iE_3'^*(0)\frac{\sin[\kappa(L-z)]}{\cos(\kappa L)}. \tag{2.36}$$

In the practical case, $E_3'(0)$ (the probe field coming into the medium) is finite and $E_4'(L)$ (the phase conjugated field at the other end of the medium) is zero. The phase conjugated field coming out of the medium at $z = 0$ is then

$$E_4'(0) = -iE_3'^*(0)\tan(\kappa L). \tag{2.37}$$

Thus the phase conjugated field depends on (i) the intensity of the pump fields, (ii) the length of the active medium, and (iii) the incoming probe field, and we notice that the magnitude of the phase conjugated field can be larger than the magnitude of the incoming probe field.

Chapter 3

The theoretical description given in the preceding chapter is not the only existing description of phase conjugation by DFWM in the macroscopic sense, but it illustrates quite well the usual line of thought when considering optical phase conjugation. As examples on theoretical papers going beyond the description in Chapter 2, let us mention that (i) polarization properties have been studied by Ducloy and Bloch (1984), (ii) descriptions taking into account the vectorial properties [see Eq. (2.20)] have been given, e.g., by Syed, Crofts, Green, and Damzen (1996), (iii) improvements to the standard theory in the form of abandoning the slowly varying envelope approximation (SVEA) have also been discussed [see, e.g., Marburger (1983) and Farzad and Tavassoly (1997)]. A feature of the standard theory [see Eq. (2.37)] is that the phase conjugated response depends on the length of the nonlinear crystal used (infinite at $\kappa L = (2p+1)\pi/2$ for any integer value of p). The standard theory has proven to be a satisfactory description for spatially nondecaying fields containing no evanescent components.

Though the overwhelming majority of optical phase conjugation experiments can be described without inclusion of evanescent components of the electromagnetic field, the possible phase conjugation of these components has been discussed from time to time. With the experimental observation of Bozhevolnyi, Keller, and Smolyaninov (1994, 1995), the need for inclusion of near-field components and thus evanescent modes in the description of optical phase conjugation has drawn renewed attention.

In an important paper by Agarwal and Gupta (1995) the treatment was focused on an analysis of the phase conjugated replica produced by a so-called ideal phase conjugator, characterized phenomenologically by a polarization- and angle of incidence independent nonlinear amplitude reflection coefficient, and in recent articles by Keller (1996b, 1996c) attention was devoted to an investigation of the spatial confinement problem of the phase conjugated field. Macroscopic theories including near-field components in the optical phase conjugation process have also appeared recently (Bozhevolnyi, Bozhevolnaya, and Berntsen 1995; Arnoldus and George 1995).

In their work Bozhevolnyi, Keller, and Smolyaninov used degenerate four-wave mixing (DFWM) produced by a 10mW HeNe laser with a wavelength of 633nm in an iron-doped lithium-niobate (Fe:LiNbO$_3$) crystal and an external-reflection near-field optical microscope to achieve phase conjugated light foci, which with a diameter of ~ 180nm were well below the classical diffraction limit. The main conclusion of their experiments

was that to achieve a spot size as small as 180nm phase conjugation of at least parts of the optical near-field emitted from the source must have taken place.

In the present work we go one step further in the theoretical study of the phase conjugation of optical signals which include near-field components by abandoning the ideal phase conjugator assumption. For simplicity our description is limited to cover only the degenerate four-wave mixing configuration for which the interacting optical fields all have the same cyclic frequency ω.

Because of the small range of the optical evanescent fields from the (mesoscopic) source a substantial part of the near-field phase conjugation process is bound to take place in the surface region of the phase conjugating medium. It is thus from the very outset necessary to focus the attention on the surface region of the nonlinear mirror and investigate the phase conjugation process on a length scale (much) smaller than the optical wavelength. This fact in itself makes use of the ideal phase conjugator assumption doubtful. For a bulk phase conjugator it may furthermore be difficult to assure an effective nonlinear mixing in a surface layer as thin as the field penetration depth. Thus, experimentally it might be advantageous to use a thin film or even a quantum well as the nonlinear medium (see Fig. 3.1). From a different perspective the use of a thin film as the nonlinear medium has already drawn attention (Montemezzani and Günter 1996).

The present theory has been constructed in such a manner that it offers a framework for microscopic studies of degenerate four-wave mixing at surfaces of bulk media, in thin films and quantum wells, and in small particles. To carry out in detail a rigorous microscopic numerical analysis of the DFWM process it is, however, necessary to consider mesoscopic media with a particularly simple electronic structure, and we shall demonstrate later how the present theory can be applied to a simple quantum well structure.

In conventional descriptions of optical phase conjugation by DFWM it is assumed that the interaction length is long compared to the wavelength of the probe fields, thus building up pictorially speaking from one of the pump beams and the probe beam a grating, from which the other pump beam is scattered into a phase conjugated replica (the 'real-time holography' picture). Furthermore it is assumed that the amplitudes of the fields are slowly varying on the optical wavelength scale [Slowly varying envelope (SVE) approximation] and thus also constant across the individual scattering units (atoms, molecules, . . .) [Electric dipole (ED) approximation] of the phase conjugating medium. Considering optical near fields, which contain components varying rapidly in space, the aforementioned approximations do not hold and we thus exclude them in the present formalism. We also avoid other approximations often made in the literature, namely (i) the assumption of a lossless medium, (ii) the *ab initio* requirement of phase matching between the interacting optical signals, and (iii) the assumption that the probe field is weak compared to the pump fields.

To illustrate the need for a theory going beyond the SVE and ED approximations, we have in Fig. 3.2 shown the component of the probe wavevector perpendicular to the surface, inside as well as outside the phase conjugator, as a function of its parallel component. When the parallel component of the probe wavevector becomes larger than ω/c_0, the perpendicular component of the wavevector becomes purely imaginary
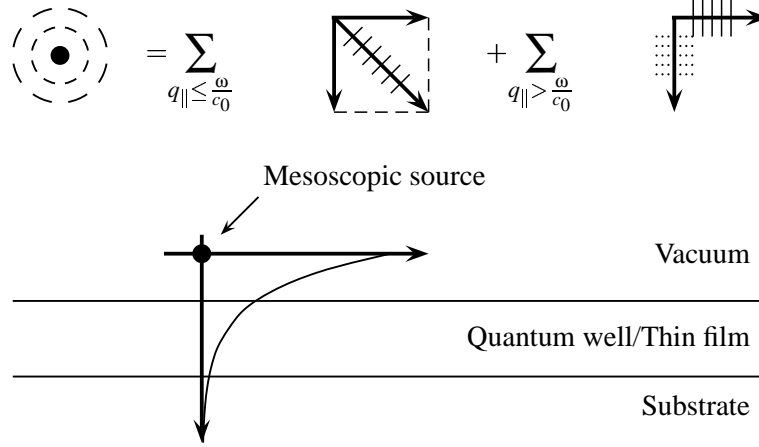
Figure 3.1: The upper part is a schematic illustration showing the Weyl representation of a spherical wave-field from a point (mesoscopic) source. In this representation the field is expanded in plane waves over a plane, in practice the surface in consideration. The two-dimensional wavevector ($\vec{q}_\parallel$) expansion consists of those terms for which $q_\parallel \leq \omega/c_0$ (c_0 being the vacuum speed of light) plus those having $q_\parallel > \omega/c_0$. In the first group of terms the component of the wavevector perpendicular to the surface (vertical arrow) is real so that the individual plane-wave modes are propagating, and in the second group, consisting of evanescent modes, this component is purely imaginary. The solid lines attached to two of the arrows indicate planes of constant phase, and the dotted lines attached to the evanescent modes indicate lines of constant amplitude. The lower part is a schematic illustration showing an exponentially decaying mode from a mesoscopic source placed near a thin film (quantum well) phase conjugator. To phase conjugate an evanescent mode in an effective manner the near field of the source must overlap the phase conjugator, and as indicated it is not always correct to assume that the selfconsistently determined evanescent field is constant across the thin film.

in the vacuum, but it is still real inside the phase conjugating mirror. A purely imaginary wavevector component means that the electromagnetic field is evanescent, whereas a real component indicates that the field is propagating and nondecaying (in the absense of absorption). When the parallel component becomes larger than $n\omega/c_0$ (where n is the refractive index of the substrate) the perpendicular component of the probe wavevector becomes evanescent also inside the phase conjugating mirror, and the larger the parallel component, the more wrong the SVE and ED approximations become. Thus to study, for instance, the phase conjugation of all field components possibly emitted from a mesoscopic source in the vicinity of the phase conjugator it is necessary to abandon these approximations.

As already mentioned, the present theory not only allows one to investigate the optical phase conjugation of evanescent waves with small penetration depths, it also enables one to investigate the possibility of achieving DFWM in mesoscopic films (quantum wells),
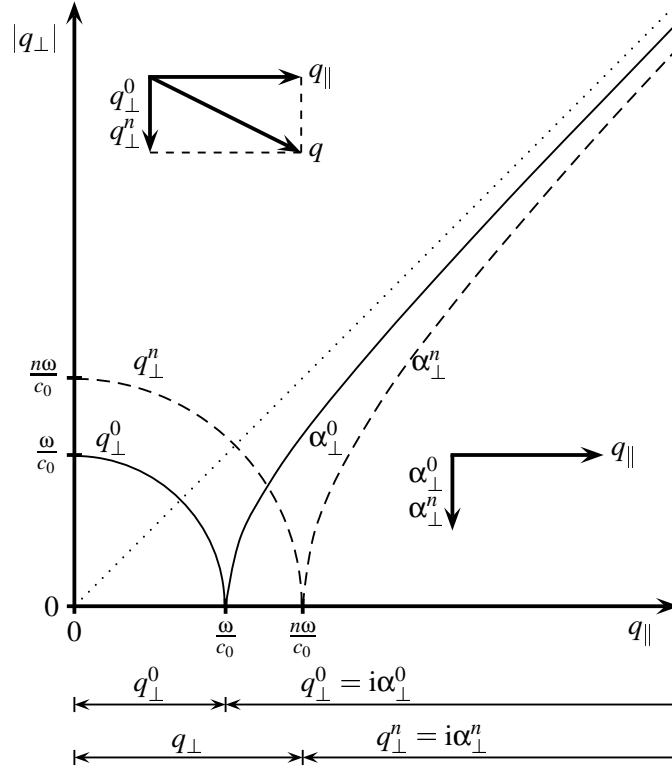
Figure 3.2: The component of the probe wavevector perpendicular to ($q_\perp$) a vacuum/bulk phase conjugator interface as a function of its real parallel component ($q_\parallel$) in vacuum (solid line, $q_\perp^0$) and in the substrate (dashed line, $q_\perp^n$). For $q_\parallel \leq \omega/c_0$, $q_\perp^0 = [(\omega/c_0)^2 - q_\parallel^2]^{1/2}$, and $q_\perp^n = [(n\omega/c_0)^2 - q_\parallel^2]^{1/2}$ are both real, and the associated plane waves are thus propagating (and nondecaying) in both the vacuum and the phase conjugator, neglecting absorption. In the region $\omega/c_0 < q_\parallel \leq n\omega/c_0$ (n being the linear (real) refractive index of the phase conjugator), $q_\perp^0 = i\alpha_\perp^0$ becomes purely imaginary (we plot $\alpha_\perp^0 = [q_\parallel^2 - (\omega/c_0)^2]^{1/2}$), but $q_\perp$ is still real. The field in the vacuum is thus evanescent in this region. In the region $q_\parallel > n\omega/c_0$, also $q_\perp = i\alpha_\perp$ is a purely imaginary number (we plot $\alpha_\perp^n = [q_\parallel^2 - (n\omega/c_0)^2]^{1/2}$), so that also the field in the phase conjugator is evanescent.

a subject of interest in its own right. The main reason that the present formulation may be used in near-field optics as well as in mesoscopic-film electrodynamics originates in the fact that in both cases the microscopic local-field calculation is the crucial quantity. A further advantage of the present theory is that it allows us to study phase conjugation when one or more of the interacting fields are surface-wave fields.

   The construction of such a theoretical model begins with the microscopic Maxwell–Lorentz equations, which combined with the nonlocal linear and third-order nonlinear constitutive equations are used to set up the basic wave equation for the phase conjugated field. The linear and nonlinear conductivity responses of the electrons will be calculated

within the framework of the random-phase-approximation theory, the starting point being the Liouville equation of motion for the density matrix operator. In the description we include in the interaction Hamiltonian not only the standard $\vec{p} \cdot \vec{A}$ term ($\vec{p}$ being the momentum operator and $\vec{A}$ being the vector potential) but also the term proportional to the square of the vector potential, i.e., $\vec{A} \cdot \vec{A}$. For a monochromatic driving field (of cyclic frequency ω), this term contains 2ω- and DC-parts, and both of these are in general important for the description of the microscopic phase conjugation process. In the current density operator we include the term containing the vector potential. This term, needed in order to ensure the gauge invariance of quantum electrodynamics, also turns out to be of importance in some cases. Starting from a dipolar interaction Hamiltonian the first explicit microscopic derivation of the third-order conductivity (susceptibility) response appears to be due to Bloembergen, Lotem, and Lynch Jr. (1978). The result of Bloembergen, Lotem, and Lynch Jr. is based on a $\vec{r} \cdot \vec{E}$ calculation and only the vector-potential independent part of the current density operator is kept. Apart from a single study dealing with the electromagnetic self-action in a BCS-paired superconductor (Keller 1995), it seems that in all theoretical investigations of the DFWM-process in which microscopic considerations have appeared, the Bloembergen, Lotem, and Lynch Jr. expression has been used. We cannot use this expression here, however, since we need to address a local-field problem when dealing with mesoscopic interaction volumes, and such a problem necessitates that we take into account values of $q_\parallel$ much larger than ω/c_0, and thus that the calculation goes beyond the ED approximation. To account for local-field effects it is necessary to perform a spatially nonlocal calculation of the third-order conductivity, and this is most adequately done beginning with the minimal coupling interaction Hamiltonian which contains both the $\vec{p} \cdot \vec{A}$ and $\vec{A} \cdot \vec{A}$ terms. In the local limit where the vector potential only depends on time our expression for the nonlinear conductivity and the $\vec{r} \cdot \vec{E}$ based one of Bloembergen, Lotem, and Lynch Jr. are physically equivalent, *provided* the terms stemming from the gauge conserving vector potential dependent part of the current density operator are neglected. Though physically equivalent, the explicit forms of the relation between the nonlinear current density and the electric field only coincides after having performed a relevant unitary transformation on the minimal coupling Hamiltonian and the related electronic wave functions. In stead of using the minimal coupling Hamiltonian to describe the nonlocal dynamics one could in principle have used the multipolar Hamiltonian. In practice this is less convenient for the present purpose due to the fact that the pronounced nonlocality we sometimes are facing in mesoscopic media would require that many multipole terms were kept in the Hamiltonian. The essentially nonlocal terms in the nonlinear conductivity are included in our treatment because they in certain cases—especially for very small interaction volumes—are the only contributing ones, and in other cases they dominate the phase conjugated response. Since we deal with a spatially nonlocal description it is important to characterize the spatial structure involved in the physical processes behind the phase conjugation, and the various physical processes hidden in the nonlinear and nonlocal constitutive equation are therefore identified. Following the identification of the physical processes, an expression for the so-called conductivity response tensor describing the nonlinear material response in the

DFWM process is established, and the eigensymmetries of the conductivity tensors belonging to each of the processes occuring in the DFWM process are discussed. Rather than solving the full spatial problem (which would be cumbersome, if not impossible), we consider a simplified system possessing infinitesimal translational invariance in two directions. For such a system the potential of the related Schrödinger equation only varies in the direction perpendicular to the plane of translational invariance. The fundamental solutions to the time-independent Schrödinger equation are inserted into the linear and nonlinear conductivity tensors thus giving us the framework for a theoretical description of the DFWM process in mesoscopic films (quantum wells) as well as for evanescent waves. Compared to conventional descriptions of optical phase conjugation in bulk media the concept of phase matching (momentum conservation) now appears only in *two* dimensions. The lack of translational invariance in the third dimension implies that no phase matching occurs in this dimension. Phase matching (in one, two or three dimensions) is not a precondition set on our theory, it follows to the extent that the phase conjugating medium exhibits infinitesimal translational invariance. Despite the fact that the phase matching is lost in the third dimension, phase conjugation may still take place in quantum wells and thin films, and with evanescent fields, just as second harmonic generation can occur in quantum-well systems, at metallic (and semiconducting) surfaces and from nonlinear (sub)monolayer films deposited on linear substrates (Richmond, Robinson, and Shannon 1988). To complete our local-field calculation of the optical phase conjugation by degenerate four-wave mixing in mesoscopic interaction volumes, we use a Green's function formalism to establish new integral equations for the phase conjugated field in the general case, and in the case where the nonlinear medium exhibits translational invariance in two dimensions. The microscopic local-field theory thus established is then used to describe the DFWM in one- and two-level quantum-well phase conjugators.

Part II

Microscopic model for degenerate four-wave mixing

Chapter 4

<div align="right">The electromagnetic field</div>

In this chapter a description of the electromagnetic field from a phase conjugating medium is established, starting from the microscopic Maxwell equations. First, we derive the relevant wave equation for the phase conjugated field. The field–matter interaction is then described through the use of constitutive relations. In the final step of this basic framework, a self-consistent description of the phase conjugated field is established.

4.1 Wave equation for the phase conjugated field

As a starting point we take the microscopic Maxwell-Lorentz equations, in which the material response at the space-time point $(\vec{r}, t)$ is completely described via the microscopic current density $\vec{J}(\vec{r}, t)$, and the related charge density, $\rho(\vec{r}, t)$. They are

$$\vec{\nabla} \times \vec{E}(\vec{r}, t) = -\frac{\partial \vec{B}(\vec{r}, t)}{\partial t}, \tag{4.1}$$

$$\vec{\nabla} \times \vec{B}(\vec{r}, t) = \mu_0 \vec{J}(\vec{r}, t) + \frac{1}{c_0^2} \frac{\partial \vec{E}(\vec{r}, t)}{\partial t}, \tag{4.2}$$

$$\vec{\nabla} \cdot \vec{E}(\vec{r}, t) = \frac{1}{\varepsilon_0} \rho(\vec{r}, t), \tag{4.3}$$

$$\vec{\nabla} \cdot \vec{B}(\vec{r}, t) = 0, \tag{4.4}$$

$\vec{E}(\vec{r}, t)$ and $\vec{B}(\vec{r}, t)$ being the electric and magnetic fields prevailing at the space point $\vec{r}$ at the time t.

Taking the curl of Eq. (4.1) and inserting the result into Eq. (4.2) we obtain the following wave equation for the prevailing local electric field $\vec{E}(\vec{r}, t)$:

$$\left(\vec{\vec{1}} \Box + \vec{\nabla} \otimes \vec{\nabla} \right) \cdot \vec{E}(\vec{r}, t) = -\mu_0 \frac{\partial \vec{J}(\vec{r}, t)}{\partial t}, \tag{4.5}$$

where $\Box = \frac{1}{c^2} \frac{\partial^2}{\partial t^2} - \nabla^2$ is the d'Alembertian operator, $\vec{\vec{1}}$ is the (3×3) unit tensor, and $\otimes$ is the outer (dyadic) product operator.

Introducing the electric field as a Fourier series in the cyclic frequency ω, viz.

$$\vec{E}(\vec{r}, t) = \frac{1}{2} \sum_{\alpha=0}^{\infty} \vec{E}_{-\alpha\omega}(\vec{r}) e^{-i\alpha\omega t} + \text{c.c.}, \tag{4.6}$$

where α is an integer and "c.c." denotes the complex conjugate of the first terms, we subsequently can limit ourselves to a harmonic analysis. Since $\vec{E}(\vec{r},t)$ is a real quantity, $\vec{E}^*_{-\alpha\omega}(\vec{r}) = \vec{E}_{\alpha\omega}(\vec{r})$.

Likewise, we write the current density as a Fourier series in ω, in which each component implicitly is expressed as a power series in the electric field. Thus

$$\vec{J}(\vec{r},t) = \frac{1}{2} \sum_{\alpha=0}^{\infty} \sum_{\beta=0}^{\infty} \left(\vec{J}^{(\alpha+2\beta)}_{-\alpha\omega}(\vec{r}) e^{-i\alpha\omega t} + \text{c.c.} \right), \tag{4.7}$$

where α and β are integers. Looking for solutions at the cyclic frequency ω, only fields and current densities with $\alpha = 1$ in Eqs. (4.6) and (4.7) contributes. Accordingly we in the following write the phase conjugated (PC) electric field without the reference to the cyclic frequency, i.e., $\vec{E}_{-\omega}(\vec{r}) \equiv \vec{E}_{PC}(\vec{r})$. In the case of DFWM we will assume that the lowest order nonlinear interaction dominates over higher order mixing processes. Thus, in order to describe the DFWM response of our medium we retain only the two currents of lowest order in β, namely the linear contribution $\vec{J}^{(1)}_{-\omega}(\vec{r})$ and the lowest order nonlinear contribution $\vec{J}^{(3)}_{-\omega}(\vec{r})$. The wave equation for the negative frequency part of the phase conjugated response hence takes the form

$$\left[\vec{\mathbb{1}} \left(\frac{\omega^2}{c^2} + \nabla^2 \right) - \vec{\nabla} \otimes \vec{\nabla} \right] \cdot \vec{E}_{PC}(\vec{r}) = -i\mu_0\omega \left(\vec{J}^{(1)}_{-\omega}(\vec{r}) + \vec{J}^{(3)}_{-\omega}(\vec{r}) \right). \tag{4.8}$$

4.2 Constitutive relations for the current densities

To close the loop for the calculation of the phase conjugated field, the microscopic current densities $\vec{J}^{(1)}_{-\omega}(\vec{r})$ and $\vec{J}^{(3)}_{-\omega}(\vec{r})$ are given in terms of the local electric field through constitutive relations describing the field–matter interaction in a perturbative manner. Choosing a gauge where the time-dependent part of the scalar potential is zero, the electric field is related to the vector potential via $\vec{E}(\vec{r}) = i\omega\vec{A}(\vec{r})$. Thus the microscopic current densities can be related via the constitutive relations to the vector potentials of the phase conjugated field ($\vec{A}_{PC}$) and the fields driving the process ($\vec{A}$). The linear constitutive relation we therefore write in the form

$$\vec{J}^{(1)}_{-\omega}(\vec{r}) = i\omega \int \vec{\sigma}(\vec{r},\vec{r}') \cdot \vec{A}_{PC}(\vec{r}') d^3r', \tag{4.9}$$

where $\vec{\sigma}(\vec{r},\vec{r}') \equiv \vec{\sigma}(\vec{r},\vec{r}';\omega)$ is the linear conductivity tensor. The i'th element of the first order current density is proportional to the integral of $[\vec{\sigma} \cdot \vec{A}_{PC}]_i = \sum_j \sigma_{ij} A_{PC,j}$. The nonlinear DFWM constitutive relation is written in a similar fashion, i.e.,

$$\vec{J}^{(3)}_{-\omega}(\vec{r}) = (i\omega)^3 \int \int \int \vec{\Xi}(\vec{r},\vec{r}',\vec{r}'',\vec{r}''') \vdots \vec{A}(\vec{r}''')\vec{A}(\vec{r}'')\vec{A}^*(\vec{r}') d^3r''' d^3r'' d^3r', \tag{4.10}$$

where $\overset{\leftrightarrow}{\Xi}(\vec{r},\vec{r}\,',\vec{r}\,'',\vec{r}\,''') \equiv \overset{\leftrightarrow}{\Xi}(\vec{r},\vec{r}\,',\vec{r}\,'',\vec{r}\,''';\omega)$ is the nonlocal third order conductivity tensor.

The three-dimensional sum-product operator "$\vdots$" is here meant to be interpreted for the i'th element of the third order current density in the following way:

$$\left[\overset{\leftrightarrow}{\Xi}(\vec{r},\vec{r}\,',\vec{r}\,'',\vec{r}\,''') \vdots \vec{A}(\vec{r}\,''')\vec{A}(\vec{r}\,'')\vec{A}^*(\vec{r}\,') \right]_i = \sum_{jkh} \Xi_{ijkh}(\vec{r},\vec{r}\,',\vec{r}\,'',\vec{r}\,''') A_h(\vec{r}\,''') A_k(\vec{r}\,'') A_j^*(\vec{r}\,').$$

(4.11)

By inserting Eqs. (4.9) and (4.10), with $\vec{A}_{\mathrm{PC}} = \vec{E}_{\mathrm{PC}}/(\mathrm{i}\omega)$, into Eq. (4.8) the loop for the phase conjugated field is closed.

4.3 The phase conjugated field

From the outset we assume that the parametric approximation can be adopted, i.e., we assume that the generated phase conjugated field does not affect the dynamics of the pump and signal fields. In the present case, where the phase conjugated field originates mainly in evanescent modes or from a quantum well, the interaction volume is small and the magnitude of the phase conjugated field thus very limited so that one may expect the parametric approximation to be quite good. The inherent spatial nonlocality of the processes which underlies the microscopic calculation of the local fields and currents is crucial and must be kept throughout the following analysis.

Above we used the microscopic Maxwell-Lorentz equations to establish a wave equation [Eq. (4.8)] for the phase conjugated electric field. Since this equation holds not only inside the phase conjugator but also in the medium possibly in contact with the phase conjugator, it is adequate to divide the linear part of the induced current density into two, i.e.,

$$\vec{J}(\vec{r}) = \vec{J}_{\mathrm{cont}}(\vec{r};\omega) + \vec{J}_{\mathrm{PC}}^{(1)}(\vec{r};\omega),$$

(4.12)

where $\vec{J}_{\mathrm{cont}}(\vec{r};\omega)$ is the linear current density of the medium in contact (cont) with the phase conjugator, and $\vec{J}_{\mathrm{PC}}^{(1)}(\vec{r};\omega)$ is the linear current density of the phase conjugator. In setting up the above-mentioned equation we have implicitly assumed that there is no (significant) electronic overlap between the phase conjugator and the contact medium. The two electron distributions can still be electromagnetically coupled, of course. In the quantum well case, $\vec{J}_{\mathrm{cont}}(\vec{r};\omega)$ is to be identified as the current density induced in the (assumed linear) response of the substrate. To deal with the evanescent response of a (semiinfinite) phase conjugator one just puts $\vec{J}_{\mathrm{cont}}(\vec{r};\omega) = \vec{0}$.

Instead of proceeding directly with the differential equation [Eq. (4.8)] for the phase conjugated local field we convert it into an integral relation between the phase conjugated electric field and the prevailing current density, namely

$$\vec{E}_{\mathrm{PC}}(\vec{r};\omega) = \vec{E}_{\mathrm{PC}}^{\mathrm{ext}}(\vec{r};\omega) - \mathrm{i}\mu_0\omega \int \overset{\leftrightarrow}{G}_0(\vec{r},\vec{r}\,';\omega) \cdot \left[\vec{J}_{\mathrm{cont}}(\vec{r}\,';\omega) + \vec{J}_{\mathrm{PC}}^{(1)}(\vec{r}\,';\omega) \right] d^3r', \quad (4.13)$$

where $\vec{E}_{PC}^{ext}(\vec{r};\omega)$ is the so-called external (ext) field driving the phase conjugation process, and $\overleftrightarrow{G}_0(\vec{r},\vec{r}';\omega)$ is the electromagnetic vacuum propagator. Instead of proceeding with Eq. (4.13) as it stands, if possible, it is often advantageous to eliminate the current density of the contact medium in favour of a so-called pseudo-vacuum (or contact-medium) propagator, $\overleftrightarrow{G}(\vec{r},\vec{r}';\omega)$. Doing this, one obtains

$$\vec{E}_{PC}(\vec{r};\omega) = \vec{E}_{PC}^{B}(\vec{r};\omega) - i\mu_0\omega \int \overleftrightarrow{G}(\vec{r},\vec{r}';\omega)\cdot\vec{J}_{PC}^{(1)}(\vec{r}';\omega)d^3r', \tag{4.14}$$

where $\vec{E}_{PC}^{B}(\vec{r};\omega)$ is the so-called background (B) response of the phase conjugator. The background field is effectively the field driving the phase conjugated response. From a knowledge of the nonlinear part, $\vec{J}_{-\omega}^{(3)}(\vec{r})$, of the current density of the phase conjugator, the background field can be calculated from the integral relation

$$\vec{E}_{PC}^{B}(\vec{r};\omega) = -i\mu_0\omega \int \overleftrightarrow{G}(\vec{r},\vec{r}';\omega)\cdot\vec{J}_{-\omega}^{(3)}(\vec{r}')d^3r'. \tag{4.15}$$

In the parametric approximation adopted here the background field can be considered as a prescribed quantity. By inserting the linear constitutive equation

$$\vec{J}_{PC}^{(1)}(\vec{r};\omega) = \int \overleftrightarrow{\sigma}(\vec{r},\vec{r}';\omega)\cdot\vec{E}_{PC}(\vec{r}';\omega)d^3r' \tag{4.16}$$

into Eq. (4.14) one obtains the following integral equation for the phase conjugated field:

$$\vec{E}_{PC}(\vec{r};\omega) = \vec{E}_{PC}^{B}(\vec{r};\omega) - i\mu_0\omega \int\int \overleftrightarrow{G}(\vec{r},\vec{r}'';\omega)\cdot\overleftrightarrow{\sigma}(\vec{r}'',\vec{r}';\omega)\cdot\vec{E}_{PC}(\vec{r}';\omega)d^3r''d^3r'. \tag{4.17}$$

The formal solution of this equation is given by

$$\vec{E}_{PC}(\vec{r};\omega) = \int \overleftrightarrow{\Gamma}(\vec{r},\vec{r}';\omega)\cdot\vec{E}_{PC}^{B}(\vec{r}';\omega)d^3r', \tag{4.18}$$

where the nonlocal field-field response tensor $\overleftrightarrow{\Gamma}(\vec{r},\vec{r}';\omega)$ is to be derived from the dyadic integral equation

$$\overleftrightarrow{\Gamma}(\vec{r},\vec{r}';\omega) = \overleftrightarrow{\mathbb{1}}\delta(\vec{r}-\vec{r}') + \int \overleftrightarrow{K}(\vec{r},\vec{r}'';\omega)\cdot\overleftrightarrow{\Gamma}(\vec{r}'',\vec{r}';\omega)d^3r''. \tag{4.19}$$

In Eq. (4.19) the tensor

$$\overleftrightarrow{K}(\vec{r},\vec{r}'';\omega) = -i\mu_0\omega \int \overleftrightarrow{G}(\vec{r},\vec{r}';\omega)\cdot\overleftrightarrow{\sigma}(\vec{r}',\vec{r}'';\omega)d^3r' \tag{4.20}$$

is the kernel of the integral equation in Eq. (4.17). This kernel formally is identical to the one playing a prominent role in the electrodynamics of mesoscopic media and small particles [see Keller (1996a), section 4].

By inserting Eq. (4.15) into Eq. (4.18) and thereafter making use of Eq. (4.10), the phase conjugated field may in principle be calculated from known quantities. In practice it is not so easy, since the integral equation in Eq. (4.17) for the phase conjugated field in general is too difficult to handle numerically even if rather simple linear conductivity response tensors are used, the reason being the inherent three-dimensional ($\vec{r}$) nature of the problem. One therefore has to resort to one sort of approximation or another. Just as in other linear and nonlinear studies of mesoscopic media, or media with a small interaction volume, a tractable problem is obtained if the medium in question possesses translational invariance in two directions as discussed in Part III.

Chapter 5

Single-electron current density response

In this chapter the Liouville equation of motion for the single-body density matrix operator is used together with the single-particle Hamiltonian to establish a more general quantum mechanical expression for the third-order current density than those hitherto found in the literature. The generalisation is of significant importance for the theory of near-field phase conjugation and for DFWM in mesoscopic films. Following the derivation of the linear and the DFWM responses, we end this chapter by a discussion of the underlying physical processes.

5.1 Density matrix operator approach

The starting point for this calculation is the Liouville equation of motion for the single-body density matrix operator ρ, i.e.,

$$\mathrm{i}\hbar\frac{\partial\rho}{\partial t} = [\mathcal{H},\rho]. \tag{5.1}$$

In the equation above, the single-particle Hamiltonian $\mathcal{H}$ appearing in the commutator $[\mathcal{H},\rho]$ in the present description is given by

$$\mathcal{H} = \mathcal{H}_0 + \mathcal{H}_{\mathrm{R}} + \mathcal{H}_0^{(2)} + \frac{1}{2}\sum_{\alpha=1}^{2}\left(\mathcal{H}_{-\alpha\omega}^{(\alpha)}e^{-\mathrm{i}\alpha\omega t} + \mathrm{H.a.}\right), \tag{5.2}$$

where $\mathcal{H}_0$ is the Hamiltonian operator for the electron in the material when the perturbing optical field is absent, $\mathcal{H}^{(1)}$ is the interaction Hamiltonian of first order in the vector potential $\vec{A}(\vec{r})$, $\mathcal{H}^{(2)}$ is the interaction Hamiltonian of second order in $\vec{A}(\vec{r})$, $\mathcal{H}_{\mathrm{R}}$ represents the irreversible coupling to the "surroundings", and "H.a." denotes the Hermitian adjoint. Although the spin and spin-orbit dynamics may be included in the formalism in a reasonably simple fashion we have omitted to do so because spin effects are judged to be significant only for nonlinear phenomena of even order. Hence

$$\mathcal{H}_0 = \frac{1}{2m_e}\vec{p}\cdot\vec{p} + V(\vec{r}), \tag{5.3}$$

$$\mathcal{H}_{-\omega}^{(1)} = \left(\mathcal{H}_{\omega}^{(1)}\right)^{\dagger} = \frac{e}{2m_e}\left(\vec{p}\cdot\vec{A}(\vec{r}) + \vec{A}(\vec{r})\cdot\vec{p}\right), \tag{5.4}$$

$$\mathcal{H}^{(2)}_{-2\omega} = \left(\mathcal{H}^{(2)}_{2\omega}\right)^{\dagger} = \frac{e^2}{4m_e}\vec{A}(\vec{r})\cdot\vec{A}(\vec{r}), \tag{5.5}$$

$$\mathcal{H}^{(2)}_{0} = \frac{e^2}{4m_e}\vec{A}(\vec{r})\cdot\vec{A}^*(\vec{r}), \tag{5.6}$$

where † stands for Hermitian adjugation, $V(\vec{r})$ is the scalar potential of the field-unperturbed Schrödinger equation, $\vec{p} = -i\hbar\vec{\nabla}$ denotes the momentum operator, m_e is the mass of the electron, and $-e$ is its electric charge.

As often is the practice in optics we assume that the irreversible coupling to the surrounding reservoir can be described using a phenomenological relaxation-time ansatz in the Liouville equation, so that

$$\frac{1}{i\hbar}\left[\mathcal{H}_{\mathrm{R}}, \rho_{nm}\right] = \frac{\rho^{(0)}_{nm} - \rho_{nm}}{\tau_{nm}}, \qquad n \neq m, \tag{5.7}$$

$\rho^{(0)}_{nm}$ being the nm'th element of the thermal equilibrium density matrix operator, and τ_{nm} the associated relaxation time.

In the present harmonic analysis we also use a combined Fourier and power series expansion of the density matrix operator, namely

$$\rho = \frac{1}{2}\sum_{\alpha=0}^{\infty}\sum_{\beta=0}^{\infty}\left(\rho^{(\alpha+2\beta)}_{-\alpha\omega}e^{-i\alpha\omega t} + \mathrm{H.a.}\right), \tag{5.8}$$

where α and β are integers, as before. The density matrix operator is Hermitian, i.e., $(\rho^{(\alpha+2\beta)}_{-\alpha\omega})^{\dagger} = \rho^{(\alpha+2\beta)}_{\alpha\omega}$, and we solve the Liouville equation of motion in the usual iterative manner.

To determine the conductivity response tensors, $\vec{\vec{\sigma}}(\vec{r},\vec{r}')$ and $\vec{\vec{\Xi}}(\vec{r},\vec{r}',\vec{r}'',\vec{r}''')$, appropriate for describing the phase conjugation process, we consider the ensemble average $\vec{J}(\vec{r},t)$ of the microscopic single-body current-density operator $\vec{j}(\vec{r},t)$. This ensemble average is obtained as the trace of $\rho\vec{j}$, carried out in the usual manner as a quantum mechanical double sum over states, i.e.,

$$\vec{J}(\vec{r},t) = \mathrm{Tr}\left\{\rho\vec{j}\right\} \equiv \sum_{nm}\rho_{nm}\vec{j}_{mn}. \tag{5.9}$$

In Eq. (5.9) and hereafter the ab'th matrix element of a single-body operator O as usual is denoted by $O_{ab} = \langle a|O|b\rangle$. In the absence of spin effects the microscopic current-density operator is given by (Bloembergen 1965)

$$\vec{j}(\vec{r},t) = \vec{j}^{(0)}(\vec{r}) + \frac{1}{2}\left(\vec{j}^{(1)}_{-\omega}e^{-i\omega t} + \mathrm{H.a.}\right), \tag{5.10}$$

where

$$\vec{j}^{(0)}(\vec{r}) = -\frac{e}{2m_e}\left(\vec{p}(\vec{r}_e)\delta(\vec{r}-\vec{r}_e) + \delta(\vec{r}-\vec{r}_e)\vec{p}(\vec{r}_e)\right) \tag{5.11}$$

$$\vec{j}^{(1)}_{-\omega} = -\frac{e^2}{m_e}\vec{A}(\vec{r}_e)\delta(\vec{r}-\vec{r}_e). \tag{5.12}$$

5.2 Linear response

Because of its usefulness for a subsequent comparison to the forced DFWM current density we first present the well known result for the linear response (Feibelman 1975, 1982). Thus, by using the expressions for the current density [Eq. (5.10)] and density matrix [Eq. (5.8)] operators it is realised that the linear current density is to be obtained from

$$\vec{J}^{(1)}_{-\omega}(\vec{r}) = \text{Tr}\left\{\rho^{(0)}\vec{j}^{(1)}_{-\omega}\right\} + \text{Tr}\left\{\rho^{(1)}_{-\omega}\vec{j}^{(0)}\right\}. \tag{5.13}$$

In explicit form the two traces are

$$\text{Tr}\left\{\rho^{(0)}\vec{j}^{(1)}_{-\omega}\right\} = \sum_n f_n \vec{j}^{(1)}_{-\omega,nn}. \tag{5.14}$$

$$\text{Tr}\left\{\rho^{(1)}_{-\omega}\vec{j}^{(0)}\right\} = \sum_{nm} \frac{f_n - f_m}{\hbar} \frac{\mathcal{H}^{(1)}_{-\omega,nm}}{\tilde{\omega}_{nm} - \omega} \vec{j}^{(0)}_{mn}. \tag{5.15}$$

In the equations above, we have introduced the complex cyclic transition frequency $\tilde{\omega}_{nm} = \omega_{nm} - i\tau_{nm}^{-1}$ between states n and m. The respective energies $\mathcal{E}_n$ and $\mathcal{E}_m$ of these states appear in the usual transition frequency $\omega_{nm} = (\mathcal{E}_n - \mathcal{E}_m)/\hbar$. The quantity

$$f_a = \left[1 + \exp\left(\frac{\mathcal{E}_a - \mu}{k_B T}\right)\right]^{-1} \tag{5.16}$$

denotes the Fermi–Dirac distribution function for state a ($a \in \{m, n\}$ above), k_B being the Boltzmann constant, μ the chemical potential of the electron system, and T the absolute temperature.

5.3 DFWM response

The nonlinear current density at $-\omega$, which originates in third order effects in the electric field, and which is the driving source for the DFWM process is given by

$$\vec{J}^{(3)}_{-\omega}(\vec{r}) = \frac{1}{2}\text{Tr}\left\{\rho^{(2)}_{-2\omega}\vec{j}^{(1)}_{\omega}\right\} + \text{Tr}\left\{\rho^{(2)}_0 \vec{j}^{(1)}_{-\omega}\right\} + \text{Tr}\left\{\rho^{(3)}_{-\omega}\vec{j}^{(0)}\right\}, \tag{5.17}$$

as one readily realises from Eqs. (4.7), (5.8), and (5.10). The tedious calculation of the three traces can be carried out in a fashion similar to that used for the linear case, finally leading to

$$\begin{aligned}
\frac{1}{2}\text{Tr}\left\{\rho^{(2)}_{-2\omega}\vec{j}^{(1)}_{\omega}\right\} = &\sum_{nm} \frac{f_n - f_m}{2\hbar} \frac{\mathcal{H}^{(2)}_{-2\omega,nm}\vec{j}^{(1)}_{\omega,mn}}{\tilde{\omega}_{nm} - 2\omega} \\
&+ \sum_{nmv} \left(\frac{f_m - f_v}{\tilde{\omega}_{vm} - \omega} + \frac{f_n - f_v}{\tilde{\omega}_{nv} - \omega}\right) \frac{\mathcal{H}^{(1)}_{-\omega,nv}\mathcal{H}^{(1)}_{-\omega,vm}\vec{j}^{(1)}_{\omega,mn}}{4\hbar^2(\tilde{\omega}_{nm} - 2\omega)},
\end{aligned} \tag{5.18}$$

$$\mathrm{Tr}\left\{\rho_0^{(2)}\vec{J}_{-\omega}^{(1)}\right\} = \sum_{nm}\frac{f_n - f_m}{\hbar}\frac{\mathcal{H}_{0,nm}^{(2)}\vec{J}_{-\omega,mn}^{(1)}}{\tilde{\omega}_{nm}} + \sum_{nmv}\left\{\left(\frac{f_m - f_v}{\tilde{\omega}_{vm}-\omega} + \frac{f_n - f_v}{\tilde{\omega}_{nv}+\omega}\right)\right.$$

$$\left.\times\frac{\mathcal{H}_{\omega,nv}^{(1)}\mathcal{H}_{-\omega,vm}^{(1)}\vec{J}_{-\omega,mn}^{(1)}}{4\hbar^2\tilde{\omega}_{nm}} + \left(\frac{f_m - f_v}{\tilde{\omega}_{vm}+\omega} + \frac{f_n - f_v}{\tilde{\omega}_{nv}-\omega}\right)\frac{\mathcal{H}_{-\omega,nv}^{(1)}\mathcal{H}_{\omega,vm}^{(1)}\vec{J}_{-\omega,mn}^{(1)}}{4\hbar^2\tilde{\omega}_{nm}}\right\}, \quad (5.19)$$

$$\mathrm{Tr}\left\{\rho_{-\omega}^{(3)}\vec{J}^{(0)}\right\} = \sum_{nmv}\frac{1}{2\hbar^2(\tilde{\omega}_{nm}-\omega)}\left\{\left(\frac{f_m - f_v}{2(\tilde{\omega}_{vm}-2\omega)} + \frac{f_n - f_v}{2(\tilde{\omega}_{nv}+\omega)}\right)\mathcal{H}_{\omega,nv}^{(1)}\mathcal{H}_{-2\omega,vm}^{(2)}\right.$$

$$+ \left(\frac{f_n - f_v}{2(\tilde{\omega}_{nv}-2\omega)} + \frac{f_m - f_v}{2(\tilde{\omega}_{vm}+\omega)}\right)\mathcal{H}_{-2\omega,nv}^{(2)}\mathcal{H}_{\omega,vm}^{(1)} + \left(\frac{f_m - f_v}{\tilde{\omega}_{vm}} + \frac{f_n - f_v}{\tilde{\omega}_{nv}-\omega}\right)$$

$$\times\mathcal{H}_{-\omega,nv}^{(1)}\mathcal{H}_{0,vm}^{(2)} + \left(\frac{f_n - f_v}{\tilde{\omega}_{nv}} + \frac{f_m - f_v}{\tilde{\omega}_{vm}-\omega}\right)\mathcal{H}_{0,nv}^{(2)}\mathcal{H}_{-\omega,vm}^{(1)}\left.\right\}\vec{J}_{mn}^{(0)}$$

$$+ \sum_{nmvl}\frac{1}{2\hbar(\tilde{\omega}_{nm}-\omega)}\left\{\left[\left(\frac{f_l - f_m}{\tilde{\omega}_{lm}-\omega} + \frac{f_l - f_v}{\tilde{\omega}_{vl}-\omega}\right)\frac{1}{4\hbar^2(\tilde{\omega}_{vm}-2\omega)}\right.\right.$$

$$+ \left(\frac{f_l - f_v}{\tilde{\omega}_{vl}-\omega} + \frac{f_n - f_v}{\tilde{\omega}_{nv}+\omega}\right)\frac{1}{4\hbar^2\tilde{\omega}_{nl}}\left]\mathcal{H}_{\omega,nv}^{(1)}\mathcal{H}_{-\omega,vl}^{(1)}\mathcal{H}_{-\omega,lm}^{(1)}\right.$$

$$+ \left[\left(\frac{f_l - f_m}{\tilde{\omega}_{lm}-\omega} + \frac{f_l - f_v}{\tilde{\omega}_{vl}+\omega}\right)\frac{1}{4\hbar^2\tilde{\omega}_{vm}} + \left(\frac{f_l - f_v}{\tilde{\omega}_{vl}+\omega} + \frac{f_n - f_v}{\tilde{\omega}_{nv}-\omega}\right)\frac{1}{4\hbar^2\tilde{\omega}_{nl}}\right]$$

$$\times\mathcal{H}_{-\omega,nv}^{(1)}\mathcal{H}_{\omega,vl}^{(1)}\mathcal{H}_{-\omega,lm}^{(1)} + \left[\left(\frac{f_l - f_m}{\tilde{\omega}_{lm}+\omega} + \frac{f_l - f_v}{\tilde{\omega}_{vl}-\omega}\right)\frac{1}{4\hbar^2\tilde{\omega}_{vm}}\right.$$

$$+ \left(\frac{f_l - f_v}{\tilde{\omega}_{vl}-\omega} + \frac{f_n - f_v}{\tilde{\omega}_{nv}-\omega}\right)\frac{1}{4\hbar^2(\tilde{\omega}_{nl}-2\omega)}\left]\mathcal{H}_{-\omega,nv}^{(1)}\mathcal{H}_{-\omega,vl}^{(1)}\mathcal{H}_{\omega,lm}^{(1)}\right\}\vec{J}_{mn}^{(0)}. \quad (5.20)$$

Though quite complicated in its appearence the expression for the driving current density of the DFWM process is needed in order to understand the near-field phase conjugation process from a general point of view.[1] Special scattering configurations of course can lead to analytical simplifications of the general result. The above result also enables us to establish a microscopic theory for DFWM in quantum wells and thin films as described in Parts III, IV, and V.

5.4 Physical processes underlying the current densities

To gain insight into the physics underlying the nonlinear constitutive equation, given implicitly in Eqs. (5.18)–(5.20), we next discuss the processes connecting in a nonlocal fashion the current density at a given point in space to the field points of the surroundings. To facilitate the understanding of the nonlinear response we start by a brief summary of the linear response.

---

[1]With respect to the result published in Andersen and Keller (1998) the last sum in Eq. (5.20) above is written in a more compact form than in Eq. (22) of Andersen and Keller (1998). The compact form in Eq. (5.20) is obtained by exchanging indices v and l in the last three terms of Andersen and Keller (1998), Eq. (22). As a consequence of this, the same difference occur between Eqs. (6.14) and (8.23) and Eqs. (34) and (51) of Andersen and Keller (1998), respectively.
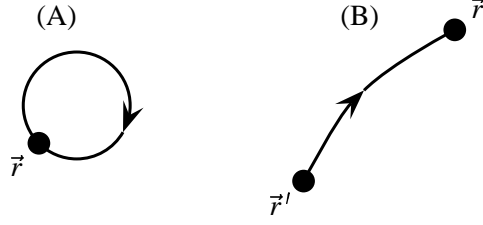
Figure 5.1: Schematic illustration of the two processes described by the linear response tensor. The process in diagram A is purely diamagnetic whereas the process in diagram B is purely paramagnetic.

5.4.1 Linear part

The electrodynamic coupling connecting a source point for the field to an observation point for the current density associated to each of the two linear processes underlying Eqs. (5.14) and (5.15) is adequately illustrated in diagrammatic form as shown in Fig. 5.1.

Hence, Fig. 5.1.A represents a picture of the well known diamagnetic process originating in the quantity $\vec{j}^{(1)}_{-\omega,nn}$ in Eq. (5.14). In this process, a photon is absorbed at the observation point $\vec{r}$ for the current density. Fig. 5.1.B is a picture of the paramagnetic process stemming from the term $\mathcal{H}^{(1)}_{-\omega,nm}$ appearing in Eq. (5.15). In this case, a photon is absorbed at space point $\vec{r}'$, and observation takes place at $\vec{r}$.

5.4.2 Nonlinear part

In the DFWM process, the coupling between the three source points for the field and the observation point for the current density, described in Eqs. (5.18)–(5.20), can be pictured in diagrammatic form as shown in Fig. 5.2.

Hence, in Fig. 5.2.A the mixing process contained in the product $\mathcal{H}^{(2)}_{-2\omega,nm}\vec{j}^{(1)}_{\omega,mn}$ in Eq. (5.18) is illustrated. Here, two photons are *simultaneously* absorbed at space point $\vec{r}''$, and one photon is emitted at the point of observation $\vec{r}$ for the current density. Fig. 5.2.B pictures the other mixing process in Eq. (5.18), namely that associated with the product $\mathcal{H}^{(1)}_{-\omega,nv}\mathcal{H}^{(1)}_{-\omega,vm}\vec{j}^{(1)}_{\omega,mn}$. In this process, one photon is absorbed at $\vec{r}''$, another at $\vec{r}'''$, and the last one is emitted at $\vec{r}$. Fig. 5.2.C gives a view of the mixing process from the terms in Eq. (5.19) containing the product $\mathcal{H}^{(2)}_{0,nm}\vec{j}^{(1)}_{-\omega,mn}$. In this case a photon is absorbed and another is emitted *simultaneously* at space point $\vec{r}'$, and the third photon is absorbed at $\vec{r}$. Fig. 5.2.D shows the other type of mixing process occuring in Eq. (5.19). This process is described by the products $\mathcal{H}^{(1)}_{\omega,nv}\mathcal{H}^{(1)}_{-\omega,vm}\vec{j}^{(1)}_{-\omega,mn}$ and $\mathcal{H}^{(1)}_{-\omega,nv}\mathcal{H}^{(1)}_{\omega,vm}\vec{j}^{(1)}_{-\omega,mn}$. Here, photons are absorbed at $\vec{r}'$ and at the point of observation $\vec{r}$, while a photon is emitted at $\vec{r}''$. Fig. 5.2.E represents the diagram for the mixing process appearing in the terms containing the product $\mathcal{H}^{(1)}_{\omega,nv}\mathcal{H}^{(2)}_{-2\omega,vm}$ (and the equivalent product $\mathcal{H}^{(2)}_{-2\omega,vm}\mathcal{H}^{(1)}_{\omega,nv}$)
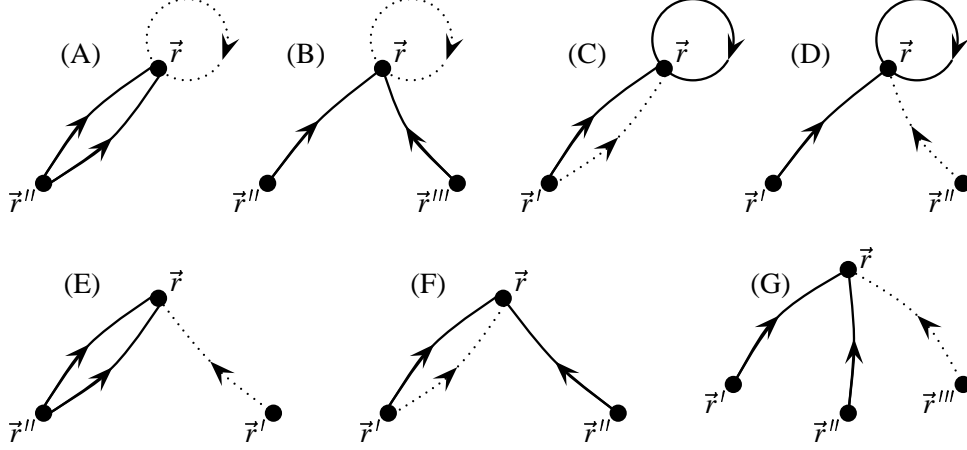
Figure 5.2: Schematic illustration of the processes underlying the DFWM response tensor. In this illustration, the solid paths results from the $-\omega$ terms, and the dotted paths from the $+\omega$ terms. The processes in diagrams A–D include both diamagnetic effects (drawn as circles) and paramagnetic effects (lines). The processes in diagrams E–G are purely paramagnetic. The standard theory for the DFWM susceptibility (conductivity) is obtained from diagram G in the local limit.

in Eq. (5.20). Here two photons are *simultanously* absorbed at $\vec{r}''$, and one is emitted at $\vec{r}'$. Fig. 5.2.F is the diagrammatic representation of the terms containing the product $\mathcal{H}_{0,nv}^{(2)}\mathcal{H}_{-\omega,vm}^{(1)}$ (and the equivalent one $\mathcal{H}_{-\omega,nv}^{(1)}\mathcal{H}_{0,vm}^{(2)}$) in Eq. (5.20). In these terms a photon is absorbed at $\vec{r}'$ and at the *same time* one is emitted from there. The last photon is absorbed at $\vec{r}''$. Finally, Fig. 5.2.G gives a picture of one of six equivalent products of the last type appearing in Eq. (5.20). These are of the form $\mathcal{H}_{\omega,nv}^{(1)}\mathcal{H}_{-\omega,vl}^{(1)}\mathcal{H}_{-\omega,lm}^{(1)}$ or equivalent forms (all six possible permutations of one "ω"-term and two "$-\omega$"-terms). Here, a photon is absorbed at $\vec{r}'$, another at $\vec{r}''$, and the last photon is emitted at $\vec{r}'''$.

At this stage it is fruitful to compare the nonlocal result for the DFWM current density, shown in diagrammatic form in Fig. 5.2, with the commonly used standard (textbook) result. In the standard description all diamagnetic effects are neglected from the outset. The diamagnetic process is hidden in the diagrams containing a closed loop, cf. Fig. 5.1. This means that all the processes depicted in Figs. 5.2.A–5.2.D are absent in the standard description. Omission of diamagnetic effects in the nonlinear optics of quantum wells and in mesoscopic near-field optics is known to be dangerous (Keller 1996a), and thus we *cannot* omit these terms here. We shall substantiate on this point later. Also the interaction channels given by the diagrams in Figs. 5.2.E and 5.2.F are absent in textbook formulations. This is so because simultaneous two-photon processes originating in the $\vec{A}\cdot\vec{A}$ part of the interaction Hamiltonian are left out from the beginning. These processes however are known to be important in mesoscopic electrodynamics and can not be omitted *a priori*. In the local limit the result given by the diagram in Fig. 5.2.G

is identical to the $\vec{r} \cdot \vec{E}$ dipolar interaction Hamiltonian, since a unitary transformation of the form $S = \exp(-\mathrm{i}e\vec{A}(t) \cdot \vec{r}/\hbar)$ performed on the wave functions and the minimal coupling Hamiltonian would display the equivalence of the two formalisms (Ackerhalt and Milonni 1984; Milonni, Cook, and Ackerhalt 1989).

Chapter 6

Conductivity tensors for DFWM response

In the preceding two chapters, we have found expressions for the phase conjugated field and the single-electron current density response. In the present chapter the connection between the single-electron current densities [Eqs. (5.13) and (5.17)] and their related conductivity tensors [Eqs. (4.9) and (4.10)] is established. First, the matrix elements of the Hamiltonian and the current density operator are written in terms of the vector potential. Then the symmetries of the various contributions to the conductivity tensors are studied. Finally, the expressions for the nonzero and independent elements of the conductivity tensors are written on explicit form.

6.1 General considerations

In order to determine (i) the linear conductivity response tensor $\overset{\leftrightarrow}{\sigma}(\vec{r}, \vec{r}')$ introduced in Eq. (4.9) from the expression for the linear current density in Eq. (5.13) [with insertion of Eqs. (5.14) and (5.15)], and (ii) the nonlinear conductivity response function $\overset{\leftrightarrow}{\Xi}(\vec{r}, \vec{r}', \vec{r}'', \vec{r}''')$ introduced in Eq. (4.10) from the expression for the DFWM current density given in Eq. (5.17) [with Eqs. (5.18)–(5.20) inserted] we by now essentially just need to relate the various matrix elements appearing in Eqs. (5.14), (5.15), and (5.18)–(5.20) to the vector potential.

Taking the *nm* matrix element of the "$-\omega$" part of the part of the Hamiltonian which is linear in the vector potential one finds on integral form

$$\mathcal{H}^{(1)}_{-\omega,nm} = \left(\mathcal{H}^{(1)}_{\omega,mn} \right)^* = - \int \vec{J}_{mn}(\vec{r}) \cdot \vec{A}(\vec{r}) d^3 r, \tag{6.1}$$

where we have introduced the transition current density *from* state *m to* state *n*, i.e., $\vec{j}^{(0)}_{nm} \equiv \vec{J}_{mn}$, in its explicit form, viz.

$$\vec{J}_{mn}(\vec{r}) = \frac{e\hbar}{2im_e} \left(\psi_m(\vec{r}) \vec{\nabla} \psi_n^*(\vec{r}) - \psi_n^*(\vec{r}) \vec{\nabla} \psi_m(\vec{r}) \right), \tag{6.2}$$

ψ_a ($a \in \{m, n\}$) being the electronic eigenstate satisfying the unperturbed Schrödinger equation $\mathcal{H}_0 \psi_a = \mathcal{E}_a \psi_a$. From Eq. (6.2) we note that $\vec{J}_{nm}(\vec{r}) = \vec{J}^*_{mn}(\vec{r})$. Similarly, the *nm* matrix elements of the "-2ω" part of the Hamiltonian becomes

$$\mathcal{H}^{(2)}_{-2\omega,nm} = \frac{e^2}{4m_e} \int \psi_n^*(\vec{r}) \psi_m(\vec{r}) \vec{A}(\vec{r}) \cdot \vec{A}(\vec{r}) d^3 r \tag{6.3}$$

33

on integral form. Next, the matrix elements of the part of the Hamiltonian which is proportional to $\vec{A} \cdot \vec{A}^*$ are given by

$$\mathcal{H}_{0,nm}^{(2)} = \frac{e^2}{4m_e} \int \psi_n^*(\vec{r})\psi_m(\vec{r})\vec{A}(\vec{r}) \cdot \vec{A}^*(\vec{r})d^3r. \tag{6.4}$$

Finally, the matrix elements of the current density operator $\vec{j}^{(1)}$ are found to be

$$\vec{j}_{-\omega,nm}^{(1)} = \vec{j}_{\omega,mn}^{(1)*} = -\frac{e^2}{m_e}\psi_n^*(\vec{r})\psi_m(\vec{r})\vec{A}(\vec{r}). \tag{6.5}$$

The calculation of the DFWM conductivity tensor is finalized in two steps. Thus we start by inserting Eqs. (6.1)–(6.5) into the three traces in Eqs. (5.18)–(5.20), and thereafter we extract the vector potential in such a manner that the result takes the general form given in Eq. (4.10). For convenience, we in the following divide the nonlinear conductivity tensor into a sum of subparts A–G referring to the processes (A)–(G) shown in Fig. 5.2.

Since we are using the linear response function in the description of the phase conjugated field it is adequate for consistency again to describe the linear process, although it is already well known. The calculation is done in a similar manner as for the DFWM response, by inserting Eqs. (6.1), (6.2) and (6.5) into the two traces in Eqs. (5.14) and (5.15), and thereafter isolating the vector potential so that the result takes the form of Eq. (4.9). In the following the linear conductivity tensor is divided into a sum of subparts A–B referring to the two processes shown in Fig. 5.1.

6.2 Symmetry properties of the conductivity tensors

In order to study the symmetries of the various contributions to the conductivity tensors $\overset{\leftrightarrow}{\sigma}(\vec{r},\vec{r}')$ and $\overset{\leftrightarrow}{\Xi}(\vec{r},\vec{r}',\vec{r}'',\vec{r}''')$ one notices that the vector potential only appears via $\mathcal{H}_{-\omega}^{(1)}$, $\mathcal{H}_{\omega}^{(1)}$, $\mathcal{H}_{-2\omega}^{(2)}$, $\mathcal{H}_0^{(2)}$, $\vec{j}_{-\omega}^{(1)}$, and $\vec{j}_{\omega}^{(1)}$ of Eqs. (6.1) and (6.3)–(6.5). One further observes from Eq. (6.1) that the matrix elements of $\mathcal{H}_{-\omega}^{(1)}$ and $\mathcal{H}_{\omega}^{(1)}$ contain inner products between a transition current density and a vector potential and that those of $\mathcal{H}_{-2\omega}^{(2)}$ and $\mathcal{H}_0^{(2)}$ involve inner products between two vector potentials, see Eqs. (6.3) and (6.4). These last inner products may conveniently be written in the form $\overset{\leftrightarrow}{\mathbb{1}} : \vec{A}\vec{A}$ and $\overset{\leftrightarrow}{\mathbb{1}} : \vec{A}\vec{A}^*$, respectively. The matrix elements of the current densities $\vec{j}_{-\omega}^{(1)}$ and $\vec{j}_{\omega}^{(1)}$ are directly proportional to the vector potential and may thus for the present purpose adequately be written in the forms $\overset{\leftrightarrow}{\mathbb{1}} \cdot \vec{A}$ and $\overset{\leftrightarrow}{\mathbb{1}} \cdot \vec{A}^*$, respectively.

6.2.1 Linear conductivity tensor

In the view of the aforementioned remarks it is concluded that part A of the linear conductivity tensor, given by Eq. (5.14) has the symmetry of the unit tensor $\overset{\leftrightarrow}{\mathbb{1}}$. Part A thus
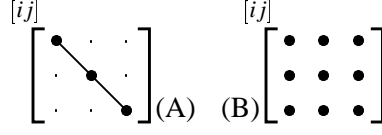
Figure 6.1: Symmetry schemes for the linear conductivity tensor. Tensor elements labeled with a "•" are nonzero, elements labeled with a "·" are zero, and the solid line connect equal nonzero elements.

have 3 nonzero elements. Furthermore, of these 3 nonzero elements only 1 is independent, since the Cartesian index of the linear current density follows that of the vector potential appearing in $\vec{j}_\omega^{(1)}$, and thus $i = j$. The other part of the linear conductivity tensor (part B) is extracted from Eq. (5.15), and it shows a symmetry to the outer product $\vec{J}_1 \otimes \vec{J}_2$, where $\vec{J}_1$ and $\vec{J}_2$ in general are different, and part B of the linear conductivity tensor thus has 9 independent nonzero elements. The symmetry schemes of the linear conductivity tensor are shown in Fig. 6.1.

6.2.2 DFWM conductivity tensor

Taking our symmetry analysis to the DFWM conductivity tensor we conclude that part A, given by the first sum on the right hand side of Eq. (5.18), has a symmetry given by the outer product $\bar{\bar{\mathbb{1}}} \otimes \bar{\bar{\mathbb{1}}}$. Part A thus have 9 nonzero elements. Furthermore, since the Cartesian index of the DFWM current density follows that of the vector potential appearing in $\vec{j}_\omega^{(1)}$, $i = j$ in the index notation of Eq. (4.11). From the form of the $\mathcal{H}_{-2\omega}^{(2)}$ term we next conclude that $k = h$. Altogether it is realised that the 9 nonzero elements are identical. To get an overview of the conclusion, we show in Fig. 6.2.A the result in terms of a symmetry scheme.

Utilising the same type of arguments it is concluded that each term in the second sum in Eq. (5.18), which gives rise to part B of the conductivity tensor, when written in the form of Eq. (4.11) has a symmetry identical to the outer product $\bar{\bar{\mathbb{1}}} \otimes \vec{J}_1 \otimes \vec{J}_2$, where $\vec{J}_1$ and $\vec{J}_2$ are two generally different transition current densities. The form of this outer product leaves us with 27 nonzero elements. Also here the coordinate convention of Eq. (4.11) implies that $i = j$. Furthermore we observe that elements with $i = x$, $i = y$, and $i = z$ are identical, since the two $\mathcal{H}_{-\omega}^{(1)}$ terms essentially produces numbers. Finally, we see that the independent nature of the two $\mathcal{H}_{-\omega}^{(1)}$ terms makes them interchangeable, and thus gives us two different ways of constructing the sum in Eq. (4.11). Of the 27 nonzero elements only 9 are independent, since as we have realised, $\Xi_{xxkh}^{B} = \Xi_{yykh}^{B} = \Xi_{zzkh}^{B}$ for all permutations of k and h in the three Cartesian coordinates $\{x, y, z\}$. Expressed in terms of a symmetry scheme, the deductions above lead to the symmetry scheme shown in Fig. 6.2.B.

The first sum in Eq. (5.19) gives rise to part C of the DFWM conductivity tensor, and the second sum in this equation leads to part D. Looking at the first sum it appears that

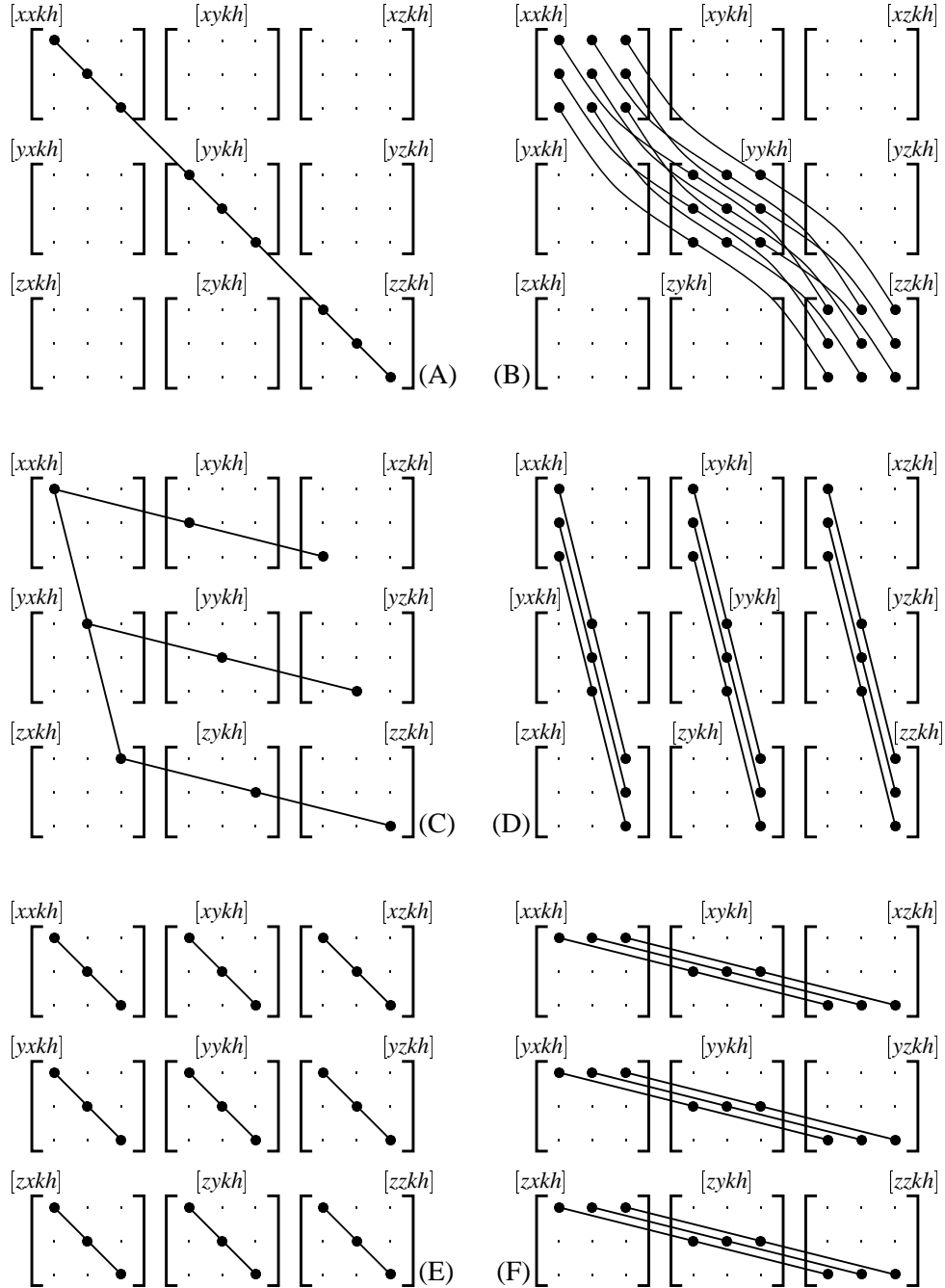Figure 6.2: The symmetry schemes for parts A–F of the DFWM conductivity tensor in their most general spin-less forms. Tensor elements labeled with a "•" are nonzero, elements labeled with a "·" are zero, and the solid lines connect nonzero elements of equal magnitude.

Conductivity	Tensor symmetry
$\vec{\sigma}^{A}(\vec{r},\vec{r}')$	$\bar{\bar{\mathbb{1}}}$
$\vec{\sigma}^{B}(\vec{r},\vec{r}')$	$\vec{J}_1 \otimes \vec{J}_2$
$\bar{\bar{\Xi}}^{A}(\vec{r},\vec{r}',\vec{r}'',\vec{r}''')$	$\bar{\bar{\mathbb{1}}} \otimes \bar{\bar{\mathbb{1}}}$
$\bar{\bar{\Xi}}^{B}(\vec{r},\vec{r}',\vec{r}'',\vec{r}''')$	$\bar{\bar{\mathbb{1}}} \otimes \vec{J}_1 \otimes \vec{J}_2$
$\bar{\bar{\Xi}}^{C}(\vec{r},\vec{r}',\vec{r}'',\vec{r}''')$	$\vec{e}_A \otimes \bar{\bar{\mathbb{1}}} \otimes \vec{e}_A$
$\bar{\bar{\Xi}}^{D}(\vec{r},\vec{r}',\vec{r}'',\vec{r}''')$	$\vec{e}_A \otimes \vec{J}_1 \otimes \vec{J}_2 \otimes \vec{e}_A$
$\bar{\bar{\Xi}}^{E}(\vec{r},\vec{r}',\vec{r}'',\vec{r}''')$	$\vec{J}_1 \otimes \bar{\bar{\mathbb{1}}} \otimes \vec{J}_2$
$\bar{\bar{\Xi}}^{F}(\vec{r},\vec{r}',\vec{r}'',\vec{r}''')$	$\vec{J}_1 \otimes \vec{J}_2 \otimes \bar{\bar{\mathbb{1}}}$
$\bar{\bar{\Xi}}^{G}(\vec{r},\vec{r}',\vec{r}'',\vec{r}''')$	$\vec{J}_1 \otimes \vec{J}_2 \otimes \vec{J}_3 \otimes \vec{J}_4$

Table 6.1: The tensor symmetries of the various parts A–B of the linear, and A–G of the DFWM conductivity. As explained in the text, $\vec{J}_1$–$\vec{J}_4$ are four in general different vectors obtained by a weighted superposition of single-particle transition current densities, and $\vec{e}_A = \vec{A}/A$.

this is proportional to $(\bar{\bar{\mathbb{1}}} : \vec{A}\vec{A}^*)\vec{A}$, a fact which in relation to the form given in Eq. (4.11) implies that the symmetry of the conductivity tensor is given by the outer product $\vec{e}_A \otimes \bar{\bar{\mathbb{1}}} \otimes \vec{e}_A$, with $\vec{e}_A = \vec{A}/A$. This product form leaves us with 9 nonzero elements. As far as the Cartesian indices are concerned the above symmetry implies that $j = h$ and $i = k$. Finally we observe that the same constant appears in front of the vector potential indexed k. This leads to the conclusion that the cases $i = x$, $i = y$, and $i = z$ are equal, leaving at the end only one independent nonzero element of part C of the conductivity tensor. The symmetry scheme for part C is shown in Fig. 6.2.C.

In the second sum of Eq. (5.19) the symmetry is proportional to the outer product $\vec{e}_A \otimes \vec{J}_1 \otimes \vec{J}_2 \otimes \vec{e}_A$ and thus we are left with 27 nonzero elements. Then, in the form of Eq. (4.11), $i = h$, and the permutations over i are seen to be equal, so that we end up with only 9 independent elements. Using the fact that $\Xi^{D}_{xjkx} = \Xi^{D}_{yjky} = \Xi^{D}_{zjkz}$ one obtains the symmetry scheme shown in Fig. 6.2.D.

Let us now take a closer look at the third trace in Eq. (5.20). It is convenient to split the first sum in this equation into two parts related to the two different processes that occur. The first part of the sum, which refers to the $\mathcal{H}^{(2)}_{-2\omega,nv}\mathcal{H}^{(1)}_{\omega,vm}$-type of terms, gives rise to part E of the third order conductivity tensor corresponding to process (E) of Fig. 5.2. The second part of the first sum is related to part F of the third order conductivity tensor [process (F) of Fig. 5.2]. Finally, the second sum on the right side of Eq. (5.20) produces part G of the third order conductivity tensor, corresponding to process (G) of Fig. 5.2.

The first part of the first sum, in relation to the representation in Eq. (4.11), has a symmetry which can be represented by the outer product $\vec{J}_1 \otimes \bar{\bar{\mathbb{1}}} \otimes \vec{J}_2$, leaving 27 nonzero elements. From the term $\mathcal{H}^{(2)}_{-2\omega}$, we see that $k = h$ in the chosen representation of coordinate sets, and furthermore we realise that elements with $k = x$, $k = y$, and $k = z$ are equal. These deductions reduce the number of independent nonzero elements to 9, which fulfils $\Xi^{E}_{ijxx} = \Xi^{E}_{ijyy} = \Xi^{E}_{ijzz}$ for all permutations of i and j in the three Cartesian coordinates

$\{x,y,z\}$. The result is shown on schematic form in terms of the symmetry scheme in Fig. 6.2.E.

In the second part of the first sum in Eq. (5.20) we observe that the symmetry of part F of the conductivity tensor, in relation to the form of Eq. (4.11), is proportional to the outer product $\vec{J}_1 \otimes \vec{J}_2 \otimes \bar{\bar{\mathbb{1}}}$, again leaving 27 nonzero elements. Due to the chosen convention of the coordinate sets, we realise from the $\mathcal{H}_0^{(2)}$ term that the condition $k = j$ applies. We furthermore notice from this that terms with $j = x$, $j = y$, and $j = z$ are equal, leaving 9 independent nonzero elements related by $\Xi_{ixxh}^{\mathrm{F}} = \Xi_{iyyh}^{\mathrm{F}} = \Xi_{izzh}^{\mathrm{F}}$ for all permutations of i and h in the three Cartesian coordinates $\{x,y,z\}$. This means that the symmetry scheme is as shown in Fig. 6.2.F.

Part G of the third order conductivity tensor, which originates in the second sum in Eq. (5.20), obviously has the tensor form $\vec{J}_1 \otimes \vec{J}_2 \otimes \vec{J}_3 \otimes \vec{J}_4$, and there will hence in general be 81 independent nonzero elements in the associated symmetry scheme.

The considerations laying the foundations for the symmetry schemes of the various parts of the linear and nonlinear conductivity tensors are displayed in Tab. 6.1, where the relevant combinations of $\vec{J}$'s and $\bar{\bar{\mathbb{1}}}$'s are given.

6.3 Expressions for the conductivity tensors

We end this chapter by giving the explicit expressions for the independent tensor elements of $\bar{\bar{\sigma}}(\vec{r},\vec{r}')$ and $\bar{\bar{\Xi}}(\vec{r},\vec{r}',\vec{r}'',\vec{r}''')$. Thus, the only independent tensor element in part A of the linear conductivity tensor is

$$\sigma_{xx}^{\mathrm{A}}(\vec{r},\vec{r}') = \frac{2\mathrm{i}}{\omega}\frac{e^2}{m_e}\sum_n f_n|\psi_n|^2\delta(\vec{r}-\vec{r}'), \tag{6.6}$$

and the nine independent elements of part B are

$$\sigma_{ij}^{\mathrm{B}}(\vec{r},\vec{r}') = \frac{2\mathrm{i}}{\omega}\frac{1}{\hbar}\sum_{nm}\frac{f_n-f_m}{\tilde{\omega}_{nm}-\omega}J'_{j,mn}J_{i,nm}. \tag{6.7}$$

The only independent tensor element in part A of the third order conductivity tensor thus is

$$\Xi_{xxxx}^{\mathrm{A}}(\vec{r},\vec{r}',\vec{r}'',\vec{r}''') = \frac{2\mathrm{i}}{\omega^3}\frac{e^4}{8m_e^2\hbar}\sum_{nm}\frac{f_n-f_m}{\tilde{\omega}_{nm}-2\omega}\psi_n^*(\vec{r}'')\psi_m(\vec{r}'')\psi_m^*(\vec{r})\psi_n(\vec{r})$$
$$\times\delta(\vec{r}-\vec{r}')\delta(\vec{r}''-\vec{r}'''), \tag{6.8}$$

and the nine independent elements of part B are

$$\Xi_{xxkh}^{\mathrm{B}}(\vec{r},\vec{r}',\vec{r}'',\vec{r}''') = \frac{2\mathrm{i}}{\omega^3}\frac{e^2}{4m_e\hbar^2}\sum_{nmv}\frac{1}{\tilde{\omega}_{nm}-2\omega}\left(\frac{f_m-f_v}{\tilde{\omega}_{vm}-\omega}+\frac{f_n-f_v}{\tilde{\omega}_{nv}-\omega}\right)$$
$$\times J_{h,vn}(\vec{r}''')J_{k,mv}(\vec{r}'')\psi_m^*(\vec{r})\psi_n(\vec{r})\delta(\vec{r}-\vec{r}'). \tag{6.9}$$

The only independent nonzero element of part C of the third order conductivity tensor is given by

$$\Xi^{\mathrm{C}}_{xxxx}(\vec{r},\vec{r}\,',\vec{r}\,'',\vec{r}\,''') = \frac{2\mathrm{i}}{\omega^3}\frac{e^4}{4m_e^2\hbar}\sum_{nm}\frac{f_n-f_m}{\tilde{\omega}_{nm}}\psi_n^*(\vec{r}\,')\psi_m(\vec{r}\,')\psi_m^*(\vec{r})\psi_n(\vec{r})$$
$$\times\delta(\vec{r}\,'-\vec{r}\,''')\delta(\vec{r}-\vec{r}\,''), \tag{6.10}$$

and the nine independent nonzero elements of part D of the third order conductivity tensor are

$$\Xi^{\mathrm{D}}_{xjkx}(\vec{r},\vec{r}\,',\vec{r}\,'',\vec{r}\,''') = \frac{2\mathrm{i}}{\omega^3}\frac{e^2}{4m_e\hbar^2}\sum_{nmv}\frac{1}{\tilde{\omega}_{nm}}\left\{\left(\frac{f_m-f_v}{\tilde{\omega}_{vm}-\omega}+\frac{f_n-f_v}{\tilde{\omega}_{nv}+\omega}\right)J_{j,vn}(\vec{r}\,')J_{k,mv}(\vec{r}\,'')\right.$$
$$\left.+\left(\frac{f_m-f_v}{\tilde{\omega}_{vm}+\omega}+\frac{f_n-f_v}{\tilde{\omega}_{nv}-\omega}\right)J_{k,vn}(\vec{r}\,'')J_{j,mv}(\vec{r}\,')\right\}\psi_m^*(\vec{r})\psi_n(\vec{r})\delta(\vec{r}-\vec{r}\,'''). \tag{6.11}$$

The nine independent elements of part E have the explicit form

$$\Xi^{\mathrm{E}}_{ijxx}(\vec{r},\vec{r}\,',\vec{r}\,'',\vec{r}\,''') = \frac{2\mathrm{i}}{\omega^3}\frac{e^2}{16m_e\hbar^2}$$
$$\times\sum_{nmv}\frac{1}{\tilde{\omega}_{nm}-\omega}\left\{\left(\frac{f_m-f_v}{\tilde{\omega}_{vm}-2\omega}+\frac{f_n-f_v}{\tilde{\omega}_{nv}+\omega}\right)J_{j,vn}(\vec{r}\,')\psi_v^*(\vec{r}\,'')\psi_m(\vec{r}\,'')\right.$$
$$\left.+\left(\frac{f_n-f_v}{\tilde{\omega}_{nv}-2\omega}+\frac{f_m-f_v}{\tilde{\omega}_{vm}+\omega}\right)J_{j,mv}(\vec{r}\,')\psi_n^*(\vec{r}\,'')\psi_v(\vec{r}\,'')\right\}J_{i,nm}(\vec{r})\delta(\vec{r}\,''-\vec{r}\,'''), \tag{6.12}$$

and the nine independent elements of part F of the third order conductivity tensor are

$$\Xi^{\mathrm{F}}_{ixxh}(\vec{r},\vec{r}\,',\vec{r}\,'',\vec{r}\,''') = \frac{2\mathrm{i}}{\omega^3}\frac{e^2}{8m_e\hbar^2}$$
$$\times\sum_{nmv}\frac{1}{\tilde{\omega}_{nm}-\omega}\left\{\left(\frac{f_m-f_v}{\tilde{\omega}_{vm}}+\frac{f_n-f_v}{\tilde{\omega}_{nv}-\omega}\right)J_{h,vn}(\vec{r}\,'')\psi_v^*(\vec{r}\,')\psi_m(\vec{r}\,')\right.$$
$$\left.+\left(\frac{f_n-f_v}{\tilde{\omega}_{nv}}+\frac{f_m-f_v}{\tilde{\omega}_{vm}-\omega}\right)J_{h,mv}(\vec{r}\,'')\psi_n^*(\vec{r}\,')\psi_v(\vec{r}\,')\right\}J_{i,nm}(\vec{r})\delta(\vec{r}\,'-\vec{r}\,'''). \tag{6.13}$$

Finally, the eighty-one independent elements of part G of the third order conductivity tensor are given by

$$\Xi^{\mathrm{G}}_{ijkh}(\vec{r},\vec{r}\,',\vec{r}\,'',\vec{r}\,''') = \frac{2\mathrm{i}}{\omega^3}\frac{1}{8\hbar^3}\sum_{nmvl}\frac{1}{\tilde{\omega}_{nm}-\omega}\left\{\left[\left(\frac{f_l-f_m}{\tilde{\omega}_{lm}-\omega}+\frac{f_l-f_v}{\tilde{\omega}_{vl}-\omega}\right)\frac{1}{\tilde{\omega}_{vm}-2\omega}\right.\right.$$
$$\left.+\left(\frac{f_l-f_v}{\tilde{\omega}_{vl}-\omega}+\frac{f_n-f_v}{\tilde{\omega}_{nv}+\omega}\right)\frac{1}{\tilde{\omega}_{nl}}\right]J_{h,ml}(\vec{r}\,''')J_{k,lv}(\vec{r}\,'')J_{j,vn}(\vec{r}\,')$$
$$+\left[\left(\frac{f_l-f_m}{\tilde{\omega}_{lm}-\omega}+\frac{f_l-f_v}{\tilde{\omega}_{vl}+\omega}\right)\frac{1}{\tilde{\omega}_{vm}}+\left(\frac{f_l-f_v}{\tilde{\omega}_{vl}+\omega}+\frac{f_n-f_v}{\tilde{\omega}_{nv}-\omega}\right)\frac{1}{\tilde{\omega}_{nl}}\right]$$
$$\times J_{h,ml}(\vec{r}\,''')J_{k,vn}(\vec{r}\,'')J_{j,lv}(\vec{r}\,')+\left[\left(\frac{f_l-f_m}{\tilde{\omega}_{lm}+\omega}+\frac{f_l-f_v}{\tilde{\omega}_{vl}-\omega}\right)\frac{1}{\tilde{\omega}_{vm}}\right.$$
$$\left.\left.+\left(\frac{f_l-f_v}{\tilde{\omega}_{vl}-\omega}+\frac{f_n-f_v}{\tilde{\omega}_{nv}-\omega}\right)\frac{1}{\tilde{\omega}_{nl}-2\omega}\right]J_{h,lv}(\vec{r}\,''')J_{k,vn}(\vec{r}\,'')J_{j,ml}(\vec{r}\,')\right\}J_{i,nm}(\vec{r}). \tag{6.14}$$

The number 2 appearing in the first fraction of each part of the conductivity tensors represents the degeneracy of the spin energies, thus giving two electrons in each energy eigenstate.

Chapter 7

<div style="text-align: right">Discussion</div>

In Chapters 4–6 we have established a spatially nonlocal theoretical model for optical phase conjugation in mesoscopic media. The comparison to the existing (local) descriptions of the degenerate four-wave mixing response can be made by taking the local limit of our nonlocal response tensor and abandoning the contributions stemming from the microscopic current density of first order in $\vec{A}$.

In the local limit, the amplitudes of the interacting vector potentials are assumed not to vary with the spatial coordinates, and thus the expressions for the nonlocal DFWM conductivity tensor can be integrated over the $\vec{r}'''$, $\vec{r}''$, and $\vec{r}'$ spaces to obtain the local DFWM conductivity tensor, i.e.,

$$\stackrel{\leftrightarrow}{\Xi}(\vec{r}) = \iiint \stackrel{\leftrightarrow}{\Xi}(\vec{r},\vec{r}',\vec{r}'',\vec{r}''')d^3r'''d^3r''d^3r'. \tag{7.1}$$

Using an orthogonal set of wave equations, parity teaches

$$\int \psi_n^*(\vec{r})\psi_m(\vec{r})d^3r = \delta_{nm}, \tag{7.2}$$

where δ_{nm} is the Kronecker delta. The integrals over the current densities gives zero if the two quantum numbers are identical, otherwise they depend on the individual wave functions. The consequences are the following: (i) Integration over the spatial coordinates $\vec{r}'''$ and $\vec{r}''$ in Eq. (6.8) gives $n = m$, and thus $f_n = f_m$, such that part A of the DFWM conductivity tensor vanish. (ii) In part C, given by Eq. (6.10), the effect is similar, but is here obtained after integration over $\vec{r}'''$, $\vec{r}''$, and $\vec{r}'$. (iii) In part E, integration over $\vec{r}'''$ and $\vec{r}''$ in Eq. (6.12) makes two terms disappear immediately, and an inspection of the remaining two terms shows that they are of equal magnitude, but with opposite sign, ultimately cancelling the rest of part E. (iv) In part F, integration over $\vec{r}'''$ and $\vec{r}'$ in Eq. (6.13) gives a result similar in consequences as for part E. Thus, parts A, C, E, and F of the DFWM conductivity tensor are inherently nonlocal, while parts B, D, and G also contributes to the response in the local limit.

Abandoning parts B and D of the DFWM conductivity tensor because they are based on the response of the microscopic current density of first order in $\vec{A}$, we conclude that only the local contribution from part G is included in the previous descriptions of the DFWM response (Bloembergen, Lotem, and Lynch Jr. 1978), as postulated on page 30.

The single-electron model for degenerate four-wave mixing established in the previous chapters can be used to study the four-wave mixing response from a number of different materials. For example, one could study (i) systems built from molecules or atoms with no electronic overlap (dielectrics), in which case the response from each molecule (atom) can be found separately. The coupling between the individual molecules would then be described using electromagnetic propagators. Another approach (ii) can be taken for studies of the response from metals, where a number of electrons from each ion in the metallic structure is shared with the other ions in a free-electron-like cloud, or (iii) one could study semiconductors, in which the behaviour of the electrons are strongly coupled.

In the present work, we will concentrate on the metallic case, and we proceed to give a simplified description of potential interest for DFWM in mesoscopic films and in near-field optics.

Part III

Degenerate four-wave mixing
in quantum well structures

Chapter 8

DFWM in two-dimensionally translational invariant media

After having established and analyzed the DFWM conductivity response in its most general form we now turn the attention towards the specific case in which the medium under consideration *effectively* exhibits translational invariance in two directions, say x and y in a Cartesian (x, y, z) coordinate system. We study such a case because it appears to be of particular importance for optical phase conjugation (i) in mesoscopic films (quantum wells), and (ii) related to evanescent waves in near-field optics. In neither of these cases a microscopic theory exists today to our knowledge. For mesoscopic films the dynamics perpendicular to the film plane (here, the x-y-plane) has to be treated from a microscopic nonlocal point of view, whereas the dynamics in the plane of the film often is well modelled by a local conductivity (dielectric) function. In the following we assume for simplicity that the electron motion in the plane of the film is free-electron-like. It is possible to replace the free-electron-like behaviour with extended Bloch-function (or tight-binding) dynamics if necessary but we shall not do this here, since after all, in the local limit only matrix elements are changed in the oscillator model when the free-electron dynamics is replaced by a more complicated one. In the optical near-field case where evanescent waves with extremely small penetration depths in say the z-direction appear, it is crucial to keep the microscopic dynamics perpendicular to the surface of the phase conjugating mirror when calculating the DFWM response. So far, four-wave mixing in media with two-dimensional translational invariance has only been studied in the context of phase conjugation of electromagnetic surface waves (Fukui, Sipe, So, and Stegeman 1978; Ujihara 1982a, 1982b), and of a bulk wave by surface waves (Zel'dovich, Pilipetskii, Sudarkin, and Shkunov 1980; Ujihara 1983; Stegeman and Karaguleff 1983; Nunzi and Ricard 1984; Mamaev, Mel'nikov, Pilipetskiĭ, Sudarkin, and Shkunov 1984; Mukhin, Pilipetskiĭ, Sudarkin, and Ushakov 1985; Arutyunyan and Dzhotyan 1987; Pilipetskiĭ, Sudarkin, and Ushakov 1987). In these investigations macroscopic approaches was used.

8.1 General DFWM response

The assumed two-dimensional translational invariance against displacements parallel to the x-y-plane makes it natural to express the various vector and tensor quantities in a

mixed Fourier representation. Thus, by a Fourier analysis in the *x*- and *y*-coordinates, the vector potential is

$$\vec{A}(z,\vec{r}_\parallel) = \frac{1}{(2\pi)^2} \int \vec{A}(z;\vec{q}_\parallel) e^{i\vec{q}_\parallel \cdot \vec{r}_\parallel} d^2 q_\parallel, \tag{8.1}$$

where $\vec{q}_\parallel = (q_x, q_y, 0)$ and $\vec{r}_\parallel = (x, y, 0)$. Likewise, the inverse relation reads for the current density of order α and linear in the cyclic frequency ω

$$\vec{J}_{-\omega}^{(\alpha)}(z;\vec{q}_\parallel) = \int \vec{J}_{-\omega}^{(\alpha)}(z,\vec{r}_\parallel) e^{-i\vec{q}_\parallel \cdot \vec{r}_\parallel} d^2 r_\parallel. \tag{8.2}$$

In the mixed Fourier representation the relevant constitutive relations takes the form

$$\vec{J}_{-\omega}^{(1)}(z;\vec{q}_\parallel) = i\omega \int \overset{\leftrightarrow}{\sigma}(z,z';\vec{q}_\parallel) \cdot \vec{A}(z';\vec{q}_\parallel) dz', \tag{8.3}$$

$$\vec{J}_{-\omega}^{(3)}(z;\vec{q}_\parallel) = \frac{(i\omega)^3}{(2\pi)^4} \int \cdots \int \overset{\leftrightarrow}{\Xi}(z,z',z'',z''';\vec{q}_\parallel,\vec{q}_\parallel',\vec{q}_\parallel'',\vec{q}_\parallel''')$$

$$\vdots \vec{A}(z''';\vec{q}_\parallel''')\vec{A}(z'';\vec{q}_\parallel'')\vec{A}^*(z';\vec{q}_\parallel') d^2 q_\parallel''' d^2 q_\parallel'' d^2 q_\parallel' dz''' dz'' dz'. \tag{8.4}$$

Due to the manner in which the nonlinear conductivity response tensor was constructed in Chapter 5, the various components parallel to the *x*-*y*-plane are not completely independent but satisfy the momentum conservation criterion

$$\vec{q}_\parallel''' + \vec{q}_\parallel'' - \vec{q}_\parallel' - \vec{q}_\parallel = \vec{0}. \tag{8.5}$$

In passing we stress again that Eq. (8.5) is *not* an extra condition put on the dynamics, the equation is *derived* from the general theory [see Appendix A]. To study the phase conjugated response originating in the mixing of three incoming waves one must choose for the fields of the two pump waves, denoted by (1) and (2), the vector potentials with the double and triple primes in Eq. (8.4). The incoming probe field [indexed (p)] is represented via the vector potential with the single prime.

8.2 Phase conjugation DFWM response

So far, we have not utilized the translational invariance condition on the properties of the medium. We do this first indirectly by assuming that each of the three incoming electromagnetic fields contains only one plane-wave component parallel to the *x*-*y*-plane. Further limiting our study to the case where the DFWM response becomes the phase conjugated response, i.e., the wavevector of the response must be counterpropagating to the probe field, conservation of pseudomomentum requires that the two pump fields are counterpropagating. Thus we take for the pump fields

$$\vec{A}(z''';\vec{q}_\parallel''') \equiv \vec{A}(z''';-\vec{k}_\parallel)\delta(\vec{q}_\parallel''' + \vec{k}_\parallel), \tag{8.6}$$

$$\vec{A}(z'';\vec{q}_\parallel'') \equiv \vec{A}(z'';\vec{k}_\parallel)\delta(\vec{q}_\parallel'' - \vec{k}_\parallel), \tag{8.7}$$

where $\vec{k}_\parallel$ is the common wavevector for the two pump fields. With these substitutions we can perform the integrals over $q_\parallel'''$ and $q_\parallel''$ in Eq. (8.4), and the conservation of pseudo-momentum is reduced from its general degenerate four-wave mixing form, $\vec{q}_\parallel''' + \vec{q}_\parallel'' - \vec{q}_\parallel' - \vec{q}_\parallel = \vec{0}$, to $\vec{q}_\parallel' + \vec{q}_\parallel = \vec{0}$. This allows us also to solve the integral over $q_\parallel'$ in Eq. (8.4).

In relation to the conventional theory of three-dimensional (bulk) phase conjugation, the relation $\vec{q}_\parallel' + \vec{q}_\parallel = \vec{0}$ expresses the fact that the two-dimensional wavevector $\vec{q}_\parallel$ of the phase conjugated field is equal in magnitude to the two-dimensional probe wavevector ($\vec{q}_\parallel'$) but points in the opposite direction. Using the aforementioned criteria, the nonlinear constitutive equation is reduced to the form

$$\vec{J}_{-\omega}^{(3)}(z;\vec{q}_\parallel) = \frac{(i\omega)^3}{(2\pi)^4} \int \int \int \overline{\overline{\Xi}}(z,z',z'',z''';\vec{q}_\parallel,\vec{k}_\parallel)$$
$$\vdots \vec{A}(z''';-\vec{k}_\parallel)\vec{A}(z'';\vec{k}_\parallel)\vec{A}^*(z';-\vec{q}_\parallel)dz'''dz''dz' + \text{i.t.}, \tag{8.8}$$

where appropriate integration over $\vec{q}_\parallel'''$, $\vec{q}_\parallel''$, and $\vec{q}_\parallel'$ has been performed. The term "i.t." denotes the so-called "interchanged term". This term is obtained from the first one by interchanging the two pump fields. The reason that such a term has to be added arises from the fact that each of the vector potentials basically consists of a sum of all three incoming fields, and that the phase conjugated term from the product of the three vector potentials thus must include both permutations of the pump fields. The new phase conjugation DFWM (PCDFWM) conductivity tensor appearing after integration over $\vec{q}_\parallel'''$, $\vec{q}_\parallel''$, and $\vec{q}_\parallel'$ is denoted $\overline{\overline{\Xi}}(z,z',z'',z''';\vec{q}_\parallel,\vec{k}_\parallel)$.

In order to calculate the nonlinear conductivity tensor $\overline{\overline{\Xi}}(z,z',z'',z''';\vec{q}_\parallel,\vec{k}_\parallel)$ in the mixed Fourier representation [as well as the linear one, $\overline{\overline{\sigma}}(z,z';\vec{q}_\parallel)$], we begin by looking at the energy eigenstates for the light-unperturbed Schrödinger equation. Hence, since the potential energy of the individual electrons is independent of x and y, i.e., $V(\vec{r}) = V(z)$ under our translational invariance assumption, the basis set may be taken in the generic form

$$\psi_n(z,\vec{r}_\parallel) \equiv \psi_{n,\vec{\kappa}_\parallel}(z,\vec{r}_\parallel) = \frac{1}{2\pi}\psi_n(z)e^{i\vec{\kappa}_\parallel \cdot \vec{r}_\parallel} \tag{8.9}$$

where $\vec{\kappa}_\parallel = (\kappa_x,\kappa_y,0)$ is the wavevector describing the free-particle motion perpendicular to the z-direction. For a medium of macroscopic extension in the x- and y-directions, the set of wavevectors commonly denoted by $\vec{\kappa}_\parallel$ forms a two-dimensional quasi-continuum. Albeit the index n in the wave function $\psi_n(z,\vec{r}_\parallel)$ stands for a triple set of quantum numbers we also use this index to classify the various wave function parts, $\psi_n(z)$, belonging to the single indexed z-dynamics. In a readily understandable notation the energy eigenstates, $\mathcal{E}_n$, associated with the generic solution in Eq. (8.9) is

$$\mathcal{E}_n = \varepsilon_n + \frac{\hbar^2}{2m_e}|\vec{\kappa}_\parallel|^2, \tag{8.10}$$

where we have introduced ε_n as the energy of state n in the solution dependent on the z-coordinate only. In the view of the abovementioned considerations the cyclic transition frequency becomes

$$\omega_{nm} = \frac{1}{\hbar} \left[\varepsilon_n - \varepsilon_m + \frac{\hbar^2}{2m_e} \left(|\vec{\kappa}_{\parallel,\bar{n}}|^2 - |\vec{\kappa}_{\parallel,\bar{m}}|^2 \right) \right], \tag{8.11}$$

in a notation where adequate subscripts $\bar{n}$ and $\bar{m}$ have been put on the wavevectors. In abbreviated form the complex transition frequency, which includes the relaxation time, is for the sake of the following analysis written in the form

$$\tilde{\omega}_{nm} = \tilde{\omega}_{nm}(\vec{\kappa}_{\parallel,\bar{n}}, \vec{\kappa}_{\parallel,\bar{m}}), \tag{8.12}$$

omitting the reference to ε_n and ε_m, since this is already implicitly given by the *nm* subscript. The Fermi-Dirac distribution function we also present in an abbreviated form, viz.

$$f_n(\mathcal{E}_n) = f_n \left(\varepsilon_n + \frac{\hbar^2 \kappa_{\parallel,\bar{n}}^2}{2m_e} \right) \equiv f_n(\vec{\kappa}_{\parallel,\bar{n}}). \tag{8.13}$$

By inserting the generic solution in Eq. (8.9) into the expression for the transition current density in Eq. (6.2), we obtain

$$\vec{J}_{mn}(\vec{r}) = -\frac{e\hbar}{2im_e} \frac{1}{(2\pi)^2} \left[i(\vec{\kappa}_{\parallel,\bar{m}} + \vec{\kappa}_{\parallel,\bar{n}}) \psi_n^*(z) \psi_m(z) \right.$$
$$+ \vec{e}_z \left(\psi_n^*(z) \frac{\partial \psi_m(z)}{\partial z} - \psi_m(z) \frac{\partial \psi_n^*(z)}{\partial z} \right) \left] e^{i(\vec{\kappa}_{\parallel,\bar{m}} - \vec{\kappa}_{\parallel,\bar{n}}) \cdot \vec{r}_\parallel} \right.$$
$$\equiv \frac{1}{(2\pi)^2} \vec{j}_{mn}(z; \vec{\kappa}_{\parallel,\bar{m}} + \vec{\kappa}_{\parallel,\bar{n}}) e^{i(\vec{\kappa}_{\parallel,\bar{m}} - \vec{\kappa}_{\parallel,\bar{n}}) \cdot \vec{r}_\parallel}, \tag{8.14}$$

where for convenience we have defined a new transition current density $\vec{j}_{mn}(z; \vec{\kappa}_{\parallel,\bar{m}} + \vec{\kappa}_{\parallel,\bar{n}})$ to separate out the dependence on the Cartesian coordinates $\vec{r}_\parallel$. For the various Cartesian components of this current density, we use the notation $j_{i,nm}(z; \vec{\kappa}_{\parallel,\bar{m}} + \vec{\kappa}_{\parallel,\bar{n}})$, $i \in \{x, y, z\}$.

8.3 Conductivity tensors

The explicit expression for the phase conjugation degenerate four-wave mixing (PCD-FWM) conductivity tensor $\overset{\leftrightarrow}{\Xi}(z, z', z'', z'''; \vec{q}_\parallel, \vec{k}_\parallel)$ is calculated by insertion of (i) the solutions to the time-independent Schrödinger equation given in Eq. (8.9), (ii) the Fourier representation of the vector potential given by Eq. (8.1), and (iii) the new form of the transition current given in Eq. (8.14) into the nonlinear DFWM constitutive relation in Eq. (4.10) with the phase conjugation conductivity tensor in real space given by Eqs. (6.8)–(6.14), and thereafter inserting the outcome of these steps into the expression for the nonlinear current density in the mixed Fourier representation in Eq. (8.2).

Finally, we perform the integrals over the two dimensions (x and y) in real space and over relevant sets of $\vec{\kappa}_\parallel$-states. Altogether we are left with an expression on the form of Eq. (8.8). For the processes in Figs. 5.1 and 5.2, the abovementioned calculations are supplied in Appendix A, where also the general DFWM conductivity tensors are given. The nonzero element of the linear conductivity tensor part A become

$$\sigma_{xx}^{\mathrm{A}}(z,z';\vec{q}_\parallel) = \frac{2\mathrm{i}}{\omega}\frac{e^2}{m_e}\frac{1}{(2\pi)^2}\sum_n \int f_n(\vec{\kappa}_\parallel)d^2\kappa_\parallel |\psi_n(z)|^2\delta(z-z'), \tag{8.15}$$

and the nine nonzero elements of part B are

$$\sigma_{ij}^{\mathrm{B}}(z,z';\vec{q}_\parallel) = \frac{2\mathrm{i}}{\omega}\frac{1}{\hbar}\frac{1}{(2\pi)^2}\sum_{nm} \int \frac{f_n(\vec{\kappa}_\parallel + \vec{q}_\parallel) - f_m(\vec{\kappa}_\parallel)}{\tilde{\omega}_{nm}(\vec{\kappa}_\parallel + \vec{q}_\parallel, \vec{\kappa}_\parallel) - \omega}$$
$$\times j_{j,mn}(z';2\vec{\kappa}_\parallel + \vec{q}_\parallel)j_{i,nm}(z;2\vec{\kappa}_\parallel + \vec{q}_\parallel)d^2\kappa_\parallel. \tag{8.16}$$

The nonzero element of the PCDFWM conductivity tensor part A are

$$\Xi_{xxxx}^{\mathrm{A}}(z,z',z'',z''';\vec{q}_\parallel,\vec{k}_\parallel) = \frac{e^4}{8m_e^2\hbar}\frac{1}{(2\pi)^2}\frac{2\mathrm{i}}{\omega^3}\sum_{nm} \psi_n^*(z'')\psi_m(z'')\psi_m^*(z)\psi_n(z)$$
$$\times\delta(z-z')\delta(z''-z''')\int \frac{f_n(\vec{\kappa}_\parallel) - f_m(\vec{\kappa}_\parallel)}{\tilde{\omega}_{nm}(\vec{\kappa}_\parallel,\vec{\kappa}_\parallel) - 2\omega}d^2\kappa_\parallel, \tag{8.17}$$

and the nine nonzero elements of part B become

$$\Xi_{xxkh}^{\mathrm{B}}(z,z',z'',z''';\vec{q}_\parallel,\vec{k}_\parallel) = \frac{e^2}{4m_e\hbar^2}\frac{1}{(2\pi)^2}\frac{2\mathrm{i}}{\omega^3}\sum_{nmv} \psi_m^*(z)\psi_n(z)\delta(z-z')$$
$$\times\int \frac{1}{\tilde{\omega}_{nm}(\vec{\kappa}_\parallel,\vec{\kappa}_\parallel) - 2\omega}\left(\frac{f_m(\vec{\kappa}_\parallel) - f_v(\vec{\kappa}_\parallel + \vec{k}_\parallel)}{\tilde{\omega}_{vm}(\vec{\kappa}_\parallel + \vec{k}_\parallel, \vec{\kappa}_\parallel) - \omega} + \frac{f_n(\vec{\kappa}_\parallel) - f_v(\vec{\kappa}_\parallel + \vec{k}_\parallel)}{\tilde{\omega}_{nv}(\vec{\kappa}_\parallel, \vec{\kappa}_\parallel + \vec{k}_\parallel) - \omega}\right)$$
$$\times j_{h,vn}(z''';2\vec{\kappa}_\parallel + \vec{k}_\parallel)j_{k,mv}(z'';2\vec{\kappa}_\parallel + \vec{k}_\parallel)d^2\kappa_\parallel. \tag{8.18}$$

In part C of the nonlinear conductivity tensor the nonzero element is

$$\Xi_{xxxx}^{\mathrm{C}}(z,z',z'',z''';\vec{q}_\parallel,\vec{k}_\parallel) = \frac{e^4}{4m_e^2\hbar}\frac{1}{(2\pi)^2}\frac{2\mathrm{i}}{\omega^3}\sum_{nm} \psi_n^*(z')\psi_m(z')\psi_m^*(z)\psi_n(z)$$
$$\times\delta(z'-z''')\delta(z-z'')\int \frac{f_n(\vec{\kappa}_\parallel - \vec{k}_\parallel + \vec{q}_\parallel) - f_m(\vec{\kappa}_\parallel)}{\tilde{\omega}_{nm}(\vec{\kappa}_\parallel - \vec{k}_\parallel + \vec{q}_\parallel, \vec{\kappa}_\parallel)}d^2\kappa_\parallel, \tag{8.19}$$

and the nine nonzero tensor elements in part D become

$$\Xi_{xjkx}^{\mathrm{D}}(z,z',z'',z''';\vec{q}_\parallel,\vec{k}_\parallel) = \frac{e^2}{4m_e\hbar^2}\frac{1}{(2\pi)^2}\frac{2\mathrm{i}}{\omega^3}\sum_{nmv} \psi_m^*(z)\psi_n(z)\delta(z-z''')$$
$$\times\int \frac{1}{\tilde{\omega}_{nm}(\vec{\kappa}_\parallel + \vec{k}_\parallel + \vec{q}_\parallel, \vec{\kappa}_\parallel)}\left\{\left(\frac{f_m(\vec{\kappa}_\parallel) - f_v(\vec{\kappa}_\parallel + \vec{k}_\parallel)}{\tilde{\omega}_{vm}(\vec{\kappa}_\parallel + \vec{k}_\parallel, \vec{\kappa}_\parallel) - \omega}\right.\right.$$

$$+ \frac{f_n(\vec{\kappa}_\parallel + \vec{k}_\parallel + \vec{q}_\parallel) - f_v(\vec{\kappa}_\parallel + \vec{k}_\parallel)}{\tilde{\omega}_{nv}(\vec{\kappa}_\parallel + \vec{k}_\parallel + \vec{q}_\parallel, \vec{\kappa}_\parallel + \vec{k}_\parallel) + \omega} \Bigg) j_{j,vn}(z'; 2\vec{\kappa}_\parallel + 2\vec{k}_\parallel + \vec{q}_\parallel) j_{k,mv}(z''; 2\vec{\kappa}_\parallel + \vec{k}_\parallel)$$

$$+ \left(\frac{f_m(\vec{\kappa}_\parallel) - f_v(\vec{\kappa}_\parallel + \vec{q}_\parallel)}{\tilde{\omega}_{vm}(\vec{\kappa}_\parallel + \vec{q}_\parallel, \vec{\kappa}_\parallel) + \omega} + \frac{f_n(\vec{\kappa}_\parallel + \vec{k}_\parallel + \vec{q}_\parallel) - f_v(\vec{\kappa}_\parallel + \vec{q}_\parallel)}{\tilde{\omega}_{nv}(\vec{\kappa}_\parallel + \vec{k}_\parallel + \vec{q}_\parallel, \vec{\kappa}_\parallel + \vec{q}_\parallel) - \omega} \right)$$

$$\times j_{k,vn}(z''; 2\vec{\kappa}_\parallel + \vec{k}_\parallel + 2\vec{q}_\parallel) j_{j,mv}(z'; 2\vec{\kappa}_\parallel + \vec{q}_\parallel) \Bigg\} d^2\kappa_\parallel. \tag{8.20}$$

The nonlinear conductivity tensor part E has the nine nonzero elements

$$\Xi^{\mathrm{E}}_{ijxx}(z, z', z'', z'''; \vec{q}_\parallel, \vec{k}_\parallel) = \frac{e^2}{16 m_e \hbar^2} \frac{1}{(2\pi)^2} \frac{2\mathrm{i}}{\omega^3} \sum_{nmv} \delta(z'' - z''') \int \frac{1}{\tilde{\omega}_{nm}(\vec{\kappa}_\parallel + \vec{q}_\parallel, \vec{\kappa}_\parallel) - \omega}$$

$$\times \Bigg\{ \left(\frac{f_m(\vec{\kappa}_\parallel) - f_v(\vec{\kappa}_\parallel)}{\tilde{\omega}_{vm}(\vec{\kappa}_\parallel, \vec{\kappa}_\parallel) - 2\omega} + \frac{f_n(\vec{\kappa}_\parallel + \vec{q}_\parallel) - f_v(\vec{\kappa}_\parallel)}{\tilde{\omega}_{nv}(\vec{\kappa}_\parallel + \vec{q}_\parallel, \vec{\kappa}_\parallel) + \omega} \right) j_{j,vn}(z'; 2\vec{\kappa}_\parallel + \vec{q}_\parallel) \psi^*_v(z'') \psi_m(z'')$$

$$+ \left(\frac{f_m(\vec{\kappa}_\parallel) - f_v(\vec{\kappa}_\parallel + \vec{q}_\parallel)}{\tilde{\omega}_{vm}(\vec{\kappa}_\parallel + \vec{q}_\parallel, \vec{\kappa}_\parallel) + \omega} + \frac{f_n(\vec{\kappa}_\parallel + \vec{q}_\parallel) - f_v(\vec{\kappa}_\parallel + \vec{q}_\parallel)}{\tilde{\omega}_{nv}(\vec{\kappa}_\parallel + \vec{q}_\parallel, \vec{\kappa}_\parallel + \vec{q}_\parallel) - 2\omega} \right)$$

$$\times j_{j,mv}(z'; 2\vec{\kappa}_\parallel + \vec{q}_\parallel) \psi^*_n(z'') \psi_v(z'') \Bigg\} j_{i,nm}(z; 2\vec{\kappa}_\parallel + \vec{q}_\parallel) d^2\kappa_\parallel. \tag{8.21}$$

Part F also has nine nonzero elements, which are

$$\Xi^{\mathrm{F}}_{ixxh}(z, z', z'', z'''; \vec{q}_\parallel, \vec{k}_\parallel) = \frac{e^2}{8 m_e \hbar^2} \frac{1}{(2\pi)^2} \frac{2\mathrm{i}}{\omega^3} \sum_{nmv} \delta(z' - z''') \int \frac{1}{\tilde{\omega}_{nm}(\vec{\kappa}_\parallel + \vec{q}_\parallel, \vec{\kappa}_\parallel) - \omega}$$

$$\times \Bigg\{ \left(\frac{f_m(\vec{\kappa}_\parallel) - f_v(\vec{\kappa}_\parallel - \vec{k}_\parallel + \vec{q}_\parallel)}{\tilde{\omega}_{vm}(\vec{\kappa}_\parallel - \vec{k}_\parallel + \vec{q}_\parallel, \vec{\kappa}_\parallel)} + \frac{f_n(\vec{\kappa}_\parallel + \vec{q}_\parallel) - f_v(\vec{\kappa}_\parallel - \vec{k}_\parallel + \vec{q}_\parallel)}{\tilde{\omega}_{nv}(\vec{\kappa}_\parallel + \vec{q}_\parallel, \vec{\kappa}_\parallel - \vec{k}_\parallel + \vec{q}_\parallel) - \omega} \right)$$

$$\times j_{h,vn}(z''; 2\vec{\kappa}_\parallel - \vec{k}_\parallel + \vec{q}_\parallel) \psi^*_v(z') \psi_m(z')$$

$$+ \left(\frac{f_m(\vec{\kappa}_\parallel) - f_v(\vec{\kappa}_\parallel + \vec{k}_\parallel)}{\tilde{\omega}_{vm}(\vec{\kappa}_\parallel + \vec{k}_\parallel, \vec{\kappa}_\parallel) - \omega} + \frac{f_n(\vec{\kappa}_\parallel + \vec{q}_\parallel) - f_v(\vec{\kappa}_\parallel + \vec{k}_\parallel)}{\tilde{\omega}_{nv}(\vec{\kappa}_\parallel + \vec{q}_\parallel, \vec{\kappa}_\parallel + \vec{k}_\parallel)} \right)$$

$$\times j_{h,mv}(z''; 2\vec{\kappa}_\parallel + \vec{k}_\parallel) \psi^*_n(z') \psi_v(z') \Bigg\} j_{i,nm}(z; 2\vec{\kappa}_\parallel + \vec{q}_\parallel) d^2\kappa_\parallel. \tag{8.22}$$

Finally, the PCDFWM conductivity tensor part G has the eightyone nonzero elements

$$\Xi^{\mathrm{G}}_{ijkh}(z, z', z'', z'''; \vec{q}_\parallel, \vec{k}_\parallel) = \frac{1}{8\hbar^3} \frac{1}{(2\pi)^2} \frac{2\mathrm{i}}{\omega^3} \sum_{nmvl} \int \frac{1}{\tilde{\omega}_{nm}(\vec{\kappa}_\parallel + \vec{q}_\parallel, \vec{\kappa}_\parallel) - \omega}$$

$$\times \Bigg\{ \left[\left(\frac{f_l(\vec{\kappa}_\parallel - \vec{k}_\parallel) - f_m(\vec{\kappa}_\parallel)}{\tilde{\omega}_{lm}(\vec{\kappa}_\parallel - \vec{k}_\parallel, \vec{\kappa}_\parallel) - \omega} + \frac{f_l(\vec{\kappa}_\parallel - \vec{k}_\parallel) - f_v(\vec{\kappa}_\parallel)}{\tilde{\omega}_{vl}(\vec{\kappa}_\parallel, \vec{\kappa}_\parallel - \vec{k}_\parallel) - \omega} \right) \frac{1}{\tilde{\omega}_{vm}(\vec{\kappa}_\parallel, \vec{\kappa}_\parallel) - 2\omega} \right.$$

$$+ \left. \left(\frac{f_l(\vec{\kappa}_\parallel - \vec{k}_\parallel) - f_v(\vec{\kappa}_\parallel)}{\tilde{\omega}_{vl}(\vec{\kappa}_\parallel, \vec{\kappa}_\parallel - \vec{k}_\parallel) - \omega} + \frac{f_n(\vec{\kappa}_\parallel + \vec{q}_\parallel) - f_v(\vec{\kappa}_\parallel)}{\tilde{\omega}_{nv}(\vec{\kappa}_\parallel + \vec{q}_\parallel, \vec{\kappa}_\parallel) + \omega} \right) \frac{1}{\tilde{\omega}_{nl}(\vec{\kappa}_\parallel + \vec{q}_\parallel, \vec{\kappa}_\parallel - \vec{k}_\parallel)} \right]$$

$$\times j_{h,ml}(z'''; 2\vec{\kappa}_\parallel - \vec{k}_\parallel) j_{k,lv}(z''; 2\vec{\kappa}_\parallel - \vec{k}_\parallel) j_{j,vn}(z'; 2\vec{\kappa}_\parallel + \vec{q}_\parallel)$$

$$
\begin{aligned}
&+ \left[\left(\frac{f_l(\vec{\kappa}_\parallel - \vec{k}_\parallel) - f_m(\vec{\kappa}_\parallel)}{\tilde{\omega}_{lm}(\vec{\kappa}_\parallel - \vec{k}_\parallel, \vec{\kappa}_\parallel) - \omega} + \frac{f_l(\vec{\kappa}_\parallel - \vec{k}_\parallel) - f_v(\vec{\kappa}_\parallel - \vec{k}_\parallel + \vec{q}_\parallel)}{\tilde{\omega}_{vl}(\vec{\kappa}_\parallel - \vec{k}_\parallel + \vec{q}_\parallel, \vec{\kappa}_\parallel - \vec{k}_\parallel) + \omega} \right) \right. \\
&\times \frac{1}{\tilde{\omega}_{vm}(\vec{\kappa}_\parallel - \vec{k}_\parallel + \vec{q}_\parallel, \vec{\kappa}_\parallel)} + \left(\frac{f_l(\vec{\kappa}_\parallel - \vec{k}_\parallel) - f_v(\vec{\kappa}_\parallel - \vec{k}_\parallel + \vec{q}_\parallel)}{\tilde{\omega}_{vl}(\vec{\kappa}_\parallel - \vec{k}_\parallel + \vec{q}_\parallel, \vec{\kappa}_\parallel - \vec{k}_\parallel) + \omega} \right. \\
&\left. \left. + \frac{f_n(\vec{\kappa}_\parallel + \vec{q}_\parallel) - f_v(\vec{\kappa}_\parallel - \vec{k}_\parallel + \vec{q}_\parallel)}{\tilde{\omega}_{nv}(\vec{\kappa}_\parallel + \vec{q}_\parallel, \vec{\kappa}_\parallel - \vec{k}_\parallel + \vec{q}_\parallel) - \omega} \right) \frac{1}{\tilde{\omega}_{nl}(\vec{\kappa}_\parallel + \vec{q}_\parallel, \vec{\kappa}_\parallel - \vec{k}_\parallel)} \right] \\
&\times j_{h,ml}(z'''; 2\vec{\kappa}_\parallel - \vec{k}_\parallel) j_{k,vn}(z''; 2\vec{\kappa}_\parallel - \vec{k}_\parallel + 2\vec{q}_\parallel) j_{j,lv}(z'; 2\vec{\kappa}_\parallel - 2\vec{k}_\parallel + \vec{q}_\parallel) \\
&+ \left[\left(\frac{f_l(\vec{\kappa}_\parallel + \vec{q}_\parallel) - f_m(\vec{\kappa}_\parallel)}{\tilde{\omega}_{lm}(\vec{\kappa}_\parallel + \vec{q}_\parallel, \vec{\kappa}_\parallel) + \omega} + \frac{f_l(\vec{\kappa}_\parallel + \vec{q}_\parallel) - f_v(\vec{\kappa}_\parallel - \vec{k}_\parallel + \vec{q}_\parallel)}{\tilde{\omega}_{vl}(\vec{\kappa}_\parallel - \vec{k}_\parallel + \vec{q}_\parallel, \vec{\kappa}_\parallel + \vec{q}_\parallel) - \omega} \right) \right. \\
&\times \frac{1}{\tilde{\omega}_{vm}(\vec{\kappa}_\parallel - \vec{k}_\parallel + \vec{q}_\parallel, \vec{\kappa}_\parallel)} + \left(\frac{f_l(\vec{\kappa}_\parallel + \vec{q}_\parallel) - f_v(\vec{\kappa}_\parallel - \vec{k}_\parallel + \vec{q}_\parallel)}{\tilde{\omega}_{vl}(\vec{\kappa}_\parallel - \vec{k}_\parallel + \vec{q}_\parallel, \vec{\kappa}_\parallel + \vec{q}_\parallel) - \omega} \right. \\
&\left. \left. + \frac{f_n(\vec{\kappa}_\parallel + \vec{q}_\parallel) - f_v(\vec{\kappa}_\parallel - \vec{k}_\parallel + \vec{q}_\parallel)}{\tilde{\omega}_{nv}(\vec{\kappa}_\parallel + \vec{q}_\parallel, \vec{\kappa}_\parallel - \vec{k}_\parallel + \vec{q}_\parallel) - \omega} \right) \frac{1}{\tilde{\omega}_{nl}(\vec{\kappa}_\parallel + \vec{q}_\parallel, \vec{\kappa}_\parallel + \vec{q}_\parallel) - 2\omega} \right] \\
&\times j_{h,lv}(z'''; 2\vec{\kappa}_\parallel - \vec{k}_\parallel + 2\vec{q}_\parallel) j_{k,vn}(z''; 2\vec{\kappa}_\parallel - \vec{k}_\parallel + 2\vec{q}_\parallel) j_{j,ml}(z'; 2\vec{\kappa}_\parallel + \vec{q}_\parallel) \Bigg\} \\
&\times j_{i,nm}(z; 2\vec{\kappa}_\parallel + \vec{q}_\parallel) d^2\kappa_\parallel .
\end{aligned}
\tag{8.23}
$$

In Eqs. (8.15)–(8.23) above we have dropped the now superfluous index on $\vec{\kappa}_\parallel$.

8.4 Phase conjugated field

After having sketched the calculation of the nonlinear DFWM response we turn our attention to the phase conjugated electric field. In the present case where the main parts of the interaction takes place in very small interaction volumes, we can expect that the generated phase conjugated field does not affect the dynamics of the pump and probe fields much, and thus take the parametric approximation.

Then the loop equation in Eq. (4.17) is reduced to the single-coordinate form in the two-dimensional phase matching case (Keller 1996a)

$$
\begin{aligned}
\vec{E}_{\text{PC}}(z; \vec{q}_\parallel, \omega) &= \vec{E}_{\text{PC}}^{\text{B}}(z; \vec{q}_\parallel, \omega) \\
&- i\mu_0 \omega \int \int \vec{\vec{G}}(z, z''; \vec{q}_\parallel, \omega) \cdot \vec{\vec{\sigma}}(z'', z'; \vec{q}_\parallel, \omega) \cdot \vec{E}_{\text{PC}}(z'; \vec{q}_\parallel, \omega) dz'' dz',
\end{aligned}
\tag{8.24}
$$

possibly with $\vec{\vec{G}}(z, z''; \vec{q}_\parallel, \omega)$ replaced by $\vec{\vec{G}}_0(z, z''; \vec{q}_\parallel, \omega)$. In the quantum-well case the explicit form of $\vec{\vec{G}}(z, z''; \vec{q}_\parallel, \omega)$ is known (Bagchi, Barrera, and Rajagopal 1979), and also $\vec{\vec{G}}_0(z, z''; \vec{q}_\parallel, \omega)$, adequate in near-field optics, is of course known. For few (one, two, three, ...)-level quantum wells several schemes exist for the handling of the integral equation problem in Eq. (8.24), cf., e.g., Keller (1996a). The only factor which in the

parametric approximation makes the DFWM loop problem different from those hitherto investigated is the background field. In the present case this is given by

$$\vec{E}^{\mathrm{B}}_{\mathrm{PC}}(z;\vec{q}_{\parallel},\omega) = -\mathrm{i}\mu_0\omega \int \ddot{G}(z,z';\vec{q}_{\parallel},\omega)\cdot\vec{J}^{(3)}_{-\omega}(z';\vec{q}_{\parallel},\omega)dz', \qquad (8.25)$$

with $\vec{J}^{(3)}_{-\omega}(z';\vec{q}_{\parallel},\omega)$ taken from Eq. (8.8) in the case of simple two-dimensional plane-wave mixing, or in general from Eq. (8.4).

In the quantum well case, the pseudo-vacuum propagator $\ddot{G}(z,z'';\vec{q}_{\parallel},\omega)$ can be written as a sum of three terms

$$\ddot{G}(z,z';\vec{q}_{\parallel},\omega) = \ddot{D}(z-z';\vec{q}_{\parallel},\omega) + \ddot{I}(z+z';\vec{q}_{\parallel},\omega) + \ddot{g}(z-z';\omega), \qquad (8.26)$$

where the first two are named after the processes they describe. Thus the term $\ddot{D}(z-z';\vec{q}_{\parallel},\omega)$ describes the direct propagation of the electromagnetic field from a source point at z' to the observation point at z. It is given by

$$\ddot{D}(z-z';\vec{q}_{\parallel},\omega) = \frac{e^{\mathrm{i}q_\perp|z-z'|}}{2\mathrm{i}q_\perp}\left[\vec{e}_y\otimes\vec{e}_y + \Theta(z-z')\vec{e}_i\otimes\vec{e}_i + \Theta(z'-z)\vec{e}_r\otimes\vec{e}_r\right]. \qquad (8.27)$$

The indirect term, $\ddot{I}(z+z';\vec{q}_{\parallel},\omega)$, describes the propagation from the source point of the part of the electromagnetic field that is going to the point of observation via the surface of the bulk medium. The expression for the indirect term reads

$$\ddot{I}(z+z';\vec{q}_{\parallel},\omega) = \frac{e^{-\mathrm{i}q_\perp(z+z')}}{2\mathrm{i}q_\perp}[r^s\vec{e}_y\otimes\vec{e}_y + r^p\vec{e}_r\otimes\vec{e}_i]. \qquad (8.28)$$

Finally, the self-field term characterizes the field generated at the observation point by the current density at the same point. The self-field part of the propagator is given by

$$\ddot{g}(z-z';\omega) = q^{-2}\delta(z-z')\vec{e}_z\otimes\vec{e}_z, \qquad (8.29)$$

where $q = \omega/c_0$ is the vacuum wavenumber. In the above equations, $q_\perp = [q^2 - q_\parallel^2]^{1/2}$, $\vec{e}_i = q^{-1}(q_\perp,0,-q_\parallel)$, and $\vec{e}_r = q^{-1}(-q_\perp,0,-q_\parallel)$, taking $\vec{q}_\parallel = q_\parallel\vec{e}_x$. The quantities r^s and r^p are the amplitude reflection coefficients of the vacuum/substrate interface in the absence of the quantum well. In general these are functions of $\vec{q}_\parallel$. The appropriate propagators for a single quantum well system are shown in Fig. 8.1.

8.5 Some limits of the PCDFWM conductivity tensor

8.5.1 Local limit in the z-coordinates

In the local limit the three interacting fields are independent of the z-coordinate, and thus we may calculate the local PCDFWM response tensor as

$$\ddot{\Xi}(z;\vec{q}_{\parallel},\vec{k}_{\parallel}) = \iiint \ddot{\Xi}(z,z',z'',z''';\vec{q}_{\parallel},\vec{k}_{\parallel})dz'''dz''dz'. \qquad (8.30)$$
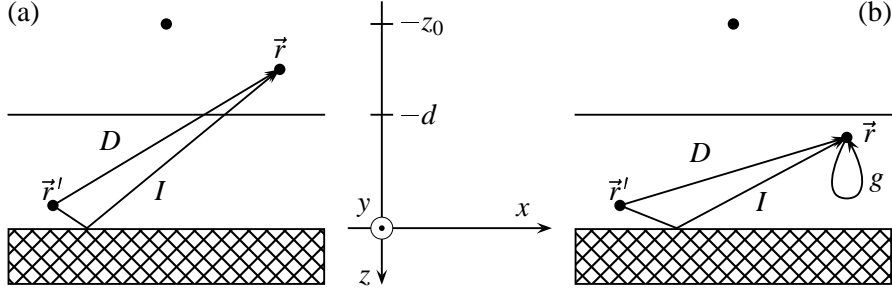
Figure 8.1: The propagators appearing in the calculation of the phase conjugated field in the system we consider in this communication. The system consists of a three layer thin film structure, namely vacuum, film (quantum well, extending from 0 to $-d$) and substrate (crosshatched). In the vacuum may be placed different kinds of sources, e.g., a quantum wire with its axis along the y-direction (shown as a dot). In Fig. (a) the propagation of the electromagnetic field from a source point $\vec{r}'$ inside the quantum well to an observation point $\vec{r}$ outside the quantum well is shown, while in (b) the propagation of the electromagnetic field is illustrated in the case where both source and observation point are inside the quantum well. D is the propagation path described by the direct propagator, I is the propagation path described by the indirect propagator, and g denotes the self-field action propagator. In the center of the figure is shown the Cartesian coordinate system used in our calculations.

Since the dependence on the three coordinates z''', z'', and z' are fairly simple we may draw some conclusions directly from looking at Eqs. (8.17)–(8.23). Using an orthogonal set of wave functions, parity teaches

$$\int \psi_n(z)\psi_m(z)dz = \delta_{nm}, \tag{8.31}$$

where δ_{nm} is the Kronecker delta. By inspection of Eq. (8.14), this is the type of integral appearing when considering the x and y coordinates of this current density.

Then we may conclude that (i) the only independent element of part A of the PCD-FWM conductivity tensor is zero in the local limit, since the two Fermi-Dirac distribution functions in Eq. (8.17) becomes identical for $n = m$. This occurs when taking the local limit in the coordinate z''. In addition, (ii) the five independent elements of part E of the PCDFWM conductivity tensor also becomes zero, since the two pure interband terms are zero by themselves, and the two other terms are of the same magnitude but with opposite sign. This occurs when taking the local limit in the coordinates z''' and z''. Furthermore, (iii) for part G of the PCDFWM conductivity tensor, elements with the Cartesian index $i = z$ and the other indices different from z becomes zero, since the other indices implies that all quantum numbers in the summation become identical. Finally, (iv) the only independent element of part C of the PCDFWM conductivity tensor is reduced to a pure intraband contribution. The same reduction appears in tensor elements of parts D, F, and G with no Cartesian coordinate index z in indices jk, ih, and $ijkh$, respectively. In part B of the PCDFWM conductivity tensor, the elements with no Cartesian index z in
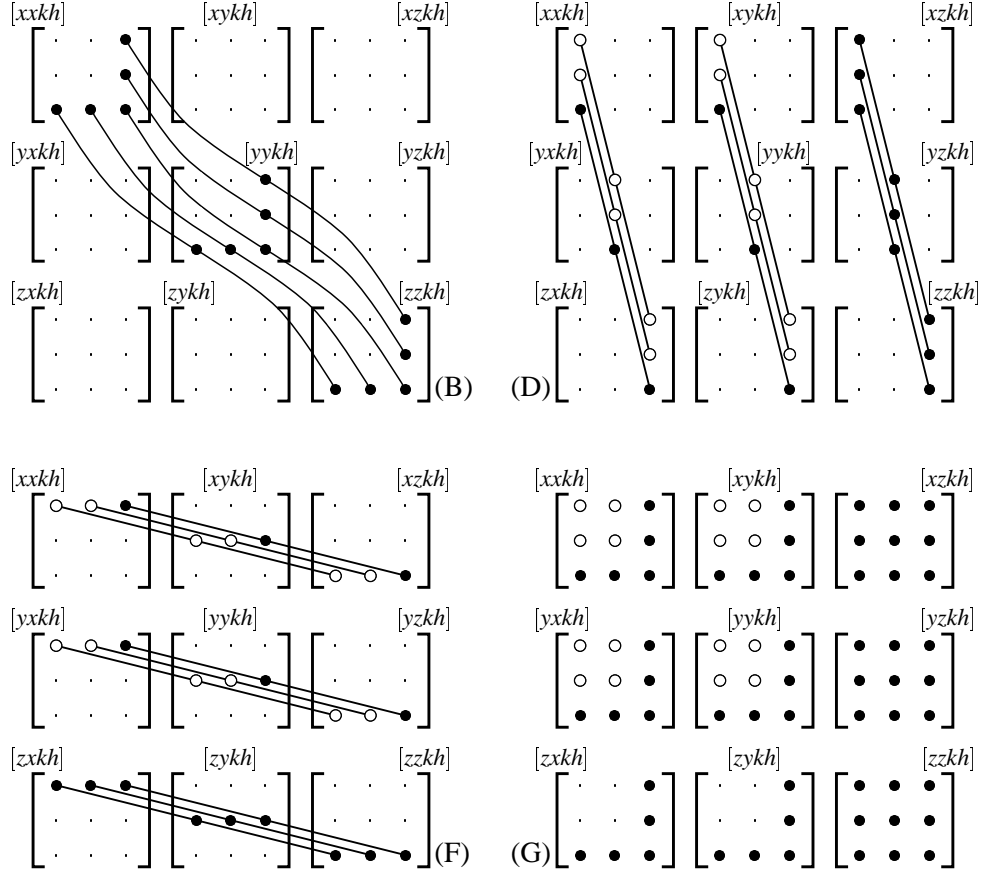
Figure 8.2: Symmetry schemes for the PCDFWM conductivity tensor parts B, D, F, and G in (i) the local limit in the z coordinates, and (ii) the single level quantum well case. In the local limit, tensor elements labeled with a "•" gives nonzero mixed interband/intraband contributions, elements labeled with a "∘" gives nonzero pure intraband contributions, and elements labeled with a "·" are zero. In the single level quantum well case, only elements labeled with a "∘" contributes to the solution. The solid lines connect equal nonzero elements.

kh apparantly gives the same result, but the following integration over $\vec{\kappa}_\parallel$ makes them vanish. These conclusions are shown in the form of symmetry schemes in Fig. 8.2.

8.5.2 Local limit along the surface

Taking the local limit along the surface coordinates, the wavenumbers are considered to be much less than the Fermi wavenumber, i.e., we take the limit where $\vec{q}_\parallel \to \vec{0}$ and $\vec{k}_\parallel \to \vec{0}$ (the dipole limit).

Then from Eq. (8.11) we observe that the transition frequencies become independent of $\vec{\kappa}_\parallel$, and thus we conclude that this approximation makes the integration over $\vec{\kappa}_\parallel$ particularly simple in the low temperature limit, since no integration variables appears in any of the denominators in Eqs. (8.17)–(8.23). We further observe that only interband contributions are left compared to the full description.

8.5.3 Local limit in three coordinates

Locality in all three coordinates is achieved by a combination of the two limits mentioned in Secs. 8.5.1 and 8.5.2 above. Thus, in this limit (i) parts A and E of the DFWM conductivity tensor does not contribute for the same reasons as before. Furthermore (ii) the integration over z' in part C makes this part vanish, (iii) the integration over z' in part F of the DFWM conductivity tensor cancels two terms, and the other two are of the same magnitude, but with opposite signs, resulting in the fact that part F does not contribute to the response in this limit. Finally (iv), all purely intraband contributing tensor elements found in the local limit vanish. All in all we are left with five independent nonzero elements of parts B and D, and fiftyseven independent nonzero elements of G, all labeled with a "•" in Fig. 8.2.

8.5.4 Single level quantum well

A substantial simplification of Eqs. (8.17)–(8.23) occur in *one* special case, namely in the case where the thin film is a single level quantum well in the z-direction. In the single level quantum well, the summation indices are all equal to 1.

Special attention is in this case devoted to the current density defined in Eq. (8.14), which in a single level quantum well is reduced to

$$j_{h,11}(z;\kappa_h) = -\frac{e\hbar}{2m_e}(\delta_{hx}+\delta_{hy})\kappa_h|\psi_1(z)|^2, \tag{8.32}$$

for $h \in \{x,y\}$, since the z-dependent part vanish for any $n = m$. This observation leads to a drastic reduction of the number of contributing elements in most of the symmetry schemes associated with the occuring processes.

The only nonzero element in part A of the nonlinear conductivity tensor vanish for $n = m$. In part B of the conductivity tensor all elements with k or h equal to z vanish for $n = m = v$, and the rest of the elements vanish by integration over $\vec{\kappa}_\parallel$. The only nonzero element of part C of the nonlinear conductivity tensor is conserved, but simplified. Part D of the nonlinear conductivity tensor is reduced somewhat, since either combination of $j = z$ or $k = z$ gives zero. Then we are left with four nonzero independent elements, as shown in Fig. 8.2.D. Part E does not give any contributions to the intraband transitions, since two terms in the sum gives no intraband contributions in general, and the other two terms cancel each other. Part F is reduced in a manner similar to parts B and D, since any combination of $i = z$ or $h = z$ gives zero. The resulting four nonzero independent

elements are shown in Fig. 8.2.F. In the last part (G) of the nonlinear conductivity tensor any combination of $i = z$, $j = z$, $k = z$, or $h = z$ gives zero. As a consequence of this rather drastic reduction we are left with sixteen nonzero elements, as shown in Fig. 8.2.G.

Chapter 9

Polarized light in the *x*-*z*-plane

Restricting ourselves to consider light propagating in the *x*-*z*-plane, which furthermore is polarized either in the *x*-*z*-plane (*p*-polarized) or perpendicular to the *x*-*z*-plane (*s*-polarized), the treatment can be split into eight separate parts related to the possible combinations of polarization of the three different incident fields. In this scattering geometry $\vec{q}_\parallel$ (and $\vec{k}_\parallel$) lie along the *x*-axis, giving a mirror plane at $y = 0$. Consequently, only tensor elements in the $(3 \times 3 \times 3 \times 3)$ PCDFWM response tensor with a Cartesian index even numbered in *y* contributes, and the 81 tensor elements generally appearing are reduced to 41.

Applying the two polarization states *s* and *p* chosen above to the three interacting fields, the resulting eight different combinations uses different matrix elements in the nonlinear conductivity tensor, and (as would be expected) these eight combinations together make use of *all* elements of the nonlinear conductivity tensor. This division is shown in Fig. 9.1 for the 41 contributing tensor elements as described in the following. The noncontributing elements of the nonlinear conductivity tensor is denoted using the symbol "·" in Fig. 9.1.

9.1 Eight sets of contributing matrix elements

From the point of view of the probe, the eight different combinations of polarized light can be divided into two groups of four, namely four giving a PCDFWM response with the same polarization as the probe and four giving the other polarization as the PCDFWM response. In the four combinations giving response of the same polarization as the probe, the two pump fields have the same polarization states. These configurations are sketched in Fig. 9.2. The other four combinations, where the two pump fields are differently polarized are sketched in Fig. 9.3.

Two out of the first four combinations describe *s* to *s* transitions, seen from the point of view of the probe. (i) The simplest combination arises when both pump fields and the probe field are *s*-polarized, as shown in Fig. 9.2.a. In this case, only the *yyyy* element of the nonlinear conductivity tensor is present. In Fig. 9.1 it is marked with a "●". It should be noted that this is the *only* case of the eight, in which a single matrix element can be determined independently in an actual experiment. (ii) When both pump fields
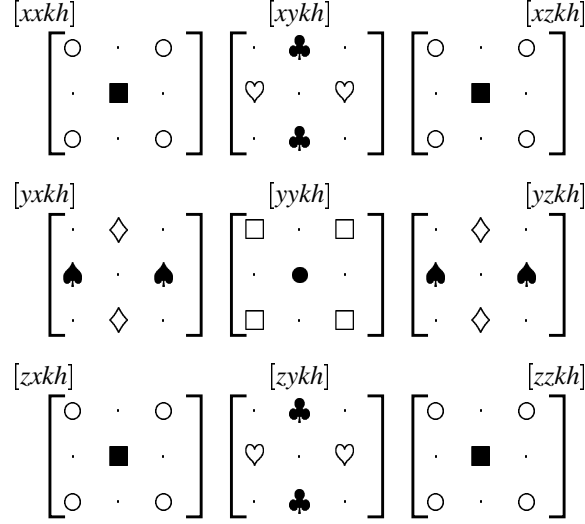
$$
[xxkh] \quad\quad [xykh] \quad\quad [xzkh]
$$

$$
\begin{bmatrix} \circ & \cdot & \circ \\ \cdot & \blacksquare & \cdot \\ \circ & \cdot & \circ \end{bmatrix}
\begin{bmatrix} \cdot & \clubsuit & \cdot \\ \heartsuit & \cdot & \heartsuit \\ \cdot & \clubsuit & \cdot \end{bmatrix}
\begin{bmatrix} \circ & \cdot & \circ \\ \cdot & \blacksquare & \cdot \\ \circ & \cdot & \circ \end{bmatrix}
$$

$$
[yxkh] \quad\quad [yykh] \quad\quad [yzkh]
$$

$$
\begin{bmatrix} \cdot & \diamondsuit & \cdot \\ \spadesuit & \cdot & \spadesuit \\ \cdot & \diamondsuit & \cdot \end{bmatrix}
\begin{bmatrix} \square & \cdot & \square \\ \cdot & \bullet & \cdot \\ \square & \cdot & \square \end{bmatrix}
\begin{bmatrix} \cdot & \diamondsuit & \cdot \\ \spadesuit & \cdot & \spadesuit \\ \cdot & \diamondsuit & \cdot \end{bmatrix}
$$

$$
[zxkh] \quad\quad [zykh] \quad\quad [zzkh]
$$

$$
\begin{bmatrix} \circ & \cdot & \circ \\ \cdot & \blacksquare & \cdot \\ \circ & \cdot & \circ \end{bmatrix}
\begin{bmatrix} \cdot & \clubsuit & \cdot \\ \heartsuit & \cdot & \heartsuit \\ \cdot & \clubsuit & \cdot \end{bmatrix}
\begin{bmatrix} \circ & \cdot & \circ \\ \cdot & \blacksquare & \cdot \\ \circ & \cdot & \circ \end{bmatrix}
$$

Figure 9.1: The contributing matrix elements of the third order conductivity tensor in the cases where (•) both the pump fields and the probe field are *s*-polarized, (○) both the pump fields and the probe field are *p*-polarized, (■) both pump fields are *s*-polarized, and the probe field is *p*-polarized, (□) both pump fields are *p*-polarized, and the probe field is *s*-polarized, (♣) (and ♡ for the "interchanged term") pump 1 is *s*-polarized, pump 2 is *p*-polarized, and the probe is *s*-polarized, (♡) (and ♣ for the "interchanged term") pump 1 is *p*-polarized, pump 2 is *s*-polarized, and the probe is *s*-polarized, (◇) (and ♠ for the "interchanged term") pump 1 is *s*-polarized, pump 2 is *p*-polarized, and the probe is *p*-polarized, and (♠) (and ◇ for the "interchanged term") pump 1 is *p*-polarized, pump 2 is *s*-polarized, and the probe is *p*-polarized.

are *p*-polarized and the probe field is *s*-polarized (see Fig. 9.2.b), the four contributing matrix elements in the nonlinear conductivity tensor have indices *i* and *j* equal to *y* and indices *k* and *h* different from *y*. Each of these four elements is marked with a "□" in Fig. 9.1.

From the same point of view the other two of the first four combinations describe *p* to *p* transitions. (iii) If both pump fields are *s*-polarized and the probe field is *p*-polarized the configuration is sketched in Fig. 9.2.c, and four matrix elements in the nonlinear conductivity tensor contribute to the solution. They have indices *k* and *h* equal to *y* and indices *i* and *j* different from *y*. In Fig. 9.1, each of these elements is marked with a "■". (iv) The other extreme case [the simple extreme has been described in item (i)] is the combination where both pump fields and the probe field are *p*-polarized, as shown in Fig. 9.2.d. In order to obtain the solution for this combination as many as sixteen elements of the nonlinear conductivity tensor are required, since every element with an index without *y*'s in it contributes. Each of these elements is marked in Fig. 9.1 with a "○".
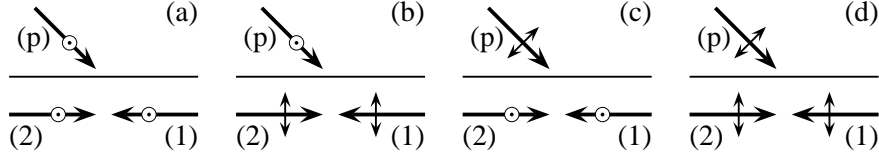
Figure 9.2: Schematic illustration showing the four possible field polarization combinations giving rise to the same polarization of the phase conjugated response as the probe field. Figs. a and b shows the *s* to *s* response for *s*-polarized and *p*-polarized pump fields, respectively, while Figs. c and d shows the *p* to *p* response corresponding to these pump field polarizations. In Figs. a–d the pump fields are denoted (1) and (2) and the probe field is denoted (p).
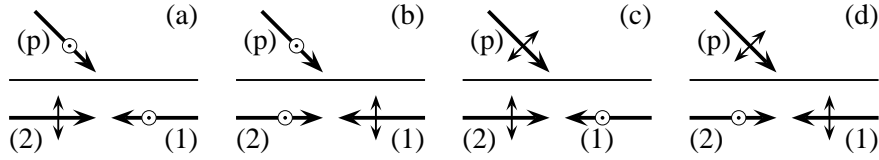

Figure 9.3: Schematic illustration showing the four possible field polarization combinations giving rise to different polarization of the phase conjugated response seen from the point of view of the probe field. Figs. a and b shows the combinations of the fields giving a *s* to *p* response, while Figs. c and d shows the *p* to *s* response configurations. In all four cases the two pump fields are differently polarized with respect to each other. In Figs. a–d the pump fields are denoted (1) and (2) and the probe field is denoted (p).

Still taking the "probe to response" point of view, two of the remaining four cases represent a probe to response transition from *s* to *p*. (v) If pump field 1 is *s*-polarized, pump field 2 is *p*-polarized, and the probe field is *s*-polarized (the corresponding diagram is showed in Fig. 9.3.a), the four contributing matrix elements have indices *j* and *k* equal to *y* and indices *i* and *h* different from *y*. In Fig. 9.1 each of these elements is marked with the symbol "♣". In the other of these cases, (vi), pump field 1 is *p*-polarized and pump field 2 is *s*-polarized, and we take the probe field to be *s*-polarized. This combination is sketched in Fig. 9.3.b, and the four contributing elements in the nonlinear conductivity tensor then have indices *j* and *k* equal to *y* and indices *i* and *h* different from *y*. In Fig. 9.1 the symbol "♡" is used to show these elements. As a direct consequence of the conservation of momentum criterion these two combinations are equivalent, since by replacing $\vec{q}_\parallel$ with $-\vec{q}_\parallel$ and $\vec{k}_\parallel$ with $-\vec{k}_\parallel$ the situation in (vi) changes to the situation in (v).

The last two combinations represent a transition from *p* to *s* in the picture from probe to response. (vii) If pump field 1 is *s*-polarized and pump field 2 is *p*-polarized, but the probe field is *p*-polarized, the situation is as sketched in Fig. 9.3.c. Then again four elements of the nonlinear conductivity tensor contribute to the solution. These four elements have indices *i* and *h* equal to *y* and indices *j* and *k* different from *y*, and each element is marked using the symbol "◇" in Fig. 9.1. Finally, (viii), when pump field

1 is p-polarized and pump field 2 is s-polarized, but the probe field is p-polarized, the configuration appears as shown in Fig. 9.3.d, which again gives four elements of the nonlinear conductivity tensor contributing to the solution, the indices i and k being equal to y and the indices j and h being different from y. We mark each of these elements with the symbol "♠" in Fig. 9.1. For the same reason as before, cases (vii) and (viii) are equivalent.

9.2 Simplified description by choice of pump fields

Although the two pump fields has been drawn parallel to the interface in Figs. 9.2 and 9.3, this is not a requirement, as long as they are counterpropagating to each other. If we are looking for a simplification in the treatment of optical phase conjugation from a quantum well structure, a reduction in the number of tensor elements to be calculated could be one alternative. Two immediate possibilities comes to mind. In the first case, the pump fields are taken to be parallel to the x-axis. The second case has the pump fields parallel to the z-axis. The consequences of these two cases are described in the following.

If the pump fields propagate in a direction parallel to the x-axis, the number of contributing tensor elements in the nonlinear conductivity tensor $\overset{\leftrightarrow}{\Xi}(z,z',z'',z''';\vec{q}_\parallel,\vec{k}_\parallel)$ is reduced from 41 to 18 when considering s- and p-polarized light only. The surviving elements can be divided into four cases following the four possible combinations of polarization of the pump fields. When (i) both pump fields are p-polarized, their respective electric fields have only a z-component, and hence $h = k = z$. Similarly (ii), when both pump fields are s-polarized, their electric fields only have a y-component, that is, $h = k = y$. In case (iii) pump field 1 is p-polarized while pump field 2 is s-polarized, giving $h = z$ and $k = y$. In the final case (iv) the pump fields are polarized oppositely to those in case (iii), i.e., $h = y$ and $k = z$.

If we choose the pump fields to propagate in a direction parallel to the z axis instead, the number of contributing tensor elements in the nonlinear conductivity tensor $\overset{\leftrightarrow}{\Xi}(z,z',z'',z''';\vec{q}_\parallel,\vec{k}_\parallel)$ is again reduced from 41 to 18 when considering s- and p-polarized light, and again the surviving elements are divided into four groups following the four possible combinations of polarization the pump fields can have. Thus, (i) when both pump fields are p-polarized, the electric fields representing them have only x-components, i.e., $h = k = x$, (ii) for the pump fields both being s-polarized, the same elements as when the pump fields are parallel to the x-axis contributes to the solution, giving again $h = k = y$. In the cases of differently polarized pump fields, (iii) $h = x$ and $k = y$ when pump field 1 is p-polarized and pump field 2 is s-polarized, and (iv) $h = y$ and $k = x$ when the opposite polarizations occur.

In conclusion, these two possibilities of choice have five common contributing elements, namely the ones where $k = h = y$. At the same time, ten elements of the nonlinear conductivity tensor does not contribute to either simplification. They have $kh \in \{xz, zx\}$.

Part IV

Optical phase conjugation
in a single-level metallic quantum well

Chapter 10

Having discussed the properties of optical phase conjugation in quantum well structures in general, let us consider here the simplest configuration of a mesoscopic metallic optical quantum-well phase conjugator. In this case only a single bound state exists below the Fermi level and it is assumed that no levels above the Fermi level can be reached with the applied optical field. Such a quantum well is called a single-level quantum well.

10.1 Phase conjugated field

In a mesoscopic film the electric field generated via the direct and indirect processes at a given point is roughly speaking of the order $(\mu_0\omega/q_\perp)\int \vec{J}_{-\omega}^{(3)}dz'$, whereas the self-field has the magnitude $(\mu_0\omega/q^2)\vec{J}_{-\omega}^{(3)}$. Since $qd \ll 1$, where d is the thickness of the film, we judge the self-field term to dominate the phase conjugated field inside the quantum well, at least for single-level metallic quantum wells which have thicknesses on the atomic length scale. In the following we therefore use the so-called self-field (electrostatic) approximation to calculate the phase conjugated field inside the quantum well. With the propagator $\vec{G}(z,z'';\vec{q}_\parallel,\omega)$ replaced by $\vec{g}(z-z';\omega)$, the phase conjugated field fulfills the integral equation

$$\vec{E}_{\text{PC}}(z;\vec{q}_\parallel,\omega) = \vec{E}_{\text{PC}}^{\text{B}}(z;\vec{q}_\parallel,\omega) + \frac{\vec{e}_z \otimes \vec{e}_z}{i\epsilon_0\omega} \cdot \int \vec{\sigma}(z,z';\vec{q}_\parallel,\omega) \cdot \vec{E}_{\text{PC}}(z';\vec{q}_\parallel,\omega)dz' \tag{10.1}$$

inside the well, and the background field is now

$$\vec{E}_{\text{PC}}^{\text{B}}(z;\vec{q}_\parallel,\omega) = \frac{\vec{e}_z \otimes \vec{e}_z}{i\epsilon_0\omega} \vec{J}_{-\omega}^{(3)}(z;\vec{q}_\parallel,\omega). \tag{10.2}$$

In the self-field approach the phase conjugated field has only a component perpendicular to the surface (the z-component) inside the well and only the z-component of the nonlinear current density $\vec{J}_{-\omega}^{(3)}$ drives the process.

Once the phase conjugated field inside the quantum well has been determined in a self-consistent manner from Eq. (10.1), it can be determined outside using Eq. (8.24). The self-field does of course not contribute to the exterior field, and no loop problem is

involved. All that need to be done is to integrate known quantities in the z-direction over the well.

10.2 Nonlinear conductivity tensor

As we may recall, the nonlinear conductivity tensor appearing in Eq. (8.8) may in general be written as a sum of seven parts (A–G) after the physical processes they describe. These have the tensor symmetries shown in Tab. 6.1. In this chapter we use this conductivity tensor in the form it takes for media with two-dimensional translational invariance as it was developed in Part II, but for quantum wells so thin that only a single bound level exists. The quantum well may be free standing, or it may be deposited on a substrate that can be described by a refractive index n relative to the vacuum on the other side of the film. The surface of the film is parallel to the x-y-plane in a Cartesian coordinate system, and the interface between the film and the substrate is placed at $z = 0$ as shown in Fig. 8.1. We further limit our study to the case where (i) all scattering takes place in the x-z-plane, (ii) the interacting fields are linearly polarized in (p) or perpendicular to (s) the scattering plane, (iii) the pump fields in the phase conjugating system are counterpropagating monochromatic plane waves with a uniform amplitude along the z-axis and propagating in a direction parallel to the x-axis, and (iv) the field is calculated within the self-field approximation.

From (i) above we get a mirror plane at $y = 0$, leaving only tensor elements of the conductivity tensors with an even number $(0, 2, 4)$ of y's in the Cartesian index nonzero. Condition (iii) implies as a consequence of condition (ii) that no tensor elements of the nonlinear conductivity tensor with one or both of the last two Cartesian indices as x contributes to the phase conjugated response. Requirement (iv) above implies that the first Cartesian index of a tensor element should be z in order to contribute to the phase conjugated response. The choice of a single level quantum well in itself restricts the transition current density to contain x- and y- components only. Together with the fact that part B gives zero after integration over $\vec{\kappa}_{\parallel}$ and E gives pure interband contributions, these choices leave two nonzero elements of the nonlinear conductivity tensor, namely

$$\Xi^{\mathrm{C}}_{zyyz}(z, z', z'', z'''; q_{\parallel} - k_{\parallel}) = \Xi^{\mathrm{C}}_{zzzz}(z, z', z'', z'''; q_{\parallel} - k_{\parallel}) =$$
$$\frac{e^4}{2^4 \pi^2 \mathrm{i} \hbar \omega^3 m_e^2} C(q_{\parallel} - k_{\parallel}) \delta(z' - z''') \delta(z - z'') |\psi(z')|^2 |\psi(z)|^2, \tag{10.3}$$

$$\Xi^{\mathrm{D}}_{zyyz}(z, z', z'', z'''; q_{\parallel}, k_{\parallel}) = \frac{e^4}{2^6 \pi^2 i \omega^3 m_e^3} \mathcal{D}(q_{\parallel}, k_{\parallel}) \delta(z - z''') |\psi(z'')|^2 |\psi(z')|^2 |\psi(z)|^2, \tag{10.4}$$

where

$$C(q_{\parallel} - k_{\parallel}) = 2 \int \frac{f(\vec{\kappa}_{\parallel} + [q_{\parallel} - k_{\parallel}] \vec{e}_x) - f(\vec{\kappa}_{\parallel})}{\hbar (q_{\parallel} - k_{\parallel}) [2\kappa_x + q_{\parallel} - k_{\parallel}] / (2m_e) - \mathrm{i}/\tau} d^2 \kappa_{\parallel}, \tag{10.5}$$

$$\mathcal{D}(q_\parallel, k_\parallel) = 2 \int \frac{\kappa_y^2}{\hbar(q_\parallel + k_\parallel)[2\kappa_x + q_\parallel + k_\parallel]/(2m_e) - i/\tau}$$
$$\times \left(\frac{f(\vec{\kappa}_\parallel) - f(\vec{\kappa}_\parallel + k_\parallel \vec{e}_x)}{\hbar k_\parallel[2\kappa_x + k_\parallel]/(2m_e) - i/\tau - \omega} + \frac{f(\vec{\kappa}_\parallel + [k_\parallel + q_\parallel]\vec{e}_x) - f(\vec{\kappa}_\parallel + k_\parallel \vec{e}_x)}{\hbar q_\parallel[2\kappa_x + q_\parallel + 2k_\parallel]/(2m_e) - i/\tau + \omega} \right.$$
$$\left. + \frac{f(\vec{\kappa}_\parallel) - f(\vec{\kappa}_\parallel + q_\parallel \vec{e}_x)}{\hbar q_\parallel[2\kappa_x + q_\parallel]/(2m_e) - i/\tau + \omega} + \frac{f(\vec{\kappa}_\parallel + [k_\parallel + q_\parallel]\vec{e}_x) - f(\vec{\kappa}_\parallel + q_\parallel \vec{e}_x)}{\hbar k_\parallel[2\kappa_x + k_\parallel + 2q_\parallel]/(2m_e) - i/\tau - \omega} \right) d^2\kappa_\parallel .$$

$$(10.6)$$

The number 2 appearing in front of the integrals above represents the summation over the degenerate spin energies.

The free-particle character of the electron motion in the plane of the quantum well enables us to write the solutions to the light-unperturbed Schrödinger equation in the form $\Psi(\vec{r}) = (2\pi)^{-1}\psi(z)\exp(i\vec{\kappa}_\parallel \cdot \vec{r})$, where $\vec{\kappa}_\parallel = (\kappa_x, \kappa_y, 0)$ is the wavevector of the electron in consideration and $\psi(z)$, appearing in Eqs. (10.3) and (10.4), is the z-dependent part of the wave function, common to all electrons. The x-y-dependent parts of the wave functions, $(2\pi)^{-1}\exp(i\vec{\kappa}_\parallel \cdot \vec{r})$, are orthonormalized in the Dirac sense, i.e., they obey the equation $(2\pi)^{-2}\int \exp[i(\vec{\kappa}_\parallel - \vec{\kappa}'_\parallel) \cdot \vec{r}]d^2r = \delta(\vec{\kappa}_\parallel - \vec{\kappa}'_\parallel)$, and the z-dependent part fulfills the separate normalization condition $\int |\psi(z)|^2 dz = 1$. In Eqs. (10.5) and (10.6) the response of all electrons is taken into account by integrating over all possible $\vec{\kappa}_\parallel$ wavevectors. The eigenenergy $\mathcal{E}(\vec{\kappa}_\parallel)$ belonging to the state $\Psi(\vec{r})$ is obtained by adding to the common bound-state energy ε, the kinetic energy in the parallel motion. Thus

$$\mathcal{E}(\vec{\kappa}_\parallel) = \varepsilon + \frac{\hbar^2}{2m_e}\kappa_\parallel^2 . \tag{10.7}$$

The quantity $f(\vec{\kappa}_\parallel) = [1 + \exp\{(\mathcal{E}(\vec{\kappa}_\parallel) - \mu)/(k_B T)\}]^{-1}$ denotes the Fermi-Dirac distribution function for this eigenstate, μ being the chemical potential of the electron system, k_B the Boltzmann constant, and T the absolute temperature.

10.3 Probe with single Fourier component

In the following we calculate the phase conjugated field generated by a probe field which consists of only one plane-wave component of wavevector $\vec{q} = (q_\parallel, 0, q_\perp)$. A probe field of the form $\vec{E}(z; \vec{q}_\parallel) = \vec{E}e^{iq_\perp z}$ is hence inserted in Eq. (8.8).

Then, when using linearly polarized light, three different combinations of polarization gives a nonlinear current density, namely (i) the one in which all participating fields are p-polarized (ppp), and (ii) the two combinations where the pump fields are differently polarized and the probe field is s-polarized (sps and pss). In all cases, the phase conjugated response is p-polarized, and thus characterized in terms of the polarization states of the probe and phase conjugated fields, case (i) may be classified as a p to p tran-
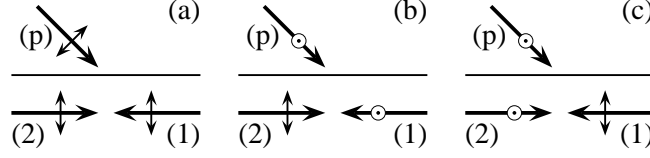
Figure 10.1: Schematic illustration showing three of the possible field polarization combinations which may give rise to a phase conjugated response in a single-level quantum well, viz. (a) the purely *p*-polarized configuration, and (b–c) the mixed polarization configurations where the pump fields are differently polarized while the probe is *s*-polarized. The two mixed polarization states are closely related, since replacing $\vec{q}_\parallel$ with $-\vec{q}_\parallel$ in one of them yields the other. In both (a and b–c) cases, the phase conjugated response is *p*-polarized. The schemes are shown in the Cartesian coordinate system given in Fig. 8.1, such that the small arrows in the plane represents *p*-polarized states and the circles represents *s*-polarized states. The large arrows show the direction of (one Fourier component of) the wavevectors of the pump fields (1 and 2) and the probe field (p).

sition, and cases (ii) as *s* to *p* transitions. A schematic illustration of these interaction configurations is shown in Fig. 10.1. Defining the *z*-independent quantity

$$\mathcal{J}_{-\omega,z}^{(3)}(\vec{q}_\parallel) \equiv \frac{J_{-\omega,z}^{(3)}(z;\vec{q}_\parallel)}{|\psi(z)|^2}, \tag{10.8}$$

the above conditions yields for the *p* to *p* transition

$$\mathcal{J}_{-\omega,z}^{(3)}(\vec{q}_\parallel) = \frac{e^4}{2^8\pi^6 i\hbar\omega^3 m_e^2} \left[C(q_\parallel - k_\parallel) + C(q_\parallel + k_\parallel) \right] E_z^{(1)} E_z^{(2)} E_z^*$$
$$\times \int |\psi(z')|^2 e^{-iq_\perp^* z'} dz' \tag{10.9}$$

and for the *s* to *p* transitions

$$\mathcal{J}_{-\omega,z}^{(3)}(\vec{q}_\parallel) = \frac{e^4}{2^8\pi^6 i\hbar\omega^3 m_e^2} \left[C(q_\parallel + k_\parallel) + \frac{\hbar}{4m_e} \mathcal{D}(\vec{q}_\parallel, -\vec{k}_\parallel) \right] E_y^{(1)} E_z^{(2)} E_y^*$$
$$\times \int |\psi(z')|^2 e^{-iq_\perp^* z'} dz', \tag{10.10}$$

$$\mathcal{J}_{-\omega,z}^{(3)}(\vec{q}_\parallel) = \frac{e^4}{2^8\pi^6 i\hbar\omega^3 m_e^2} \left[C(q_\parallel - k_\parallel) + \frac{\hbar}{4m_e} \mathcal{D}(q_\parallel, k_\parallel) \right] E_z^{(1)} E_y^{(2)} E_y^*$$
$$\times \int |\psi(z')|^2 e^{-iq_\perp^* z'} dz'. \tag{10.11}$$

In the above three equations, the superscript (1) refers to the pump field propagating along the *x*-axis in the positive direction ($\vec{k}_\parallel = k_\parallel \vec{e}_x$), and the superscript (2) refers to the other pump field. The *s* to *p* transitions are symmetric in the sense that if the probe wavevector $\vec{q}_\parallel$ is replaced by $-\vec{q}_\parallel$ in Eq. (10.10), then the result of Eq. (10.11) is obtained, and vice versa. The *p* to *p* transition is symmetric to itself in this sense.

For a single-level quantum well, the *zz*-component of the linear conductivity tensor is given by (Feibelman 1982)

$$\sigma_{zz}(z,z';\vec{q}_\parallel) = \frac{ie^2\mathcal{N}}{m_e(\omega+i/\tau)}|\psi(z)|^2\delta(z-z'),\tag{10.12}$$

where

$$\mathcal{N} = \frac{2}{(2\pi)^2}\int f(\vec{\kappa}_\parallel)d^2\kappa_\parallel.\tag{10.13}$$

In order to take into account the coupling to surroundings we have introduced a phenomenological relaxation time τ in the diamagnetic expression for σ_{zz} [Eq. (10.12)] (Feibelman 1982). A factor of two in this equation again stems from the spin summation, and the quantity $\mathcal{N}|\psi(z)|^2$ is the conduction electron density. The phase conjugated field inside the quantum well has a *z*-component, $E_{\mathrm{PC},z}(z;\vec{q}_\parallel)$, only, and by combining Eqs. (10.1), (10.2), and (10.12) it appears that this is given by

$$E_{\mathrm{PC},z}(z;\vec{q}_\parallel) = \frac{im_e(\omega+i/\tau)}{e^2\mathcal{N}|\psi(z)|^2-\varepsilon_0 m_e\omega(\omega+i/\tau)}J^{(3)}_{-\omega,z}(z;\vec{q}_\parallel).\tag{10.14}$$

Using now Eq. (8.24), the *z*-components of the phase conjugated field outside the quantum well can be calculated, and the result is

$$E_{\mathrm{PC},z}(z;\vec{q}_\parallel) = \mathcal{J}^{(3)}_{-\omega,z}(\vec{q}_\parallel)e^{-iq_\perp z}\frac{q_\parallel^2 m_e(\omega+i/\tau)}{2q_\perp}\int\frac{(e^{iq_\perp z'}+r^p e^{-iq_\perp z'})|\psi(z')|^2}{e^2\mathcal{N}|\psi(z')|^2-\varepsilon_0 m_e\omega(\omega+i/\tau)}dz',\tag{10.15}$$

where the relevant expression for $\mathcal{J}^{(3)}_{-\omega,z}(\vec{q}_\parallel)$ is taken from Eq. (10.9), (10.10), or (10.11). Given the *z*-component of the phase conjugated field, the *x*-component may be found from

$$E_{\mathrm{PC},x}(z;\vec{q}_\parallel) = \frac{q_\perp}{q_\parallel}E_{\mathrm{PC},z}(z;\vec{q}_\parallel),\tag{10.16}$$

which follows from the expression for the electromagnetic propagator, or equivalently from the demand that the phase conjugated field must be transverse in vacuum.

The integral in Eq. (10.15) is different from zero only in the region of the quantum well [from around $z'=-d$ to around $z'=0$ in the chosen coordinate system, the exact domain depending on the extent of the electronic wave function $\psi(z')$]. Since the width ($\sim d$) of a single-level metallic quantum well is in the Ångström range, and $q_\perp$ is typically in the micrometer range for optical signals such that $q_\perp d\ll 1$, it is a good approximation to put $\exp(\pm iq_\perp z')=1$ in Eq. (10.15). For electromagnetic frequencies so high that $q_\perp\sim d^{-1}$, the present theory would anyway be too simple to rely on [the Bloch function character of the wave functions along the surface and excitation to the continuum (photoemission) should be incorporated at least]. With the above-mentioned approximation, Eq. (10.15) is reduced to

$$E_{\mathrm{PC},z}(z;\vec{q}_\parallel) = \mathcal{J}^{(3)}_{-\omega,z}(\vec{q}_\parallel)e^{-iq_\perp z}\frac{(1+r^p)q_\parallel^2}{2\varepsilon_0\omega q_\perp}\int\frac{|\psi(z')|^2}{\gamma|\psi(z')|^2-1}dz',\tag{10.17}$$

where $\gamma = e^2 \mathcal{N}/[\varepsilon_0 m_e \omega(\omega + i/\tau)]$. Using the approximation $\exp(iq_\perp z') = 1$ and the normalization condition on $\psi(z')$, Eqs. (10.9)–(10.11) are reduced to

$$\mathcal{J}^{(3)}_{-\omega,z}(\vec{q}_\parallel) = \frac{e^4}{2^8 \pi^6 i \hbar \omega^3 m_e^2} \left[C(q_\parallel - k_\parallel) + C(q_\parallel + k_\parallel) \right] E_z^{(1)} E_z^{(2)} E_z^*, \tag{10.18}$$

$$\mathcal{J}^{(3)}_{-\omega,z}(\vec{q}_\parallel) = \frac{e^4}{2^8 \pi^6 i \hbar \omega^3 m_e^2} \left[C(q_\parallel + k_\parallel) + \frac{\hbar}{4m_e} \mathcal{D}(\vec{q}_\parallel, -\vec{k}_\parallel) \right] E_y^{(1)} E_z^{(2)} E_y^*, \tag{10.19}$$

and

$$\mathcal{J}^{(3)}_{-\omega,z}(\vec{q}_\parallel) = \frac{e^4}{2^8 \pi^6 i \hbar \omega^3 m_e^2} \left[C(q_\parallel - k_\parallel) + \frac{\hbar}{4m_e} \mathcal{D}(q_\parallel, k_\parallel) \right] E_z^{(1)} E_y^{(2)} E_y^*, \tag{10.20}$$

respectively.

Thus the phase conjugated field from a single-level quantum well is described in the mixed Fourier space by Eq. (10.17) with insertion of Eq. (10.18), (10.19), or (10.20), the expressions for C [Eq. (10.5)] and $\mathcal{D}$ [Eq. (10.6)] carrying the information on the two-dimensional electron dynamics.

So far, the description of the phase conjugated response has been independent of the actual wave functions in the active medium, and thus independent of the form of the quantum well potential. In order to prepare our theory for a numerical study we now introduce a model potential in our quantum well system, namely the infinite barrier potential.

10.4 Infinite barrier model

To achieve a qualitative impression of the phase conjugation from a single-level metallic quantum well it is sufficient to carry out numerical calculations on the basis of the simple infinite barrier (IB) model. In this model the one-dimensional potential $V(z)$ is taken to be zero in the interval $-d \leq z \leq 0$ (inside the quantum well) and infinite elsewhere. The stationary state wave function now is given by $\psi(z) = \sqrt{2/d} \sin(\pi z/d)$ inside the well and $\psi(z) = 0$ outside, and the associated energy is $\varepsilon = (\pi \hbar)^2/(2m_e d^2)$. In the IB model the number of bound states is of course infinite, and to use this model in the context of a single level calculation, one must be sure that only one of the bound states (the ground state) has an energy below the Fermi energy, and that the optical frequency is so low that interlevel excitations are negligible.

For a metallic quantum well one may even at room temperature approximate the Fermi-Dirac distribution function appearing in the expressions for C, $\mathcal{D}$, and $\mathcal{N}$ in Eqs. (10.5), (10.6), and (10.13) by its value at zero temperature, i.e.,

$$\lim_{T \to 0} f(\vec{\kappa}_\parallel) = \Theta \left\{ \mathcal{E}_F - \frac{\hbar^2}{2m_e} \left[\left(\frac{\pi}{d}\right)^2 + \kappa_\parallel^2 \right] \right\}, \tag{10.21}$$

where Θ is the Heaviside step function and $\mathcal{E}_F$ is the Fermi energy of the system. In the low temperature limit it is possible to find analytical solutions to the integrals over

$\vec{\kappa}_{\parallel}$ appearing in Eqs. (10.5) and (10.6). This is adequately achieved by performing a co-ordinate transformation into cylindrical coordinates, since each Heaviside step function gives nonzero values in the κ_x-κ_y-space only inside a circle with radius, say, α. The explicit calculations are tedious but trivial to carry out, and since the final expressions for $\mathcal{C}$ and $\mathcal{D}$ are rather long we do not present them here. For the interested reader these calculations are reproduced in Appendices B and C [specifically, Section C.11].

The Fermi energy is calculated from the global charge neutrality condition [see Keller (1996a) and the calculation performed in Appendix D], which for a single level quantum well takes the form

$$\mathcal{N} = ZN_+d, \tag{10.22}$$

where N_+ is the number of positive ions per unit volume and Z is the valence of these ions. Since $\mathcal{N} = m_e(\mathcal{E}_F - \varepsilon)/(\pi\hbar^2)$, cf. the calculation in the Section C.11, one gets

$$\mathcal{E}_F = \frac{\pi\hbar^2}{m_e}\left[ZN_+d + \frac{\pi}{2d^2}\right]. \tag{10.23}$$

In order that just the ground state (energy ε) has an energy less than the Fermi energy, the film thickness must be less than a certain maximum value $d_{\max}$. When the thickness of the well becomes so large that the Fermi energy equals the energy $\varepsilon_2 = (2\pi\hbar)^2/(2m_ed^2)$ of the first excited state a second bound state of energy less than $\mathcal{E}_F$ will appear. From the condition $\mathcal{E}_F(d_{\max}) = \varepsilon_2(d_{\max})$, $d_{\max}$ can be calculated, and one gets by means of Eq. (10.23)

$$d_{\max} = \sqrt[3]{3\pi/(2ZN_+)}, \tag{10.24}$$

i.e., a result which depends on the number of conduction electrons in the film. The minimum thickness is in the IB model zero, but in reality the smallest thickness is a single monolayer.

Inserting the IB model into the integral over the source region appearing in Eq. (10.17) we get

$$\int \frac{|\psi(z')|^2}{\gamma|\psi(z')|^2 - 1}dz' = \int_{-d}^{0} \frac{2\sin^2(\pi z'/d)}{2\gamma\sin^2(\pi z'/d) - d}dz', \tag{10.25}$$

which by substitution of $\theta = \pi z'/d$, addition and subtraction of d in the nominator of the integral, and use of $2\gamma\sin^2\theta - d = 2\gamma[\sqrt{1 - d/(2\gamma)} - \cos\theta][\sqrt{1 - d/(2\gamma)} + \cos\theta]$ gives

$$\frac{d}{\pi\gamma}\left[\pi - \frac{d}{4\gamma}\frac{1}{\sqrt{1 - d/(2\gamma)}}\int_0^{2\pi}\frac{d\theta}{\sqrt{1 - d/(2\gamma)} + \cos\theta}\right] = \frac{d}{\gamma}\left[1 - \frac{1}{\sqrt{2\gamma/d - 1}}\right] \approx \frac{d}{\gamma}. \tag{10.26}$$

The solution to the integral in Eq. (10.26) is obtained by use of Eq. (B.32), and since $2|\gamma|/d \gg 1$ [for metals, $|\gamma|$ lies typically between 1 and 100 in the optical region (e.g., for copper $|\gamma| \approx 85$ in the present study) and d is in the Ångström range]. Using this result

and the expression for the Fermi energy given in Eq. (10.23), we obtain by insertion into Eq. (10.17) the result

$$
E_{\text{PC},z}(z;\vec{q}_{\parallel}) = \frac{q_{\parallel}^2 m_e(\omega + \text{i}/\tau)(1 + r^p)}{2q_{\perp}e^2 Z N_+} \mathcal{I}^{(3)}_{-\omega,z}(\vec{q}_{\parallel}) e^{-\text{i}q_{\perp}z}. \tag{10.27}
$$

By insertion of the relevant expressions for $\mathcal{I}^{(3)}_{-\omega,z}(\vec{q}_{\parallel})$ we finally obtain the following results for the z-component of the phase conjugated field outside the quantum well:

$$
\begin{aligned}
E_{\text{PC},z}(z;\vec{q}_{\parallel}) = {} & \frac{e^2(\omega + \text{i}/\tau)(1 + r^p)}{2^9 \pi^6 \hbar \omega^3 Z N_+ m_e} \frac{q_{\parallel}^2}{\text{i}q_{\perp}} \left[C(q_{\parallel} - k_{\parallel}) + C(q_{\parallel} + k_{\parallel}) \right] \\
& \times E_z^{(1)} E_z^{(2)} E_z^* e^{-\text{i}q_{\perp}z},
\end{aligned} \tag{10.28}
$$

for the purely p-polarized configuration, and

$$
\begin{aligned}
E_{\text{PC},z}(z;\vec{q}_{\parallel}) = {} & \frac{e^2(\omega + \text{i}/\tau)(1 + r^p)}{2^9 \pi^6 \hbar \omega^3 Z N_+ m_e} \frac{q_{\parallel}^2}{\text{i}q_{\perp}} \left[C(q_{\parallel} + k_{\parallel}) + \frac{\hbar}{4m_e} \mathcal{D}(q_{\parallel}, -k_{\parallel}) \right] \\
& \times E_y^{(1)} E_z^{(2)} E_y^* e^{-\text{i}q_{\perp}z},
\end{aligned} \tag{10.29}
$$

$$
\begin{aligned}
E_{\text{PC},z}(z;\vec{q}_{\parallel}) = {} & \frac{e^2(\omega + \text{i}/\tau)(1 + r^p)}{2^9 \pi^6 \hbar \omega^3 Z N_+ m_e} \frac{q_{\parallel}^2}{\text{i}q_{\perp}} \left[C(q_{\parallel} - k_{\parallel}) + \frac{\hbar}{4m_e} \mathcal{D}(q_{\parallel}, k_{\parallel}) \right] \\
& \times E_z^{(1)} E_y^{(2)} E_y^* e^{-\text{i}q_{\perp}z}
\end{aligned} \tag{10.30}
$$

for the configurations with mixed polarization of the pump fields. The x-component of the phase conjugated field is obtained using Eq. (10.16).

Chapter 11

The theoretical description presented in the previous chapter resulted in expressions for the phase conjugated field from a single level quantum well. Thus for the numerical work, the phase conjugated field is given completely by Eqs. (10.28)–(10.30) and (10.16) with the insertion of the expressions for the electron dynamics parallel to the surface plane, given by Eqs. (C.179)–(C.180) in Appendix C. In the following we will present the phase conjugation reflection coefficient, succeeded by a discussion of a possible excitation scheme which might be adequate for studies of phase conjugation of optical near fields (Bozhevolnyi, Keller, and Smolyaninov 1994).

11.1 Phase conjugation reflection coefficient

To estimate the amount of light we get back through the phase conjugated channel, we define the phase conjugation (energy) reflection coefficient as

$$R_{PC}(z; \vec{q}_{\parallel}) = \frac{I_{PC}(z; \vec{q}_{\parallel})}{I^{(1)} I^{(2)} I_{Probe}(-d; \vec{q}_{\parallel})}, \tag{11.1}$$

in which $I^{(1)}$, $I^{(2)}$, I_{Probe}, and I_{PC} are the intensities of the two pump beams, the probe and the phase conjugated field, respectively. Each of the intensities are given by

$$I = \frac{\varepsilon_0 c_0}{2} \frac{\vec{E} \cdot \vec{E}^*}{(2\pi)^4}, \tag{11.2}$$

where the factor of $(2\pi)^{-4}$ originates from the manner in which we have introduced the Fourier amplitudes of the fields. If the probe field is evanescent the intensity of the phase conjugated field, $I_{PC}(z; \vec{q}_{\parallel})$, will depend on the distance from the surface, and consequently the reflection coefficient is z-dependent in such a case.

For the remaining part of this work we choose a copper quantum well with $N_+ = 8.47 \times 10^{28} \text{m}^{-3}$ and $Z = 1$ [data taken from Ashcroft and Mermin (1976)]. Then from Eq. (10.24), the maximal thickness becomes $d_{max} = 3.82\text{Å}$, which is more than two monolayers and less than three. Thus we have two obvious choices for the thickness of the quantum well, namely a single monolayer or two monolayers. We thus take a look
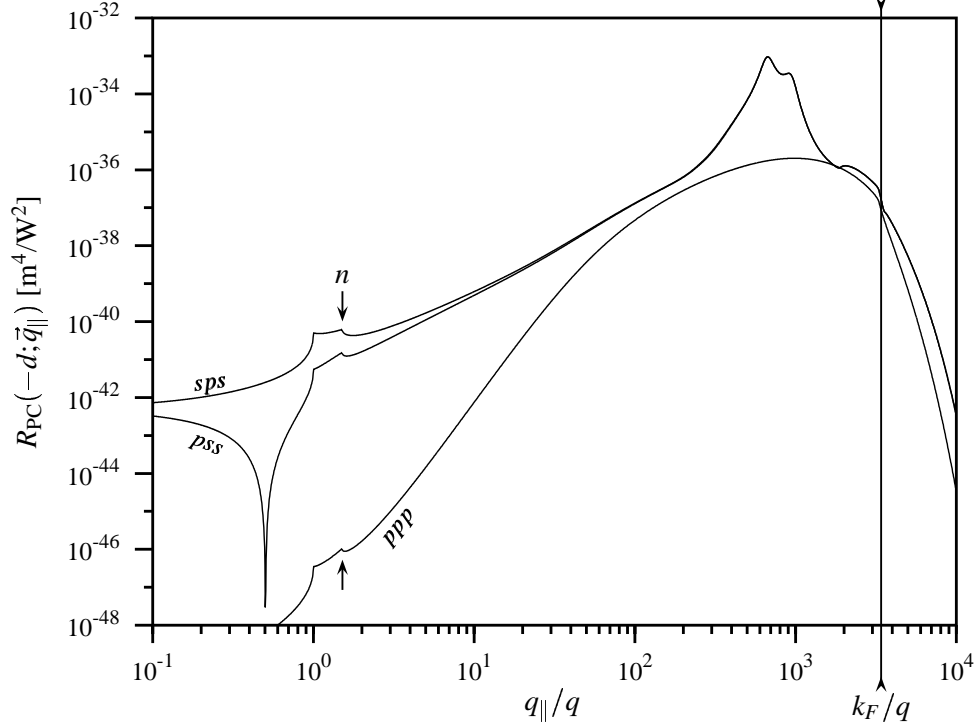
Figure 11.1: The phase conjugation reflection coefficient at the vacuum/film interface of a single monolayer copper quantum well, $R_{PC}(-d;\vec{q}_\parallel)$, is plotted for ($ppp$) the p to p transition (corresponding to diagram (a) in Fig. 10.1), (sps) one of the s to p transitions (corresponding to diagram (b) in Fig. 10.1), and (pss) the other s to p transition (corresponding to diagram (c) in Fig. 10.1), as a function of the normalized component of the probe wavevector along the interface, $q_\parallel/q$. The normalized Fermi wavenumber is indicated by the vertical line. It is for a single monolayer of copper $k_F/q = 3.38 \times 10^3$. The set of arrows labeled n are placed at $q_\parallel = nq$.

at both possibilities in the following, corresponding to a thickness of $d = 1.8\text{Å}$ for one monolayer and $d = 3.6\text{Å}$ for two monolayers. The Cu quantum well can adequately be deposited on a glass substrate for which we use a refractive index n of 1.51. With this substrate, a reasonable description of the linear vaccum/substrate amplitude reflection coefficient r^p is obtained by use of the classical Fresnel formula

$$r^p = \frac{n^2 q_\perp - (n^2 q^2 - q_\parallel^2)^{\frac{1}{2}}}{n^2 q_\perp + (n^2 q^2 - q_\parallel^2)^{\frac{1}{2}}}, \tag{11.3}$$

$q = \omega/c_0$ being the vacuum wavenumber, as before. Then, having the pump fields parallel to the x-axis gives a pump wavenumber $k_\parallel = 1.51q$. The wavelength λ of the light is chosen to be $\lambda = 1061\text{nm}$.

The phase conjugation reflection coefficient at the vacuum/film interface, $R_{PC}(-d;\vec{q}_\parallel)$ is plotted in Figs. 11.1 and 11.2 as a function of the parallel component ($q_\parallel$) of the
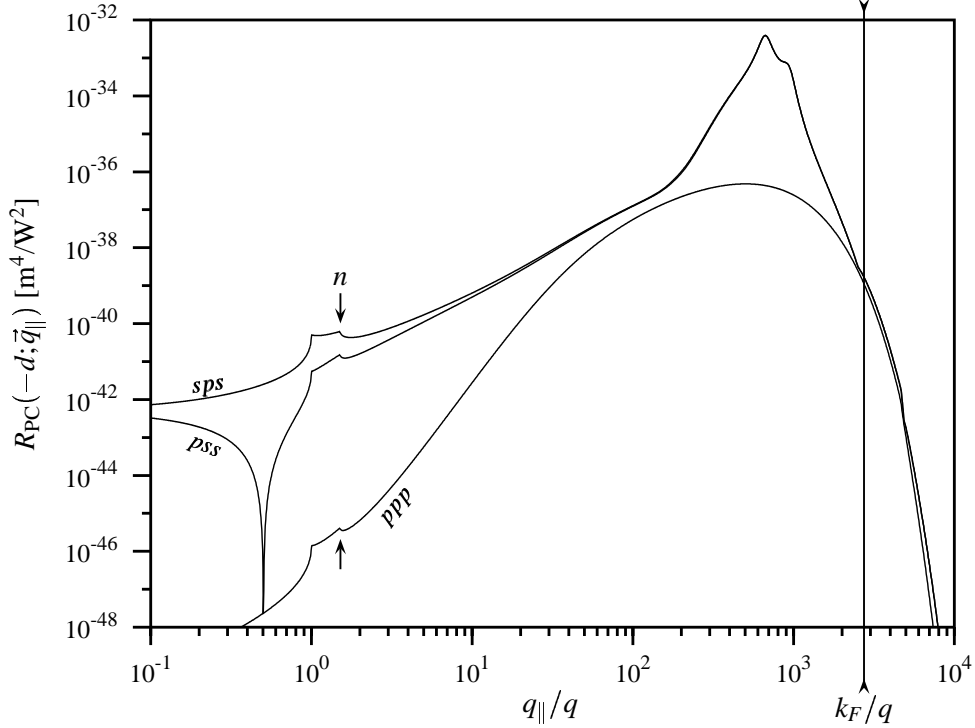
Figure 11.2: The phase conjugation reflection coefficient at the vacuum/film interface of a two-monolayer copper quantum well, $R_{PC}(-d; \vec{q}_{\parallel})$, is plotted for ($ppp$) the p to p transition (corresponding to diagram (a) in Fig. 10.1), (sps) one of the s to p transitions (corresponding to diagram (b) in Fig. 10.1), and (pss) the other s to p transition (corresponding to diagram (c) in Fig. 10.1), as a function of the normalized component of the probe wavevector along the interface, $q_{\parallel}/q$. The normalized Fermi wavenumber is indicated by the vertical line. For a two-monolayer copper film it is $k_F/q = 2.78 \times 10^3$. The set of arrows labeled n are placed at $q_{\parallel} = nq$.

wavevector for both the p to p transition and the two s to p transitions. The reason that the two curves for the s to p transitions appear the same in the high end of the $q_{\parallel}/q$ spectrum is due to the fact that for $k_{\parallel} \ll q_{\parallel}$ we have $C(q_{\parallel} - k_{\parallel}) \simeq C(q_{\parallel} + k_{\parallel})$ and $\mathcal{D}(q_{\parallel}, k_{\parallel}) \simeq \mathcal{D}(q_{\parallel}, -k_{\parallel})$. The "bubble" appearing on the sps and pss curves from around $q_{\parallel}/q \sim 100$ to $q_{\parallel}/q \sim k_F/q$ is due to the two-dimensional electron dynamics hidden in $\mathcal{D}(q_{\parallel}, k_{\parallel})$. To be a little more specific, the left of the two peaks stems from the second term, while the peak to the right in the bubble stems from the third term.

To illustrate the similarity between the two possible s to p transitions, we can take Eq. (10.29) to describe the phase conjugated field, which for positive values of $q_{\parallel}/q$ gives the result in Fig. 11.2 (sps). Using the other s to p transition, given by Eq. (10.30), instead we get the result in Fig. 11.2 (pss) for positive values of $q_{\parallel}/q$. The symmetry between the two configurations is obtained by looking at the negative values of $q_{\parallel}/q$, since Eq. (10.29) plotted for negative values of $q_{\parallel}/q$ gives the (pss) curve in Fig. 11.2.
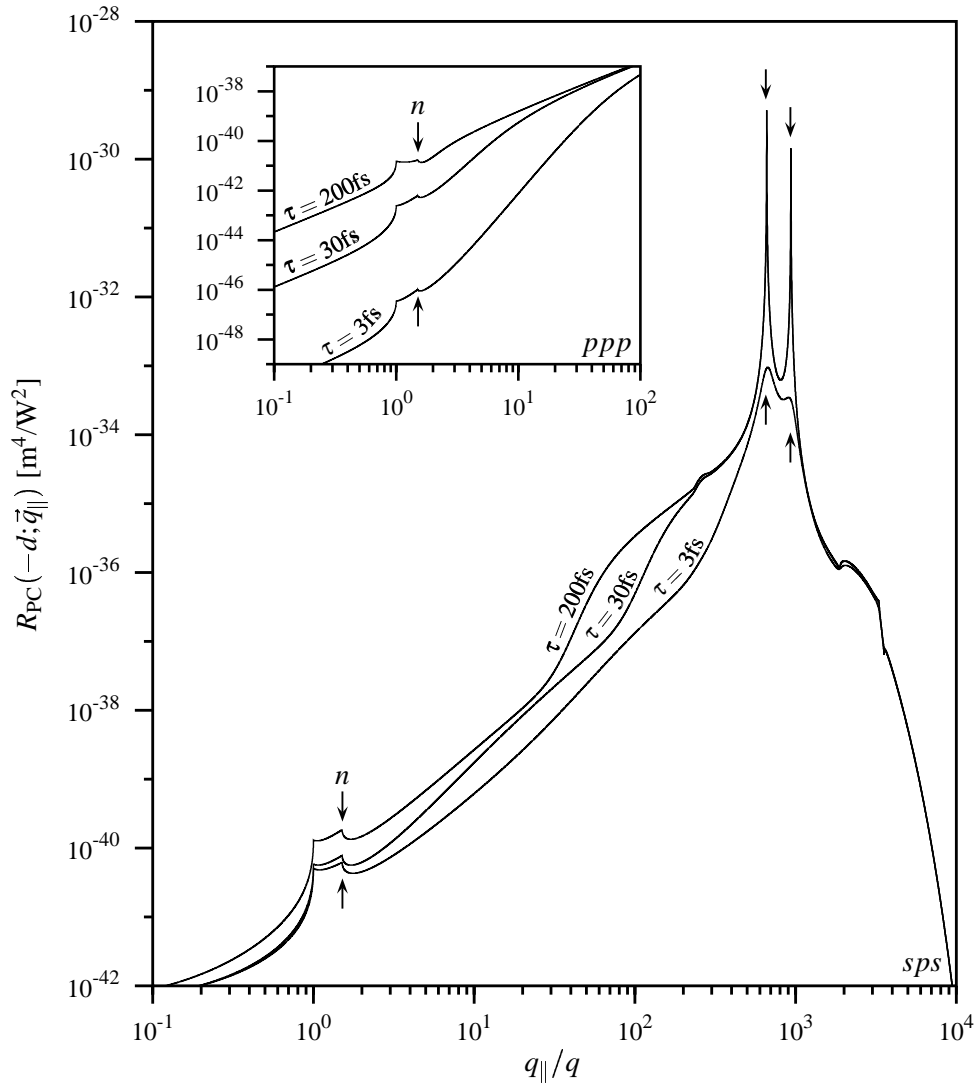
Figure 11.3: The phase conjugation reflection coefficient at the surface of the phase conjugator (single monolayer Cu film) is plotted for different values ($\tau \in \{200, 30, 3\}$ femtoseconds) of the relaxation time. The main figure shows the result for the *sps* configuration, while the inserted picture shows the *ppp* result. The two sets of arrows labeled *n* are placed at $q_{\parallel} = nq$. The other two sets of arrows are explained in the main text.

Similarly, by starting with Eq. (10.30), the resulting curve for negative values of $q_{\parallel}/q$ gives the (*sps*) result in Fig. 11.2.

The choice of an adequate relaxation time τ is a difficult problem and it appears from Figs. 11.3 and 11.4 that the value of the relaxation time has a great impact on the phase conjugation reflection coefficient. We have plotted the reflection coefficent for three val-
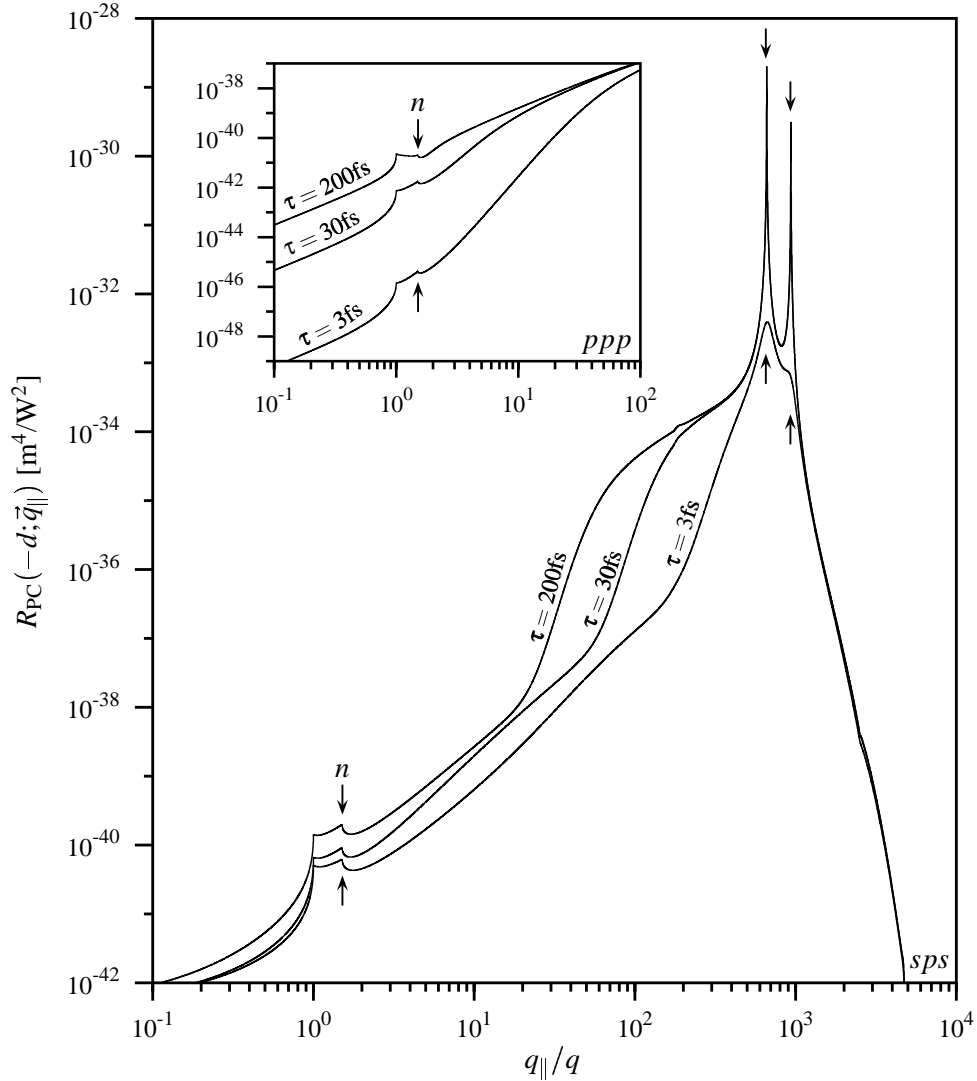
Figure 11.4: The phase conjugation reflection coefficient at the surface of the phase conjugator (two-monolayer Cu film) is plotted for different values ($\tau \in \{200, 30, 3\}$ femtoseconds) of the relaxation time. The main figure shows the result for the *sps* configuration, while the inserted picture shows the *ppp* result. The two sets of arrows labeled *n* are placed at $q_\parallel = nq$. The other two sets of arrows are explained in the main text.

ues of the relaxation time, namely (i) 30fs and (ii) 200fs, which are typical values one would find for bulk copper (Ashcroft and Mermin 1976) at (i) room temperature and (ii) at 77K, and (iii) 3fs. The value in case (iii) is obtained by a conjecture based on the difference between measured data for a lead quantum well (Jałochowski, Stróżak, and Zdyb 1997) and the bulk value for lead at room temperature. The difference be-

tween the relaxation time measured by Jalochowski, Strόżak, and Zdyb (1997) is for two monolayers approximately one order of magnitude. Based on the results of Jalochowski, Strόżak, and Zdyb (1997) we have for the data presented in this work chosen the value of the relaxation time to be 3fs. As it can be seen from Fig. 11.4, the bubble in the curve corresponding to the *sps* configuration appears earlier in the $q_{\parallel}/q$-spectrum for higher values of τ. For the *ppp* configuration the lower end of the spectrum is damped when τ becomes smaller.

So what is the difference between using a single monolayer or two monolayers in the quantum well? In the single monolayer quantum well, the distance between the occupied energy level and the first free energy level in the infinite barrier model, and between the occupied energy level and the continuum states in a finite barrier model is larger than for a two monolayer well. Thus the single-monolayer well should behave more ideally like a single-level quantum well at higher frequencies than the two-monolayer well. If we take a look at Figs. 11.1 and 11.2 we observe that the bubble in the *sps* and *pss* curves has the highest maximal magnitude for the two-monolayer well, and the earliest falloff in the high end of the $q_{\parallel}/q$-spectrum. The value of each of the two peaks in the bubble is reached at the same $q_{\parallel}/q$-value in the two cases, as is also evident from Figs. 11.3 and 11.4 (shown using a set of arrows for each peak). From these two figures we also observe that the relaxation-time dependent low-$q_{\parallel}/q$ beginning of the bubble occurs a little earlier and is increasing faster in the two-monolayer well compared to the other. In the low end of the $q_{\parallel}/q$-spectrum the *sps* and *pss* curves are of equal magnitude. Looking at the *ppp* curve, we observe that it is damped roughly by a factor of two in the low end of the $q_{\parallel}/q$-spectrum using a single-monolayer film in stead of two monolayers. In the high end it takes its maximal value for the single-monolayer well at rougly twice the value of $q_{\parallel}/q$ than for the two-monolayer film. In conclusion, the differences between the phase conjugated response for a single-monolayer film and a two-monolayer film will probably be very difficult, if not impossible, to observe in an experiment with single mode excitation. In the rest of this chapter we thus present results for the two-monolayer film only.

We have in Fig. 11.5 plotted the phase conjugation reflection coefficient for the *p* to *p* transition and one of the *s* to *p* transitions, respectively, for different distances from the surface of the phase conjugator. Due to our particular interest in the phase conjugation of the evanescent modes in the Fourier spectrum the chosen distances are fractions of the vacuum wavelength. In Fig. 11.6 we have plotted the part of the Fourier spectrum for all three configurations which is judged to be the most easily accessible to single-mode excitation in experimental investigations.

It appears from Fig. 11.5 (*ppp*) that the phase conjugation reflection coefficient is independent of the distance from the metal film in the region where $q_{\parallel}/q \leq 1$. This is so because the probe field, and hence also the phase conjugated field, are of propagating character ($q_{\perp} = [q^2 - q_{\parallel}^2]^{1/2}$ is real). In the region where $q_{\parallel}/q > 1$, both the probe field and the phase conjugated field are evanescent ($q_{\perp} = i[q_{\parallel}^2 - q^2]^{1/2}$ is a purely imaginary quantity), and in consequence the reflection coefficient decreases rapidly with the dis-
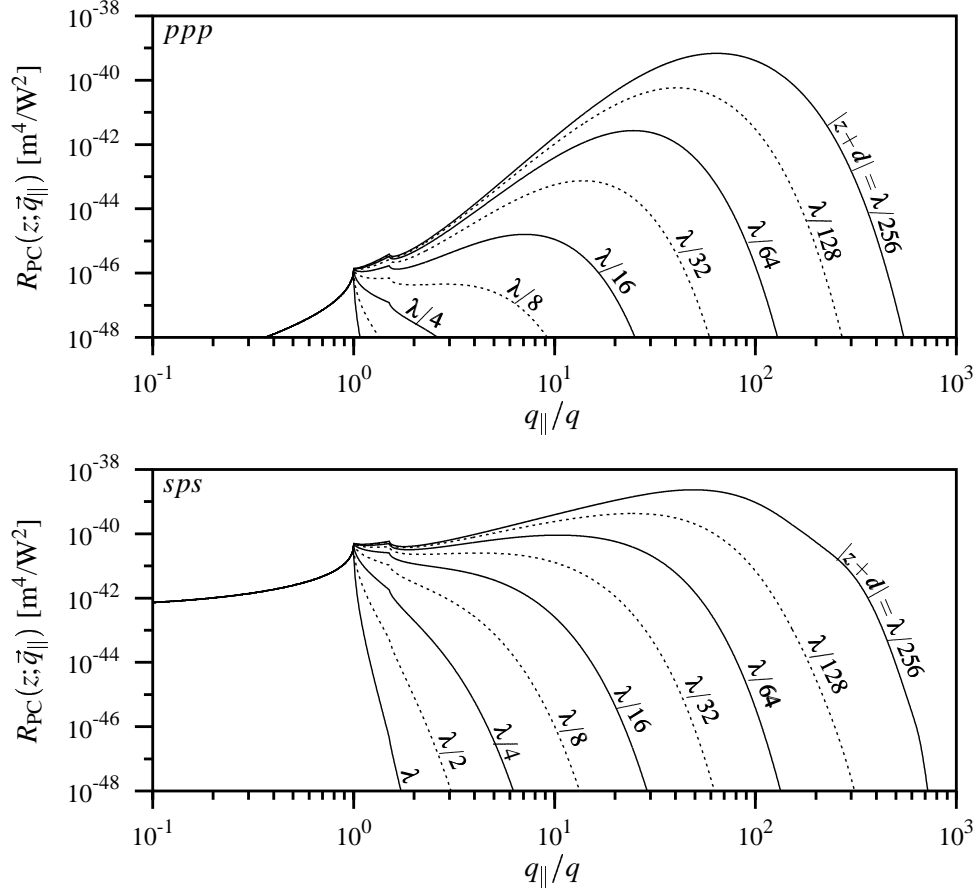
Figure 11.5: The $q_\parallel/q$-dependence of the phase conjugation reflection coefficient, $R_{PC}(z;\vec{q}_\parallel)$, is plotted at different distances $|z+d| \in \{\lambda,\lambda/2,\lambda/4,\lambda/8,\lambda/16,\lambda/32,\lambda/64,\lambda/128,\lambda/256\}$ from the vacuum/film interface. The upper figure shows the results for the p to p transition. The lower figure shows the results for the s to p transition which corresponds to configuration (b) in Fig. 10.1.

tance from the phase conjugator. Already a single wavelength away from the surface of the phase conjugator the evanescent modes of the phase conjugated field have essentially vanished and only propagating modes are detectable. Although the evanescent Fourier components of the phase conjugated field are present only less than an optical wavelength from the surface, this *does not* imply that the nonlinear mixing of the electromagnetic waves is less effective in the regime of the evanescent modes. It is in fact opposite, as may be seen for instance from Fig. 11.2. The maximum coupling for the p to p transition is obtained for $q_\parallel/q \simeq 500$, and in comparison with R_{PC} at $q_\parallel/q \simeq 1$, the maximum in R_{PC} is nine orders of magnitude larger, and seven, respectively eight orders of magnitude larger for the two s to p transitions, which have their maxima at around $q_\parallel/q \simeq 700$. As we observe from Fig. 11.5, as the distance from the film increases the

maximum value decreases and is shifted downwards in the $q_{\parallel}/q$ spectrum. But only when the distance from the phase conjugator becomes larger than $\sim \lambda/10$ (*ppp*) respectively $\sim \lambda/60$ (*sps*), the phase conjugated signal is largest at $q_{\parallel}/q \approx 1$.

The absolute value of the reflection coefficients may seem very small, but utilizing a high-power Nd:YAG laser with, say an energy of 100mJ per pulse available for each of the three incoming fields, a pulse (assumed square for simplicity) duration of 4ns and an interaction area of 25mm^2, the intensity of each of these fields will be in the order of 1TW/m^2, and the phase conjugated intensity lies between 100pW/m^2 and 1W/m^2 in the full range of $q_{\parallel}/q$ for which the reflection coefficient has been plotted in Fig. 11.5 (*ppp*), and between $1\mu\text{W/m}^2$ and 1kW/m^2 in relation to the data in Fig. 11.5 (*sps*).

In many theoretical studies of the properties of phase conjugated fields it is assumed that the phase conjugator is ideal (Hendriks and Nienhuis 1989; Agarwal and Gupta 1995; Keller 1996c). By this is meant that the phase conjugation reflection coefficient is independent of the angle of incidense of the (propagating) probe field (and maybe also of the state of polarization). In the present case, the ideal phase conjugator assumption is certainly not good. Prior to the observation that evanescent fields could be phase conjugated (Bozhevolnyi, Keller, and Smolyaninov 1994) it was often assumed in theory (Yariv 1982) that $R_{\text{PC}} = 0$ in the region $q_{\parallel}/q > 1$, and in later studies (Agarwal and Gupta 1995; Keller 1996c) it has been assumed that also the phase conjugation of evanescent waves is ideal, i.e., independent of $q_{\parallel}/q$ ($\gtrsim 1$). When it comes to the phase conjugation from quantum well systems our analysis indicates that use of an energy reflection coefficient independent of $q_{\parallel}/q$ in general is bad. Only at specific distances the ideal phase conjugator assumption might be justified, see, e.g., the results representing R_{PC} at $|z + d| = \lambda/8$ in Fig. 11.6. The kink in the reflection coefficient (which is most pronounced close to the metal/vacuum interface) found at $q_{\parallel}/q = n$ ($= 1.51$) appears when the probe field changes from being propagating to being evanescent inside the substrate.

Above we have discussed the nonlinear reflection coefficient for the *p* to *p* configuration. It appears from Figs. 11.5 and 11.6 that the quantitative picture is the same for the *s* to *p* cases, though the reflection coefficient for the *s* to *p* transitions roughly speaking are five orders of magnitude larger in the experimentally most adequate evanescent region of the Fourier spectrum ($1 \leq q_{\parallel}/q \lesssim 2.5$) for single mode excitation.

The IB model only offers a crude description of the electronic properties of a quantum well. Among other things, the electron density profile at the ion/vacuum edge is poorly accounted for in this model, which gives too sharp a profile and underestimates the spill-out of the wave function. Altogether one should be careful to put too much reality into the IB model when treating local-field variations (related to, say, $q_{\parallel}$ or $q_{\perp}$) on the atomic length scale. Also the neclect of the Bloch character of the wave functions accounting for the dynamics in the plane of the well is doubtful in investigations of the local field among the atoms of the quantum well. The crucial quantity in the above-mentioned context is the Fermi wavenumber $k_F = (2m_e \mathcal{E}_F)^{1/2}/\hbar$, and in relation to Fig. 11.5, only
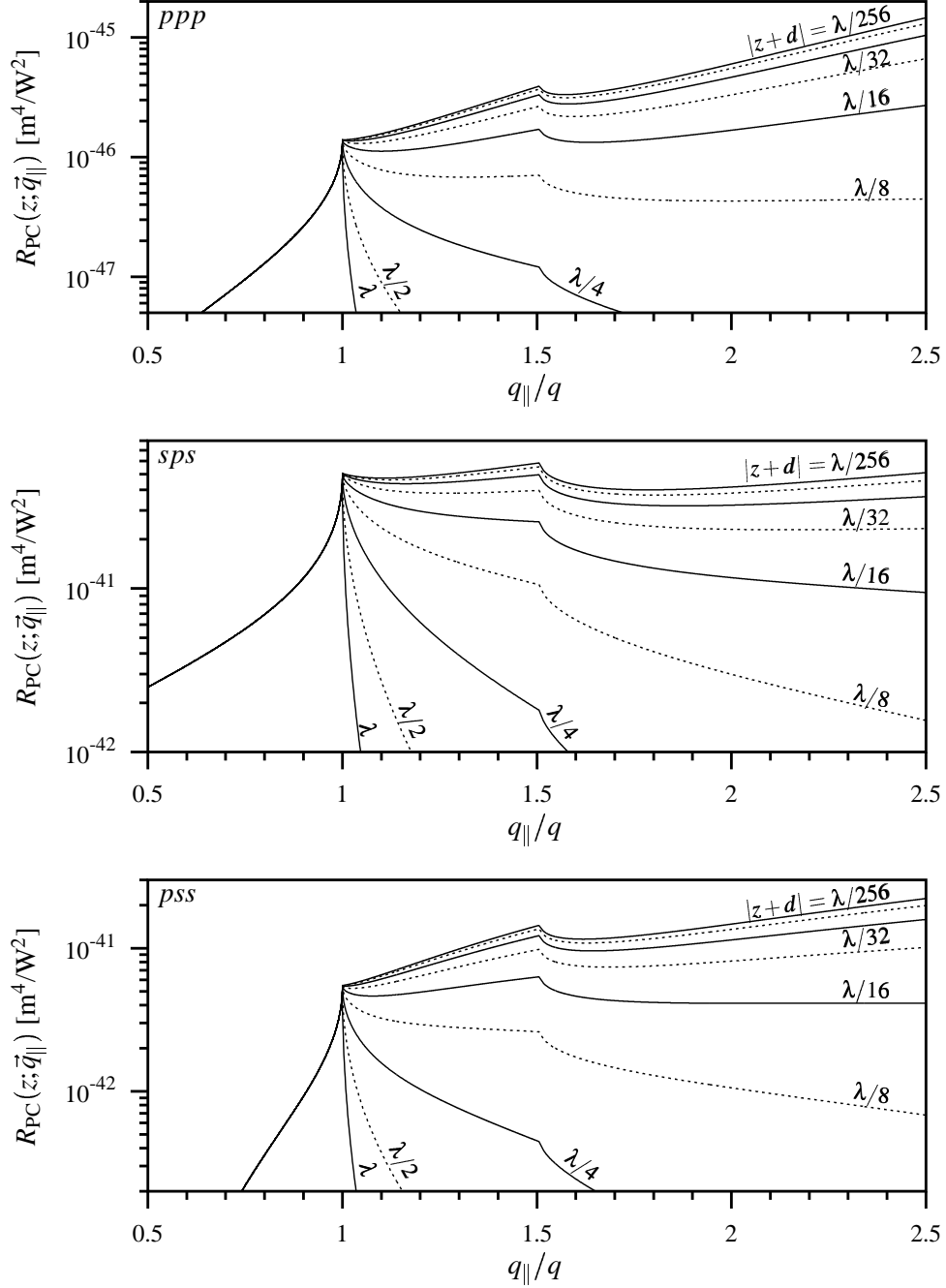
Figure 11.6: The phase conjugation reflection coefficient, $R_{PC}(z; \vec{q}_\parallel)$, is plotted at different distances $|z + d| \in \{\lambda, \lambda/2, \lambda/4, \lambda/8, \lambda/16, \lambda/32, \lambda/64, \lambda/128, \lambda/256\}$ from the vacuum/film interface as a function of the normalized probe wave number $q_\parallel/q$. Results for a two-monolayer thick quantum-well phase conjugator are here shown for the three polarization combinations ppp, sps, and pss in the range where we expect single mode excitation to be experimentally feasible.

results for $q_\parallel/q$ ratios less than approximately

$$\frac{k_F}{q} = \lambda\sqrt{\frac{ZN_+d}{2\pi} + \frac{1}{4d^2}}, \tag{11.4}$$

appears reliable. Insertion of the appropriate values for copper: $ZN_+ = 8.47 \times 10^{28}$, $d = 1.8\text{Å}$ (single monolayer film) or $d = 3.6\text{Å}$ (two-monolayer film), and the wavelength $\lambda = 1061\text{nm}$ gives $k_F = 3.38 \times 10^3 q$ for a single monolayer of copper, and $k_F = 2.76 \times 10^3 q$ for two monolayers of copper, respectively. The data presented in Fig. 11.5 should therefore be well within this limit of our model.

Returning to the curve in Fig. 11.5 (ppp) which represents the reflection coefficient closest to the surface of the phase conjugator ($|z+d| = \lambda/256$) one finds approximately a relation of the form $R_{PC} = b(q_\parallel/q)^a$ with $a \simeq 5$ in the lower wavenumber end of the evanescent region. The falloff of R_{PC} with $q_\parallel/q$ after the maximum (located at $q_\parallel/q \sim 50$) is much stronger than the increase towards the maximum. As the distance from the phase conjugator is increased the value of a gradually decreases. In Fig. 11.5 (b) we observe a similar behaviour, but this time the value of a in the approximate relation in the low end of the evanescent part of the Fourier spectrum is smaller, namely $a \simeq 1.5$.

The energy reflection coefficient calculated at the vacuum/quantum well interface, $R_{PC}(-d; \vec{q}_\parallel)$, characterizes the effectiveness with which a given ($q_\parallel$) plane-wave probe field (propagating or evanescent) may be phase conjugated, and the results presented in Fig. 11.2 indicate that this effectiveness (nonlinear coupling) is particularly large for (part of the) evanescent modes. The maximum in the effectivity is reached for a value of $q_\parallel/q$ as large as ~ 500–700. The strong coupling in part of the evanescent region does not necessarily reflect itself in any easy manner experimentally. First of all, one must realize that the strong coupling effect only may be observed close to the quantum well, i.e., at distances $z \lesssim \lambda$. Secondly, one must be able to produce evanescent probe fields with relatively large values of $q_\parallel/q$. This is in itself by no means simple outside the range when the standard Otto (1968, 1976) [or possibly Kretschmann (Kretschmann and Raether 1968; Raether 1988)] techniques can be adopted. Roughly speaking, this range coincides with the ones shown in Fig. 11.6. To create probe fields with larger $q_\parallel/q$ values other kinds of experimental techniques must be used, and in the following we shall consider a particular example and in a qualitative manner discuss the resulting Fourier spectrum of the phase conjugated field.

11.2 Phase conjugated response using a wire source

In near-field optics evanescent fields with relatively large values of $q_\parallel/q$ are produced by various methods, all aiming at compressing the source field to subwavelength spatial extension [see, e.g., Pohl and Courjon (1993) and Nieto-Vesperinas and García (1996)]. From a theoretical point of view the radiation from a subwavelength source may in some cases be modelled by the radiation from an (electric) point-dipole source, or an assembly of such sources. It is a straightforward matter to decompose an electric point-dipole field

into its relevant evanescent and propagating modes, and thereby estimate the intensity of the phase conjugated field in each of the $q_\parallel$-components. However, in order to determine the characteristics of the phase conjugated light focus generated by the quantum well one would have to calculate the four-wave mixing also for probe fields with wavevectors not confined to the x-z-plane, and to do this our theory must first be generalized to non-planar phase conjugation.

Within the framework of the present theory, it is possible, however, to study the spatial confinement (focusing) of the phase conjugated field generated by a quantum wire adequately placed above the surface of the quantum well (Keller 1998), and let us therefore as an example consider the case where the source of the probe field is a (quantum) wire. We imagine that the axis of the wire is placed parallel to the y-axis and cuts the x-z-plane in the point $(0, -z_0)$, cf. Fig. 8.1. Under the assumption that the spatial electron confinement in the wire is perfect (complete) and the wire current density is the same all along the wire at a given time, the harmonic source current density is given by

$$\vec{J}(\vec{r};\omega) = \vec{J}_0(\omega)\delta(x)\delta(z+z_0), \tag{11.5}$$

where $\vec{J}_0(\omega)$ is its possibly frequency dependent vectorial amplitude. The spatial distribution of the field from this source is

$$\vec{E}(x,z;\omega) = \frac{1}{(2\pi)^2}\int_{-\infty}^{\infty}\vec{E}(z;\vec{q}_\parallel,\omega)e^{i\vec{q}_\parallel\cdot\vec{r}}\delta(q_{\parallel,y})d^2q_\parallel,$$

$$= \frac{1}{(2\pi)^2}\int_{-\infty}^{\infty}\vec{E}(z;\vec{q}_\parallel,\omega)e^{iq_\parallel x}dq_\parallel, \tag{11.6}$$

where

$$\vec{E}(z;\vec{q}_\parallel,\omega) = -\frac{e^{iq_\perp(z+z_0)}}{2\varepsilon_0\omega q_\perp}\begin{bmatrix} q_\perp^2 & 0 & -q_\parallel q_\perp \\ 0 & q^2 & 0 \\ -q_\parallel q_\perp & 0 & q_\parallel^2 \end{bmatrix}\cdot\vec{J}_0(\omega), \tag{11.7}$$

where as hitherto $q_\parallel^2 + q_\perp^2 = q^2$. At the phase conjugating mirror, the Fourier components of the wire probe are $\vec{E}(-d;\vec{q}_\parallel,\omega)$.

To illustrate the angular spectral distribution of the field from this kind of wire source at the phase conjugator, we look closer at the cases, where (i) the current density is polarized along the x-axis, and (ii) along the y-axis. Thus, in case (i) we use $\vec{J}_0(\omega) = J_0(\omega)\vec{e}_x$, and by normalizing the electric fields to the amplitude of the current density, the corresponding normalized differential intensity $[\Delta I_{\text{Probe}} \equiv \frac{1}{2}\varepsilon_0c_0\vec{E}(-d;\vec{q}_\parallel,\omega)\cdot\vec{E}^*(-d;\vec{q}_\parallel,\omega)/(2\pi)^4]$ becomes

$$\frac{\Delta I_{\text{Probe}}(-d;\vec{q}_\parallel)}{|J_0(\omega)|^2} = \frac{1}{2^7\pi^4\varepsilon_0c_0}\left\{\Theta\left(1-(q_\parallel/q)\right) + \Theta\left((q_\parallel/q)-1\right)\left[2(q_\parallel/q)^2-1\right]\right.$$

$$\left.\times\exp\left(-2(z_0-d)q\sqrt{(q_\parallel/q)^2-1}\right)\right\} \tag{11.8}$$
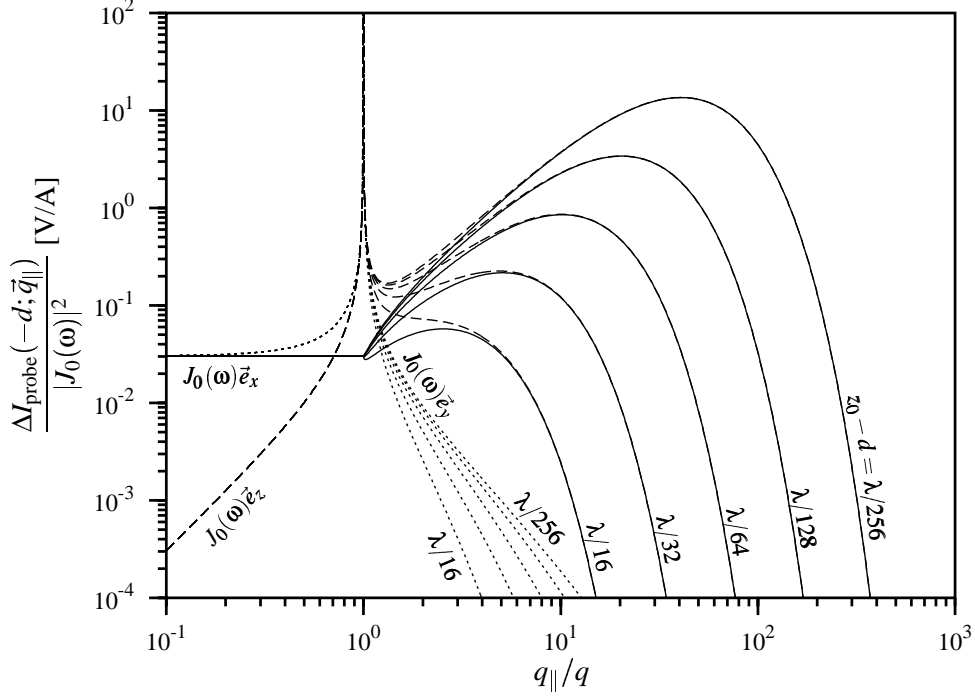
Figure 11.7: The angular Fourier spectrum reaching the surface of the phase conjugating medium when the probe field is radiated from a (quantum) wire. The dotted curves ($J_0(\omega)\vec{e}_y$) show the Fourier components when the wire current density is polarized along the y axis. Similarly, the dashed curves ($J_0(\omega)\vec{e}_z$) and the fully drawn curves ($J_0(\omega)\vec{e}_x$) show the Fourier components from a wire source with its current density oscillating along the z-axis and the x-axis, respectively. The angular Fourier spectrum is for all three cases shown for five different distances $z_0 - d \in \{\lambda/16, \lambda/32, \lambda/64, \lambda/128, \lambda/256\}$ of the wire from the phase conjugator.

is shown in Fig. 11.7 for different values of the distance $z_0 - d$ from the wire to the vacuum/film interface. In case (ii), $\vec{J}_0(\omega) = J_0(\omega)\vec{e}_y$, and the associated normalized intensity which is given by

$$\frac{\Delta I_{\text{Probe}}(-d;\vec{q}_\parallel)}{|J_0(\omega)|^2} = \frac{1}{2^7\pi^4\varepsilon_0 c_0} \left\{ \frac{\Theta\left(1-(q_\parallel/q)\right)}{1-(q_\parallel/q)^2} + \frac{\Theta\left((q_\parallel/q)-1\right)}{(q_\parallel/q)^2-1} \right.$$
$$\left. \times \exp\left(-2(z_0-d)q\sqrt{(q_\parallel/q)^2-1}\right) \right\}, \tag{11.9}$$

is also presented in Fig. 11.7, for the same distances as in case (i). The third curve in Fig. 11.7 represents the case where $\vec{J}_0(\omega) = J_0(\omega)\vec{e}_z$, and is shown for reference.

Looking at the curve in Fig. 11.7 corresponding to $\vec{J}_0(\omega) = J_0(\omega)\vec{e}_y$ (and the curve corresponding to $\vec{J}_0(\omega) = J_0(\omega)\vec{e}_z$), we notice that a singularity occurs when $q_\parallel/q = 1$, or equivalently where $q_\perp = 0$. The presence of this singularity is an artifact originating in the (model) assumption that the electron confinement is complete in the x- and

z-directions (see Eq. (11.5)). If we had started from a quantum wire current density of finite (but small) extension in x and z the singularity would have been replaced by a (narrow) peak of finite height. Not only in quantum wire optics, but also in optical studies of quantum dots and wells singularities would appear if complete electron confinement was assumed (in 3D and 1D, respectively). In the present context the assumption of perfect electron confinement works well because we only consider the generated field outside the self-field region of the wire [see, e.g., Keller (1997b)]. In an experiment one would always end up integrating over some finite interval of $q_\parallel$ around the singularity, and this integral can in all cases be proven finite. At each distance of the wire from the phase conjugator the two curves $J_0\vec{e}_x$ and $J_0\vec{e}_z$ in Fig. 11.7 becomes identical when $(q_\parallel/q)^2 \gg 1$, since from Eq. (11.7) we may draw the relation $E_z = -(q_\parallel/q_\perp)E_x$, and since $q_\parallel/q_\perp \simeq 1$ when $(q_\parallel/q)^2 \gg 1$.

When the current oscillates in the direction of the wire, it appears that the field intensity in the evanescent probe modes is very small. An appreciable amount of the radiated energy is stored in components in the region $q_\parallel/q \sim 1$ (and in the propagating modes). To study the phase conjugation of evanescent modes it is therefore better to start from $\vec{J}_0(\omega) = J_0(\omega)\vec{e}_x$ or from $\vec{J}_0(\omega) = J_0(\omega)\vec{e}_z$ because these two probe current densities give rise to significant probe intensities in the evanescent regime. If we look at the curve in Fig. 11.7 representing the field at the surface of the phase conjugator when the probe is placed at $z_0 - d = \lambda/256$, I_{Probe} peaks in both these cases at $q_\parallel/q \sim 50$ in the evanescent regime. When the current density oscillates along the surface (in the x-direction) there is no singularity (and no peak) at $q_\parallel/q \sim 1$, and the maximum value of I_{Probe}, occuring at $q_\parallel/q \sim 50$, is three orders of magnitude larger than the probe intensities of every one of the propagating modes. Above $q_\parallel/q \approx 50$ the amplitude of the $q_\parallel$ components descends rapidly and has lost six orders of magnitude within the next order of magnitude of $q_\parallel/q$. At larger probe to surface distances the maximum in the $q_\parallel/q$ spectrum of the probe field at the vacuum/film interface is shifted downwards, and the magnitude becomes smaller, too. That is, compared to the raw p to p reflection coefficient, the intensity of each of the Fourier components available from the probe field begin their own falloff about one to two orders of magnitude before the reflection coefficient descends, depending on the distance from the probe to the surface of the phase conjugator. The s-polarized probe field starts the descending tendency already where the character of the Fourier components shifts from being propagating to evanescent ($q_\perp$ becoming imaginary), cf. the remarks above.

Using a quantum wire as the source for the probe field, the angular spectrum of the phase conjugated response, normalized to the pump fields and the absolute square of the amplitude of the wire current density, is given by

$$R_{\text{PC}}(z;\vec{q}_\parallel)\frac{I_{\text{Probe}}(-d;\vec{q}_\parallel)}{|J_0(\omega)|^2} = \frac{I_{\text{PC}}(z;\vec{q}_\parallel)}{I^{(1)}I^{(2)}|J_0(\omega)|^2}, \qquad (11.10)$$

and is obtained numerically by multiplying the energy reflection coefficient, $R_{\text{PC}}(z;\vec{q}_\parallel)$, with the normalized probe intensity, $I_{\text{Probe}}(-d;\vec{q}_\parallel)/|J_0(\omega)|^2$. In Fig. 11.8, the angular spectrum at the vacuum/quantum-well interface ($z = -d$) given by Eq. (11.10) is shown
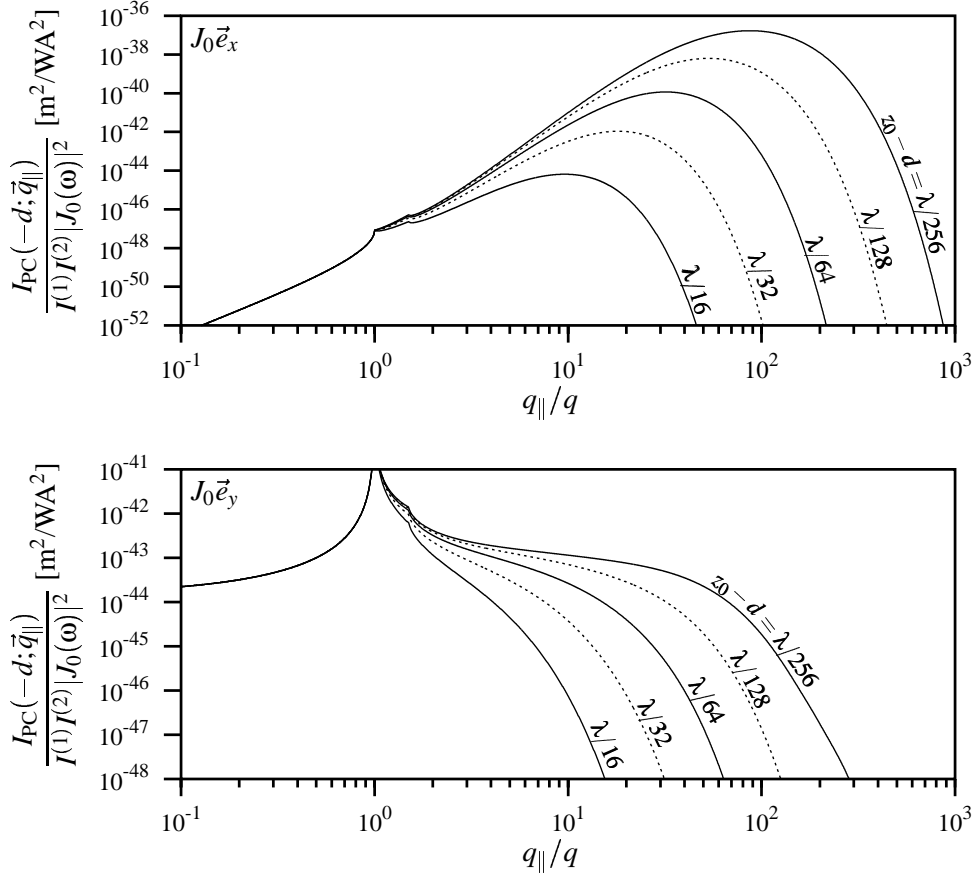
Figure 11.8: The convolution of the probe field from a wire source with the phase conjugation reflection coefficient at the vacuum/film interface is shown for different distances between the wire source and the vacuum/film interface, namely $z_0 - d \in \{\lambda/16, \lambda/32, \lambda/64, \lambda/128, \lambda/256\}$ as a function of the normalized probe wavenumber $q_{\parallel}/q$. In the top figure the current density of the wire oscillates along the x-axis, and in the bottom figure along the y-axis.

for the cases where $\vec{J}_0(\omega) = J_0(\omega)\vec{e}_x$ and $\vec{J}_0(\omega) = J_0(\omega)\vec{e}_y$. It is plotted for the two-monolayer film, but since the main contribution is in the low end of the $q_{\parallel}/q$-spectrum, the similar curves for the single-monolayer film would be indistinguishable from the ones plotted (apart from a factor of two in the ppp case). In both cases data are presented for the wire placed at different distances from the vacuum/film interface. By comparison with the raw reflection data in Fig. 11.2 it appears that the high end of the reflected $q_{\parallel}$-spectrum is strongly damped. For the s to p transition we see that the energy of the phase conjugated signal is concentrated around $q_{\parallel}/q = 1$, which is mainly due to the fact that the concentration of the radiated energy spectrum from the wire lies around that same point. In the p to p transition the evanescent components are still by far dominating the response at the place of the wire compared to the propagating components.

Chapter 12

Two-dimensional confinement of light
in front of a single-level quantum-well phase conjugator

The possibility of compressing light in space to a degree (much) better than predictable by classical diffraction theory has gained widespread attention only with the birth of near-field optics (Pohl and Courjon 1993; Nieto-Vesperinas and García 1996).

As stated in Chapter 1, sub-wavelength electrodynamics was discussed only sporadically until near-field optics evolved in the mid-eighties in the wake of the experimental works by the groups of Pohl, Lewis, and Fischer (Pohl, Denk, and Lanz 1984; Lewis, Isaacson, Harootunian, and Murray 1984; Fischer 1985). The first investigations are usually attributed to Synge, who presented a proposal for sub-wavelength microscopy as early as in 1928. The subject was studied again in 1944 by Bethe, by Bouwkamp in 1950, and a proposal much similar to that of Synge was made by O'Keefe in 1956. Using microwaves, Ash and Nichols resolved a grating with a linewidth of $\lambda/60$ in 1972.

In the wake of theoretical studies of the possibility for phase conjugating the field emitted from a mesoscopic object carried out by Keller (1992), creation of light foci with a diameter below the classical diffraction limit was demonstrated experimentally by Bozhevolnyi, Keller, and Smolyaninov (1994, 1995), who used the fibre tip of a near field optical microscope to create source spots of red light (633nm) in front of a photorefractive Fe:LiNbO$_3$ crystal, which acted as a phase conjugator. After creation, the phase conjugated replica of these light spots could be detected using the near field microscope, since they were maintained for approximately ten minutes because of the long memory of the phase conjugation process in the crystal. The resulting phase conjugated light foci had diameters of around 180nm, and the conclusion of their work was therefore that at least some of the evanescent field components of the source also must have been phase conjugated in order to achieve the observed size of the phase conjugated image.

The above-mentioned observation drew renewed attention to the description of focusing of electromagnetic fields in front of phase conjugating mirrors, and required inclusion of evanescent modes in the description of the optical phase conjugation process. In an important paper, Agarwal and Gupta (1995), extending an original idea of Agarwal (1982), undertook an analysis of the phase conjugated replica of the field from a point particle as it is produced by a so-called ideal phase conjugator, and in recent articles by Keller (1996b, 1996c) attention was devoted to an investigation of microscopic aspects of the spatial confinement problem of the phase conjugated field.

In the previous chapters, we developed a microscopic theory for optical phase con-

jugation by degenerate four-wave mixing in mesoscopic interaction volumes, with the aim of establishing a theoretical framework for inclusion of near field components in the analysis. In order for near field components to give a significant contribution to the phase conjugated response, the phase conjugation process must be effective in a surface layer of thickness (much) less than the optical wavelength. This makes quantum well systems particularly adequate candidates for the nonlinear mixing process.

In this chapter we employ the developed microscopic theory to a study of the spatial confinement of an electromagnetic field emitted from an ideal line source (quantum wire with complete electron confinement), paying particular attention to the evanescent part of the angular spectrum. As phase conjugator a single-level metallic quantum well, particularly effective in phase conjugating evanescent field components, albeit with an overall small conversion efficiency, is used. The relevant expression for the phase conjugated field is given and the result of a numerical calculation of the nonlinear energy reflection coefficient for a copper well presented. Finally, the intensity distribution of the phase conjugated field in the region between the line source and the phase conjugator is calculated and the two-dimensional spatial focusing investigated.

12.1 Quantum wire as a two-dimensional point source

As starting point, we consider a line source (quantum wire) placed parallel to the y-axis of a Cartesian coordinate system and cutting the x-z-plane in the point $(0, -z_0)$. In the description of the source we assume (i) perfect spatial electron confinement in the wire and (ii) constant current density along the wire at a given time. Choosing the wire current to oscillate along the x-direction, the above-mentioned assumptions lead to a harmonic source current density given by

$$\vec{J}(\vec{r};\omega) = J_0(\omega)\delta(x)\delta(z+z_0)\vec{e}_x, \tag{12.1}$$

where $\vec{J}_0(\omega) = J_0(\omega)\vec{e}_x$ is its possibly frequency dependent vectorial amplitude, $\vec{e}_x$ being a unit vector in the x-direction. In order to calculate the phase conjugated response using the developed microscopic model we perform a Fourier analysis of the source field along the x-axis. The electric field of the quantum wire at the surface ($z = -d$) of the phase conjugating mirror thus becomes

$$\vec{E}(x,-d;\omega) = \frac{1}{(2\pi)^2}\int_{-\infty}^{\infty}\vec{E}(-d;\vec{q}_\parallel,\omega)e^{iq_\parallel x}dq_\parallel, \tag{12.2}$$

where the parallel component of the probe wavevector lies along the x-axis, i.e., $\vec{q}_\parallel = q_\parallel\vec{e}_x$, and (Keller 1998)

$$\vec{E}(-d;\vec{q}_\parallel,\omega) = -\frac{e^{iq_\perp(z_0-d)}}{2\varepsilon_0\omega}\begin{bmatrix} q_\perp \\ 0 \\ -q_\parallel \end{bmatrix}J_0(\omega). \tag{12.3}$$
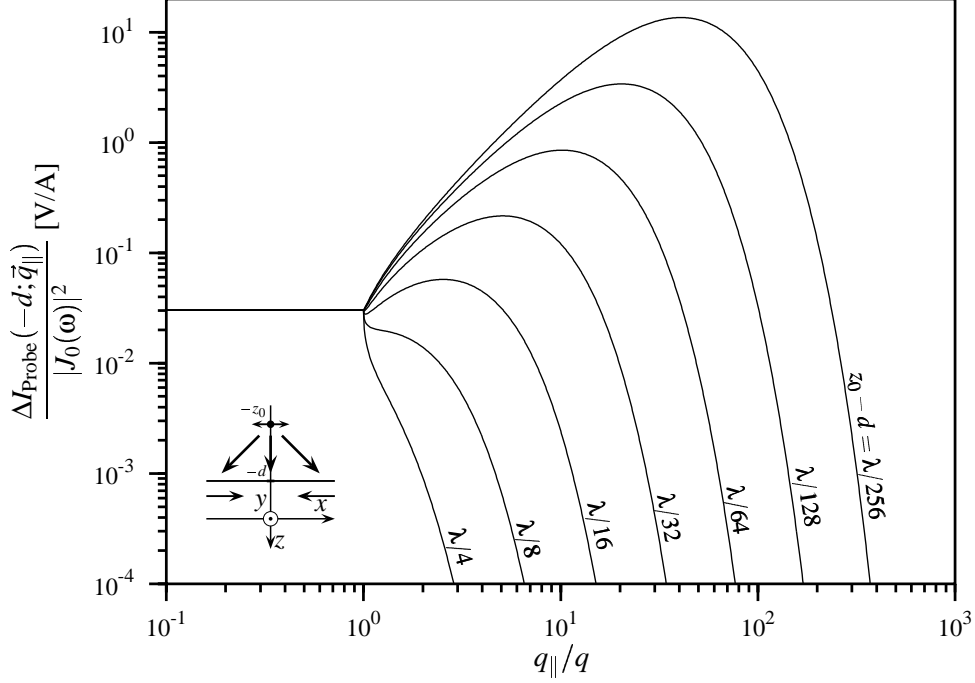
Figure 12.1: The angular spectral distribution of the field generated by a quantum wire at the surface of the phase conjugator is shown for the seven different distances $z_0 - d \in \{\lambda/4, \lambda/8, \lambda/16, \lambda/32, \lambda/64, \lambda/128, \lambda/256\}$ of the wire from the phase conjugating film. Inserted is shown the scattering geometry. The film/substrate and vacuum/film interfaces are at $z = 0$ and $z = -d$, respectively, and the wire crosses the x-z-plane in the point $(x, z) = (0, -z_0)$. As indicated by the double arrow the current oscillations of the wire is along the x-direction. The arrows between the vacuum/film and film/substrate interfaces indicate the two pump wavevectors. The arrows drawn from the source towards the vacuum/film interface indicate the angular spreading of the source field.

In Eq. (12.3), $q_\perp$ is determined from the vacuum dispersion relation for the field, i.e., $(q_\perp^2 + q_\parallel^2)^{1/2} = q$, where $q = \omega/c_0$ is the vacuum wavenumber. For propagating modes, satisfying the inequality $|q_\parallel| < q$, $q_\perp = (q^2 - q_\parallel^2)^{1/2}$ is real (and positive), whereas for evanescent modes having $|q_\parallel| > q$, $q_\perp = i(q_\parallel^2 - q^2)^{1/2}$ is purely imaginary. To illustrate the angular spectral distribution of the field from the wire at the phase conjugator, we calculate the magnitude of the differential source (probe) field intensity, i.e., $\Delta I_{\text{probe}}(-d; \vec{q}_\parallel, \omega) = \frac{1}{2}\varepsilon_0 c_0 \vec{E}(-d; \vec{q}_\parallel, \omega) \cdot \vec{E}^*(-d; \vec{q}_\parallel, \omega)/(2\pi)^4$. From Eq. (12.3) one obtains [Eq. (11.8)]

$$\frac{\Delta I_{\text{probe}}(-d; \vec{q}_\parallel)}{|J_0(\omega)|^2} = \frac{1}{2^7 \pi^4 \varepsilon_0 c_0} \left\{ \Theta\left(1 - (q_\parallel/q)\right) + \Theta\left((q_\parallel/q) - 1\right) \left[2(q_\parallel/q)^2 - 1\right] \right\}$$

$$\times \exp\left(-2(z_0 - d)q\sqrt{(q_\parallel/q)^2 - 1}\right)\bigg\},\tag{12.4}$$

where Θ is the Heaviside unit step function. It appears from Eq. (12.4), that ΔI_{probe} is independent of $q_\parallel$ for the propagating modes. In Fig. 12.1, the normalized differential probe distribution $\Delta I_{\text{probe}}/|J_0(\omega)|^2$ is shown as a function of $q_\parallel/q$ for various distances $z_0 - d$ between the wire and the vaccum/phase-conjugator interface. It is seen that the evanescent components tend to dominate the angular spectrum when $z_0 - d \lesssim \lambda/4$.

12.2 Single-level metallic quantum-well phase conjugator

We take as the active medium a metallic quantum well, and we describe the conduction electron dynamics using the infinite barrier model potential. While such a model potential from a quantitative point of view of course is too naïve, in particular in cases where the conduction electrons of the well are allowed to mix with those of a semiconducting or metallic substrate, it suffices in the present context. We further assume that only the lowest lying band is below the Fermi energy and that the photon energy is so small that interband transitions do not contribute to the electrodynamics. The quantum well is deposited on a substrate that can be described alone by its refractive index n. Because of the chosen polarization of the wire current density we have limited the description to cover only the case where all interacting electric fields are polarized in the scattering plane (p-polarization). Then, within the limits of a self-field approximation, the z-component of the phase conjugated field becomes [Eq. (10.28)]

$$E_{\text{PC},z}(z;\vec{q}_\parallel,\omega) = \frac{e^2(\omega + i/\tau)(1 + r^p)}{2^9\pi^6\hbar\omega^3 Z N_+ m_e}\frac{q_\parallel^2}{iq_\perp}\left[C(q_\parallel - k_\parallel) + C(q_\parallel + k_\parallel)\right]$$
$$\times E_z^{(1)} E_z^{(2)} E_z^* e^{-iq_\perp z},\tag{12.5}$$

where

$$C(q_\parallel \pm k_\parallel) = \frac{4\pi}{a^2}\left\{\sqrt{b^2 - a^2\alpha^2} - a(q_\parallel \pm k_\parallel) - \sqrt{\left[b - a(q_\parallel \pm k_\parallel)\right]^2 - a^2\alpha^2}\right\},\tag{12.6}$$

with $a = \hbar(q_\parallel \pm k_\parallel)/m_e$ and $b = \hbar(q_\parallel \pm k_\parallel)^2/(2m_e) - i/\tau$. The quantity α is the radius of the (two-dimensional) Fermi circle, given by $\alpha = [k_F^2 - (\pi/d)^2]^{1/2}$. Given the z-component of the phase conjugated field, the x-component is also known, since the electric field must be transverse in vacuum. Above, $-e$ and m_e are the electron charge and mass, respectively, ω and τ are the cyclic frequency of the optical field and the electron relaxation time, and $k_\parallel > 0$ is the parallel component of the wavevector of pump field number 1 having a z-component $E_z^{(1)}$. The corresponding quantities for pump field number 2 are $-k_\parallel$ and $E_z^{(2)}$. When the two pump fields have numerically equal wavevector components in the plane of the phase conjugator, conservation of momentum parallel to the surface implies that given angular components of the probe and phase conjugated
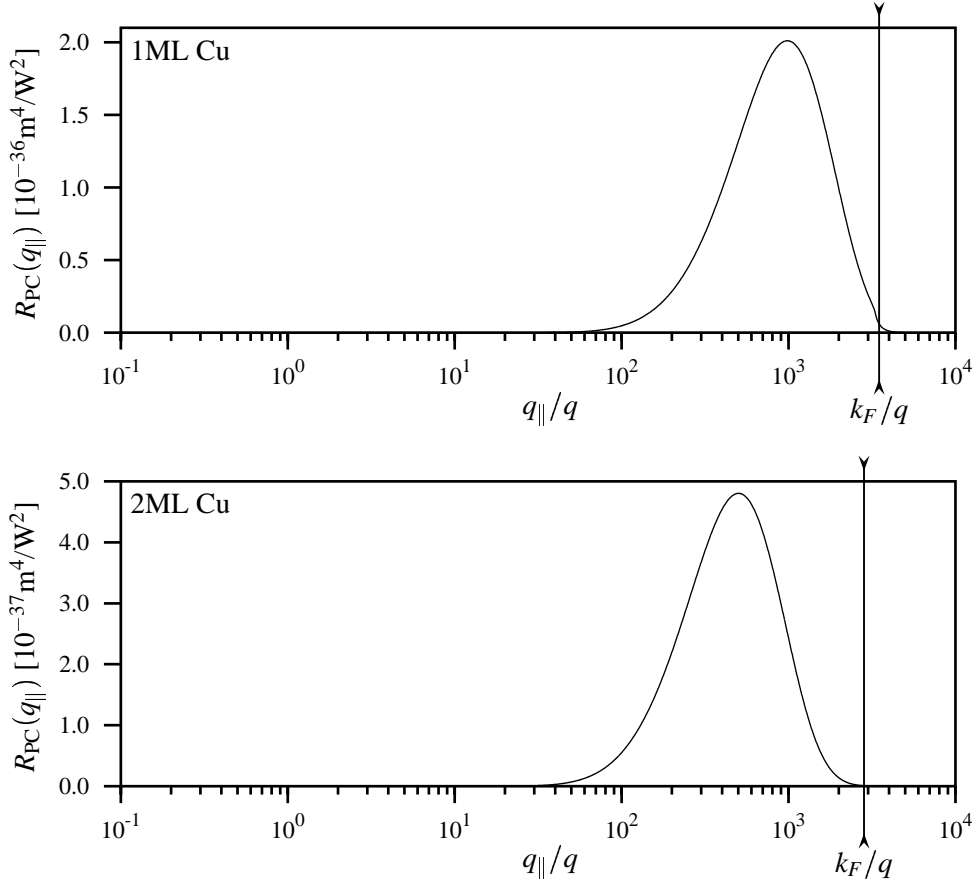
Figure 12.2: The phase conjugation energy reflection coefficient $R_{PC}(q_\parallel) \equiv R_{PC}(-d, \vec{q}_\parallel)$ is shown on a linear scale as a function of the probe wavevector component parallel to the film plane, normalized to the vacuum wavenumber. The upper figure shows the result for a single monolayer (1ML) copper film [linear plot of Fig. 11.1 (ppp)]. The lower figure gives the result for the two-monolayer (2ML) film [linear plot of Fig. 11.2 (ppp)].

fields are counterpropagating along the surface. Moreover, Z is the number of conduction electrons each atom in the quantum well contributes to the assumed free-electron gas, N_+ is the number of atoms per unit volume in the quantum well, and k_F is the Fermi wavenumber. Since the two pump fields are counterpropagating, the wavevectors of the probe field ($\vec{q}_\parallel'$) and the phase conjugated field ($\vec{q}_\parallel$) are related through the conservation of momentum, $\vec{q}_\parallel' + \vec{q}_\parallel = \vec{0}$. This property was used in the derivation of Eq. (12.5). Thus, the z-component of the probe field in Eq. (12.3), E_z, is given by $E_z = \int E_z(-d; \vec{q}_\parallel', \omega) \delta(\vec{q}_\parallel' + \vec{q}_\parallel) d^2 q_\parallel'$, where $E_z(-d; \vec{q}_\parallel', \omega)$ is taken from Eq. (12.3).

12.3 Numerical results and discussion

For the numerical calculation we consider a copper quantum well [$d = 1.8$Å (for single-monolayer film), respectively 3.6Å (two monolayers), $N_+ = 8.47 \times 10^{28}\,\mathrm{m}^{-3}$ and $Z = 1$ (Ashcroft and Mermin 1976)] deposited on a glass substrate with $n = 1.51$, giving $k_\| = 1.51q$ when the wavevectors of the pump fields are parallel to the x-axis. The wavelength of the light is chosen to be $\lambda = 1061$nm. For a glass substrate it is adequate to calculate the linear vaccum/substrate amplitude reflection coefficient r^p by means of the classical Fresnel formula $r^p = [n^2 q_\perp - (n^2 q^2 - q_\|^2)^{\frac{1}{2}}]/[n^2 q_\perp + (n^2 q^2 - q_\|^2)^{\frac{1}{2}}]$. In the view of the recent experimental data discussed in Section 11.1 (Jalochowski, Stróżak, and Zdyb 1997), we have chosen an intraband relaxation time of $\tau = 3$fs for the electrons in the ultrathin quantum-well film.

To give an impression of the efficiency of the phase conjugation process for the various evanescent modes, the nonlinear energy reflection coefficient of the phase conjugator at the vacuum/film interface, $R_{\mathrm{PC}}(q_\|)$, is shown in Fig. 12.2 as a function of the parallel component ($q_\|$) of the probe wavevector for the two possible single-level quantum wells. It appears from this figure that in particular high spatial frequency components ($10^2 \lesssim q_\|/q \lesssim 10^3$) are phase conjugated in an effective manner. This is associated with the fact that in a single-level quantum well the two-dimensional intraband electron dynamics along the plane of the well is responsible for the main part of the phase conjugation process.

Using a square-potential barrier model to describe the quantum well the integration limits should not extend beyond the (two-dimensional) Fermi wavenumber $k_F = [2\pi Z N_+ d + (\pi/d)^2]^{1/2}$ for the single level quantum well. Looking at the phase conjugation reflection coefficient shown in Fig. 12.2, we not only notice that the main contribution to the phase conjugated signal is well above the point where the probe field becomes evanescent in vaccum, but also does not extend beyond the Fermi wavenumber. The phase conjugated image of our quantum-wire source field is then given by

$$\vec{E}_{\mathrm{PC}}(x, z; \omega) = \frac{1}{2\pi} \int_{-k_F}^{k_F} \vec{E}_{\mathrm{PC}}(z; \vec{q}_\|, \omega) e^{i q_\| x} dq_\|, \tag{12.7}$$

in the x-z-plane.

It appears from Eq. (12.5), that the individual angular components of the phase conjugated field decay exponentially with the distance from the phase conjugator in the evanescent part of the Fourier spectrum. The evanescent components of the source likewise decay exponentially with the distance from the quantum wire. Therefore, the contribution from the evanescent components to the total phase conjugated field is expected to increase significantly when the distance between the source and the phase conjugator becomes smaller. Experimentally, it is feasible presently to carry out measurements at distances from the surface down to ~ 40Å (using near-field microscopes). For the chosen system this leads to an intensity distribution in the x-z-plane between the probe and the phase conjugator as shown in Figs. 12.3 and 12.4 for different distances between the probe and the film, $z_0 - d \in \{\lambda/4, 3\lambda/16, \lambda/8, 3\lambda/32, \lambda/16\}$, Fig. 12.3 corresponding

to the single-monolayer film and Fig. 12.4 to the two-monolayer film. For $z_0 - d \gtrsim \lambda/2$, the effect of the near-field components are negligible. In both Figs. 12.3 and 12.4, the figures to the left show by equal-intensity contours the intensity distribution of the phase conjugated field in the area of the x-z-plane between the quantum wire and the surface of the phase conjugator. The width (along the x-axis) of the shown area is in all cases twice the height (along the z-axis) on both sides of $x = 0$. The contours are drawn in an exponential sequence, so that if the first contour corresponds to the intensity $I_{\mathrm{PC}}^{(1)}$ the n-th contour is associated with the intensity $I_{\mathrm{PC}}^{(n)} = I_{\mathrm{PC}}^{(1)} \exp[(1-n)\alpha]$, α varying from figure to figure. To further illustrate the capabilities of light focusing the chosen system possess, we have to the right on a linear scale shown the phase conjugated intensity at (i) the surface of the phase conjugator (solid lines) and (ii) along an axis parallel to the x-axis placed at the same distance from the phase conjugator as the wire (dashed lines). The two curves in each of the plots to the right are adjusted by multiplication of the curve in case (ii) by a factor of (a) 2590, (b) 545, (c) 271, (d) 353, and (e) 586 in Fig. 12.3, and by a factor of (a) 555, (b) 212, (c) 204, (d) 322, and (e) 528 in Fig. 12.4, respectively, so that the maximum values coincide in the plots.

It is seen from Figs. 12.3 and 12.4 that the width of the focus created by the phase conjugated field in all cases is smallest at the surface of the phase conjugator. Furthermore one observe that the focus becomes narrower when the distance between the source and the film becomes smaller, as one should expect when evanescent field components give a significant contribution to the process. At the surface the width of the main peak decreases roughly by a factor of two every time the source-film distance decreases by the same factor. This tendency continues closer to the surface of the phase conjugator, at least down to around $\lambda/256 \approx 4$nm, where the structure of the intensity distribution looks more or less like Fig. 12.3.e [and Fig. 12.4.e], scaled appropriately with the distance.

The difference between the ability of the single-monolayer film and the two-monolayer film to focus the field emitted from the source is small, as we would expect from the analysis in the previous chapter. We observe from Fig. 12.3 that when the source is far away from the film (a–b), the intensity of the phase conjugated field decays faster in the case of a single-monolayer film than in the other case. Furthermore, we observe that the width of the centre peak is somewhat smaller for the focus in front of the single-monolayer phase conjugator, and that the height of the first sidelobe is slightly higher compared to the centre peak. Taking the source closer to the surface (c–e) we observe that the distance between minima in Fig. 12.3 is still smaller than in Fig. 12.4, but that the width of the centre peak becomes more and more equal in the two cases.

To give an impression of the size of the phase conjugated focus, let us take a look at Fig. 12.4.e, where the distance from the probe to the surface is $\lambda/16 \approx 66$nm. The distance between the two minima at the surface of the phase conjugator is in this case around 40nm (approximately $\lambda/25$). In the plane of the probe the distance between the two minima is around 100nm ($\sim \lambda/10$).
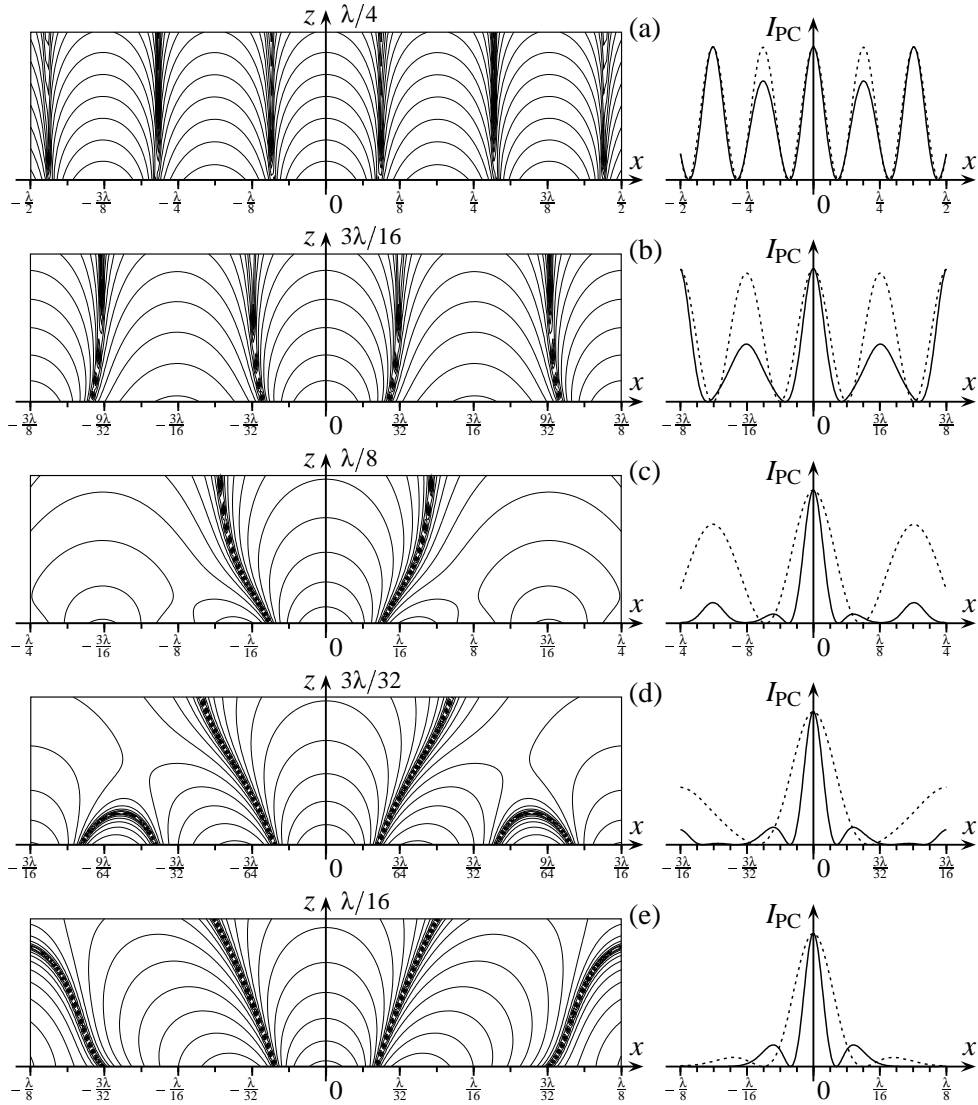
Figure 12.3: The intensity of the phase conjugated field from a quantum wire is plotted for different distances between the wire and the surface of a single-monolayer copper quantum-well phase conjugator. The figures to the left show lines of equal intensity on a logarithmic scale of the phase conjugated intensity in the x-z-plane between the surface of the phase conjugator and the wire. The figures to the right show the phase conjugated intensity (i) at the surface of the phase conjugator (solid lines) and (ii) at the height of the wire, $z = -z_0$ (dashed lines). The intensity in these figures is plotted on a linear scale (arbitrary units). In order to make the two curves in these plots comparable, the curve associated with case (ii) has been multiplied by a factor of (a) 2590, (b) 545, (c) 271, (d) 353, and (e) 586. The sets of figures are shown for distances $z_0 - d$ of (a) $\lambda/4$, (b) $3\lambda/16$, (c) $\lambda/8$, (d) $3\lambda/32$, and (e) $\lambda/16$ between the quantum wire and the surface of the phase conjugating mirror.
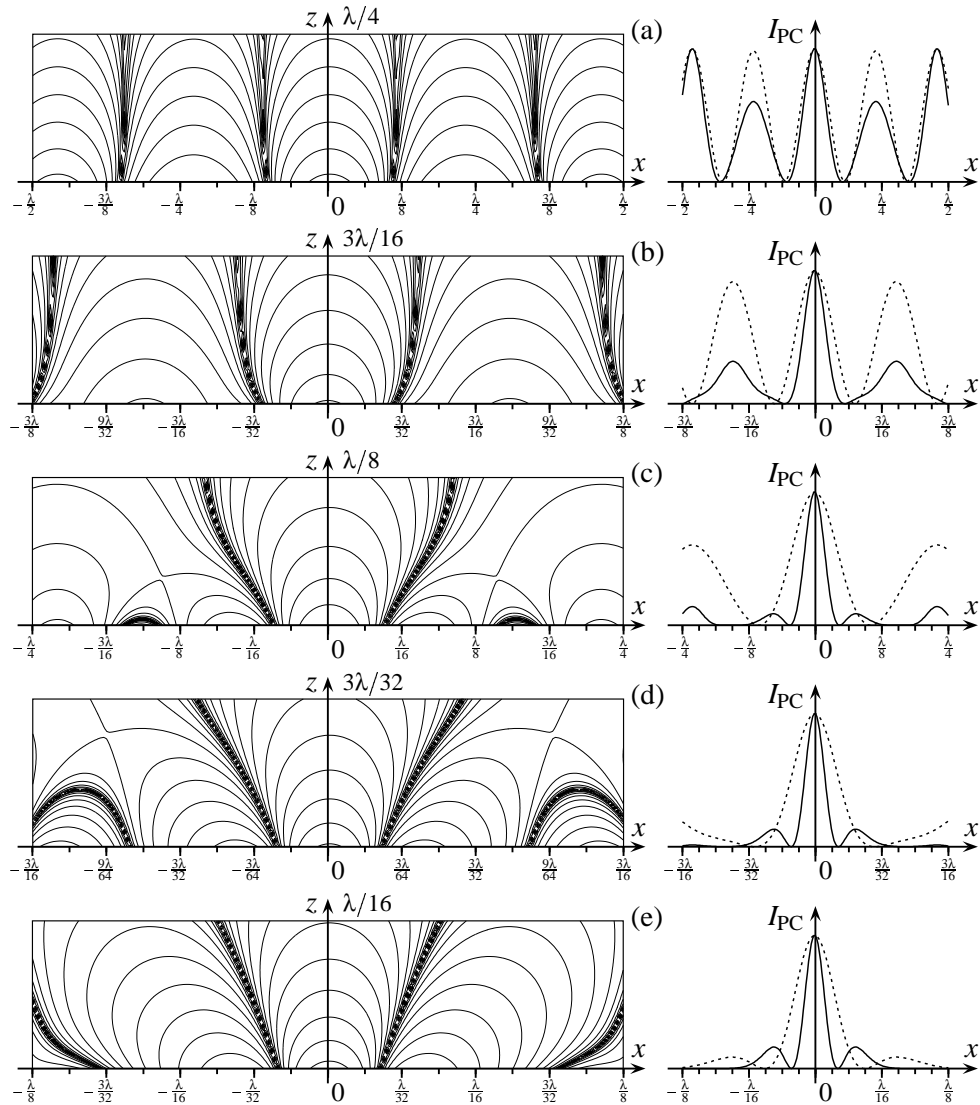
Figure 12.4: The intensity of the phase conjugated field from a quantum wire is plotted for different distances between the wire and the surface of a two-monolayer copper quantum-well phase conjugator. The figures to the left show lines of equal intensity on a logarithmic scale of the phase conjugated intensity in the x-z-plane between the surface of the phase conjugator and the wire. The figures to the right show the phase conjugated intensity (i) at the surface of the phase conjugator (solid lines) and (ii) at the height of the wire, $z = -z_0$ (dashed lines). The intensity in these figures is plotted on a linear scale (arbitrary units). In order to make the two curves in these plots comparable, the curve associated with case (ii) has been multiplied by a factor of (a) 555, (b) 212, (c) 204, (d) 322, and (e) 528. The sets of figures are shown for distances $z_0 - d$ of (a) $\lambda/4$, (b) $3\lambda/16$, (c) $\lambda/8$, (d) $3\lambda/32$, and (e) $\lambda/16$ between the quantum wire and the surface of the phase conjugating mirror.

Chapter 13

We have in the previous three chapters discussed the phase conjugation response of a single-level quantum well, where only intraband transitions are possible. It is evident from our analysis that in this case the phase conjugated response depends strongly on the component of the probe wavevector that is parallel to the surface of the phase conjugator ($q_\parallel$). Consequently, the assumption of an ideal phase conjugator with constant reflection coefficient throughout the full $q_\parallel$-spectrum must be abandoned, at least when a single-level quantum-well phase conjugator is considered. The nonlinear coupling is strongest in the evanescent part of the $q_\parallel$-spectrum above the point up to which the probe field is propagating in the substrate ($q_\parallel/q = n$). As a consequence, if one wants to observe the phase conjugation of a broad Fourier spectrum of evanescent modes, both the observation and the excitation are required to take place near the surface of the phase conjugator.

As a possible method to excite the Fourier components in the high end of the $q_\parallel$-spectrum we have analyzed the consequences of using a quantum wire. When the quantum wire is placed close to the phase conjugator the phase conjugated response contains a broad range of evanescent components. This property made it a good candidate for investigations of the problem of focusing light to a spatial extent less than the Rayleigh limit. The spatial focusing of the phase conjugated response from a quantum wire was studied, and the problem of the resolution limit has been addressed. The conclusion of this study is in agreement with previous studies and mainly shows that the focus gets narrower when the distance from the quantum wire to the phase conjugator gets shorter. Judging from this we may conclude that in order to establish a better estimate of the limit of resolution the present model has to be improved, since continuing to get closer becomes meaningless at some point.

In examining the phase conjugation response of the single-level quantum well we have chosen a specific frequency of the interacting electromagnetic fields, which should be feasible for an experiment. It would be interesting to give a more detailed account of how (i) the phase conjugated response and (ii) the focusing of the phase conjugated field varies with the frequency. These properties will not be discussed in detail in this dissertation, but let us at this point just mention that (i) it seems like the evanescent components in the high end of the Fourier spectrum becomes better phase conjugated when the interacting fields move to longer wavelengths, and (ii) the spatial distance

between minima in the intensity of the phase conjugated response when using a quantum wire becomes smaller when measured in fractions of the wavelength. Going to shorter wavelengths, the tendency goes in the opposite direction.

Part V

Optical phase conjugation in
multi-level metallic quantum wells

Chapter 14

From the simple description of a quantum well where only intraband transitions contributed to the phase conjugated response we now turn our attention to the case where transitions between energy levels in the quantum well (interband transitions) can take place. In this chapter we therefore give the theoretical description that is necessary to describe the phase conjugated response from a quantum well where both interband and intraband transitions contribute to the response. In the following we adopt the same scattering geometry as in the previous treatment, i.e., scattering takes place in the *x-z*-plane and we use light that is polarized either in (*p*-polarized) or perpendicular to (*s*-polarized) the scattering plane.

14.1 Phase conjugated field

Unlike in the case of a single-level quantum well, we cannot rely on the self-field approximation when considering multi-level quantum wells (with resonances). We therefore begin this treatment with the loop equation for the phase conjugated field in the two-dimensional Fourier space [Eq. (8.24)]. It is repeated here for convenience:

$$\vec{E}_{PC}(z;\vec{q}_{\parallel},\omega) = \vec{E}_{PC}^{B}(z;\vec{q}_{\parallel},\omega)$$
$$-i\mu_0\omega \iint \vec{\vec{G}}(z,z'';\vec{q}_{\parallel},\omega) \cdot \vec{\vec{\sigma}}(z'',z';\vec{q}_{\parallel},\omega) \cdot \vec{E}_{PC}(z';\vec{q}_{\parallel},\omega)dz''dz'. \tag{14.1}$$

The background field in Eq. (14.1) is given by

$$\vec{E}_{PC}^{B}(z;\vec{q}_{\parallel},\omega) = -i\mu_0\omega \int \vec{\vec{G}}(z,z';\vec{q}_{\parallel},\omega) \cdot \vec{J}_{-\omega}^{(3)}(z';\vec{q}_{\parallel},\omega)dz', \tag{14.2}$$

and can be determined from the previous analysis. The linear conductivity tensor consists in general of a diamagnetic and a paramagnetic part (see the discussion in Chapters 5 and 6). It is, however, possible to combine the two parts in such a way that the diamagnetic conductivity tensor can be written as a correction to the paramagnetic one (Keller 1996a, 1997a, 1997b). Then the expression for the total linear conductivity tensor becomes

$$\vec{\vec{\sigma}}(\vec{r},\vec{r}';\omega) = -\frac{2}{i\omega}\frac{1}{\hbar}\sum_{nm}\frac{\omega}{\tilde{\omega}_{nm}}\frac{f_n - f_m}{\tilde{\omega}_{nm} - \omega}\vec{J}_{nm}(\vec{r}) \otimes \vec{J}_{mn}(\vec{r}'), \tag{14.3}$$

the correction from the diamagnetic term to the paramagnetic response being the factor $\omega/\tilde{\omega}_{nm}$, which close to resonance becomes 1. In the two-dimensional mixed Fourier space this is

$$\vec{\sigma}(z,z';\vec{q}_\parallel,\omega) = -\frac{2}{i\omega}\frac{1}{\hbar}\frac{1}{(2\pi)^2}\sum_{nm}\int \frac{\omega}{\tilde{\omega}_{nm}(\vec{\kappa}_\parallel+\vec{q}_\parallel,\vec{\kappa}_\parallel)}\frac{f_n(\vec{\kappa}_\parallel+\vec{q}_\parallel)-f_m(\vec{\kappa}_\parallel)}{\tilde{\omega}_{nm}(\vec{\kappa}_\parallel+\vec{q}_\parallel,\vec{\kappa}_\parallel)-\omega}$$
$$\times \vec{j}_{nm}(z;2\vec{\kappa}_\parallel+\vec{q}_\parallel)\otimes\vec{j}_{mn}(z';2\vec{\kappa}_\parallel+\vec{q}_\parallel)d^2\kappa_\parallel. \tag{14.4}$$

The transition frequency appearing in Eq. (14.4) is

$$\tilde{\omega}_{nm}(\vec{\kappa}_\parallel+\vec{q}_\parallel,\vec{\kappa}_\parallel) = \frac{1}{\hbar}\left[\varepsilon_n-\varepsilon_m+\frac{\hbar^2}{2m_e}\left(2\kappa_x q_x+q_x^2\right)\right]-\frac{i}{\tau_{nm}}, \tag{14.5}$$

which by insertion into Eq. (14.4) gives the five nonzero elements of the linear conductivity tensor

$$\sigma_{xx}(z,z';\vec{q}_\parallel,\omega) = \sum_{nm}Q_{nm}^{xx}(\vec{q}_\parallel,\omega)\mathcal{Z}_{nm}^x(z)\mathcal{Z}_{mn}^x(z'), \tag{14.6}$$

$$\sigma_{xz}(z,z';\vec{q}_\parallel,\omega) = -i\sum_{nm}Q_{nm}^{xz}(\vec{q}_\parallel,\omega)\mathcal{Z}_{nm}^x(z)\mathcal{Z}_{mn}^z(z'), \tag{14.7}$$

$$\sigma_{yy}(z,z';\vec{q}_\parallel,\omega) = \sum_{nm}Q_{nm}^{yy}(\vec{q}_\parallel,\omega)\mathcal{Z}_{nm}^x(z)\mathcal{Z}_{mn}^x(z'), \tag{14.8}$$

$$\sigma_{zx}(z,z';\vec{q}_\parallel,\omega) = -i\sum_{nm}Q_{nm}^{xz}(\vec{q}_\parallel,\omega)\mathcal{Z}_{nm}^z(z)\mathcal{Z}_{mn}^x(z'), \tag{14.9}$$

$$\sigma_{zz}(z,z';\vec{q}_\parallel,\omega) = -\sum_{nm}Q_{nm}^{zz}(\vec{q}_\parallel,\omega)\mathcal{Z}_{nm}^z(z)\mathcal{Z}_{mn}^z(z'), \tag{14.10}$$

where we for the sake of notational simplicity have divided the total expression for each element into a z-dependent part and a z-independent part, the z-independent quantities being

$$Q_{nm}^{xx}(\vec{q}_\parallel,\omega) = \frac{2i\hbar}{(2\pi)^2}\left(\frac{e\hbar}{2m_e}\right)^2\int \frac{4\kappa_x^2+4\kappa_x q_x+q_x^2}{\varepsilon_n-\varepsilon_m+\hbar(2\kappa_x q_x+q_x^2)/(2m_e)-i\hbar/\tau_{nm}}$$
$$\times\frac{f_n(\vec{\kappa}_\parallel+\vec{q}_\parallel)-f_m(\vec{\kappa}_\parallel)}{\varepsilon_n-\varepsilon_m+\hbar(2\kappa_x q_x+q_x^2)/(2m_e)-i\hbar/\tau_{nm}-\hbar\omega}d^2\kappa_\parallel, \tag{14.11}$$

$$Q_{nm}^{xz}(\vec{q}_\parallel,\omega) = \frac{2i\hbar}{(2\pi)^2}\left(\frac{e\hbar}{2m_e}\right)^2\int \frac{2\kappa_x+q_x}{\varepsilon_n-\varepsilon_m+\hbar(2\kappa_x q_x+q_x^2)/(2m_e)-i\hbar/\tau_{nm}}$$
$$\times\frac{f_n(\vec{\kappa}_\parallel+\vec{q}_\parallel)-f_m(\vec{\kappa}_\parallel)}{\varepsilon_n-\varepsilon_m+\hbar(2\kappa_x q_x+q_x^2)/(2m_e)-i\hbar/\tau_{nm}-\hbar\omega}d^2\kappa_\parallel, \tag{14.12}$$

$$Q_{nm}^{yy}(\vec{q}_\parallel,\omega) = \frac{2i\hbar}{(2\pi)^2}\left(\frac{e\hbar}{2m_e}\right)^2\int \frac{4\kappa_y^2}{\varepsilon_n-\varepsilon_m+\hbar(2\kappa_x q_x+q_x^2)/(2m_e)-i\hbar/\tau_{nm}}$$
$$\times\frac{f_n(\vec{\kappa}_\parallel+\vec{q}_\parallel)-f_m(\vec{\kappa}_\parallel)}{\varepsilon_n-\varepsilon_m+\hbar(2\kappa_x q_x+q_x^2)/(2m_e)-i\hbar/\tau_{nm}-\hbar\omega}d^2\kappa_\parallel, \tag{14.13}$$

$$Q_{nm}^{zz}(\vec{q}_\parallel,\omega) = \frac{2i\hbar}{(2\pi)^2}\left(\frac{e\hbar}{2m_e}\right)^2\int \frac{1}{\varepsilon_n-\varepsilon_m+\hbar(2\kappa_x q_x+q_x^2)/(2m_e)-i\hbar/\tau_{nm}}$$

$$\times \frac{f_n(\vec{\kappa}_\parallel + \vec{q}_\parallel) - f_m(\vec{\kappa}_\parallel)}{\varepsilon_n - \varepsilon_m + \hbar(2\kappa_x q_x + q_x^2)/(2m_e) - i\hbar/\tau_{nm} - \hbar\omega} d^2\kappa_\parallel, \tag{14.14}$$

since $Q_{nm}^{xz}(\vec{\kappa}_\parallel, \omega) = Q_{nm}^{zx}(\vec{\kappa}_\parallel, \omega)$. The z-dependent quantities in Eqs. (14.6)–(14.10) above are

$$\mathcal{Z}_{nm}^{x}(z) = \mathcal{Z}_{nm}^{y}(z) = \psi_m^*(z)\psi_n(z), \tag{14.15}$$

$$\mathcal{Z}_{nm}^{z}(z) = \psi_m^*(z)\frac{\partial \psi_n(z)}{\partial z} - \psi_n(z)\frac{\partial \psi_m^*(z)}{\partial z}. \tag{14.16}$$

Eqs. (14.11)–(14.14) has the solutions given in Appendix C, section C.12 in terms of the analytic solution to the integrals given in Appendix B. Inserting this solution into Eq. (14.1), we get

$$\vec{E}_{PC}(z; \vec{q}_\parallel, \omega) = \vec{E}_{PC}^{B}(z; \vec{q}_\parallel, \omega) + \sum_{nm} \overleftrightarrow{F}_{nm}(z; \vec{q}_\parallel, \omega) \cdot \vec{\Gamma}_{mn}(\vec{q}_\parallel, \omega), \tag{14.17}$$

in which we have introduced the 3×3 tensor $\overleftrightarrow{F}_{nm}(z; \vec{q}_\parallel, \omega)$ with the nonzero elements

$$F_{nm}^{xx}(z; \vec{q}_\parallel, \omega) = -i\mu_0\omega \left\{ Q_{nm}^{xx}(\vec{q}_\parallel, \omega) \int G_{xx}(z, z''; \vec{q}_\parallel, \omega) \mathcal{Z}_{nm}^{x}(z'')dz'' \right.$$

$$\left. -iQ_{nm}^{xz}(\vec{q}_\parallel, \omega) \int G_{xz}(z, z''; \vec{q}_\parallel, \omega) \mathcal{Z}_{nm}^{z}(z'')dz'' \right\}, \tag{14.18}$$

$$F_{nm}^{xz}(z; \vec{q}_\parallel, \omega) = i\mu_0\omega \left\{ iQ_{nm}^{xz}(\vec{q}_\parallel, \omega) \int G_{xx}(z, z''; \vec{q}_\parallel, \omega) \mathcal{Z}_{nm}^{x}(z'')dz'' \right.$$

$$\left. +Q_{nm}^{zz}(\vec{q}_\parallel, \omega) \int G_{xz}(z, z''; \vec{q}_\parallel, \omega) \mathcal{Z}_{nm}^{z}(z'')dz'' \right\}, \tag{14.19}$$

$$F_{nm}^{yy}(z; \vec{q}_\parallel, \omega) = -i\mu_0\omega Q_{nm}^{yy}(\vec{q}_\parallel, \omega) \int G_{yy}(z, z''; \vec{q}_\parallel, \omega) \mathcal{Z}_{nm}^{x}(z'')dz'', \tag{14.20}$$

$$F_{nm}^{zx}(z; \vec{q}_\parallel, \omega) = \frac{q_\parallel}{q_\perp} F_{nm}^{xx}(z; \vec{q}_\parallel, \omega), \tag{14.21}$$

$$F_{nm}^{zz}(z; \vec{q}_\parallel, \omega) = \frac{q_\parallel}{q_\perp} F_{nm}^{xz}(z; \vec{q}_\parallel, \omega), \tag{14.22}$$

and the vector

$$\vec{\Gamma}_{mn}(\vec{q}_\parallel, \omega) = \begin{pmatrix} \int \mathcal{Z}_{mn}^{x}(z') E_{PC,x}(z'; \vec{q}_\parallel, \omega)dz' \\ \int \mathcal{Z}_{mn}^{x}(z') E_{PC,y}(z'; \vec{q}_\parallel, \omega)dz' \\ \int \mathcal{Z}_{mn}^{z}(z') E_{PC,z}(z'; \vec{q}_\parallel, \omega)dz' \end{pmatrix} \tag{14.23}$$

can be determined from the following set of algebraic equations:

$$\vec{\Gamma}_{mn}(\vec{q}_\parallel, \omega) - \sum_{vl} \overleftrightarrow{K}_{mn}^{vl}(\vec{q}_\parallel, \omega) \cdot \vec{\Gamma}_{vl}(\vec{q}_\parallel, \omega) = \vec{\Omega}_{mn}(\vec{q}_\parallel, \omega). \tag{14.24}$$

Since we may now determine the different Γ values independently of their dependence on the phase conjugated field, $\vec{E}_{PC}(z; \vec{q}_\parallel, \omega)$, we have by this operation kept the self-consistency in Eq. (14.17), but the problem of solution has been reduced to a problem of

solving a linear algebraic set of equations with just as many unknowns. This problem can be treated as a matrix problem and is thus in principle fairly easy to solve numerically. In Eq. (14.24) above, the vectorial quantity $\vec{\Omega}_{mn}$ is given by

$$\vec{\Omega}_{mn}(\vec{q}_{\parallel},\omega) = \begin{pmatrix} \int \mathcal{Z}^x_{mn}(z)E^{\mathrm{B}}_{\mathrm{PC},x}(z;\vec{q}_{\parallel},\omega)dz \\ \int \mathcal{Z}^x_{mn}(z)E^{\mathrm{B}}_{\mathrm{PC},y}(z;\vec{q}_{\parallel},\omega)dz \\ \int \mathcal{Z}^z_{mn}(z)E^{\mathrm{B}}_{\mathrm{PC},z}(z;\vec{q}_{\parallel},\omega)dz \end{pmatrix} \tag{14.25}$$

and the 3×3 tensorial quantity $\vec{\vec{K}}^{vl}_{mn}(\vec{q}_{\parallel},\omega)$ has the five nonzero elements

$$K^{vl}_{xx,mn}(\vec{q}_{\parallel},\omega) = \int \mathcal{Z}^x_{mn}(z)F^{xx}_{lv}(z;\vec{q}_{\parallel},\omega)dz, \tag{14.26}$$

$$K^{vl}_{xz,mn}(\vec{q}_{\parallel},\omega) = \int \mathcal{Z}^x_{mn}(z)F^{xz}_{lv}(z;\vec{q}_{\parallel},\omega)dz, \tag{14.27}$$

$$K^{vl}_{yy,mn}(\vec{q}_{\parallel},\omega) = \int \mathcal{Z}^x_{mn}(z)F^{yy}_{lv}(z;\vec{q}_{\parallel},\omega)dz, \tag{14.28}$$

$$K^{vl}_{zx,mn}(\vec{q}_{\parallel},\omega) = \frac{q_{\parallel}}{q_{\perp}} \int \mathcal{Z}^z_{mn}(z)F^{xx}_{lv}(z;\vec{q}_{\parallel},\omega)dz, \tag{14.29}$$

$$K^{vl}_{zz,mn}(\vec{q}_{\parallel},\omega) = \frac{q_{\parallel}}{q_{\perp}} \int \mathcal{Z}^z_{mn}(z)F^{xz}_{lv}(z;\vec{q}_{\parallel},\omega)dz. \tag{14.30}$$

If we limit our treatment to polarized light perpendicular to the scattering plane (s) and in the scattering plane (p), we get for s-polarized light the set of equations

$$\Gamma_{y,mn} - \sum_{vl}K^{vl}_{yy,mn}\Gamma_{y,vl} = \Omega_{y,mn}, \tag{14.31}$$

which is $m \times n$ equations with just as many unknowns, and for p-polarized light the set of equations

$$\Gamma_{x,mn} - \sum_{vl}\left(K^{vl}_{xx,mn}\Gamma_{x,vl} + K^{vl}_{xz,mn}\Gamma_{z,vl}\right) = \Omega_{x,mn}, \tag{14.32}$$

$$\Gamma_{z,mn} - \sum_{vl}\left(K^{vl}_{zx,mn}\Gamma_{x,vl} + K^{vl}_{zz,mn}\Gamma_{z,vl}\right) = \Omega_{z,mn}, \tag{14.33}$$

which is $2m \times n$ equations with just as many unknowns.

14.2 Infinite barrier quantum well

Applying the infinite barrier quantum well to the above formalism, we are able to determine the integrals over the Cartesian coordinates in explicit form. The wave function constructs $\mathcal{Z}(z)$ becomes in the infinite barrier model

$$\mathcal{Z}^{x,\mathrm{IB}}_{nm}(z) = \frac{1}{d}\left[\cos\left(\frac{(n-m)\pi z}{d}\right) - \cos\left(\frac{(n+m)\pi z}{d}\right)\right], \tag{14.34}$$

$$\mathcal{Z}^{z,\mathrm{IB}}_{nm}(z) = \frac{\pi}{d^2}\left[(n-m)\sin\left(\frac{(n+m)\pi z}{d}\right) - (n+m)\sin\left(\frac{(n-m)\pi z}{d}\right)\right]. \tag{14.35}$$

With this result the integrals over the source region apperaing in Eqs. (14.18)– (14.22) and (14.26)–(14.30) can be solved (see Appendix E), and the K quantities thus become

$$K_{xx,mn}^{vl}(\vec{q}_\parallel, \omega) = -\frac{8\pi^4 nmlvq_\perp d \left[1 - e^{iq_\perp d}(-1)^{n+m}\right]}{\varepsilon_0\omega[(iq_\perp d)^2 + \pi^2(n-m)^2][(iq_\perp d)^2 + \pi^2(n+m)^2]}$$
$$\times \frac{1 + r^p - \left(e^{-iq_\perp d} + r^p e^{iq_\perp d}\right)(-1)^{l+v}}{[(iq_\perp d)^2 + \pi^2(l-v)^2][(iq_\perp d)^2 + \pi^2(l+v)^2]}$$
$$\times \left\{ Q_{lv}^{xx}(\vec{q}_\parallel, \omega)q_\perp^2 d + Q_{lv}^{xz}(\vec{q}_\parallel, \omega)\frac{\pi^2(l^2 - v^2)q_\parallel}{d} \right\}, \tag{14.36}$$

$$K_{xz,mn}^{vl}(\vec{q}_\parallel, \omega) = \frac{8\pi^4 inmlvq_\perp d \left[1 - e^{iq_\perp d}(-1)^{n+m}\right]}{\varepsilon_0\omega[(iq_\perp d)^2 + \pi^2(n-m)^2][(iq_\perp d)^2 + \pi^2(n+m)^2]}$$
$$\times \frac{1 + r^p - \left(e^{-iq_\perp d} + r^p e^{iq_\perp d}\right)(-1)^{l+v}}{[(iq_\perp d)^2 + \pi^2(l-v)^2][(iq_\perp d)^2 + \pi^2(l+v)^2]}$$
$$\times \left\{ Q_{lv}^{xz}(\vec{q}_\parallel, \omega)q_\perp^2 d + Q_{lv}^{zz}(\vec{q}_\parallel, \omega)\frac{\pi^2(l^2 - v^2)q_\parallel}{d} \right\}, \tag{14.37}$$

$$K_{yy,mn}^{vl}(\vec{q}_\parallel, \omega) = Q_{lv}^{yy}(\vec{q}_\parallel, \omega)\frac{8\pi^4\mu_0 nmlv\omega q_\perp d^2[e^{iq_\perp d}(-1)^{n+m} - 1]}{[(iq_\perp d)^2 + \pi^2(n-m)^2][(iq_\perp d)^2 + \pi^2(n+m)^2]}$$
$$\times \frac{1 - r^s - \left(e^{-iq_\perp d} - r^s e^{iq_\perp d}\right)(-1)^{l+v}}{[(iq_\perp d)^2 + \pi^2(l-v)^2][(iq_\perp d)^2 + \pi^2(l+v)^2]} \tag{14.38}$$

$$K_{zx,mn}^{vl}(\vec{q}_\parallel, \omega) = -\frac{2\pi^2 ilv}{\varepsilon_0\omega}\frac{4\pi^4 nm(n^2 - m^2)[e^{iq_\perp d}(-1)^{n+m} - 1]}{d[(iq_\perp d)^2 + \pi^2(n-m)^2][(iq_\perp d)^2 + \pi^2(n+m)^2]}$$
$$\times \frac{1 + r^p - \left(e^{-iq_\perp d} + r^p e^{iq_\perp d}\right)(-1)^{l+v}}{[(iq_\perp d)^2 + \pi^2(l-v)^2][(iq_\perp d)^2 + \pi^2(l+v)^2]}$$
$$\times \left\{ Q_{lv}^{xx}(\vec{q}_\parallel, \omega)q_\perp^2 d + Q_{lv}^{xz}(\vec{q}_\parallel, \omega)\frac{\pi^2(l^2 - v^2)q_\parallel}{d} \right\} \tag{14.39}$$

$$K_{zz,mn}^{vl}(\vec{q}_\parallel, \omega) = \frac{2\pi^2 ilv}{\varepsilon_0\omega}\frac{4\pi^4 nm(n^2 - m^2)[e^{iq_\perp d}(-1)^{n+m} - 1]}{d[(iq_\perp d)^2 + \pi^2(n-m)^2][(iq_\perp d)^2 + \pi^2(n+m)^2]}$$
$$\times \frac{1 + r^p - \left(e^{-iq_\perp d} + r^p e^{iq_\perp d}\right)(-1)^{l+v}}{[(iq_\perp d)^2 + \pi^2(l-v)^2][(iq_\perp d)^2 + \pi^2(l+v)^2]}$$
$$\times \left\{ iQ_{lv}^{xz}(\vec{q}_\parallel, \omega)q_\perp^2 d - Q_{lv}^{zz}(\vec{q}_\parallel, \omega)\frac{\pi^2(l^2 - v^2)q_\parallel}{id} \right\}. \tag{14.40}$$

To find $\vec{\Omega}_{mn}(\vec{q}_\parallel, \omega)$ is in general a much more difficult task, but insertion of the expression for $\vec{E}_{\text{PC}}^{\text{B}}(z; \vec{q}_\parallel, \omega)$ gives

$$\Omega_{x,mn}(\vec{q}_\parallel, \omega) = -i\mu_0\omega \int_{-d}^0 \mathcal{Z}_{mn}^x(z) \int_{-d}^0 \left[G_{xx}(z, z'; \vec{q}_\parallel)J_{-\omega,x}^{(3)}(z'; \vec{q}_\parallel) \right.$$
$$\left. + G_{xz}(z, z'; \vec{q}_\parallel)J_{-\omega,z}^{(3)}(z'; \vec{q}_\parallel) \right] dz' dz, \tag{14.41}$$

$$\Omega_{y,mn}(\vec{q}_{\parallel},\omega) = -\mathrm{i}\mu_0\omega \int_{-d}^{0} \mathcal{Z}_{mn}^x(z) \int_{-d}^{0} G_{yy}(z,z';\vec{q}_{\parallel}) J_{-\omega,y}^{(3)}(z';\vec{q}_{\parallel}) dz' dz, \tag{14.42}$$

$$\Omega_{z,mn}(\vec{q}_{\parallel},\omega) = -\mathrm{i}\mu_0\omega \int_{-d}^{0} \mathcal{Z}_{mn}^z(z) \int_{-d}^{0} \frac{q_{\parallel}}{q_{\perp}} \Big[G_{xx}(z,z';\vec{q}_{\parallel}) J_{-\omega,x}^{(3)}(z';\vec{q}_{\parallel})$$

$$+ G_{xz}(z,z';\vec{q}_{\parallel}) J_{-\omega,z}^{(3)}(z';\vec{q}_{\parallel}) \Big] dz' dz. \tag{14.43}$$

These integrals can by insertion of the propagators and the wave functions be solved for the integral over z, and thus we find

$$\Omega_{x,mn}(\vec{q}_{\parallel},\omega) = -\frac{2\pi^2 inmq_{\perp}d \left[e^{iq_{\perp}d}(-1)^{n+m} - 1 \right]}{\varepsilon_0\omega[(iq_{\perp}d)^2 + \pi^2(n+m)^2][(iq_{\perp}d)^2 + \pi^2(n-m)^2]}$$

$$\times \int_{-d}^{0} \Big[q_{\perp} \left(e^{iq_{\perp}z} - r^p e^{-iq_{\perp}z} \right) J_{-\omega,x}^{(3)}(z;\vec{q}_{\parallel}) + q_{\parallel} \left(e^{iq_{\perp}z} + r^p e^{-iq_{\perp}z} \right) J_{-\omega,z}^{(3)}(z;\vec{q}_{\parallel}) \Big] dz, \tag{14.44}$$

$$\Omega_{y,mn}(\vec{q}_{\parallel},\omega) = -\frac{2\pi^2 \mathrm{i}\mu_0\omega nmd \left[e^{iq_{\perp}d}(-1)^{n+m} - 1 \right]}{[(iq_{\perp}d)^2 + \pi^2(n+m)^2][(iq_{\perp}d)^2 + \pi^2(n-m)^2]}$$

$$\times \int_{-d}^{0} \left(e^{iq_{\perp}z} + r^s e^{-iq_{\perp}z} \right) J_{-\omega,y}^{(3)}(z;\vec{q}_{\parallel}) dz, \tag{14.45}$$

$$\Omega_{z,mn}(\vec{q}_{\parallel},\omega) = -\frac{2\pi^4 q_{\parallel} nm(n^2 - m^2) \left[e^{iq_{\perp}d}(-1)^{m+n} - 1 \right]}{\varepsilon_0\omega d[(iq_{\perp}d)^2 + \pi^2(n+m)^2][(iq_{\perp}d)^2 + \pi^2(n-m)^2]}$$

$$\times \int_{-d}^{0} \left[\left(e^{iq_{\perp}z} - r^p e^{-iq_{\perp}z} \right) J_{-\omega,x}^{(3)}(z;\vec{q}_{\parallel}) + \frac{q_{\parallel}}{q_{\perp}} \left(e^{iq_{\perp}z} + r^p e^{-iq_{\perp}z} \right) J_{-\omega,z}^{(3)}(z;\vec{q}_{\parallel}) \right] dz, \tag{14.46}$$

where we have dropped the now superfluous marking z' in favor of a new z. Since the z-dependence of $\vec{J}_{-\omega}^{(3)}(z;\vec{q}_{\parallel})$ is expressed via the interacting fields and the wave functions, and we are limiting ourselves to studies where (i) the pump fields are parallel to either the x-axis or the z-axis and with uniform amplitude profile along that axis, and (ii) the probe field has only one plane-wave component on the form $\vec{E}(z;\vec{q}_{\parallel}) = \vec{E}e^{iq_{\perp}z}$, the last integral above can be solved. This solution is discussed in Appendix C, sections C.8 and C.9. Thus, in Eq. (14.24), all K's and Ω's are numbers with no inline integrals to solve numerically.

Chapter 15

Numerical results for a two-level quantum well

Besides calculation of the nonlinear current densities, the main numerical work consists of finding the solution to the appropriate sets of equations, given by Eq. (14.31) for processes with s-polarized response, and Eqs. (14.32) and (14.33) for processes with p-polarized response. Computational procedures to solve this kind of problems are well known (see, e.g., Press, Teukolsky, Vetterling, and Flannery 1992, 1996a, 1996b for description and Fortran routines).

15.1 Phase conjugation reflection coefficient

To estimate the amount of light we get back through the phase conjugated channel, we use the phase conjugation reflection coefficient $R_{\mathrm{PC}}(z; \vec{q}_\parallel)$ defined in Eq. (11.1) together with the expression for the intensities given by Eq. (11.2). As before, the reflection coefficient at the surface of the quantum well is thus $R_{\mathrm{PC}}(-d; \vec{q}_\parallel)$.

In order to give an impression of the difference between the calculation where only intraband contributions were taken into account (chapter 11) the present calculation is also based on the data for a two-monolayer thick copper quantum well [$N_+ = 8.47 \times 10^{28} \mathrm{m}^{-3}$, $Z = 1$, and $d = 3.8$Å (Ashcroft and Mermin 1976)]. As was the case for the single-level Cu quantum well, the two-level Cu quantum well can adequately be deposited on a glass substrate for which we use a refractive index n of 1.51. With this substrate, a reasonable description of the linear vaccum/substrate amplitude reflection coefficients (r^p for the p-polarized light and r^s for the s-polarized light) can be obtained by use of the classical Fresnel formulae, given by Eq. (11.3) and

$$r^s = \frac{q_\perp - (n^2 q^2 - q_\parallel^2)^{\frac{1}{2}}}{q_\perp + (n^2 q^2 - q_\parallel^2)^{\frac{1}{2}}}. \tag{15.1}$$

Keeping the pump fields parallel to the x-axis, we get a pump wavenumber $k_\parallel = 1.51q$.

In Figs. 15.1 and 15.2 we have plotted the phase conjugation reflection coefficient at the interface between the vacuum and the quantum well as a function of the parallel component of the wavevector normalized to the vacuum wavenumber, $q_\parallel/q$. The wavelength has in these plots been fixed to $\lambda = 1061$nm (the same as in the single-level case). The
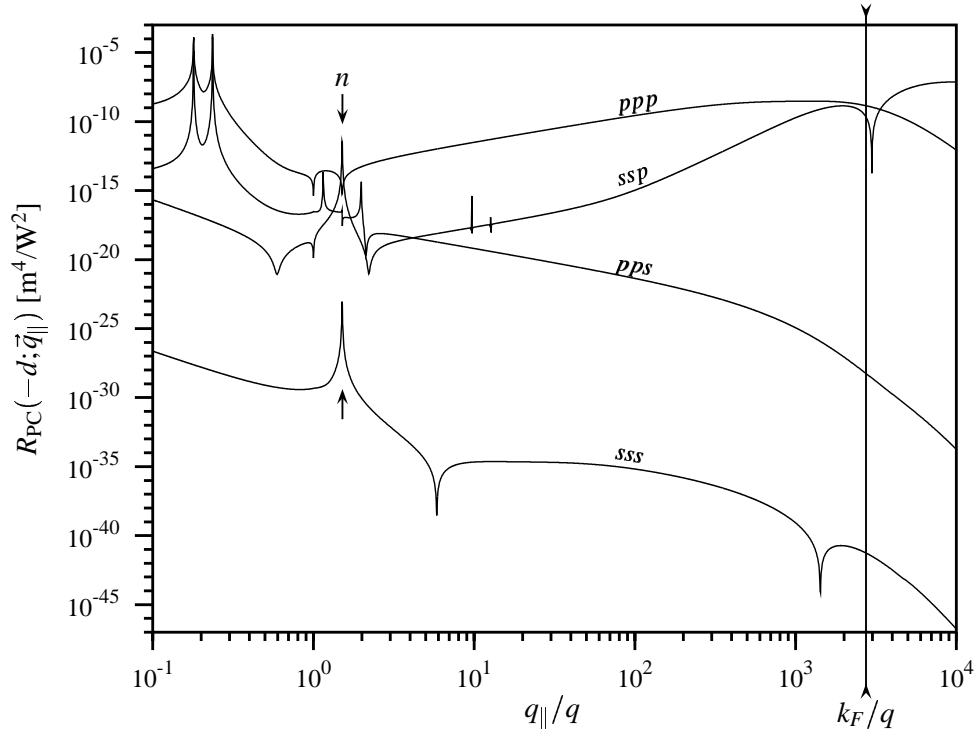
Figure 15.1: The phase conjugation reflection coefficient at the vaccum/quantum-well interface is plotted as a function of the normalized component of the probe wavevector along the surface, $q_\parallel/q$, for the four combinations of polarization of the three interacting fields, in which the two pump fields have the same polarization (ppp, sss, ssp, and pps), corresponding to the four diagrams shown in Fig. 9.2. The vertical line indicates the normalized Fermi wavenumber, which for the two-monolayer Cu quantum well is 2.78×10^3. The set of arrows labeled n are placed at $q_\parallel = nq$.

plots have been divided into two sets, together covering all eight different combinations of polarization of the interacting fields. In Fig. 15.1 is plotted the four combinations leading to a response with the same state of polarization as the probe, i.e., (i) the purely p-polarized case where all interacting fields are polarized in the scattering plane (denoted ppp), (ii) the purely s-polarized (sss) case where all three interacting fields are polarized perpendicular to the scattering plane, (iii) the case where the two pump fields both are p-polarized and the probe field is s-polarized (pps), and (iv) the case where the probe field is p-polarized and the two pump fields are s-polarized (ssp). The results for the other four combinations of polarization has been plotted in pairs in Fig. 15.2. The upper figure in Fig. 15.2 shows the two cases where the pump fields are differently polarized and the probe field is s-polarized, while in the lower figure, the probe field is p-polarized, still with differently polarized pump fields. The vertical line inserted into Figs. 15.1 and 15.2 indicates the normalized Fermi wavenumber, which for the two-monolayer Cu quantum
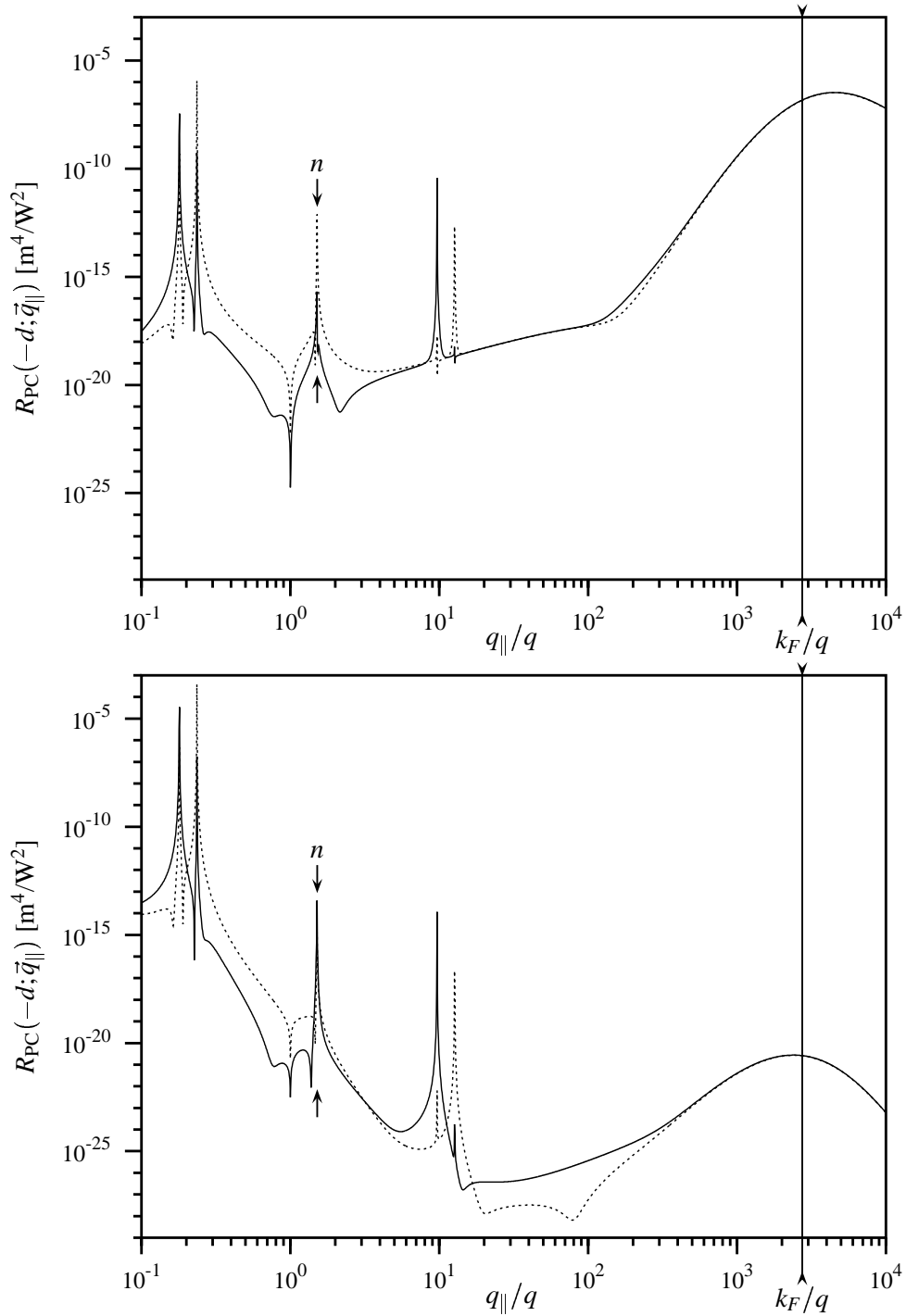
Figure 15.2: Same parameters as in Fig. 15.1, but for the other four polarization combinations (see Fig. 9.3). The upper figure shows the responses where *s*-polarized probe gives *p*-polarized response [*pss* (solid line) and *sps* (dotted line)]. The lower figure shows the opposite cases [*psp* (solid line) and *psp* (dotted line)]. Further explanation can be found in the main text.
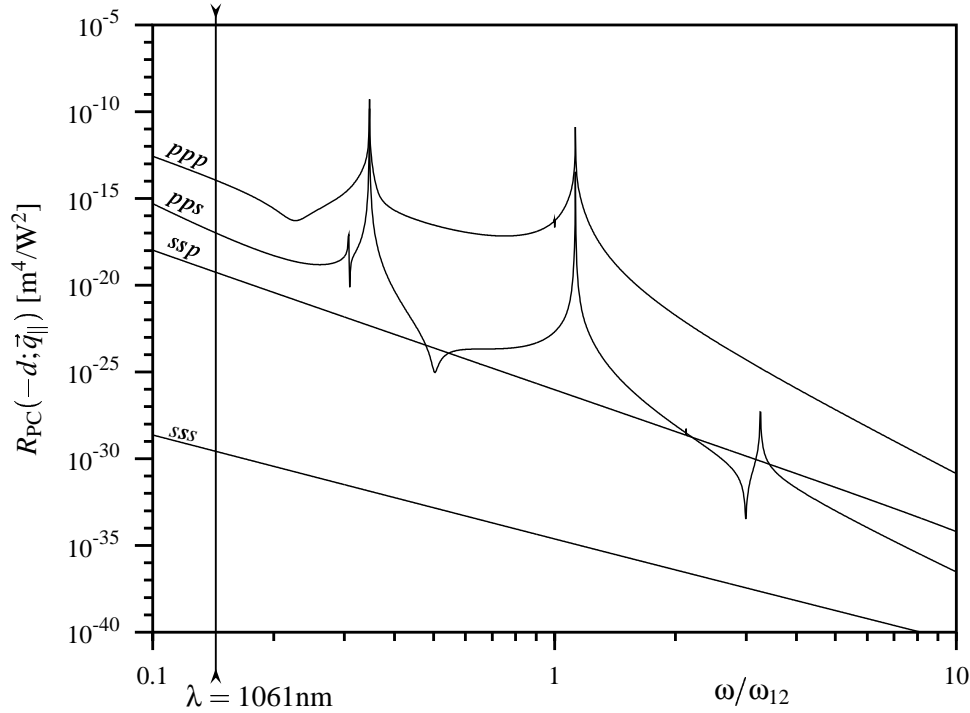
Figure 15.3: The phase conjugation reflection coefficient at the vaccum/quantum-well interface is plotted as a function of the optical frequency normalized to the transition frequency of the two-level quantum well, ω/ω_{12}, for the four combinations of polarization of the three interacting fields which have equal pump field polarization (ppp, sss, ssp, and pps). The transition frequency ω_{12} in the present case is $\omega_{12} = 1.32 \times 10^{16}$rad/s, corresponding to a wavelength of $\lambda = 142.4$nm. The vertical line indicates $\lambda = 1061$nm, the point in the frequency spectrum where Figs. 11.1 and 11.2 have been drawn.

well is 2.78×10^3. The discussion of this quantity has been given in chapter 11 (in the paragraph starting at the end of page 78).

In addition to the plots in Figs. 15.1 and 15.2, where the phase conjugation reflection coefficient was plotted as a function of $q_\parallel/q$, we have in Figs. 15.3 and 15.4 plotted the phase conjugation reflection coefficient as a function of the optical frequency normalized to the interband transition frequency, ω/ω_{12}. The parallel component of the wavevector has in this case been fixed at $q_\parallel = 0.8q$ (in the propagating regime). Again, the four cases of pump fields having the same polarization are plotted in the first of the two figures (Fig. 15.3), and the remaining four in the other figure (Fig. 15.4).

All plots in Figs. 15.1–15.4 have been plotted using a relaxation time of 200fs in the interband transition from the occupied state to the unoccupied state and a relaxation time of 3fs within the intraband transitions of the occupied state. Unlike in the case of pure intraband response, the choice of adequate relaxation times seem less important in the two-level quantum-well case. Changing either of the relaxation times (or both) an order
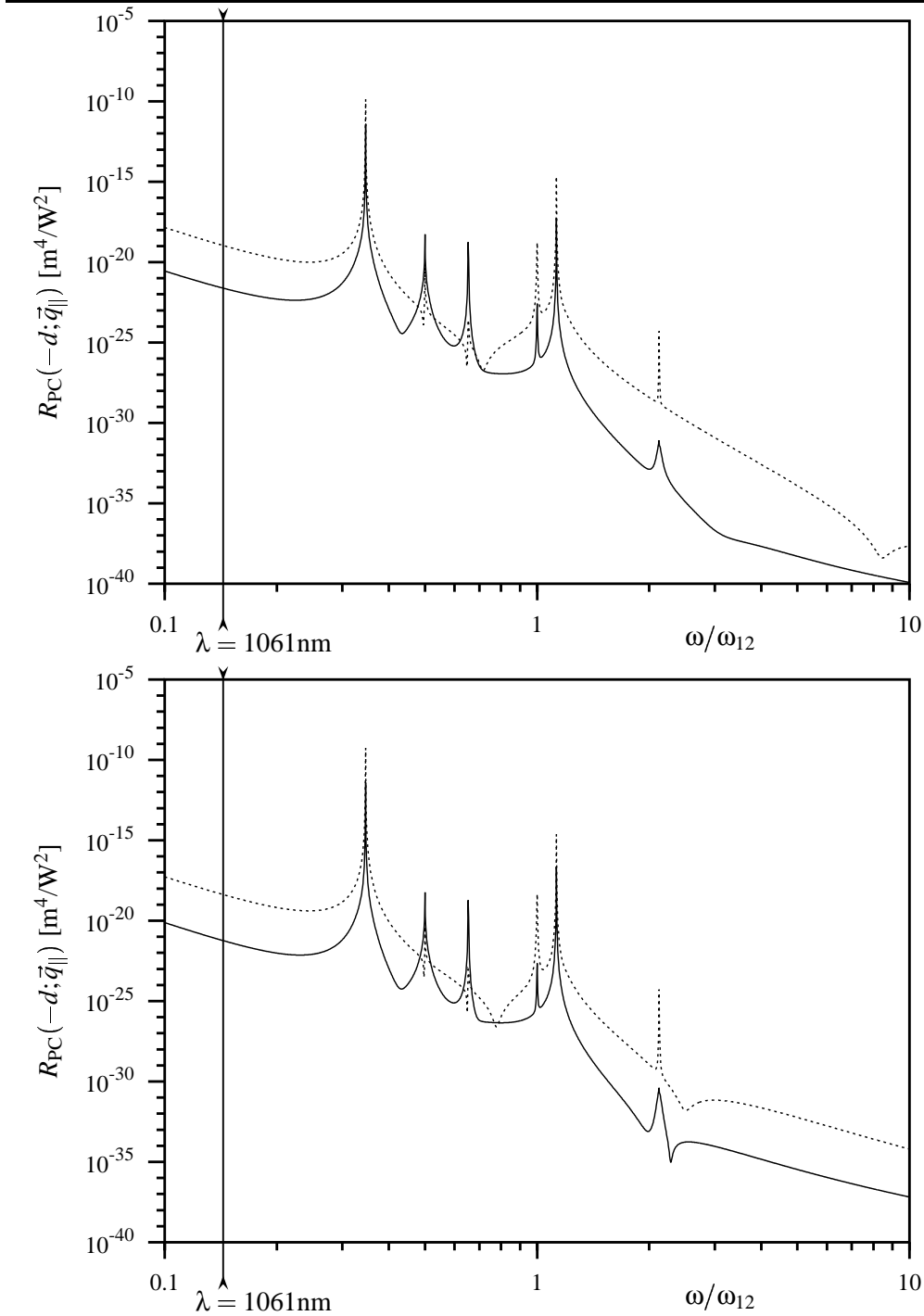
Figure 15.4: Same parameters as in Fig. 15.3, but for the other four polarization combinations. The upper figure shows the responses where *s*-polarized probe gives *p*-polarized response [*pss* (solid line) and *sps* (dotted line)]. The lower figure shows the opposite cases [*psp* (solid line) and *spp* (dotted line)]. For further explanation, please consult the main text.

of magnitude up or down doesn't change the results shown in Figs. 15.1–15.4 so much that the two curves for the respective choices of relaxation times would differ from each other, as it was the case in the single-level quantum well (see Fig. 11.4).

Returning our attention to Fig. 15.1, we observe that the purely p-polarized combination of polarization gives the strongest phase conjugated response while the purely s-polarized combination gives the weakest response of the four. Looking at the ppp curve, we see that the maximum value is reached in the propagating regime of the $q_\parallel/q$-spectrum, where two peaks occur approximately at the values of $q_\parallel = 0.18q$ and $q_\parallel = 0.22q$. These peaks must be due to the pump waves being p-polarized, since they also occur in the pps configuration, but in neither of the sss and ssp configurations. In the evanescent regime the ppp curve is increasing from the point $q_\parallel = nq$ until it reaches its maximal value at around $q_\parallel = 10^3 q$. Above $q_\parallel = 10^3 q$, the ppp response starts decaying again. The pps curve in Fig. 15.1 has, apart from the two peaks discussed above, two additional peaks occuring symmetrically around the point nq in the $q_\parallel$-spectrum, at approximately $q_\parallel = 1.1q$ and $q_\parallel = 1.9q$, respectively. After the second of these peaks, the amplitude of the response fades away with growing values of $q_\parallel$. The ssp curve has a maximum when the probe field is perpendicularly incident on the phase conjugator ($q_\parallel/q = 0$), and another one where the probe field becomes evanescent in the substrate, i.e., at $q_\parallel = nq$. In the evanescent regime of the $q_\parallel/q$-spectrum the response is increasing, with two small narrow peaks occuring at $q_\parallel \approx 10q$ and $q_\parallel \approx 13q$, and it reaches a maximum at $q_\parallel \approx 2 \times 10^3$, and after going down to a minimum right after k_F/q it increases again. This indicates that if we are able to produce probe fields with a significant amount of evanescent modes above k_F/q, the present model is probably not sufficient to describe the ssp response (and maybe not sufficient to describe the ppp response either). The last of the curves in Fig. 15.1 represents the purely s-polarized case (sss). It has maxima at $q_\parallel/q = 0$, and again at $q_\parallel/q = n$. Above $q_\parallel = nq$ it falls off rapidly.

Looking at the $q_\parallel/q$-spectrum of the phase conjugated response in the other four combinations of polarization, depicted in Fig. 15.2, we see that both pairs have peaks in the propagating regime of the $q_\parallel/q$-spectrum at the same places as the ppp and pps curves of Fig. 15.1 had. Another peak appears when $q_\parallel = nq$, and in the purely evanescent part of the $q_\parallel/q$-spectrum peaks appear at $q_\parallel \approx 10q$ and $q_\parallel \approx 13q$, the same places as in the ssp response shown in Fig. 15.1. After these two peaks the responses of the pss/sps-pair increases until they reach their maximum at around $q_\parallel = 5 \times 10^3$, after which they decrease again. This maximum is comparable in magnitude to the peaks in the propagating end of the $q_\parallel/q$-spectrum. We observe that the two curves in each of the pairs shown in Fig. 15.2 becomes identical for high values of $q_\parallel$, as they should from the previous analysis. The spp/psp-pair of curves also starts increasing in magnitude in the high end of the $q_\parallel/q$-spectrum showed. They reach their maximum at around $q_\parallel = 2.5 \times 10^3 q$, after which the magnitude decreases again. In this case, however, the magnitude of this maximum is some fifteen orders of magnitude less than the magnitude of the peaks in the propagating regime. The problem in the sps/pss-pair of curves is that the maximal value is reached after the point $q_\parallel = k_F/q$, and the conclusion must therefore be the same as in the ssp case, namely that if the probe has components of significance in the high

end of the $q_\parallel/q$-spectrum, then the model should probably be extended in one way or another.

Continuing to the frequency plots, we observe from Fig. 15.3 that the two cases where both pump fields are s-polarized has no resonances at all. Their decrease in magnitude as the frequency increases is mainly due to the factor of ω^{-3} occuring in the nonlinear conductivity tensor. The ppp curve has a peak of high magnitude at $\omega \approx \omega_{12}/3$, a small one at $\omega = \omega_{12}$, and a large one again at $\omega \approx 1.1\omega_{12}$. The pps curve has a peak of small magnitude at $\omega = 0.3\omega_{12}$, two large ones at $\omega \approx \omega_{12}/3$ and at $\omega \approx 1.1\omega_{12}$, and finally a small one at $\omega \approx 3.2\omega_{12}$. The peaks around $\omega \approx \omega_{12}$ probably arise from the combination of the denominators in the nonlinear conductivity tensors, but none of the peaks have been clearly identified from the formulas yet. Going to any of the two sides in the frequency spectrum away from this group of resonances, the curves behave like the sss and ssp curves, with the magnitude proportional to ω^{-3}. The frequency plots for the two pairs of polarization combinations where the pump fields are differently polarized (Fig. 15.4) have resonances with the approximate values of ω/ω_{12} of 1/3, 1/2, 2/3, 1, 1.1, and 2. Like in the previous case, these peaks have not been clearly identified from the formulas yet. Again one might assume that the peaks at 1 and 1.1 arise directly from (some of) the denominators in the nonlinear conductivity tensors. As before, outside of the shown frequency range, the behaviour of the response is proportional to ω^{-3}. The results presented in this chapter will be treated more thoroughly in a forthcoming paper.

Chapter 16

Discussion

In the past two chapter we have briefly shown how to calculate the phase conjugated response from a multilevel quantum well and given numerical results for a two-level quantum well. As we concluded in the single-level quantum-well case, the assumption of an ideal phase conjugator also does not hold for a two-level quantum-well phase conjugator. In this case, however, it is not so much because of the efficiency in the high end of the $q_\parallel$-spectrum, since in most of the cases shown in chapter 15 the efficiency in the evanescent regime is not so much larger than in the propagating regime. It is more because the two-level phase conjugator is much more efficient for certain values of $q_\parallel$ than for the rest of the spectrum.

However, before we can give a full description of the phase conjugated response from multi-level quantum wells, some aspects has to be addressed. Among the important ones are the fact that we need to identify (i) which terms of the nonlinear conductivity tensor that are dominating the phase conjugation response, and if it is possible by a careful choice of the system to make different terms dominate. Furthermore (ii) it is desirable to find out more precisely which individual terms in the nonlinear conductivity tensor gives rise to each of the peaks occuring in the curves in Figs. 15.1–15.4. Many other things has to be investigated, for example (i) the behaviour of the response close to the peaks in Figs. 15.1–15.4, both in the frequency spectrum and in the $q_\parallel$-spectrum, (ii) the frequency dependence in general, and (iii) the response to sources with a large number of Fourier components in the $q_\parallel$-spectrum, such as the quantum wire discussed in Chapter 12.

113

Part VI

Closing remarks

Summary of conclusions

We have developed a spatially nonlocal theoretical model of degenerate four-wave mixing of electromagnetic fields on the mesoscopic length scale. We have analyzed the physical processes involved in creating the DFWM response and identified the independent nonzero elements of the related conductivity tensor for each type of process. Following the more general treatment in real space we have specialized the treatment to take into account only cases where translational invariance against displacements in two of the three spatial dimensions occur, thereby favouring a description in which the optical processes occur in surfaces and thin films of condensed matter.

As a consequence of this choice we have transformed the response function into Fourier space in two spatial coordinates, keeping the real-space coordinate in the third dimension. From there, the emphasis has been laid on phase conjugation, although the more general DFWM response tensor has been carried out in this mixed Fourier space as well. The emphasis on phase conjugation was realized by the choice of letting two of the interacting fields be spatially counterpropagating. Letting the two counterpropagating fields act as pump fields in the phase conjugation process, the third of the interacting fields became what we have referred to as the probe field.

The choice of a scattering geometry in which the pump fields were taken to be undamped plane waves traveling parallel to the translationally invariant plane resulted in a description where the main effort could be concentrated on studying the response due to the probe field, thus letting the pump fields effectively being a part of the phase conjugator. We concluded that using different combinations of light polarized in the scattering plane or perpendicular to this plane lead to different properties of the phase conjugated field compared to the incoming probe field, including changes in polarization in some cases.

Using the developed model on a single-level metallic quantum-well phase conjugator we have shown that the phase-conjugation reflection coefficient behaves quite differently from the uniform reflection coefficient that has often been assumed in previous studies where evanescent components have been included (Agarwal and Gupta 1995; Keller 1992). The response in the high end of the $q_\parallel$-spectrum turned out to be as much as ten orders of magnitude larger than in the propagating regime. Subsequently, it was shown that by use of the single-level phase conjugator it was possible to phase conjugate light emitted from a subwavelength source in the vicinity of the phase conjugator, and that the phase conjugated light at the plane parallel to the phase conjugator, where the source has been placed, has a subwavelength distance between the minima in the intensity. Consistent with another recent prediction (Bozhevolnyi 1997; Bozhevolnyi and Vohnsen 1997) we have observed that the smallest distance between the two minima surrounding the main lobe in the phase conjugated field occur at the surface of the phase conjugator.

The theoretical model was concluded with a description of a quantum well with an arbitrary number of bound states, followed by a numerical calculation of the response from a two-level quantum well. We have shown that also the two-level quantum well does not come close to an ideal phase conjugator with a uniform reflection coefficient

in the $q_\parallel$-spectrum. Furthermore, it does not behave the same way as the single-level quantum well, even though the combinations of polarization for the interacting fields that gives a p-polarized response lead to similar results in the high end of the $q_\parallel$-spectrum. In the low end of the $q_\parallel$-spectrum the phase conjugated response from a two-level quantum well is several orders of magnitude stronger in a small number of very narrow ranges in $q_\parallel$ than in the rest.

Finally, we concluded that if one is able to excite the two-level quantum well in the $q_\parallel$-range around the point of the Fermi wave number the present model could prove insufficient, because the maximum value of the phase conjugation reflection coefficient in the high end of the $q_\parallel$-spectrum in several cases is above the Fermi wave number.

Discussion and outlook

With respect to the single-level quantum well several properties would be interesting to examine from a fundamental point of view, including (i) the response in the far-infrared and ultraviolet parts of the frequency spectrum, (ii) how the response can be divided into an electrostatic and an electrodynamic part, (iii) how the width of the phase conjugated focus from a quantum wire scales with the wavelength of the electromagnetic field used in the interaction, and (iv) the problem of a three-dimensional source.

For the two-level quantum well plenty of work remains to be done before it would be wise to take up some of the above-mentioned properties. First of all, we have to determine how much each of the terms in the nonlinear conductivity tensor contributes to the phase conjugated response. Also, the problem of phase conjugating a broad angular band should be addressed in order to study, for instance, focusing of light in front of a two-level phase conjugator.

The problem of focusing has to be addressed more carefully, since the present study has revealed only that when the mesoscopic source is moved closer to the phase conjugator the focus is narrowed. I imagine that this problem could be addressed properly using a pure engineering approach to make an adjustment of the present model by (i) abandoning the infinite barrier model by insertion of a more sophisticated potential across the barrier, and (ii) abandoning the point-source description of the probe field. Thereby one would also be able to discuss the problem of resolution in a near-field optical microscope.

Furthermore, it could be interesting to establish a model which provides a temporal resolution. It could be used to study, for example, the time delay and distortion of an electromagnetic pulse (wave packet) being phase conjugated, initially using, for example, plane waves as pumps, and ultimately to give an understanding of four-wave mixing using pulsed interacting fields. Such a model would provide a framework for a description of time-resolved optical phase conjugation in, for example, communications systems.

On the more sophisticated fundamental side it could be interesting to investigate the phase conjugated response when the phase conjugator is, for example, a mesoscopic ring, cylinder, sphere, or a quantum wire. Another possibility is to take into account

spin effects in order to treat the phase conjugation response from magnetic materials. We also believe that there is a connection between the model for electromagnetic phase conjugation presented in this work and phase conjugation of electrons and atoms [for an introduction to atomic phase conjugation and nonlinear atom optics, see Lenz, Meystre, and Wright (1993, 1994) and Goldstein, Plättner, and Meystre (1995)].

A problem that has to be taken into account when using the present formulation to describe nonlinear optical processes is the apparently divergent behaviour in the long-wavelength (low-frequency) limit stemming (in third-order problems) from the ω^{-3}-term in the beginning of the nonlinear conductivity tensor. This problem is a general one in the theoretical model, and although the linear problem has been solved (Keller 1996a), the problem has still not been solved for any nonlinear case, including DFWM.

If time permits, I shall substantiate on some of these points in future work. Otherwise, it will be left for others to do.

We are very lucky to live in an age in which we are still making discoveries.
Richard P. Feynman in *The Character of Physical Law, p. 172.*

Appendices

Appendix A

Calculation of linear and nonlinear conductivity tensors in two-dimensionally translational invariant systems [$(z;\vec{q}_\parallel)$-space]

In this appendix I present a calculation of linear and nonlinear conductivity tensors suitable for calculation of the linear and nonlinear current densities in a physical system with translational invariance only in the *x* and *y* directions of the Cartesian *x-y-z*-coordinate system. The basic ingredients in this calculation consists of (i) the Fourier integral representation of the vector potential in the *x*- and *y*-coordinates given by Eq. (8.1), (ii) the inverse relation for the current densities linear in the cyclic frequency ω (appeared as Eq. (8.2)), (iii) the basis set of the wave functions taken on the form of Eq. (8.9), and (iv) the corresponding transition current density in Eq. (8.14). Using these ingredients we start from the three-dimensional expressions in real space, which in the linear case are given by Eq. (4.9) with insertion of Eqs. (6.6)–(6.7) and in the nonlinear case are given by Eq. (4.10) with insertion of Eqs. (6.8)–(6.14). The results of these calculations are presented as expressions for the individual matrix elements according to the definitions given by Eq. (8.3) for the linear conductivity tensor and Eq. (8.8) for the nonlinear conductivity tensor, the cyclic transition frequencies being expressed in the form of Eq. (8.12).

For convenience, we in the following treatment divide the linear current density into two parts following the two processes shown in Fig. 5.1. If we define the linear current density as $J_i(z;\vec{q}_\parallel) = \sum_j J_{ij}(z;\vec{q}_\parallel)$, the result of calculating the linear conductivity tensor is presented as the individual nonzero matrix elements corresponding to the symmetry analysis presented in Chapter 6. Like in the linear case, it is convenient in the nonlinear case to define the nonlinear current density as $J_i(\vec{r}) \equiv \sum_{jkh} J_{ijkh}(\vec{r})$, with $J_{ijkh}(\vec{r}) = \Xi_{ijkh}(\vec{r},\vec{r}',\vec{r}'',\vec{r}''')A_h(\vec{r}''')A_k(\vec{r}'')A_j(\vec{r}')$, and then split the treatment of the nonlinear current density in such a way that each of the processes mentioned in Fig. 5.2 is treated separately.

A.1 Linear process A

From Eq. (6.6) we have the *xx* element of part A of the linear current, in which we insert the expressions for the wave function and the vector potential in the two-dimensional

Fourier representation, giving the result

$$
J_{xx}^{\mathrm{A}}(z;\vec{q}_\|) = -\frac{e^2}{m_e}\frac{2}{(2\pi)^4}\iiint\sum_n f_n|\psi_n(z)|^2\delta(\vec{r}-\vec{r}')A_x(z';\vec{q}_\|')e^{\mathrm{i}\vec{q}_\|'\cdot\vec{r}_\|'}d^2q_\|'d^3r'
$$
$$
\times e^{-\mathrm{i}\vec{q}_\|\cdot\vec{r}_\|}d^2r_\|. \tag{A.1}
$$

Solving the integrals over the real-space coordinates in the x-y-directions, $\int d^2r_\|'$ and $\int d^2r_\|$, we obtain

$$
J_{xx}^{\mathrm{A}}(z;\vec{q}_\|) = -\frac{e^2}{m_e}\frac{2}{(2\pi)^2}\iiint\sum_n f_n(\vec{\kappa}_{\|,\bar{n}})|\psi_n(z)|^2\delta(z-z')\delta(\vec{q}_\|'-\vec{q}_\|)
$$
$$
\times A_x(z';\vec{q}_\|')d^2\kappa_{\|,\bar{n}}d^2q_\|'dz', \tag{A.2}
$$

where the (infinite) sum over the $\kappa_\|$ coordinates has been replaced by an integral. From this expression we extract part A of the linear conductivity tensor as

$$
\sigma_{xx}^{\mathrm{A}}(z,z';\vec{q}_\|,\vec{q}_\|') = -\frac{2}{\mathrm{i}\omega}\frac{e^2}{m_e}\frac{1}{(2\pi)^2}\sum_n\int f_n(\vec{\kappa}_\|)d^2\kappa_\||\psi_n(z)|^2\delta(z-z')\delta(\vec{q}_\|'-\vec{q}_\|), \quad \text{(A.3)}
$$

where we have omitted the now superfluous reference to n from $\vec{\kappa}_\|$. Taking into account the conservation of momentum given by the Dirac delta function $\delta(\vec{q}_\|'-\vec{q}_\|)$ we may integrate over $q_\|'$ in Eq. (A.2), and thereafter extract part A of the linear conductivity tensor as presented in Eq. (8.15).

A.2 Linear process B

Taking from Eq. (6.7) element ij of part B of the linear current density and inserting the expressions for the wave function [Eq. (8.9)] and the transition current density [Eq. (8.14)] in the two-dimensional Fourier representation, we get

$$
J_{ij}^{\mathrm{B}}(z;\vec{q}_\|) = -\frac{1}{\hbar}\frac{2}{(2\pi)^6}\iiint\sum_{nm}\frac{f_n-f_m}{\tilde{\omega}_{nm}-\omega}j_{j,mn}(z';\vec{\kappa}_{\|,\bar{m}}+\vec{\kappa}_{\|,\bar{n}})j_{i,nm}(z;\vec{\kappa}_{\|,\bar{n}}+\vec{\kappa}_{\|,\bar{m}})
$$
$$
\times e^{\mathrm{i}(\vec{\kappa}_{\|,\bar{m}}-\vec{\kappa}_{\|,\bar{n}})\cdot\vec{r}_\|'}e^{\mathrm{i}(\vec{\kappa}_{\|,\bar{n}}-\vec{\kappa}_{\|,\bar{m}})\cdot\vec{r}_\|}A_j(z';\vec{q}_\|')e^{\mathrm{i}\vec{q}_\|'\cdot\vec{r}_\|'}d^2q_\|'d^3r'e^{-\mathrm{i}\vec{q}_\|\cdot\vec{r}_\|}d^2r_\|. \tag{A.4}
$$

Solving the Cartesian integrals $\int d^2r_\|'$ and $\int d^2r_\|$ along the surface and replacing the infinite sum over $\vec{\kappa}_\|$ with an integral, this is

$$
J_{ij}^{\mathrm{B}}(z;\vec{q}_\|) = -\frac{1}{\hbar}\frac{2}{(2\pi)^2}\int\cdots\int\sum_{nm}\frac{f_n(\vec{\kappa}_{\|,\bar{n}})-f_m(\vec{\kappa}_{\|,\bar{m}})}{\tilde{\omega}_{nm}(\vec{\kappa}_{\|,\bar{n}},\vec{\kappa}_{\|,\bar{m}})-\omega}j_{j,mn}(z';\vec{\kappa}_{\|,\bar{m}}+\vec{\kappa}_{\|,\bar{n}})
$$
$$
\times j_{i,nm}(z;\vec{\kappa}_{\|,\bar{n}}+\vec{\kappa}_{\|,\bar{m}})\delta(\vec{\kappa}_{\|,\bar{m}}-\vec{\kappa}_{\|,\bar{n}}+\vec{q}_\|')\delta(\vec{\kappa}_{\|,\bar{n}}-\vec{\kappa}_{\|,\bar{m}}-\vec{q}_\|)
$$
$$
\times A_j(z';\vec{q}_\|')d^2\kappa_{\|,\bar{n}}d^2\kappa_{\|,\bar{m}}d^2q_\|'dz'. \tag{A.5}
$$

Of these two integrals over the surface states, we can solve one because of the coupling between the surface states and the wavevectors introduced by the Dirac delta functions

appearing. Keeping the $\vec{\kappa}_{\parallel,\bar{m}}$ set, and thus we solve for the n set. Solving for this set, we find that $\vec{\kappa}_{\parallel,\bar{n}}$ is replaced by $\vec{\kappa}_{\parallel,\bar{m}} + \vec{q}_\parallel'$, thus giving

$$
\begin{aligned}
J_{ij}^{\mathrm{B}}(z; \vec{q}_\parallel) = & -\frac{1}{\hbar} \frac{2}{(2\pi)^2} \iiint \sum_{nm} \frac{f_n(\vec{\kappa}_{\parallel,\bar{m}} + \vec{q}_\parallel') - f_m(\vec{\kappa}_{\parallel,\bar{m}})}{\tilde{\omega}_{nm}(\vec{\kappa}_{\parallel,\bar{m}} + \vec{q}_\parallel', \vec{\kappa}_{\parallel,\bar{m}}) - \omega} j_{j,nm}(z'; 2\vec{\kappa}_{\parallel,\bar{m}} + \vec{q}_\parallel') \\
& \times j_{i,nm}(z; 2\vec{\kappa}_{\parallel,\bar{m}} + \vec{q}_\parallel') \delta(\vec{q}_\parallel' - \vec{q}_\parallel) A_j(z'; \vec{q}_\parallel') d^2\kappa_{\parallel,\bar{m}} d^2q_\parallel' dz'.
\end{aligned}
\tag{A.6}
$$

From the above expression we extract part B of the linear conductivity tensor as

$$
\begin{aligned}
\sigma_{ij}^{\mathrm{B}}(z, z'; \vec{q}_\parallel, \vec{q}_\parallel') = & -\frac{2}{i\omega} \frac{1}{\hbar} \frac{1}{(2\pi)^2} \sum_{nm} \int \frac{f_n(\vec{\kappa}_\parallel + \vec{q}_\parallel') - f_m(\vec{\kappa}_\parallel)}{\tilde{\omega}_{nm}(\vec{\kappa}_\parallel + \vec{q}_\parallel', \vec{\kappa}_\parallel) - \omega} j_{j,nm}(z'; 2\vec{\kappa}_\parallel + \vec{q}_\parallel') \\
& \times j_{i,nm}(z; 2\vec{\kappa}_\parallel + \vec{q}_\parallel') \delta(\vec{q}_\parallel' - \vec{q}_\parallel) d^2\kappa_\parallel,
\end{aligned}
\tag{A.7}
$$

where we have omitted the now superfluous index m from the surface states $\vec{\kappa}_\parallel$. Again we take into account the conservation of pseudo-momentum, $\delta(\vec{q}_\parallel' - \vec{q}_\parallel)$, letting us perform the integration over $q_\parallel'$ in Eq. (A.6). From this result the linear conductivity tensor part B is extracted on the form shown in Eq. (8.16).

A.3 Nonlinear process A

Inserting Eq. (6.8) into Eq. (4.10), we take element *xxxx* of part A of the nonlinear current density. In the result we insert the expressions for the wave function and the vector potential in the two-dimensional Fourier representation [Eqs. (8.9) and (8.1), respectively]. Then by use of Eq. (8.2) we find

$$
\begin{aligned}
J_{xxxx}^{\mathrm{A}}(z; \vec{q}_\parallel) = & -\frac{e^4}{8m_e^2\hbar} \frac{2}{(2\pi)^{10}} \int \cdots \int \sum_{nm} \frac{f_n - f_m}{\tilde{\omega}_{nm} - 2\omega} \psi_n^*(z'') \psi_m(z'') \psi_m^*(z) \psi_n(z) \\
& \times A_x(z'''; \vec{q}_\parallel''') A_x(z''; \vec{q}_\parallel'') A_x^*(z'; \vec{q}_\parallel') e^{i(\vec{\kappa}_{\parallel,\bar{m}} - \vec{\kappa}_{\parallel,\bar{n}}) \cdot \vec{r}''} e^{i(\vec{\kappa}_{\parallel,\bar{n}} - \vec{\kappa}_{\parallel,\bar{m}}) \cdot \vec{r}_\parallel} e^{i\vec{q}_\parallel''' \cdot \vec{r}_\parallel'''} e^{i\vec{q}_\parallel'' \cdot \vec{r}_\parallel''} e^{-i\vec{q}_\parallel' \cdot \vec{r}_\parallel'} \\
& \times \delta(\vec{r} - \vec{r}') \delta(\vec{r}'' - \vec{r}''') d^2q_\parallel''' d^2q_\parallel'' d^2q_\parallel' d^3r''' d^3r'' d^3r' e^{-i\vec{q}_\parallel \cdot \vec{r}_\parallel} d^2r_\parallel.
\end{aligned}
\tag{A.8}
$$

In this equation, we first solve the integrals $\int d^2r_\parallel'$ and $\int d^2r_\parallel'''$, thereafter the remaining Cartesian integrals $\int d^2r_\parallel''$ and $\int d^2r_\parallel$, and finally replace the infinite sums over the different $\vec{\kappa}_\parallel$ coordinates with integrals, thereby obtaining

$$
\begin{aligned}
J_{xxxx}^{\mathrm{A}}(z; \vec{q}_\parallel) = & -\frac{e^4}{8m_e^2\hbar} \frac{2}{(2\pi)^6} \int \cdots \int \sum_{nm} \frac{f_n(\vec{\kappa}_{\parallel,\bar{n}}) - f_m(\vec{\kappa}_{\parallel,\bar{m}})}{\tilde{\omega}_{nm}(\vec{\kappa}_{\parallel,\bar{n}}, \vec{\kappa}_{\parallel,\bar{m}}) - 2\omega} \psi_n^*(z'') \psi_m(z'') \psi_m^*(z) \psi_n(z) \\
& \times A_x(z'''; \vec{q}_\parallel''') A_x(z''; \vec{q}_\parallel'') A_x^*(z'; \vec{q}_\parallel') \delta(\vec{\kappa}_{\parallel,\bar{m}} - \vec{\kappa}_{\parallel,\bar{n}} + \vec{q}_\parallel''' + \vec{q}_\parallel'') \delta(\vec{\kappa}_{\parallel,\bar{n}} - \vec{\kappa}_{\parallel,\bar{m}} - \vec{q}_\parallel' - \vec{q}_\parallel) \\
& \times \delta(z - z') \delta(z'' - z''') d^2\kappa_{\parallel,\bar{n}} d^2\kappa_{\parallel,\bar{m}} d^2q_\parallel''' d^2q_\parallel'' d^2q_\parallel' dz''' dz'' dz'.
\end{aligned}
\tag{A.9}
$$

Of the two integrals over the $\kappa_\parallel$ quantities, we can solve one because of the coupling of these to the wavevectors introduced by the Dirac delta functions appearing. Keeping the

$\vec{\kappa}_{\parallel,\bar{m}}$ set we thus solve the integrals for the n set. Solving for this set, we find that $\vec{\kappa}_{\parallel,\bar{n}}$ is replaced by $\vec{\kappa}_{\parallel,\bar{m}} + \vec{q}_{\parallel}' + \vec{q}_{\parallel}$, which gives

$$
\begin{aligned}
J_{xxxx}^{\mathrm{A}}(z;\vec{q}_{\parallel}) = &-\frac{e^4}{8m_e^2\hbar}\frac{2}{(2\pi)^6}\int\cdots\int\sum_{nm}\frac{f_n(\vec{\kappa}_{\parallel,\bar{m}}+\vec{q}_{\parallel}'+\vec{q}_{\parallel})-f_m(\vec{\kappa}_{\parallel,\bar{m}})}{\tilde{\omega}_{nm}(\vec{\kappa}_{\parallel,\bar{m}}+\vec{q}_{\parallel}'+\vec{q}_{\parallel},\vec{\kappa}_{\parallel,\bar{m}})-2\omega}\psi_n^*(z'')\psi_m(z'') \\
&\times\psi_m^*(z)\psi_n(z)A_x(z''';\vec{q}_{\parallel}''')A_x(z'';\vec{q}_{\parallel}'')A_x^*(z';\vec{q}_{\parallel}')\delta(\vec{q}_{\parallel}'''+\vec{q}_{\parallel}''-\vec{q}_{\parallel}'-\vec{q}_{\parallel})\delta(z-z') \\
&\times\delta(z''-z''')d^2\kappa_{\parallel,\bar{m}}d^2q_{\parallel}'''d^2q_{\parallel}''d^2q_{\parallel}'dz'''dz''dz'.
\end{aligned}
\tag{A.10}
$$

From this we may extract part A of the nonlinear conductivity tensor as defined in Eq. (8.4) as

$$
\begin{aligned}
\Xi_{xxxx}^{\mathrm{A}}(z,z',z'',z''';\vec{q}_{\parallel},\vec{q}_{\parallel}',\vec{q}_{\parallel}'',\vec{q}_{\parallel}''') = &\frac{2\mathrm{i}}{\omega^3}\frac{e^4}{8m_e^2\hbar}\frac{1}{(2\pi)^2}\sum_{nm}\int\frac{f_n(\vec{\kappa}_{\parallel}+\vec{q}_{\parallel}'+\vec{q}_{\parallel})-f_m(\vec{\kappa}_{\parallel})}{\tilde{\omega}_{nm}(\vec{\kappa}_{\parallel}+\vec{q}_{\parallel}'+\vec{q}_{\parallel},\vec{\kappa}_{\parallel})-2\omega} \\
&\times\psi_n^*(z'')\psi_m(z'')\psi_m^*(z)\psi_n(z)\delta(\vec{q}_{\parallel}'''+\vec{q}_{\parallel}''-\vec{q}_{\parallel}'-\vec{q}_{\parallel})\delta(z-z')\delta(z''-z''')d^2\kappa_{\parallel},
\end{aligned}
\tag{A.11}
$$

where we have omitted the now superfluous index m from the surface states $\vec{\kappa}_{\parallel}$. Taking into account the fact that we look for the phase conjugation response we restrict ourselves to the case where the pump fields are counterpropagating, thus taking

$$
\vec{A}(z''';\vec{q}_{\parallel}''') \equiv \vec{A}(z''';-\vec{k}_{\parallel})\delta(\vec{q}_{\parallel}'''+\vec{k}_{\parallel}),
\tag{A.12}
$$

$$
\vec{A}(z'';\vec{q}_{\parallel}'') \equiv \vec{A}(z'';\vec{k}_{\parallel})\delta(\vec{q}_{\parallel}''-\vec{k}_{\parallel}),
\tag{A.13}
$$

where $\vec{k}_{\parallel}$ is the common wavevector for the two pump fields. With these substitutions we can perform the integrals over $q_{\parallel}'''$ and $q_{\parallel}''$ in Eq. (A.10), and the conservation of pseudo-momentum is reduced from its general degenerate four-wave mixing form, $\delta(\vec{q}_{\parallel}'''+\vec{q}_{\parallel}''-\vec{q}_{\parallel}'-\vec{q}_{\parallel})$, to $\delta(\vec{q}_{\parallel}'+\vec{q}_{\parallel})$. This allows us also to solve the integral over $q_{\parallel}'$ in Eq. (A.10), and on the form of Eq. (8.8) we can extract the PCDFWM conductivity tensor part A, appearing as Eq. (8.17).

A.4 Nonlinear process B

Inserting Eq. (6.9) into Eq. (4.10), we take element *xxkh* of part B of the nonlinear current density. In the result we insert the expressions for the wave function, the vector potential and the transition current density in the two-dimensional Fourier representation [Eqs. (8.9), (8.1) and (8.14), respectively]. Then by use of Eq. (8.2) we find

$$
\begin{aligned}
J_{xxkh}^{\mathrm{B}}(z;\vec{q}_{\parallel}) = &-\frac{e^2}{4m_e\hbar^2}\frac{2}{(2\pi)^{12}}\int\cdots\int\sum_{nmv}\frac{1}{\tilde{\omega}_{nm}-2\omega}\left(\frac{f_m-f_v}{\tilde{\omega}_{vm}-\omega}+\frac{f_n-f_v}{\tilde{\omega}_{nv}-\omega}\right) \\
&\times j_{h,vn}(z''';\vec{\kappa}_{\parallel,\bar{v}}+\vec{\kappa}_{\parallel,\bar{n}})j_{k,mv}(z'';\vec{\kappa}_{\parallel,\bar{m}}+\vec{\kappa}_{\parallel,\bar{v}})\psi_m^*(z)\psi_n(z) \\
&\times A_h(z''';\vec{q}_{\parallel}''')A_k(z'';\vec{q}_{\parallel}'')A_x^*(z';\vec{q}_{\parallel}')e^{\mathrm{i}(\vec{\kappa}_{\parallel,\bar{n}}-\vec{\kappa}_{\parallel,\bar{m}})\cdot\vec{r}_{\parallel}}e^{\mathrm{i}(\vec{\kappa}_{\parallel,\bar{v}}-\vec{\kappa}_{\parallel,\bar{n}})\cdot\vec{r}_{\parallel}'''}e^{\mathrm{i}(\vec{\kappa}_{\parallel,\bar{m}}-\vec{\kappa}_{\parallel,\bar{v}})\cdot\vec{r}_{\parallel}''} \\
&\times e^{\mathrm{i}\vec{q}_{\parallel}'''\cdot\vec{r}_{\parallel}'''}e^{\mathrm{i}\vec{q}_{\parallel}''\cdot\vec{r}_{\parallel}''}e^{-\mathrm{i}\vec{q}_{\parallel}'\cdot\vec{r}_{\parallel}'}d^2q_{\parallel}'''d^2q_{\parallel}''d^2q_{\parallel}'\delta(\vec{r}-\vec{r}')d^3r'''d^3r''d^3r'e^{-\mathrm{i}\vec{q}_{\parallel}\cdot\vec{r}_{\parallel}}d^2r_{\parallel}.
\end{aligned}
\tag{A.14}
$$

Solving first the integral $\int d^2 r'_\parallel$, then the integrals $\int d^2 r'''_\parallel$, $\int d^2 r''_\parallel$, and $\int d^2 r_\parallel$, and finally replacing the sums over the $\vec{\kappa}_\parallel$ quantities with integrals, we obtain

$$
\begin{aligned}
J^{\mathrm{B}}_{xxkh}(z; \vec{q}_\parallel) = & -\frac{e^2}{4 m_e \hbar^2} \frac{2}{(2\pi)^6} \int \cdots \int \sum_{nmv} \frac{1}{\tilde{\omega}_{nm}(\vec{\kappa}_{\parallel,\bar{n}}, \vec{\kappa}_{\parallel,\bar{m}}) - 2\omega} \\
& \times \left(\frac{f_m(\vec{\kappa}_{\parallel,\bar{m}}) - f_v(\vec{\kappa}_{\parallel,\bar{v}})}{\tilde{\omega}_{vm}(\vec{\kappa}_{\parallel,\bar{v}}, \vec{\kappa}_{\parallel,\bar{m}}) - \omega} + \frac{f_n(\vec{\kappa}_{\parallel,\bar{n}}) - f_v(\vec{\kappa}_{\parallel,\bar{v}})}{\tilde{\omega}_{nv}(\vec{\kappa}_{\parallel,\bar{n}}, \vec{\kappa}_{\parallel,\bar{v}}) - \omega} \right) j_{h,vn}(z'''; \vec{\kappa}_{\parallel,\bar{v}} + \vec{\kappa}_{\parallel,\bar{n}}) \\
& \times j_{k,mv}(z''; \vec{\kappa}_{\parallel,\bar{m}} + \vec{\kappa}_{\parallel,\bar{v}}) \psi_m^*(z) \psi_n(z) A_h(z'''; \vec{q}'''_\parallel) A_k(z''; \vec{q}''_\parallel) A_x^*(z'; \vec{q}'_\parallel) \\
& \times \delta(\vec{\kappa}_{\parallel,\bar{v}} - \vec{\kappa}_{\parallel,\bar{n}} + \vec{q}'''_\parallel) \delta(\vec{\kappa}_{\parallel,\bar{m}} - \vec{\kappa}_{\parallel,\bar{v}} + \vec{q}''_\parallel) \delta(\vec{\kappa}_{\parallel,\bar{n}} - \vec{\kappa}_{\parallel,\bar{m}} - \vec{q}'_\parallel - \vec{q}_\parallel) \\
& \times \delta(z - z') d^2\kappa_{\parallel,\bar{n}} d^2\kappa_{\parallel,\bar{m}} d^2\kappa_{\parallel,\bar{v}} d^2 q'''_\parallel d^2 q''_\parallel d^2 q'_\parallel dz''' dz'' dz'.
\end{aligned}
\tag{A.15}
$$

Of these three integrals over $\vec{\kappa}_\parallel$, we can solve two because of the coupling to the wave-vectors introduced by the Dirac delta functions appearing. Keeping the $\vec{\kappa}_{\parallel,\bar{m}}$ set of surface states, we thus solve the integrals for the v and n sets (in that order). Solving for the v set, we find that $\vec{\kappa}_{\parallel,\bar{v}}$ is replaced by $\vec{\kappa}_{\parallel,\bar{m}} + \vec{q}''_\parallel$, which then allows us to solve the n set by replacing $\vec{\kappa}_{\parallel,\bar{n}}$ by $\vec{\kappa}_{\parallel,\bar{m}} + \vec{q}'''_\parallel + \vec{q}''_\parallel$. Then we get

$$
\begin{aligned}
J^{\mathrm{B}}_{xxkh}(z; \vec{q}_\parallel) = & -\frac{e^2}{4 m_e \hbar^2} \frac{2}{(2\pi)^6} \int \cdots \int \sum_{nmv} \frac{1}{\tilde{\omega}_{nm}(\vec{\kappa}_{\parallel,\bar{m}} + \vec{q}'''_\parallel + \vec{q}''_\parallel, \vec{\kappa}_{\parallel,\bar{m}}) - 2\omega} \\
& \times \left(\frac{f_m(\vec{\kappa}_{\parallel,\bar{m}}) - f_v(\vec{\kappa}_{\parallel,\bar{m}} + \vec{q}''_\parallel)}{\tilde{\omega}_{vm}(\vec{\kappa}_{\parallel,\bar{m}} + \vec{q}''_\parallel, \vec{\kappa}_{\parallel,\bar{m}}) - \omega} + \frac{f_n(\vec{\kappa}_{\parallel,\bar{m}} + \vec{q}'''_\parallel + \vec{q}''_\parallel) - f_v(\vec{\kappa}_{\parallel,\bar{m}} + \vec{q}''_\parallel)}{\tilde{\omega}_{nv}(\vec{\kappa}_{\parallel,\bar{m}} + \vec{q}'''_\parallel + \vec{q}''_\parallel, \vec{\kappa}_{\parallel,\bar{m}} + \vec{q}''_\parallel) - \omega} \right) \\
& \times j_{h,vn}(z'''; 2\vec{\kappa}_{\parallel,\bar{m}} + \vec{q}'''_\parallel + 2\vec{q}''_\parallel) j_{k,mv}(z''; 2\vec{\kappa}_{\parallel,\bar{m}} + \vec{q}''_\parallel) \psi_m^*(z) \psi_n(z) \\
& \times A_h(z'''; \vec{q}'''_\parallel) A_k(z''; \vec{q}''_\parallel) A_x^*(z'; \vec{q}'_\parallel) \delta(\vec{q}'''_\parallel + \vec{q}''_\parallel - \vec{q}'_\parallel - \vec{q}_\parallel) \\
& \times \delta(z - z') d^2\kappa_{\parallel,\bar{m}} d^2 q'''_\parallel d^2 q''_\parallel d^2 q'_\parallel dz''' dz'' dz'.
\end{aligned}
\tag{A.16}
$$

On the form of Eq. (8.4) we thus get part B of the conductivity tensor as

$$
\begin{aligned}
\Xi^{\mathrm{B}}_{xxkh}(z, z', z'', z'''; & \vec{q}_\parallel, \vec{q}'_\parallel, \vec{q}''_\parallel, \vec{q}'''_\parallel) = \\
& \frac{2\mathrm{i}}{\omega^3} \frac{1}{(2\pi)^2} \frac{e^2}{4 m_e \hbar^2} \sum_{nmv} \int \frac{1}{\tilde{\omega}_{nm}(\vec{\kappa}_\parallel + \vec{q}'''_\parallel + \vec{q}''_\parallel, \vec{\kappa}_\parallel) - 2\omega} \left(\frac{f_m(\vec{\kappa}_\parallel) - f_v(\vec{\kappa}_\parallel + \vec{q}''_\parallel)}{\tilde{\omega}_{vm}(\vec{\kappa}_\parallel + \vec{q}''_\parallel, \vec{\kappa}_\parallel) - \omega} \right. \\
& \left. + \frac{f_n(\vec{\kappa}_\parallel + \vec{q}'''_\parallel + \vec{q}''_\parallel) - f_v(\vec{\kappa}_\parallel + \vec{q}''_\parallel)}{\tilde{\omega}_{nv}(\vec{\kappa}_\parallel + \vec{q}'''_\parallel + \vec{q}''_\parallel, \vec{\kappa}_\parallel + \vec{q}''_\parallel) - \omega} \right) j_{h,vn}(z'''; 2\vec{\kappa}_\parallel + \vec{q}'''_\parallel + 2\vec{q}''_\parallel) \\
& \times j_{k,mv}(z''; 2\vec{\kappa}_\parallel + \vec{q}''_\parallel) \psi_m^*(z) \psi_n(z) \delta(\vec{q}'''_\parallel + \vec{q}''_\parallel - \vec{q}'_\parallel - \vec{q}_\parallel) \delta(z - z') d^2\kappa_\parallel,
\end{aligned}
\tag{A.17}
$$

where we have omitted the now superfluous index m from the surface states $\vec{\kappa}_\parallel$. Looking for the phase conjugation response the pump fields take the form of Eqs. (A.12)–(A.13), and integration over $q'''_\parallel$ and $q''_\parallel$ in Eq. (A.16) can be performed. Thereby the Dirac delta function accounting for conservation of pseudo-momentum is reduced from its general DFWM form, $\delta(\vec{q}'''_\parallel + \vec{q}''_\parallel - \vec{q}'_\parallel - \vec{q}_\parallel)$, to $\delta(\vec{q}'_\parallel + \vec{q}_\parallel)$. Thus performing also the integral

over $q'_\parallel$, the PCDFWM conductivity tensor on the form of Eq. (8.8) can be extracted, and Eq. (8.18) appear.

A.5 Nonlinear process C

Inserting Eq. (6.10) into Eq. (4.10), we take element *xxxx* of part C of the nonlinear current density. In the result we insert the expressions for the wave function and the vector potential in the two-dimensional Fourier representation [Eqs. (8.9) and (8.1), respectively]. Then by use of Eq. (8.2) we find

$$
\begin{aligned}
J^{\mathrm{C}}_{xxxx}(z;\vec{q}_\parallel) = &-\frac{e^4}{4m_e^2\hbar}\frac{2}{(2\pi)^{10}}\int\cdots\int\sum_{nm}\frac{f_n-f_m}{\tilde{\omega}_{nm}}\psi_n^*(z')\psi_m(z')\psi_m^*(z)\psi_n(z)A_x(z''';\vec{q}_\parallel''') \\
&\times A_x(z'';\vec{q}_\parallel'')A_x^*(z';\vec{q}_\parallel')e^{i(\vec{\kappa}_{\parallel,\bar{m}}-\vec{\kappa}_{\parallel,\bar{n}})\cdot\vec{r}_\parallel'}e^{i(\vec{\kappa}_{\parallel,\bar{n}}-\vec{\kappa}_{\parallel,\bar{m}})\cdot\vec{r}_\parallel}e^{i\vec{q}_\parallel'''\cdot\vec{r}_\parallel'''}e^{i\vec{q}_\parallel''\cdot\vec{r}_\parallel''}e^{-i\vec{q}_\parallel'\cdot\vec{r}_\parallel'}\delta(\vec{r}'-\vec{r}''') \\
&\times\delta(\vec{r}-\vec{r}'')d^2q_\parallel'''d^2q_\parallel''d^2q_\parallel'd^3r'''d^3r''d^3r'e^{-i\vec{q}_\parallel\cdot\vec{r}_\parallel}d^2r_\parallel.
\end{aligned}
\tag{A.18}
$$

Solving first the integrals $\int d^2r_\parallel'''$ and $\int d^2r_\parallel''$, then the integrals $\int d^2r_\parallel'$ and $\int d^2r_\parallel$, and finally replacing the sum over the $\vec{\kappa}_\parallel$ quantities with integrals, we get

$$
\begin{aligned}
J^{\mathrm{C}}_{xxxx}(z;\vec{q}_\parallel) = &-\frac{e^4}{4m_e^2\hbar}\frac{2}{(2\pi)^6}\int\cdots\int\sum_{nm}\frac{f_n(\vec{\kappa}_{\parallel,\bar{n}})-f_m(\vec{\kappa}_{\parallel,\bar{m}})}{\tilde{\omega}_{nm}(\vec{\kappa}_{\parallel,\bar{n}},\vec{\kappa}_{\parallel,\bar{m}})}\psi_n^*(z')\psi_m(z')\psi_m^*(z)\psi_n(z) \\
&\times A_x(z''';\vec{q}_\parallel''')A_x(z'';\vec{q}_\parallel'')A_x^*(z';\vec{q}_\parallel')\delta(\vec{\kappa}_{\parallel,\bar{m}}-\vec{\kappa}_{\parallel,\bar{n}}+\vec{q}_\parallel'''-\vec{q}_\parallel'')\delta(\vec{\kappa}_{\parallel,\bar{n}}-\vec{\kappa}_{\parallel,\bar{m}}+\vec{q}_\parallel''-\vec{q}_\parallel) \\
&\times\delta(z'-z''')\delta(z-z'')d^2\kappa_{\parallel,\bar{n}}d^2\kappa_{\parallel,\bar{m}}d^2q_\parallel'''d^2q_\parallel''d^2q_\parallel'dz'''dz''dz'.
\end{aligned}
\tag{A.19}
$$

Of the two integrals over the $\vec{\kappa}_\parallel$ quantities, we can solve one because of the coupling to the wavevectors introduced by the Dirac delta functions appearing. We aim at keeping the $\vec{\kappa}_{\parallel,\bar{m}}$ set, and thus we solve the integrals for the *n* set. Solving for this set, we find that $\vec{\kappa}_{\parallel,\bar{n}}$ is replaced by $\vec{\kappa}_{\parallel,\bar{m}}-\vec{q}_\parallel''+\vec{q}_\parallel$, thus leading to the result

$$
\begin{aligned}
J^{\mathrm{C}}_{xxxx}(z;\vec{q}_\parallel) = &-\frac{e^4}{4m_e^2\hbar}\frac{2}{(2\pi)^6}\int\cdots\int\sum_{nm}\frac{f_n(\vec{\kappa}_{\parallel,\bar{m}}-\vec{q}_\parallel''+\vec{q}_\parallel)-f_m(\vec{\kappa}_{\parallel,\bar{m}})}{\tilde{\omega}_{nm}(\vec{\kappa}_{\parallel,\bar{m}}-\vec{q}_\parallel''+\vec{q}_\parallel,\vec{\kappa}_{\parallel,\bar{m}})}\psi_n^*(z')\psi_m(z') \\
&\times\psi_m^*(z)\psi_n(z)A_x(z''';\vec{q}_\parallel''')A_x(z'';\vec{q}_\parallel'')A_x^*(z';\vec{q}_\parallel')\delta(\vec{q}_\parallel'''+\vec{q}_\parallel''-\vec{q}_\parallel'-\vec{q}_\parallel)\delta(z'-z''') \\
&\times\delta(z-z'')d^2\kappa_{\parallel,\bar{m}}d^2q_\parallel'''d^2q_\parallel''d^2q_\parallel'dz'''dz''dz'.
\end{aligned}
\tag{A.20}
$$

On the form of Eq. (8.4) we thus get part C of the conductivity tensor as

$$
\begin{aligned}
\Xi^{\mathrm{C}}_{xxxx}(z,z',z'',z''';\vec{q}_\parallel,\vec{q}_\parallel',\vec{q}_\parallel'',\vec{q}_\parallel''') = &\frac{2i}{\omega^3}\frac{e^4}{4m_e^2\hbar}\frac{1}{(2\pi)^2}\sum_{nm}\int\frac{f_n(\vec{\kappa}_\parallel-\vec{q}_\parallel''+\vec{q}_\parallel)-f_m(\vec{\kappa}_\parallel)}{\tilde{\omega}_{nm}(\vec{\kappa}_\parallel-\vec{q}_\parallel''+\vec{q}_\parallel,\vec{\kappa}_\parallel)} \\
&\times\psi_n^*(z')\psi_m(z')\psi_m^*(z)\psi_n(z)\delta(\vec{q}_\parallel'''+\vec{q}_\parallel''-\vec{q}_\parallel'-\vec{q}_\parallel)\delta(z'-z''')\delta(z-z'')d^2\kappa_\parallel.
\end{aligned}
\tag{A.21}
$$

where we have omitted the now superfluous index *m* from the surface states $\vec{\kappa}_\parallel$. The phase conjugation response is found using the same procedure as before, since using the

pump fields defined in Eqs. (A.12)–(A.13) the integrals over $q_\parallel'''$ and $q_\parallel''$ in Eq. (A.20) can be performed. Then (again) the conservation of pseudo-momentum, $\delta(\vec{q}_\parallel''' + \vec{q}_\parallel'' - \vec{q}_\parallel' - \vec{q}_\parallel)$, is reduced to $\delta(\vec{q}_\parallel' + \vec{q}_\parallel)$, and after integration over $q_\parallel'$ we obtain on the form of Eq. (8.8) the PCDFWM conductivity tensor part C, appearing as Eq. (8.19).

A.6 Nonlinear process D

Inserting Eq. (6.11) into Eq. (4.10), we take element $xjkx$ of part D of the nonlinear current density. In the result we insert the expressions for the wave function, the vector potential and the transition current density in the two-dimensional Fourier representation [Eqs. (8.9), (8.1) and (8.14), respectively]. Then by use of Eq. (8.2) we find

$$
\begin{aligned}
J_{xjkx}^{\mathrm{D}}(z; \vec{q}_\parallel) = &-\frac{e^2}{4m_e\hbar^2}\frac{2}{(2\pi)^{12}} \int \cdots \int \sum_{nmv} \frac{1}{\tilde{\omega}_{nm}} \left\{ \left(\frac{f_m - f_v}{\tilde{\omega}_{vm} - \omega} + \frac{f_n - f_v}{\tilde{\omega}_{nv} + \omega} \right) \right. \\
&\times j_{j,vn}(z'; \vec{\kappa}_{\parallel,\bar{v}} + \vec{\kappa}_{\parallel,\bar{n}}) j_{k,mv}(z''; \vec{\kappa}_{\parallel,\bar{m}} + \vec{\kappa}_{\parallel,\bar{v}}) e^{\mathrm{i}(\vec{\kappa}_{\parallel,\bar{v}} - \vec{\kappa}_{\parallel,\bar{n}})\cdot\vec{r}_\parallel'} e^{\mathrm{i}(\vec{\kappa}_{\parallel,\bar{m}} - \vec{\kappa}_{\parallel,\bar{v}})\cdot\vec{r}_\parallel''} \\
&+ \left(\frac{f_m - f_v}{\tilde{\omega}_{vm} + \omega} + \frac{f_n - f_v}{\tilde{\omega}_{nv} - \omega} \right) j_{k,vn}(z''; \vec{\kappa}_{\parallel,\bar{v}} + \vec{\kappa}_{\parallel,\bar{n}}) j_{j,mv}(z'; \vec{\kappa}_{\parallel,\bar{m}} + \vec{\kappa}_{\parallel,\bar{v}}) e^{\mathrm{i}(\vec{\kappa}_{\parallel,\bar{v}} - \vec{\kappa}_{\parallel,\bar{n}})\cdot\vec{r}_\parallel''} \\
&\left. \times e^{\mathrm{i}(\vec{\kappa}_{\parallel,\bar{m}} - \vec{\kappa}_{\parallel,\bar{v}})\cdot\vec{r}_\parallel'} \right\} \psi_m^*(z)\psi_n(z)\delta(\vec{r} - \vec{r}''')A_x(z'''; \vec{q}_\parallel''')A_k(z''; \vec{q}_\parallel'')A_j^*(z'; \vec{q}_\parallel') e^{\mathrm{i}(\vec{\kappa}_{\parallel,\bar{n}} - \vec{\kappa}_{\parallel,\bar{m}})\cdot\vec{r}_\parallel} \\
&\times e^{\mathrm{i}\vec{q}_\parallel'''\cdot\vec{r}_\parallel'''} e^{\mathrm{i}\vec{q}_\parallel''\cdot\vec{r}_\parallel''} e^{-\mathrm{i}\vec{q}_\parallel'\cdot\vec{r}_\parallel'} d^2q_\parallel''' d^2q_\parallel'' d^2q_\parallel' d^3r''' d^3r'' d^3r' e^{-\mathrm{i}\vec{q}_\parallel\cdot\vec{r}_\parallel} d^2r_\parallel.
\end{aligned}
\tag{A.22}
$$

Solving in this equation the integral $\int d^2r_\parallel'''$, and then the integrals $\int d^2r_\parallel''$, $\int d^2r_\parallel'$, and $\int d^2r_\parallel$ we get, after having replaced the sums over the various $\vec{\kappa}_\parallel$ quantities with integrals as before,

$$
\begin{aligned}
J_{xjkx}^{\mathrm{D}}(z; \vec{q}_\parallel) = &-\frac{e^2}{4m_e\hbar^2}\frac{2}{(2\pi)^6} \int \cdots \int \sum_{nmv} \frac{1}{\tilde{\omega}_{nm}(\vec{\kappa}_{\parallel,\bar{n}}, \vec{\kappa}_{\parallel,\bar{m}})} \left\{ \left(\frac{f_m(\vec{\kappa}_{\parallel,\bar{m}}) - f_v(\vec{\kappa}_{\parallel,\bar{v}})}{\tilde{\omega}_{vm}(\vec{\kappa}_{\parallel,\bar{v}}, \vec{\kappa}_{\parallel,\bar{m}}) - \omega} \right. \right. \\
&+ \frac{f_n(\vec{\kappa}_{\parallel,\bar{n}}) - f_v(\vec{\kappa}_{\parallel,\bar{v}})}{\tilde{\omega}_{nv}(\vec{\kappa}_{\parallel,\bar{n}}, \vec{\kappa}_{\parallel,\bar{v}}) + \omega} \right) j_{j,vn}(z'; \vec{\kappa}_{\parallel,\bar{v}} + \vec{\kappa}_{\parallel,\bar{n}}) j_{k,mv}(z''; \vec{\kappa}_{\parallel,\bar{m}} + \vec{\kappa}_{\parallel,\bar{v}})\delta(\vec{\kappa}_{\parallel,\bar{m}} - \vec{\kappa}_{\parallel,\bar{v}} + \vec{q}_\parallel'') \\
&\times \delta(\vec{\kappa}_{\parallel,\bar{v}} - \vec{\kappa}_{\parallel,\bar{n}} - \vec{q}_\parallel') + \left(\frac{f_m(\vec{\kappa}_{\parallel,\bar{m}}) - f_v(\vec{\kappa}_{\parallel,\bar{v}})}{\tilde{\omega}_{vm}(\vec{\kappa}_{\parallel,\bar{v}}, \vec{\kappa}_{\parallel,\bar{m}}) + \omega} + \frac{f_n(\vec{\kappa}_{\parallel,\bar{n}}) - f_v(\vec{\kappa}_{\parallel,\bar{v}})}{\tilde{\omega}_{nv}(\vec{\kappa}_{\parallel,\bar{n}}, \vec{\kappa}_{\parallel,\bar{v}}) - \omega} \right) \\
&\times j_{k,vn}(z''; \vec{\kappa}_{\parallel,\bar{v}} + \vec{\kappa}_{\parallel,\bar{n}}) j_{j,mv}(z'; \vec{\kappa}_{\parallel,\bar{m}} + \vec{\kappa}_{\parallel,\bar{v}})\delta(\vec{\kappa}_{\parallel,\bar{v}} - \vec{\kappa}_{\parallel,\bar{n}} + \vec{q}_\parallel'')\delta(\vec{\kappa}_{\parallel,\bar{m}} - \vec{\kappa}_{\parallel,\bar{v}} - \vec{q}_\parallel') \right\} \\
&\times \psi_m^*(z)\psi_n(z)\delta(z - z''')\delta(\vec{\kappa}_{\parallel,\bar{n}} - \vec{\kappa}_{\parallel,\bar{m}} + \vec{q}_\parallel''' - \vec{q}_\parallel)A_x(z'''; \vec{q}_\parallel''')A_k(z''; \vec{q}_\parallel'') \\
&\times A_j^*(z'; \vec{q}_\parallel') d^2\kappa_{\parallel,\bar{n}} d^2\kappa_{\parallel,\bar{m}} d^2\kappa_{\parallel,\bar{v}} d^2q_\parallel''' d^2q_\parallel'' d^2q_\parallel' dz''' dz'' dz'.
\end{aligned}
\tag{A.23}
$$

Of the three integrals over $\vec{\kappa}_\parallel$ quantities, we can solve two because of the coupling to the wavevectors introduced by the Dirac delta functions appearing. We aim at keeping the $\vec{\kappa}_{\parallel,\bar{m}}$ set, and thus we solve the integrals for the v and n sets (in that order). Solving for the v set, we find that $\vec{\kappa}_{\parallel,\bar{v}}$ is replaced by $\vec{\kappa}_{\parallel,\bar{m}} + \vec{q}_\parallel''$ in the first part of the sum and

by $\vec{\kappa}_{\parallel,\bar{m}} - \vec{q}_{\parallel}'$ in the second part of the sum, which then allows us to solve the n set by replacing $\vec{\kappa}_{\parallel,\bar{n}}$ with $\vec{\kappa}_{\parallel,\bar{m}} + \vec{q}_{\parallel}'' - \vec{q}_{\parallel}'$ in general, giving the result

$$
\begin{aligned}
J^{\mathrm{D}}_{xjkx}(z;\vec{q}_{\parallel}) = &-\frac{e^2}{4m_e\hbar^2}\frac{2}{(2\pi)^6}\int\cdots\int\sum_{nmv}\frac{1}{\tilde{\omega}_{nm}(\vec{\kappa}_{\parallel,\bar{m}}+\vec{q}_{\parallel}''-\vec{q}_{\parallel}',\vec{\kappa}_{\parallel,\bar{m}})}\\
&\times\Bigg\{\left(\frac{f_m(\vec{\kappa}_{\parallel,\bar{m}})-f_v(\vec{\kappa}_{\parallel,\bar{m}}+\vec{q}_{\parallel}'')}{\tilde{\omega}_{vm}(\vec{\kappa}_{\parallel,\bar{m}}+\vec{q}_{\parallel}'',\vec{\kappa}_{\parallel,\bar{m}})-\omega}+\frac{f_n(\vec{\kappa}_{\parallel,\bar{m}}+\vec{q}_{\parallel}''-\vec{q}_{\parallel}')-f_v(\vec{\kappa}_{\parallel,\bar{m}}+\vec{q}_{\parallel}'')}{\tilde{\omega}_{nv}(\vec{\kappa}_{\parallel,\bar{m}}+\vec{q}_{\parallel}''-\vec{q}_{\parallel}',\vec{\kappa}_{\parallel,\bar{m}}+\vec{q}_{\parallel}'')+\omega}\right)\\
&\times j_{j,vn}(z';2\vec{\kappa}_{\parallel,\bar{m}}+2\vec{q}_{\parallel}''-\vec{q}_{\parallel}')j_{k,mv}(z'';2\vec{\kappa}_{\parallel,\bar{m}}+\vec{q}_{\parallel}'')\\
&+\left(\frac{f_m(\vec{\kappa}_{\parallel,\bar{m}})-f_v(\vec{\kappa}_{\parallel,\bar{m}}-\vec{q}_{\parallel}')}{\tilde{\omega}_{vm}(\vec{\kappa}_{\parallel,\bar{m}}-\vec{q}_{\parallel}',\vec{\kappa}_{\parallel,\bar{m}})+\omega}+\frac{f_n(\vec{\kappa}_{\parallel,\bar{m}}+\vec{q}_{\parallel}''-\vec{q}_{\parallel}')-f_v(\vec{\kappa}_{\parallel,\bar{m}}-\vec{q}_{\parallel}')}{\tilde{\omega}_{nv}(\vec{\kappa}_{\parallel,\bar{m}}+\vec{q}_{\parallel}''-\vec{q}_{\parallel}',\vec{\kappa}_{\parallel,\bar{m}}-\vec{q}_{\parallel}')-\omega}\right)\\
&\times j_{k,vn}(z'';2\vec{\kappa}_{\parallel,\bar{m}}+\vec{q}_{\parallel}''-2\vec{q}_{\parallel}')j_{j,mv}(z';2\vec{\kappa}_{\parallel,\bar{m}}-\vec{q}_{\parallel}')\Bigg\}\psi_m^*(z)\psi_n(z)\delta(z-z''')\\
&\times\delta(\vec{q}_{\parallel}'''+\vec{q}_{\parallel}''-\vec{q}_{\parallel}'-\vec{q}_{\parallel})A_x(z''';\vec{q}_{\parallel}''')A_k(z'';\vec{q}_{\parallel}'')A_j^*(z';\vec{q}_{\parallel}')d^2\kappa_{\parallel,\bar{m}}d^2q_{\parallel}'''d^2q_{\parallel}''d^2q_{\parallel}'\\
&\times dz'''dz''dz'.
\end{aligned}
\tag{A.24}
$$

On the form of Eq. (8.4) we thus get part D of the conductivity tensor as

$$
\begin{aligned}
\Xi^{\mathrm{D}}_{xjkx}(z,z',z'',z''';\vec{q}_{\parallel},\vec{q}_{\parallel}',\vec{q}_{\parallel}'',\vec{q}_{\parallel}''') = &\frac{2\mathrm{i}}{\omega^3}\frac{e^2}{4m_e\hbar^2}\frac{1}{(2\pi)^2}\sum_{nmv}\int\frac{1}{\tilde{\omega}_{nm}(\vec{\kappa}_{\parallel}+\vec{q}_{\parallel}''-\vec{q}_{\parallel}',\vec{\kappa}_{\parallel})}\\
&\times\Bigg\{\left(\frac{f_m(\vec{\kappa}_{\parallel})-f_v(\vec{\kappa}_{\parallel}+\vec{q}_{\parallel}'')}{\tilde{\omega}_{vm}(\vec{\kappa}_{\parallel}+\vec{q}_{\parallel}'',\vec{\kappa}_{\parallel})-\omega}+\frac{f_n(\vec{\kappa}_{\parallel}+\vec{q}_{\parallel}''-\vec{q}_{\parallel}')-f_v(\vec{\kappa}_{\parallel}+\vec{q}_{\parallel}'')}{\tilde{\omega}_{nv}(\vec{\kappa}_{\parallel}+\vec{q}_{\parallel}''-\vec{q}_{\parallel}',\vec{\kappa}_{\parallel}+\vec{q}_{\parallel}'')+\omega}\right)\\
&\times j_{j,vn}(z';2\vec{\kappa}_{\parallel}+2\vec{q}_{\parallel}''-\vec{q}_{\parallel}')j_{k,mv}(z'';2\vec{\kappa}_{\parallel}+\vec{q}_{\parallel}'')\\
&+\left(\frac{f_m(\vec{\kappa}_{\parallel})-f_v(\vec{\kappa}_{\parallel}-\vec{q}_{\parallel}')}{\tilde{\omega}_{vm}(\vec{\kappa}_{\parallel}-\vec{q}_{\parallel}',\vec{\kappa}_{\parallel})+\omega}+\frac{f_n(\vec{\kappa}_{\parallel}+\vec{q}_{\parallel}''-\vec{q}_{\parallel}')-f_v(\vec{\kappa}_{\parallel}-\vec{q}_{\parallel}')}{\tilde{\omega}_{nv}(\vec{\kappa}_{\parallel}+\vec{q}_{\parallel}''-\vec{q}_{\parallel}',\vec{\kappa}_{\parallel}-\vec{q}_{\parallel}')-\omega}\right)\\
&\times j_{k,vn}(z'';2\vec{\kappa}_{\parallel}+\vec{q}_{\parallel}''-2\vec{q}_{\parallel}')j_{j,mv}(z';2\vec{\kappa}_{\parallel}-\vec{q}_{\parallel}')\Bigg\}\psi_m^*(z)\psi_n(z)\delta(z-z''')\\
&\times\delta(\vec{q}_{\parallel}'''+\vec{q}_{\parallel}''-\vec{q}_{\parallel}'-\vec{q}_{\parallel})d^2\kappa_{\parallel},
\end{aligned}
\tag{A.25}
$$

where we have omitted the now superfluous index m from the surface states $\vec{\kappa}_{\parallel}$. Again, when looking for the DFWM response tensor we insert the pump fields defined in Eqs. (A.12)–(A.13) and integrate over $q_{\parallel}'''$ and $q_{\parallel}''$ in Eq. (A.24), again reducing the Dirac delta function accounting for conservation of pseudo-momentum to $\delta(\vec{q}_{\parallel}'+\vec{q}_{\parallel})$. After integration over $q_{\parallel}'$ and separation according to Eq. (8.8), Eq. (8.20) appear as the PCD-FWM conductivity tensor part D.

A.7 Nonlinear Process E

Inserting Eq. (6.12) into Eq. (4.10), we take element $ijxx$ of part E of the nonlinear current density. In the result we insert the expressions for the wave function, the vector

potential and the transition current density in the two-dimensional Fourier representation [Eqs. (8.9), (8.1) and (8.14), respectively]. Then by use of Eq. (8.2) we find

$$
\begin{aligned}
J^{\mathrm{E}}_{ijxx}(z; \vec{q}_\parallel) = &-\frac{e^2}{16 m_e \hbar^2} \frac{2}{(2\pi)^{12}} \int \cdots \int \sum_{nmv} \frac{1}{\tilde{\omega}_{nm} - \omega} \left\{ \left(\frac{f_m - f_v}{\tilde{\omega}_{vm} - 2\omega} + \frac{f_n - f_v}{\tilde{\omega}_{nv} + \omega} \right) \right. \\
&\times j_{j,vn}(z'; \vec{\kappa}_{\parallel,\bar{v}} + \vec{\kappa}_{\parallel,\bar{n}}) \psi_v^*(z'') \psi_m(z'') e^{i(\vec{\kappa}_{\parallel,\bar{v}} - \vec{\kappa}_{\parallel,\bar{n}}) \cdot \vec{r}'_\parallel} e^{i(\vec{\kappa}_{\parallel,\bar{m}} - \vec{\kappa}_{\parallel,\bar{v}}) \cdot \vec{r}''_\parallel} \\
&+ \left(\frac{f_n - f_v}{\tilde{\omega}_{nv} - 2\omega} + \frac{f_m - f_v}{\tilde{\omega}_{vm} + \omega} \right) j_{j,mv}(z'; \vec{\kappa}_{\parallel,\bar{m}} + \vec{\kappa}_{\parallel,\bar{v}}) \psi_n^*(z'') \psi_v(z'') e^{i(\vec{\kappa}_{\parallel,\bar{m}} - \vec{\kappa}_{\parallel,\bar{v}}) \cdot \vec{r}'_\parallel} \\
&\left. \times e^{i(\vec{\kappa}_{\parallel,\bar{v}} - \vec{\kappa}_{\parallel,\bar{n}}) \cdot \vec{r}''_\parallel} \right\} j_{i,nm}(z; \vec{\kappa}_{\parallel,\bar{n}} + \vec{\kappa}_{\parallel,\bar{m}}) \delta(\vec{r}'' - \vec{r}''') A_x(z'''; \vec{q}'''_\parallel) A_x(z''; \vec{q}''_\parallel) A_j^*(z'; \vec{q}'_\parallel) \\
&\times e^{i(\vec{\kappa}_{\parallel,\bar{n}} - \vec{\kappa}_{\parallel,\bar{m}}) \cdot \vec{r}_\parallel} e^{i \vec{q}'''_\parallel \cdot \vec{r}'''_\parallel} e^{i \vec{q}''_\parallel \cdot \vec{r}''_\parallel} e^{-i \vec{q}'_\parallel \cdot \vec{r}'_\parallel} d^2 q'''_\parallel d^2 q''_\parallel d^2 q'_\parallel d^3 r''' d^3 r'' d^3 r' e^{-i \vec{q}_\parallel \cdot \vec{r}_\parallel} d^2 r_\parallel. \quad \text{(A.26)}
\end{aligned}
$$

In this equation, we first solve the integral $\int d^2 r'''_\parallel$, and then the integrals $\int d^2 r''_\parallel$, $\int d^2 r'_\parallel$, and $\int d^2 r_\parallel$, which together with replacement of the sums over the different $\vec{\kappa}_\parallel$ quantities with integrals yields the result

$$
\begin{aligned}
J^{\mathrm{E}}_{ijxx}(z; \vec{q}_\parallel) = &-\frac{e^2}{16 m_e \hbar^2} \frac{2}{(2\pi)^6} \int \cdots \int \sum_{nmv} \frac{1}{\tilde{\omega}_{nm}(\vec{\kappa}_{\parallel,\bar{n}}, \vec{\kappa}_{\parallel,\bar{m}}) - \omega} \left\{ \left(\frac{f_m(\vec{\kappa}_{\parallel,\bar{m}}) - f_v(\vec{\kappa}_{\parallel,\bar{v}})}{\tilde{\omega}_{vm}(\vec{\kappa}_{\parallel,\bar{v}}, \vec{\kappa}_{\parallel,\bar{m}}) - 2\omega} \right. \right. \\
&+ \frac{f_n(\vec{\kappa}_{\parallel,\bar{n}}) - f_v(\vec{\kappa}_{\parallel,\bar{v}})}{\tilde{\omega}_{nv}(\vec{\kappa}_{\parallel,\bar{n}}, \vec{\kappa}_{\parallel,\bar{v}}) + \omega} \right) j_{j,vn}(z'; \vec{\kappa}_{\parallel,\bar{v}} + \vec{\kappa}_{\parallel,\bar{n}}) \psi_v^*(z'') \psi_m(z'') \delta(\vec{\kappa}_{\parallel,\bar{v}} - \vec{\kappa}_{\parallel,\bar{n}} - \vec{q}'_\parallel) \\
&\times \delta(\vec{\kappa}_{\parallel,\bar{m}} - \vec{\kappa}_{\parallel,\bar{v}} + \vec{q}'''_\parallel + \vec{q}''_\parallel) + \left(\frac{f_n(\vec{\kappa}_{\parallel,\bar{n}}) - f_v(\vec{\kappa}_{\parallel,\bar{v}})}{\tilde{\omega}_{nv}(\vec{\kappa}_{\parallel,\bar{n}}, \vec{\kappa}_{\parallel,\bar{v}}) - 2\omega} + \frac{f_m(\vec{\kappa}_{\parallel,\bar{m}}) - f_v(\vec{\kappa}_{\parallel,\bar{v}})}{\tilde{\omega}_{vm}(\vec{\kappa}_{\parallel,\bar{v}}, \vec{\kappa}_{\parallel,\bar{m}}) + \omega} \right) \\
&\times j_{j,mv}(z'; \vec{\kappa}_{\parallel,\bar{m}} + \vec{\kappa}_{\parallel,\bar{v}}) \psi_n^*(z'') \psi_v(z'') \delta(\vec{\kappa}_{\parallel,\bar{m}} - \vec{\kappa}_{\parallel,\bar{v}} - \vec{q}'_\parallel) \delta(\vec{\kappa}_{\parallel,\bar{v}} - \vec{\kappa}_{\parallel,\bar{n}} + \vec{q}'''_\parallel + \vec{q}''_\parallel) \right\} \\
&\times j_{i,nm}(z; \vec{\kappa}_{\parallel,\bar{n}} + \vec{\kappa}_{\parallel,\bar{m}}) \delta(z'' - z''') A_x(z'''; \vec{q}'''_\parallel) A_x(z''; \vec{q}''_\parallel) A_j^*(z'; \vec{q}'_\parallel) \\
&\times \delta(\vec{\kappa}_{\parallel,\bar{n}} - \vec{\kappa}_{\parallel,\bar{m}} - \vec{q}_\parallel) d^2 \kappa_{\parallel,\bar{n}} d^2 \kappa_{\parallel,\bar{m}} d^2 \kappa_{\parallel,\bar{v}} d^2 q'''_\parallel d^2 q''_\parallel d^2 q'_\parallel dz''' dz'' dz'. \quad \text{(A.27)}
\end{aligned}
$$

Of the three integrals over $\vec{\kappa}_\parallel$ quantities, we can solve two because of the coupling to the wavevectors introduced by the Dirac delta functions appearing. We aim at keeping the $\vec{\kappa}_{\parallel,\bar{m}}$ set, and thus we solve the integrals for the v and n sets (in that order). Solving for the v set, we find that $\vec{\kappa}_{\parallel,\bar{v}}$ is replaced by $\vec{\kappa}_{\parallel,\bar{m}} + \vec{q}'''_\parallel + \vec{q}''_\parallel$ in the first part of the sum and by $\vec{\kappa}_{\parallel,\bar{m}} - \vec{q}'_\parallel$ in the second part of the sum, which then allows us to solve the n set by replacing $\vec{\kappa}_{\parallel,\bar{n}}$ with $\vec{\kappa}_{\parallel,\bar{m}} + \vec{q}'''_\parallel + \vec{q}''_\parallel - \vec{q}'_\parallel$ in general, giving

$$
\begin{aligned}
J^{\mathrm{E}}_{ijxx}(z; \vec{q}_\parallel) = &-\frac{e^2}{16 m_e \hbar^2} \frac{2}{(2\pi)^6} \int \cdots \int \sum_{nmv} \frac{1}{\tilde{\omega}_{nm}(\vec{\kappa}_{\parallel,\bar{m}} + \vec{q}'''_\parallel + \vec{q}''_\parallel - \vec{q}'_\parallel, \vec{\kappa}_{\parallel,\bar{m}}) - \omega} \\
&\times \left\{ \left(\frac{f_m(\vec{\kappa}_{\parallel,\bar{m}}) - f_v(\vec{\kappa}_{\parallel,\bar{m}} + \vec{q}'''_\parallel + \vec{q}''_\parallel)}{\tilde{\omega}_{vm}(\vec{\kappa}_{\parallel,\bar{m}} + \vec{q}'''_\parallel + \vec{q}''_\parallel, \vec{\kappa}_{\parallel,\bar{m}}) - 2\omega} \right. \right. \\
&+ \frac{f_n(\vec{\kappa}_{\parallel,\bar{m}} + \vec{q}'''_\parallel + \vec{q}''_\parallel - \vec{q}'_\parallel) - f_v(\vec{\kappa}_{\parallel,\bar{m}} + \vec{q}'''_\parallel + \vec{q}''_\parallel)}{\tilde{\omega}_{nv}(\vec{\kappa}_{\parallel,\bar{m}} + \vec{q}'''_\parallel + \vec{q}''_\parallel - \vec{q}'_\parallel, \vec{\kappa}_{\parallel,\bar{m}} + \vec{q}'''_\parallel + \vec{q}''_\parallel) + \omega} \right)
\end{aligned}
$$

$$\times j_{j,vn}(z'; 2\vec{\kappa}_{\parallel,\bar{m}} + 2\vec{q}_{\parallel}''' + 2\vec{q}_{\parallel}'' - \vec{q}_{\parallel}')\psi_v^*(z'')\psi_m(z'')$$

$$+ \left(\frac{f_n(\vec{\kappa}_{\parallel,\bar{m}} + \vec{q}_{\parallel}''' + \vec{q}_{\parallel}'' - \vec{q}_{\parallel}') - f_v(\vec{\kappa}_{\parallel,\bar{m}} - \vec{q}_{\parallel}')}{\tilde{\omega}_{mv}(\vec{\kappa}_{\parallel,\bar{m}} + \vec{q}_{\parallel}''' + \vec{q}_{\parallel}'' - \vec{q}_{\parallel}', \vec{\kappa}_{\parallel,\bar{m}} - \vec{q}_{\parallel}') - 2\omega} + \frac{f_m(\vec{\kappa}_{\parallel,\bar{m}}) - f_v(\vec{\kappa}_{\parallel,\bar{m}} - \vec{q}_{\parallel}')}{\tilde{\omega}_{vm}(\vec{\kappa}_{\parallel,\bar{m}} - \vec{q}_{\parallel}', \vec{\kappa}_{\parallel,\bar{m}}) + \omega} \right)$$

$$\times j_{j,mv}(z'; 2\vec{\kappa}_{\parallel,\bar{m}} - \vec{q}_{\parallel}')\psi_n^*(z'')\psi_v(z'') \Big\} j_{i,nm}(z; 2\vec{\kappa}_{\parallel,\bar{m}} + \vec{q}_{\parallel}''' + \vec{q}_{\parallel}'' - \vec{q}_{\parallel}')\delta(z'' - z''')$$

$$\times A_x(z'''; \vec{q}_{\parallel}''')A_x(z''; \vec{q}_{\parallel}'')A_j^*(z'; \vec{q}_{\parallel}')\delta(\vec{q}_{\parallel}''' + \vec{q}_{\parallel}'' - \vec{q}_{\parallel}' - \vec{q}_{\parallel})d^2\kappa_{\parallel,\bar{m}}d^2q_{\parallel}'''d^2q_{\parallel}''d^2q_{\parallel}'$$

$$\times dz'''dz''dz'. \tag{A.28}$$

On the form of Eq. (8.4) we thus get part E of the conductivity tensor as

$$\Xi_{ijxx}^{E}(z, z', z'', z'''; \vec{q}_{\parallel}, \vec{q}_{\parallel}', \vec{q}_{\parallel}'', \vec{q}_{\parallel}''') =$$

$$\frac{2\mathrm{i}}{\omega^3} \frac{e^2}{16 m_e \hbar^2} \frac{1}{(2\pi)^2} \sum_{nmv} \int \frac{1}{\tilde{\omega}_{nm}(\vec{\kappa}_{\parallel} + \vec{q}_{\parallel}''' + \vec{q}_{\parallel}'' - \vec{q}_{\parallel}', \vec{\kappa}_{\parallel}) - \omega}$$

$$\times \left\{ \left(\frac{f_m(\vec{\kappa}_{\parallel}) - f_v(\vec{\kappa}_{\parallel} + \vec{q}_{\parallel}''' + \vec{q}_{\parallel}'')}{\tilde{\omega}_{vm}(\vec{\kappa}_{\parallel} + \vec{q}_{\parallel}''' + \vec{q}_{\parallel}'', \vec{\kappa}_{\parallel}) - 2\omega} + \frac{f_n(\vec{\kappa}_{\parallel} + \vec{q}_{\parallel}''' + \vec{q}_{\parallel}'' - \vec{q}_{\parallel}') - f_v(\vec{\kappa}_{\parallel} + \vec{q}_{\parallel}''' + \vec{q}_{\parallel}'')}{\tilde{\omega}_{mv}(\vec{\kappa}_{\parallel} + \vec{q}_{\parallel}''' + \vec{q}_{\parallel}'' - \vec{q}_{\parallel}', \vec{\kappa}_{\parallel} + \vec{q}_{\parallel}''' + \vec{q}_{\parallel}'') + \omega} \right) \right.$$

$$\times j_{j,vn}(z'; 2\vec{\kappa}_{\parallel} + 2\vec{q}_{\parallel}''' + 2\vec{q}_{\parallel}'' - \vec{q}_{\parallel}')\psi_v^*(z'')\psi_m(z'')$$

$$+ \left(\frac{f_n(\vec{\kappa}_{\parallel} + \vec{q}_{\parallel}''' + \vec{q}_{\parallel}'' - \vec{q}_{\parallel}') - f_v(\vec{\kappa}_{\parallel} - \vec{q}_{\parallel}')}{\tilde{\omega}_{mv}(\vec{\kappa}_{\parallel} + \vec{q}_{\parallel}''' + \vec{q}_{\parallel}'' - \vec{q}_{\parallel}', \vec{\kappa}_{\parallel} - \vec{q}_{\parallel}') - 2\omega} + \frac{f_m(\vec{\kappa}_{\parallel}) - f_v(\vec{\kappa}_{\parallel} - \vec{q}_{\parallel}')}{\tilde{\omega}_{vm}(\vec{\kappa}_{\parallel} - \vec{q}_{\parallel}', \vec{\kappa}_{\parallel}) + \omega} \right)$$

$$\times j_{j,mv}(z'; 2\vec{\kappa}_{\parallel} - \vec{q}_{\parallel}')\psi_n^*(z'')\psi_v(z'') \Big\} j_{i,nm}(z; 2\vec{\kappa}_{\parallel} + \vec{q}_{\parallel}''' + \vec{q}_{\parallel}'' - \vec{q}_{\parallel}')\delta(z'' - z''')$$

$$\times \delta(\vec{q}_{\parallel}''' + \vec{q}_{\parallel}'' - \vec{q}_{\parallel}' - \vec{q}_{\parallel})d^2\kappa_{\parallel}, \tag{A.29}$$

where we have omitted the now superfluous index m from the surface states $\vec{\kappa}_{\parallel}$. The PCDFWM response tensor part E we find by insertion of the pump fields defined by Eqs. (A.12) and (A.13) into Eq. (A.28) and perform the integrals over $q_{\parallel}'''$ and $q_{\parallel}''$, followed by integration over $q_{\parallel}'$ because of the reduction in the Dirac delta function accounting for conservation of pseudo-momentum. After these operations, the resulting expression is separated in the form of Eq. (8.8), and Eq. (8.21) is obtained.

A.8 Nonlinear process F

Inserting Eq. (6.13) into Eq. (4.10), we take element $ixxh$ of part F of the nonlinear current density. In the result we insert the expressions for the wave function, the vector potential and the transition current density in the two-dimensional Fourier representation [Eqs. (8.9), (8.1) and (8.14), respectively]. Then by use of Eq. (8.2) we find

$$J_{ixxh}^{F}(z; \vec{q}_{\parallel}) = -\frac{e^2}{8 m_e \hbar^2} \frac{2}{(2\pi)^{12}} \int \cdots \int \sum_{nmv} \frac{1}{\tilde{\omega}_{nm} - \omega} \left\{ \left(\frac{f_m - f_v}{\tilde{\omega}_{vm}} + \frac{f_n - f_v}{\tilde{\omega}_{nv} - \omega} \right) \right.$$

$$\times j_{h,vn}(z''; \vec{\kappa}_{\parallel,\bar{v}} + \vec{\kappa}_{\parallel,\bar{n}})\psi_v^*(z')\psi_m(z')e^{\mathrm{i}(\vec{\kappa}_{\parallel,\bar{v}} - \vec{\kappa}_{\parallel,\bar{n}})\cdot\vec{r}_{\parallel}''}e^{\mathrm{i}(\vec{\kappa}_{\parallel,\bar{m}} - \vec{\kappa}_{\parallel,\bar{v}})\cdot\vec{r}_{\parallel}'}$$

$$+ \left(\frac{f_n - f_v}{\tilde{\omega}_{nv}} + \frac{f_m - f_v}{\tilde{\omega}_{vm} - \omega} \right) j_{h,mv}(z''; \vec{\kappa}_{\parallel,\bar{m}} + \vec{\kappa}_{\parallel,\bar{v}}) \psi_n^*(z') \psi_v(z') e^{i(\vec{\kappa}_{\parallel,\bar{m}} - \vec{\kappa}_{\parallel,\bar{v}})\cdot \vec{r}_\parallel''} e^{i(\vec{\kappa}_{\parallel,\bar{v}} - \vec{\kappa}_{\parallel,\bar{n}})\cdot \vec{r}_\parallel'} \Big\}$$

$$\times j_{i,nm}(z; \vec{\kappa}_{\parallel,\bar{n}} + \vec{\kappa}_{\parallel,\bar{m}}) \delta(\vec{r}' - \vec{r}''') A_h(z'''; \vec{q}_\parallel''') A_x(z''; \vec{q}_\parallel'') A_x^*(z'; \vec{q}_\parallel') e^{i(\vec{\kappa}_{\parallel,\bar{n}} - \vec{\kappa}_{\parallel,\bar{m}})\cdot \vec{r}_\parallel}$$

$$\times e^{i\vec{q}_\parallel'''\cdot \vec{r}_\parallel'''} e^{i\vec{q}_\parallel''\cdot \vec{r}_\parallel''} e^{-i\vec{q}_\parallel'\cdot \vec{r}_\parallel'} d^2 q_\parallel''' d^2 q_\parallel'' d^2 q_\parallel' d^3 r''' d^3 r'' d^3 r' e^{-i\vec{q}_\parallel\cdot \vec{r}_\parallel} d^2 r_\parallel. \tag{A.30}$$

Solving in this equation first the integral $\int d^2 r_\parallel'''$, and then the integrals $\int d^2 r_\parallel''$, $\int d^2 r_\parallel'$, and $\int d^2 r_\parallel$, followed by a replacement of the sums over the various $\vec{\kappa}_\parallel$ quantities with integrals, we get

$$J_{ixxh}^F(z; \vec{q}_\parallel) = -\frac{e^2}{8 m_e \hbar^2} \frac{2}{(2\pi)^6} \int \cdots \int \sum_{nmv} \frac{1}{\tilde{\omega}_{nm}(\vec{\kappa}_{\parallel,\bar{n}}, \vec{\kappa}_{\parallel,\bar{m}}) - \omega} \left\{ \left(\frac{f_m(\vec{\kappa}_{\parallel,\bar{m}}) - f_v(\vec{\kappa}_{\parallel,\bar{v}})}{\tilde{\omega}_{vm}(\vec{\kappa}_{\parallel,\bar{v}}, \vec{\kappa}_{\parallel,\bar{m}})} \right. \right.$$

$$+ \frac{f_n(\vec{\kappa}_{\parallel,\bar{n}}) - f_v(\vec{\kappa}_{\parallel,\bar{v}})}{\tilde{\omega}_{nv}(\vec{\kappa}_{\parallel,\bar{n}}, \vec{\kappa}_{\parallel,\bar{v}}) - \omega} \right) j_{h,vn}(z''; \vec{\kappa}_{\parallel,\bar{v}} + \vec{\kappa}_{\parallel,\bar{n}}) \psi_v^*(z') \psi_m(z') \delta(\vec{\kappa}_{\parallel,\bar{m}} - \vec{\kappa}_{\parallel,\bar{v}} + \vec{q}_\parallel''' - \vec{q}_\parallel')$$

$$\times \delta(\vec{\kappa}_{\parallel,\bar{v}} - \vec{\kappa}_{\parallel,\bar{n}} + \vec{q}_\parallel'') + \left(\frac{f_n(\vec{\kappa}_{\parallel,\bar{n}}) - f_v(\vec{\kappa}_{\parallel,\bar{v}})}{\tilde{\omega}_{nv}(\vec{\kappa}_{\parallel,\bar{n}}, \vec{\kappa}_{\parallel,\bar{v}})} + \frac{f_m(\vec{\kappa}_{\parallel,\bar{m}}) - f_v(\vec{\kappa}_{\parallel,\bar{v}})}{\tilde{\omega}_{vm}(\vec{\kappa}_{\parallel,\bar{v}}, \vec{\kappa}_{\parallel,\bar{m}}) - \omega} \right)$$

$$\times j_{h,mv}(z''; \vec{\kappa}_{\parallel,\bar{m}} + \vec{\kappa}_{\parallel,\bar{v}}) \psi_n^*(z') \psi_v(z') \delta(\vec{\kappa}_{\parallel,\bar{v}} - \vec{\kappa}_{\parallel,\bar{n}} + \vec{q}_\parallel''' - \vec{q}_\parallel') \delta(\vec{\kappa}_{\parallel,\bar{m}} - \vec{\kappa}_{\parallel,\bar{v}} + \vec{q}_\parallel'') \Big\}$$

$$\times j_{i,nm}(z; \vec{\kappa}_{\parallel,\bar{n}} + \vec{\kappa}_{\parallel,\bar{m}}) \delta(z' - z''') A_h(z'''; \vec{q}_\parallel''') A_x(z''; \vec{q}_\parallel'') A_x^*(z'; \vec{q}_\parallel')$$

$$\times \delta(\vec{\kappa}_{\parallel,\bar{n}} - \vec{\kappa}_{\parallel,\bar{m}} - \vec{q}_\parallel) d^2 \kappa_{\parallel,\bar{n}} d^2 \kappa_{\parallel,\bar{m}} d^2 \kappa_{\parallel,\bar{v}} d^2 q_\parallel''' d^2 q_\parallel'' d^2 q_\parallel' dz''' dz'' dz'. \tag{A.31}$$

Of the three integrals over $\vec{\kappa}_\parallel$ quantities, we can solve two because of the coupling to the wavevectors introduced by the Dirac delta functions appearing. We aim at keeping the $\vec{\kappa}_{\parallel,\bar{m}}$ set, and thus we solve the integrals for the v and n sets (in that order). Solving for the v set, we find that $\vec{\kappa}_{\parallel,\bar{v}}$ is replaced by $\vec{\kappa}_{\parallel,\bar{m}} + \vec{q}_\parallel''' - \vec{q}_\parallel'$ in the first part of the sum and by $\vec{\kappa}_{\parallel,\bar{m}} + \vec{q}_\parallel''$ in the second part of the sum, which afterwards allows us to solve the n set by replacing $\vec{\kappa}_{\parallel,\bar{n}}$ with $\vec{\kappa}_{\parallel,\bar{m}} + \vec{q}_\parallel''' + \vec{q}_\parallel'' - \vec{q}_\parallel'$ in general, giving

$$J_{ixxh}^F(z; \vec{q}_\parallel) = -\frac{e^2}{8 m_e \hbar^2} \frac{2}{(2\pi)^6} \int \cdots \int \sum_{nmv} \frac{1}{\tilde{\omega}_{nm}(\vec{\kappa}_{\parallel,\bar{m}} + \vec{q}_\parallel''' + \vec{q}_\parallel'' - \vec{q}_\parallel', \vec{\kappa}_{\parallel,\bar{m}}) - \omega}$$

$$\times \left\{ \left(\frac{f_m(\vec{\kappa}_{\parallel,\bar{m}}) - f_v(\vec{\kappa}_{\parallel,\bar{m}} + \vec{q}_\parallel''' - \vec{q}_\parallel')}{\tilde{\omega}_{vm}(\vec{\kappa}_{\parallel,\bar{m}} + \vec{q}_\parallel''' - \vec{q}_\parallel', \vec{\kappa}_{\parallel,\bar{m}})} \right. \right.$$

$$+ \frac{f_n(\vec{\kappa}_{\parallel,\bar{m}} + \vec{q}_\parallel''' + \vec{q}_\parallel'' - \vec{q}_\parallel') - f_v(\vec{\kappa}_{\parallel,\bar{m}} + \vec{q}_\parallel''' - \vec{q}_\parallel')}{\tilde{\omega}_{nv}(\vec{\kappa}_{\parallel,\bar{m}} + \vec{q}_\parallel''' + \vec{q}_\parallel'' - \vec{q}_\parallel', \vec{\kappa}_{\parallel,\bar{m}} + \vec{q}_\parallel''' - \vec{q}_\parallel') - \omega} \right)$$

$$\times j_{h,vn}(z''; 2\vec{\kappa}_{\parallel,\bar{m}} + 2\vec{q}_\parallel''' + \vec{q}_\parallel'' - \vec{q}_\parallel') \psi_v^*(z') \psi_m(z')$$

$$+ \left(\frac{f_n(\vec{\kappa}_{\parallel,\bar{m}} + \vec{q}_\parallel''' + \vec{q}_\parallel'' - \vec{q}_\parallel') - f_v(\vec{\kappa}_{\parallel,\bar{m}} + \vec{q}_\parallel'')}{\tilde{\omega}_{nv}(\vec{\kappa}_{\parallel,\bar{m}} + \vec{q}_\parallel''' + \vec{q}_\parallel'' - \vec{q}_\parallel', \vec{\kappa}_{\parallel,\bar{m}} + \vec{q}_\parallel'')} + \frac{f_m(\vec{\kappa}_{\parallel,\bar{m}}) - f_v(\vec{\kappa}_{\parallel,\bar{m}} + \vec{q}_\parallel'')}{\tilde{\omega}_{vm}(\vec{\kappa}_{\parallel,\bar{m}} + \vec{q}_\parallel'', \vec{\kappa}_{\parallel,\bar{m}}) - \omega} \right)$$

$$\times j_{h,mv}(z''; 2\vec{\kappa}_{\parallel,\bar{m}} + \vec{q}_\parallel'') \psi_n^*(z') \psi_v(z') \Big\} j_{i,nm}(z; 2\vec{\kappa}_{\parallel,\bar{m}} + \vec{q}_\parallel''' + \vec{q}_\parallel'' - \vec{q}_\parallel') \delta(z' - z''')$$

$$\times A_h(z''';\vec{q}_\parallel''')A_x(z'';\vec{q}_\parallel'')A_x^*(z';\vec{q}_\parallel')\delta(\vec{q}_\parallel'''+\vec{q}_\parallel''-\vec{q}_\parallel'-\vec{q}_\parallel)d^2\kappa_{\parallel,\bar{m}}d^2q_\parallel'''d^2q_\parallel''d^2q_\parallel'$$
$$\times dz'''dz''dz'. \tag{A.32}$$

On the form of Eq. (8.4) we thus get part F of the conductivity tensor as

$$\Xi_{ixxh}^{\rm F}(z,z',z'',z''';\vec{q}_\parallel,\vec{q}_\parallel',\vec{q}_\parallel'',\vec{q}_\parallel''') =$$
$$\frac{2\mathrm{i}}{\omega^3}\frac{e^2}{8m_e\hbar^2}\frac{1}{(2\pi)^2}\sum_{nmv}\int \frac{1}{\tilde{\omega}_{nm}(\vec{\kappa}_\parallel+\vec{q}_\parallel'''+\vec{q}_\parallel''-\vec{q}_\parallel',\vec{\kappa}_\parallel)-\omega}$$
$$\times\left\{\left(\frac{f_m(\vec{\kappa}_\parallel)-f_v(\vec{\kappa}_\parallel+\vec{q}_\parallel'''-\vec{q}_\parallel')}{\tilde{\omega}_{vm}(\vec{\kappa}_\parallel+\vec{q}_\parallel'''-\vec{q}_\parallel',\vec{\kappa}_\parallel)}+\frac{f_n(\vec{\kappa}_\parallel+\vec{q}_\parallel'''+\vec{q}_\parallel''-\vec{q}_\parallel')-f_v(\vec{\kappa}_\parallel+\vec{q}_\parallel'''-\vec{q}_\parallel')}{\tilde{\omega}_{nv}(\vec{\kappa}_\parallel+\vec{q}_\parallel'''+\vec{q}_\parallel''-\vec{q}_\parallel',\vec{\kappa}_\parallel+\vec{q}_\parallel'''-\vec{q}_\parallel')-\omega}\right)\right.$$
$$\times j_{h,vn}(z'';2\vec{\kappa}_\parallel+2\vec{q}_\parallel'''+\vec{q}_\parallel''-\vec{q}_\parallel')\psi_v^*(z')\psi_m(z')$$
$$+\left(\frac{f_n(\vec{\kappa}_\parallel+\vec{q}_\parallel'''+\vec{q}_\parallel''-\vec{q}_\parallel')-f_v(\vec{\kappa}_\parallel+\vec{q}_\parallel'')}{\tilde{\omega}_{nv}(\vec{\kappa}_\parallel+\vec{q}_\parallel'''+\vec{q}_\parallel''-\vec{q}_\parallel',\vec{\kappa}_\parallel+\vec{q}_\parallel'')}+\frac{f_m(\vec{\kappa}_\parallel)-f_v(\vec{\kappa}_\parallel+\vec{q}_\parallel'')}{\tilde{\omega}_{vm}(\vec{\kappa}_\parallel+\vec{q}_\parallel'',\vec{\kappa}_\parallel)-\omega}\right)$$
$$\times j_{h,mv}(z'';2\vec{\kappa}_\parallel+\vec{q}_\parallel'')\psi_n^*(z')\psi_v(z')\bigg\} j_{i,nm}(z;2\vec{\kappa}_\parallel+\vec{q}_\parallel'''+\vec{q}_\parallel''-\vec{q}_\parallel')\delta(z'-z''')$$
$$\times\delta(\vec{q}_\parallel'''+\vec{q}_\parallel''-\vec{q}_\parallel'-\vec{q}_\parallel)d^2\kappa_\parallel, \tag{A.33}$$

where we have omitted the now superfluous index m from the surface states $\vec{\kappa}_\parallel$. Inserting the DFWM pump fields defined by Eqs. (A.12) and (A.13) into Eq. (A.32), the integrals over $q_\parallel'''$ and $q_\parallel''$ can be solved. The resulting expression can then be solved for $q_\parallel'$ for the same reason as before, and on the form of Eq. (8.8), the PCDFWM conductivity tensor part F appears as Eq. (8.22).

A.9 Nonlinear process G

Inserting Eq. (6.14) into Eq. (4.10), we take element $ijkh$ of part G of the nonlinear current density. In the result we insert the expressions for the wave function, the vector potential and the transition current density in the two-dimensional Fourier representation [Eqs. (8.9), (8.1) and (8.14), respectively]. Then by use of Eq. (8.2) we find

$$J_{ijkh}^{\rm G}(z;\vec{q}_\parallel) = -\frac{1}{8\hbar^3}\frac{2}{(2\pi)^{14}}\int\cdots\int\sum_{nmvl}\frac{1}{\tilde{\omega}_{nm}-\omega}\left\{\left[\left(\frac{f_l-f_m}{\tilde{\omega}_{lm}-\omega}+\frac{f_l-f_v}{\tilde{\omega}_{vl}-\omega}\right)\frac{1}{\tilde{\omega}_{vm}-2\omega}\right.\right.$$
$$+\left(\frac{f_l-f_v}{\tilde{\omega}_{vl}-\omega}+\frac{f_n-f_v}{\tilde{\omega}_{nv}+\omega}\right)\frac{1}{\tilde{\omega}_{nl}}\bigg] j_{h,ml}(z''';\vec{\kappa}_{\parallel,\bar{m}}+\vec{\kappa}_{\parallel,\bar{l}})j_{k,lv}(z'';\vec{\kappa}_{\parallel,\bar{l}}+\vec{\kappa}_{\parallel,\bar{v}})$$
$$\times j_{j,vn}(z';\vec{\kappa}_{\parallel,\bar{v}}+\vec{\kappa}_{\parallel,\bar{n}})e^{\mathrm{i}(\vec{\kappa}_{\parallel,\bar{m}}-\vec{\kappa}_{\parallel,\bar{l}})\cdot\vec{r}_\parallel'''}e^{\mathrm{i}(\vec{\kappa}_{\parallel,\bar{l}}-\vec{\kappa}_{\parallel,\bar{v}})\cdot\vec{r}_\parallel''}e^{\mathrm{i}(\vec{\kappa}_{\parallel,\bar{v}}-\vec{\kappa}_{\parallel,\bar{n}})\cdot\vec{r}_\parallel'}$$
$$+\left[\left(\frac{f_l-f_m}{\tilde{\omega}_{lm}-\omega}+\frac{f_l-f_v}{\tilde{\omega}_{vl}+\omega}\right)\frac{1}{\tilde{\omega}_{vm}}+\left(\frac{f_l-f_v}{\tilde{\omega}_{vl}+\omega}+\frac{f_n-f_v}{\tilde{\omega}_{nv}-\omega}\right)\frac{1}{\tilde{\omega}_{nl}}\right]$$
$$\times j_{h,ml}(z''';\vec{\kappa}_{\parallel,\bar{m}}+\vec{\kappa}_{\parallel,\bar{l}})j_{k,vn}(z'';\vec{\kappa}_{\parallel,\bar{v}}+\vec{\kappa}_{\parallel,\bar{n}})j_{j,lv}(z';\vec{\kappa}_{\parallel,\bar{l}}+\vec{\kappa}_{\parallel,\bar{v}})e^{\mathrm{i}(\vec{\kappa}_{\parallel,\bar{m}}-\vec{\kappa}_{\parallel,\bar{l}})\cdot\vec{r}_\parallel'''}$$
$$\times e^{\mathrm{i}(\vec{\kappa}_{\parallel,\bar{v}}-\vec{\kappa}_{\parallel,\bar{n}})\cdot\vec{r}_\parallel''}e^{\mathrm{i}(\vec{\kappa}_{\parallel,\bar{l}}-\vec{\kappa}_{\parallel,\bar{v}})\cdot\vec{r}_\parallel'}+\left[\left(\frac{f_l-f_m}{\tilde{\omega}_{lm}+\omega}+\frac{f_l-f_v}{\tilde{\omega}_{vl}-\omega}\right)\frac{1}{\tilde{\omega}_{vm}}\right.$$

$$+ \left(\frac{f_l - f_v}{\tilde\omega_{vl} - \omega} + \frac{f_n - f_v}{\tilde\omega_{nv} - \omega} \right) \frac{1}{\tilde\omega_{nl} - 2\omega} \right] j_{h,lv}(z'''; \vec{\kappa}_{\parallel,\bar{l}} + \vec{\kappa}_{\parallel,\bar{v}}) j_{k,vn}(z''; \vec{\kappa}_{\parallel,\bar{v}} + \vec{\kappa}_{\parallel,\bar{n}})$$

$$\times j_{j,ml}(z'; \vec{\kappa}_{\parallel,\bar{m}} + \vec{\kappa}_{\parallel,\bar{l}}) e^{i(\vec{\kappa}_{\parallel,\bar{l}} - \vec{\kappa}_{\parallel,\bar{v}}) \cdot \vec{r}'''_\parallel} e^{i(\vec{\kappa}_{\parallel,\bar{v}} - \vec{\kappa}_{\parallel,\bar{n}}) \cdot \vec{r}''_\parallel} e^{i(\vec{\kappa}_{\parallel,\bar{m}} - \vec{\kappa}_{\parallel,\bar{l}}) \cdot \vec{r}'_\parallel} \Big\}$$

$$\times j_{i,nm}(z; \vec{\kappa}_{\parallel,\bar{n}} + \vec{\kappa}_{\parallel,\bar{m}}) A_h(z'''; \vec{q}'''_\parallel) A_k(z''; \vec{q}''_\parallel) A_j^*(z'; \vec{q}'_\parallel) e^{i(\vec{\kappa}_{\parallel,\bar{n}} - \vec{\kappa}_{\parallel,\bar{m}}) \cdot \vec{r}_\parallel}$$

$$\times e^{i\vec{q}'''_\parallel \cdot \vec{r}'''_\parallel} e^{i\vec{q}''_\parallel \cdot \vec{r}''_\parallel} e^{-i\vec{q}'_\parallel \cdot \vec{r}'_\parallel} d^2 q'''_\parallel d^2 q''_\parallel d^2 q'_\parallel d^3 r''' d^3 r'' d^3 r' e^{-i\vec{q}_\parallel \cdot \vec{r}_\parallel} d^2 r_\parallel. \tag{A.34}$$

In the above equation, we may immediately solve the integrals $\int d^2 r'''_\parallel$, $\int d^2 r''_\parallel$, $\int d^2 r'_\parallel$, and $\int d^2 r_\parallel$, and by replacing the sums over the various $\vec{\kappa}_\parallel$ quantities with integrals, as before, we get

$$J^G_{ijkh}(z;\vec{q}_\parallel) = -\frac{1}{8\hbar^3} \frac{2}{(2\pi)^6} \int \cdots \int \sum_{nmvl} \frac{1}{\tilde\omega_{nm}(\vec{\kappa}_{\parallel,\bar{n}}, \vec{\kappa}_{\parallel,\bar{m}}) - \omega}$$

$$\times \Bigg\{ \left[\left(\frac{f_l(\vec{\kappa}_{\parallel,\bar{l}}) - f_m(\vec{\kappa}_{\parallel,\bar{m}})}{\tilde\omega_{lm}(\vec{\kappa}_{\parallel,\bar{l}}, \vec{\kappa}_{\parallel,\bar{m}}) - \omega} + \frac{f_l(\vec{\kappa}_{\parallel,\bar{l}}) - f_v(\vec{\kappa}_{\parallel,\bar{v}})}{\tilde\omega_{vl}(\vec{\kappa}_{\parallel,\bar{v}}, \vec{\kappa}_{\parallel,\bar{l}}) - \omega} \right) \frac{1}{\tilde\omega_{vm}(\vec{\kappa}_{\parallel,\bar{v}}, \vec{\kappa}_{\parallel,\bar{m}}) - 2\omega} \right.$$

$$\left. + \left(\frac{f_l(\vec{\kappa}_{\parallel,\bar{l}}) - f_v(\vec{\kappa}_{\parallel,\bar{v}})}{\tilde\omega_{vl}(\vec{\kappa}_{\parallel,\bar{v}}, \vec{\kappa}_{\parallel,\bar{l}}) - \omega} + \frac{f_n(\vec{\kappa}_{\parallel,\bar{n}}) - f_v(\vec{\kappa}_{\parallel,\bar{v}})}{\tilde\omega_{nv}(\vec{\kappa}_{\parallel,\bar{n}}, \vec{\kappa}_{\parallel,\bar{v}}) + \omega} \right) \frac{1}{\tilde\omega_{nl}(\vec{\kappa}_{\parallel,\bar{n}}, \vec{\kappa}_{\parallel,\bar{l}})} \right]$$

$$\times j_{h,ml}(z'''; \vec{\kappa}_{\parallel,\bar{m}} + \vec{\kappa}_{\parallel,\bar{l}}) j_{k,lv}(z''; \vec{\kappa}_{\parallel,\bar{l}} + \vec{\kappa}_{\parallel,\bar{v}}) j_{j,vn}(z'; \vec{\kappa}_{\parallel,\bar{v}} + \vec{\kappa}_{\parallel,\bar{n}})$$

$$\times \delta(\vec{\kappa}_{\parallel,\bar{m}} - \vec{\kappa}_{\parallel,\bar{l}} + \vec{q}'''_\parallel) \delta(\vec{\kappa}_{\parallel,\bar{l}} - \vec{\kappa}_{\parallel,\bar{v}} + \vec{q}''_\parallel) \delta(\vec{\kappa}_{\parallel,\bar{v}} - \vec{\kappa}_{\parallel,\bar{n}} - \vec{q}'_\parallel)$$

$$+ \left[\left(\frac{f_l(\vec{\kappa}_{\parallel,\bar{l}}) - f_m(\vec{\kappa}_{\parallel,\bar{m}})}{\tilde\omega_{lm}(\vec{\kappa}_{\parallel,\bar{l}}, \vec{\kappa}_{\parallel,\bar{m}}) - \omega} + \frac{f_l(\vec{\kappa}_{\parallel,\bar{l}}) - f_v(\vec{\kappa}_{\parallel,\bar{v}})}{\tilde\omega_{vl}(\vec{\kappa}_{\parallel,\bar{v}}, \vec{\kappa}_{\parallel,\bar{l}}) + \omega} \right) \frac{1}{\tilde\omega_{vm}(\vec{\kappa}_{\parallel,\bar{v}}, \vec{\kappa}_{\parallel,\bar{m}})} \right.$$

$$\left. + \left(\frac{f_l(\vec{\kappa}_{\parallel,\bar{l}}) - f_v(\vec{\kappa}_{\parallel,\bar{v}})}{\tilde\omega_{vl}(\vec{\kappa}_{\parallel,\bar{v}}, \vec{\kappa}_{\parallel,\bar{l}}) + \omega} + \frac{f_n(\vec{\kappa}_{\parallel,\bar{n}}) - f_v(\vec{\kappa}_{\parallel,\bar{v}})}{\tilde\omega_{nv}(\vec{\kappa}_{\parallel,\bar{n}}, \vec{\kappa}_{\parallel,\bar{v}}) - \omega} \right) \frac{1}{\tilde\omega_{nl}(\vec{\kappa}_{\parallel,\bar{n}}, \vec{\kappa}_{\parallel,\bar{l}})} \right]$$

$$\times j_{h,ml}(z'''; \vec{\kappa}_{\parallel,\bar{m}} + \vec{\kappa}_{\parallel,\bar{l}}) j_{k,vn}(z''; \vec{\kappa}_{\parallel,\bar{v}} + \vec{\kappa}_{\parallel,\bar{n}}) j_{j,lv}(z'; \vec{\kappa}_{\parallel,\bar{l}} + \vec{\kappa}_{\parallel,\bar{v}})$$

$$\times \delta(\vec{\kappa}_{\parallel,\bar{m}} - \vec{\kappa}_{\parallel,\bar{l}} + \vec{q}'''_\parallel) \delta(\vec{\kappa}_{\parallel,\bar{v}} - \vec{\kappa}_{\parallel,\bar{n}} + \vec{q}''_\parallel) \delta(\vec{\kappa}_{\parallel,\bar{l}} - \vec{\kappa}_{\parallel,\bar{v}} - \vec{q}'_\parallel)$$

$$+ \left[\left(\frac{f_l(\vec{\kappa}_{\parallel,\bar{l}}) - f_m(\vec{\kappa}_{\parallel,\bar{m}})}{\tilde\omega_{lm}(\vec{\kappa}_{\parallel,\bar{l}}, \vec{\kappa}_{\parallel,\bar{m}}) + \omega} + \frac{f_l(\vec{\kappa}_{\parallel,\bar{l}}) - f_v(\vec{\kappa}_{\parallel,\bar{v}})}{\tilde\omega_{vl}(\vec{\kappa}_{\parallel,\bar{v}}, \vec{\kappa}_{\parallel,\bar{l}}) - \omega} \right) \frac{1}{\tilde\omega_{vm}(\vec{\kappa}_{\parallel,\bar{v}}, \vec{\kappa}_{\parallel,\bar{m}})} \right.$$

$$\left. + \left(\frac{f_l(\vec{\kappa}_{\parallel,\bar{l}}) - f_v(\vec{\kappa}_{\parallel,\bar{v}})}{\tilde\omega_{vl}(\vec{\kappa}_{\parallel,\bar{v}}, \vec{\kappa}_{\parallel,\bar{l}}) - \omega} + \frac{f_n(\vec{\kappa}_{\parallel,\bar{n}}) - f_v(\vec{\kappa}_{\parallel,\bar{v}})}{\tilde\omega_{nv}(\vec{\kappa}_{\parallel,\bar{n}}, \vec{\kappa}_{\parallel,\bar{v}}) - \omega} \right) \frac{1}{\tilde\omega_{nl}(\vec{\kappa}_{\parallel,\bar{n}}, \vec{\kappa}_{\parallel,\bar{l}}) - 2\omega} \right]$$

$$\times j_{h,lv}(z'''; \vec{\kappa}_{\parallel,\bar{l}} + \vec{\kappa}_{\parallel,\bar{v}}) j_{k,vn}(z''; \vec{\kappa}_{\parallel,\bar{v}} + \vec{\kappa}_{\parallel,\bar{n}}) j_{j,ml}(z'; \vec{\kappa}_{\parallel,\bar{m}} + \vec{\kappa}_{\parallel,\bar{l}})$$

$$\times \delta(\vec{\kappa}_{\parallel,\bar{l}} - \vec{\kappa}_{\parallel,\bar{v}} + \vec{q}'''_\parallel) \delta(\vec{\kappa}_{\parallel,\bar{v}} - \vec{\kappa}_{\parallel,\bar{n}} + \vec{q}''_\parallel) \delta(\vec{\kappa}_{\parallel,\bar{m}} - \vec{\kappa}_{\parallel,\bar{l}} - \vec{q}'_\parallel) \Bigg\} j_{i,nm}(z; \vec{\kappa}_{\parallel,\bar{n}} + \vec{\kappa}_{\parallel,\bar{m}})$$

$$\times A_h(z'''; \vec{q}'''_\parallel) A_k(z''; \vec{q}''_\parallel) A_j^*(z'; \vec{q}'_\parallel) \delta(\vec{\kappa}_{\parallel,\bar{n}} - \vec{\kappa}_{\parallel,\bar{m}} - \vec{q}_\parallel) d^2\kappa_{\parallel,\bar{n}} d^2\kappa_{\parallel,\bar{m}} d^2\kappa_{\parallel,\bar{v}} d^2\kappa_{\parallel,\bar{l}}$$

$$\times d^2 q'''_\parallel d^2 q''_\parallel d^2 q'_\parallel dz''' dz'' dz'. \tag{A.35}$$

Of the four integrals over $\vec{\kappa}_\parallel$ quantities, we can solve three because of the coupling to the wavevectors introduced by the Dirac delta functions appearing. We aim at keeping the

$\vec{\kappa}_{\|,\bar{m}}$ set, and thus we solve the integrals for the l, v, and n sets. Thus (i), in the first part of the sum, we find that $\vec{\kappa}_{\|,\bar{l}}$ can be replaced by $\vec{\kappa}_{\|,\bar{m}} + \vec{q}_{\|}''$, then letting us replace $\vec{\kappa}_{\|,\bar{v}}$ by $\vec{\kappa}_{\|,\bar{m}} + \vec{q}_{\|}''' + \vec{q}_{\|}''$, which again let us replace $\vec{\kappa}_{\|,\bar{n}}$ by $\vec{\kappa}_{\|,\bar{m}} + \vec{q}_{\|}''' + \vec{q}_{\|}'' - \vec{q}_{\|}'$. (ii) In the second part of the sum, we find that $\vec{\kappa}_{\|,\bar{l}}$ can be replaced by $\vec{\kappa}_{\|,\bar{m}} + \vec{q}_{\|}'''$, then letting us replace $\vec{\kappa}_{\|,\bar{v}}$ by $\vec{\kappa}_{\|,\bar{m}} + \vec{q}_{\|}''' - \vec{q}_{\|}'$, which again let us replace $\vec{\kappa}_{\|,\bar{n}}$ by $\vec{\kappa}_{\|,\bar{m}} + \vec{q}_{\|}''' + \vec{q}_{\|}'' - \vec{q}_{\|}'$. (iii) In the third part of the sum, we find that $\vec{\kappa}_{\|,\bar{l}}$ can be replaced by $\vec{\kappa}_{\|,\bar{m}} - \vec{q}_{\|}'$, then letting us replace $\vec{\kappa}_{\|,\bar{v}}$ by $\vec{\kappa}_{\|,\bar{m}} + \vec{q}_{\|}''' - \vec{q}_{\|}'$, which again let us replace $\vec{\kappa}_{\|,\bar{n}}$ by $\vec{\kappa}_{\|,\bar{m}} + \vec{q}_{\|}''' + \vec{q}_{\|}'' - \vec{q}_{\|}'$. Finally (iv), we observe that the substitution of $\vec{\kappa}_{\|,\bar{n}}$ by $\vec{\kappa}_{\|,\bar{m}} + \vec{q}_{\|}''' + \vec{q}_{\|}'' - \vec{q}_{\|}'$ is global, and we thus get the resulting current density element

$$
\begin{aligned}
J^{\mathrm{G}}_{ijkh}(z;\vec{q}_{\|}) = & -\frac{1}{8\hbar^3}\frac{2}{(2\pi)^6}\int\cdots\int\sum_{nmvl}\frac{1}{\tilde{\omega}_{nm}(\vec{\kappa}_{\|,\bar{m}}+\vec{q}_{\|}'''+\vec{q}_{\|}''-\vec{q}_{\|}',\vec{\kappa}_{\|,\bar{m}})-\omega} \\
& \times\Bigg\{\Bigg[\left(\frac{f_l(\vec{\kappa}_{\|,\bar{m}}+\vec{q}_{\|}''')-f_m(\vec{\kappa}_{\|,\bar{m}})}{\tilde{\omega}_{lm}(\vec{\kappa}_{\|,\bar{m}}+\vec{q}_{\|}''',\vec{\kappa}_{\|,\bar{m}})-\omega}+\frac{f_l(\vec{\kappa}_{\|,\bar{m}}+\vec{q}_{\|}''')-f_v(\vec{\kappa}_{\|,\bar{m}}+\vec{q}_{\|}'''+\vec{q}_{\|}'')}{\tilde{\omega}_{vl}(\vec{\kappa}_{\|,\bar{m}}+\vec{q}_{\|}'''+\vec{q}_{\|}'',\vec{\kappa}_{\|,\bar{m}}+\vec{q}_{\|}''')-\omega}\right) \\
& \times\frac{1}{\tilde{\omega}_{vm}(\vec{\kappa}_{\|,\bar{m}}+\vec{q}_{\|}'''+\vec{q}_{\|}'',\vec{\kappa}_{\|,\bar{m}})-2\omega}+\left(\frac{f_l(\vec{\kappa}_{\|,\bar{m}}+\vec{q}_{\|}''')-f_v(\vec{\kappa}_{\|,\bar{m}}+\vec{q}_{\|}'''+\vec{q}_{\|}'')}{\tilde{\omega}_{vl}(\vec{\kappa}_{\|,\bar{m}}+\vec{q}_{\|}'''+\vec{q}_{\|}'',\vec{\kappa}_{\|,\bar{m}}+\vec{q}_{\|}''')-\omega}\right. \\
& \left.+\frac{f_n(\vec{\kappa}_{\|,\bar{m}}+\vec{q}_{\|}'''+\vec{q}_{\|}''-\vec{q}_{\|}')-f_v(\vec{\kappa}_{\|,\bar{m}}+\vec{q}_{\|}'''+\vec{q}_{\|}'')}{\tilde{\omega}_{nv}(\vec{\kappa}_{\|,\bar{m}}+\vec{q}_{\|}'''+\vec{q}_{\|}''-\vec{q}_{\|}',\vec{\kappa}_{\|,\bar{m}}+\vec{q}_{\|}'''+\vec{q}_{\|}'')+\omega}\right) \\
& \times\frac{1}{\tilde{\omega}_{nl}(\vec{\kappa}_{\|,\bar{m}}+\vec{q}_{\|}'''+\vec{q}_{\|}''-\vec{q}_{\|}',\vec{\kappa}_{\|,\bar{m}}+\vec{q}_{\|}''')}\Bigg]j_{h,ml}(z''';2\vec{\kappa}_{\|,\bar{m}}+\vec{q}_{\|}''') \\
& \times j_{k,lv}(z'';2\vec{\kappa}_{\|,\bar{m}}+2\vec{q}_{\|}'''+\vec{q}_{\|}'')j_{j,vn}(z';2\vec{\kappa}_{\|,\bar{m}}+2\vec{q}_{\|}'''+2\vec{q}_{\|}''-\vec{q}_{\|}') \\
& +\Bigg[\left(\frac{f_l(\vec{\kappa}_{\|,\bar{m}}+\vec{q}_{\|}''')-f_m(\vec{\kappa}_{\|,\bar{m}})}{\tilde{\omega}_{lm}(\vec{\kappa}_{\|,\bar{m}}+\vec{q}_{\|}''',\vec{\kappa}_{\|,\bar{m}})-\omega}+\frac{f_l(\vec{\kappa}_{\|,\bar{m}}+\vec{q}_{\|}''')-f_v(\vec{\kappa}_{\|,\bar{m}}+\vec{q}_{\|}'''-\vec{q}_{\|}')}{\tilde{\omega}_{vl}(\vec{\kappa}_{\|,\bar{m}}+\vec{q}_{\|}'''-\vec{q}_{\|}',\vec{\kappa}_{\|,\bar{m}}+\vec{q}_{\|}''')+\omega}\right) \\
& \times\frac{1}{\tilde{\omega}_{vm}(\vec{\kappa}_{\|,\bar{m}}+\vec{q}_{\|}'''-\vec{q}_{\|}',\vec{\kappa}_{\|,\bar{m}})}+\left(\frac{f_l(\vec{\kappa}_{\|,\bar{m}}+\vec{q}_{\|}''')-f_v(\vec{\kappa}_{\|,\bar{m}}+\vec{q}_{\|}'''-\vec{q}_{\|}')}{\tilde{\omega}_{vl}(\vec{\kappa}_{\|,\bar{m}}+\vec{q}_{\|}'''-\vec{q}_{\|}',\vec{\kappa}_{\|,\bar{m}}+\vec{q}_{\|}''')+\omega}\right. \\
& \left.+\frac{f_n(\vec{\kappa}_{\|,\bar{m}}+\vec{q}_{\|}'''+\vec{q}_{\|}''-\vec{q}_{\|}')-f_v(\vec{\kappa}_{\|,\bar{m}}+\vec{q}_{\|}'''-\vec{q}_{\|}')}{\tilde{\omega}_{nv}(\vec{\kappa}_{\|,\bar{m}}+\vec{q}_{\|}'''+\vec{q}_{\|}''-\vec{q}_{\|}',\vec{\kappa}_{\|,\bar{m}}+\vec{q}_{\|}'''-\vec{q}_{\|}')-\omega}\right) \\
& \times\frac{1}{\tilde{\omega}_{nl}(\vec{\kappa}_{\|,\bar{m}}+\vec{q}_{\|}'''+\vec{q}_{\|}''-\vec{q}_{\|}',\vec{\kappa}_{\|,\bar{m}}+\vec{q}_{\|}''')}\Bigg]j_{h,ml}(z''';2\vec{\kappa}_{\|,\bar{m}}+\vec{q}_{\|}''') \\
& \times j_{k,vn}(z'';2\vec{\kappa}_{\|,\bar{m}}+2\vec{q}_{\|}'''+\vec{q}_{\|}''-2\vec{q}_{\|}')j_{j,lv}(z';2\vec{\kappa}_{\|,\bar{m}}+2\vec{q}_{\|}'''-\vec{q}_{\|}') \\
& +\Bigg[\left(\frac{f_l(\vec{\kappa}_{\|,\bar{m}}-\vec{q}_{\|}')-f_m(\vec{\kappa}_{\|,\bar{m}})}{\tilde{\omega}_{lm}(\vec{\kappa}_{\|,\bar{m}}-\vec{q}_{\|}',\vec{\kappa}_{\|,\bar{m}})+\omega}+\frac{f_l(\vec{\kappa}_{\|,\bar{m}}-\vec{q}_{\|}')-f_v(\vec{\kappa}_{\|,\bar{m}}+\vec{q}_{\|}'''-\vec{q}_{\|}')}{\tilde{\omega}_{vl}(\vec{\kappa}_{\|,\bar{m}}+\vec{q}_{\|}'''-\vec{q}_{\|}',\vec{\kappa}_{\|,\bar{m}}-\vec{q}_{\|}')-\omega}\right) \\
& \times\frac{1}{\tilde{\omega}_{vm}(\vec{\kappa}_{\|,\bar{m}}+\vec{q}_{\|}'''-\vec{q}_{\|}',\vec{\kappa}_{\|,\bar{m}})}+\left(\frac{f_l(\vec{\kappa}_{\|,\bar{m}}-\vec{q}_{\|}')-f_v(\vec{\kappa}_{\|,\bar{m}}+\vec{q}_{\|}'''-\vec{q}_{\|}')}{\tilde{\omega}_{vl}(\vec{\kappa}_{\|,\bar{m}}+\vec{q}_{\|}'''-\vec{q}_{\|}',\vec{\kappa}_{\|,\bar{m}}-\vec{q}_{\|}')-\omega}\right.
\end{aligned}
$$

$$+ \frac{f_n(\vec{\kappa}_{\parallel,\bar{m}} + \vec{q}_\parallel''' + \vec{q}_\parallel'' - \vec{q}_\parallel') - f_v(\vec{\kappa}_{\parallel,\bar{m}} + \vec{q}_\parallel''' - \vec{q}_\parallel')}{\tilde{\omega}_{nv}(\vec{\kappa}_{\parallel,\bar{m}} + \vec{q}_\parallel''' + \vec{q}_\parallel'' - \vec{q}_\parallel', \vec{\kappa}_{\parallel,\bar{m}} + \vec{q}_\parallel''' - \vec{q}_\parallel') - \omega} \Bigg)$$

$$\times \frac{1}{\tilde{\omega}_{nl}(\vec{\kappa}_{\parallel,\bar{m}} + \vec{q}_\parallel''' + \vec{q}_\parallel'' - \vec{q}_\parallel', \vec{\kappa}_{\parallel,\bar{m}} - \vec{q}_\parallel') - 2\omega} \Bigg] j_{h,lv}(z'''; 2\vec{\kappa}_{\parallel,\bar{m}} + \vec{q}_\parallel'' - 2\vec{q}_\parallel')$$

$$\times j_{k,vn}(z''; 2\vec{\kappa}_{\parallel,\bar{m}} + 2\vec{q}_\parallel''' + \vec{q}_\parallel'' - 2\vec{q}_\parallel') j_{j,ml}(z'; 2\vec{\kappa}_{\parallel,\bar{m}} - \vec{q}_\parallel') \Big\}$$

$$\times j_{i,nm}(z; 2\vec{\kappa}_{\parallel,\bar{m}} + \vec{q}_\parallel''' + \vec{q}_\parallel'' - \vec{q}_\parallel') \delta(\vec{q}_\parallel''' + \vec{q}_\parallel'' - \vec{q}_\parallel' - \vec{q}_\parallel) A_h(z'''; \vec{q}_\parallel''') A_k(z''; \vec{q}_\parallel'')$$

$$\times A_j^*(z'; \vec{q}_\parallel') d^2\kappa_{\parallel,\bar{m}} d^2 q_\parallel''' d^2 q_\parallel'' d^2 q_\parallel' dz''' dz'' dz'. \tag{A.36}$$

On the form of Eq. (8.4) we thus get part G of the conductivity tensor as

$$\Xi_{ijkh}^G(z, z', z'', z'''; \vec{q}_\parallel, \vec{q}_\parallel', \vec{q}_\parallel'', \vec{q}_\parallel''') = \frac{2\mathrm{i}}{\omega^3} \frac{1}{(2\pi)^2} \frac{1}{8\hbar^3}$$

$$\times \sum_{nmvl} \int \frac{1}{\tilde{\omega}_{nm}(\vec{\kappa}_\parallel + \vec{q}_\parallel''' + \vec{q}_\parallel'' - \vec{q}_\parallel', \vec{\kappa}_\parallel) - \omega} \Bigg\{ \Bigg[\frac{1}{\tilde{\omega}_{vm}(\vec{\kappa}_\parallel + \vec{q}_\parallel''' + \vec{q}_\parallel'', \vec{\kappa}_\parallel) - 2\omega}$$

$$\times \left(\frac{f_l(\vec{\kappa}_\parallel + \vec{q}_\parallel''') - f_m(\vec{\kappa}_\parallel)}{\tilde{\omega}_{lm}(\vec{\kappa}_\parallel + \vec{q}_\parallel''', \vec{\kappa}_\parallel) - \omega} + \frac{f_l(\vec{\kappa}_\parallel + \vec{q}_\parallel''') - f_v(\vec{\kappa}_\parallel + \vec{q}_\parallel''' + \vec{q}_\parallel'')}{\tilde{\omega}_{vl}(\vec{\kappa}_\parallel + \vec{q}_\parallel''' + \vec{q}_\parallel'', \vec{\kappa}_\parallel + \vec{q}_\parallel''') - \omega} \right)$$

$$+ \frac{1}{\tilde{\omega}_{nl}(\vec{\kappa}_\parallel + \vec{q}_\parallel''' + \vec{q}_\parallel'' - \vec{q}_\parallel', \vec{\kappa}_\parallel + \vec{q}_\parallel''')} \left(\frac{f_l(\vec{\kappa}_\parallel + \vec{q}_\parallel''') - f_v(\vec{\kappa}_\parallel + \vec{q}_\parallel''' + \vec{q}_\parallel'')}{\tilde{\omega}_{vl}(\vec{\kappa}_\parallel + \vec{q}_\parallel''' + \vec{q}_\parallel'', \vec{\kappa}_\parallel + \vec{q}_\parallel''') - \omega} \right.$$

$$\left. + \frac{f_n(\vec{\kappa}_\parallel + \vec{q}_\parallel''' + \vec{q}_\parallel'' - \vec{q}_\parallel') - f_v(\vec{\kappa}_\parallel + \vec{q}_\parallel''' + \vec{q}_\parallel'')}{\tilde{\omega}_{nv}(\vec{\kappa}_\parallel + \vec{q}_\parallel''' + \vec{q}_\parallel'' - \vec{q}_\parallel', \vec{\kappa}_\parallel + \vec{q}_\parallel''' + \vec{q}_\parallel'') + \omega} \right) \Bigg] j_{h,ml}(z'''; 2\vec{\kappa}_\parallel + \vec{q}_\parallel''')$$

$$\times j_{k,lv}(z''; 2\vec{\kappa}_\parallel + 2\vec{q}_\parallel''' + \vec{q}_\parallel'') j_{j,vn}(z'; 2\vec{\kappa}_\parallel + 2\vec{q}_\parallel''' + 2\vec{q}_\parallel'' - \vec{q}_\parallel')$$

$$+ \Bigg[\left(\frac{f_l(\vec{\kappa}_\parallel + \vec{q}_\parallel''') - f_m(\vec{\kappa}_\parallel)}{\tilde{\omega}_{lm}(\vec{\kappa}_\parallel + \vec{q}_\parallel''', \vec{\kappa}_\parallel) - \omega} + \frac{f_l(\vec{\kappa}_\parallel + \vec{q}_\parallel''') - f_v(\vec{\kappa}_\parallel + \vec{q}_\parallel''' - \vec{q}_\parallel')}{\tilde{\omega}_{vl}(\vec{\kappa}_\parallel + \vec{q}_\parallel''' - \vec{q}_\parallel', \vec{\kappa}_\parallel + \vec{q}_\parallel''') + \omega} \right)$$

$$\times \frac{1}{\tilde{\omega}_{vm}(\vec{\kappa}_\parallel + \vec{q}_\parallel''' - \vec{q}_\parallel', \vec{\kappa}_\parallel)} + \left(\frac{f_l(\vec{\kappa}_\parallel + \vec{q}_\parallel''') - f_v(\vec{\kappa}_\parallel + \vec{q}_\parallel''' - \vec{q}_\parallel')}{\tilde{\omega}_{vl}(\vec{\kappa}_\parallel + \vec{q}_\parallel''' - \vec{q}_\parallel', \vec{\kappa}_\parallel + \vec{q}_\parallel''') + \omega} \right.$$

$$\left. + \frac{f_n(\vec{\kappa}_\parallel + \vec{q}_\parallel''' + \vec{q}_\parallel'' - \vec{q}_\parallel') - f_v(\vec{\kappa}_\parallel + \vec{q}_\parallel''' - \vec{q}_\parallel')}{\tilde{\omega}_{nv}(\vec{\kappa}_\parallel + \vec{q}_\parallel''' + \vec{q}_\parallel'' - \vec{q}_\parallel', \vec{\kappa}_\parallel + \vec{q}_\parallel''' - \vec{q}_\parallel') - \omega} \right) \frac{1}{\tilde{\omega}_{nl}(\vec{\kappa}_\parallel + \vec{q}_\parallel''' + \vec{q}_\parallel'' - \vec{q}_\parallel', \vec{\kappa}_\parallel + \vec{q}_\parallel''')} \Bigg]$$

$$\times j_{h,ml}(z'''; 2\vec{\kappa}_\parallel + \vec{q}_\parallel''') j_{k,vn}(z''; 2\vec{\kappa}_\parallel + 2\vec{q}_\parallel''' + \vec{q}_\parallel'' - 2\vec{q}_\parallel') j_{j,lv}(z'; 2\vec{\kappa}_\parallel + 2\vec{q}_\parallel''' - \vec{q}_\parallel')$$

$$+ \Bigg[\left(\frac{f_l(\vec{\kappa}_\parallel - \vec{q}_\parallel') - f_m(\vec{\kappa}_\parallel)}{\tilde{\omega}_{lm}(\vec{\kappa}_\parallel - \vec{q}_\parallel', \vec{\kappa}_\parallel) + \omega} + \frac{f_l(\vec{\kappa}_\parallel - \vec{q}_\parallel') - f_v(\vec{\kappa}_\parallel + \vec{q}_\parallel''' - \vec{q}_\parallel')}{\tilde{\omega}_{vl}(\vec{\kappa}_\parallel + \vec{q}_\parallel''' - \vec{q}_\parallel', \vec{\kappa}_\parallel - \vec{q}_\parallel') - \omega} \right)$$

$$\times \frac{1}{\tilde{\omega}_{vm}(\vec{\kappa}_\parallel + \vec{q}_\parallel''' - \vec{q}_\parallel', \vec{\kappa}_\parallel)} + \left(\frac{f_l(\vec{\kappa}_\parallel - \vec{q}_\parallel') - f_v(\vec{\kappa}_\parallel + \vec{q}_\parallel''' - \vec{q}_\parallel')}{\tilde{\omega}_{vl}(\vec{\kappa}_\parallel + \vec{q}_\parallel''' - \vec{q}_\parallel', \vec{\kappa}_\parallel - \vec{q}_\parallel') - \omega} \right.$$

$$\left. + \frac{f_n(\vec{\kappa}_\parallel + \vec{q}_\parallel''' + \vec{q}_\parallel'' - \vec{q}_\parallel') - f_v(\vec{\kappa}_\parallel + \vec{q}_\parallel''' - \vec{q}_\parallel')}{\tilde{\omega}_{nv}(\vec{\kappa}_\parallel + \vec{q}_\parallel''' + \vec{q}_\parallel'' - \vec{q}_\parallel', \vec{\kappa}_\parallel + \vec{q}_\parallel''' - \vec{q}_\parallel') - \omega} \right)$$

$$\times \frac{1}{\tilde{\omega}_{nl}(\vec{\kappa}_\parallel + \vec{q}_\parallel''' + \vec{q}_\parallel'' - \vec{q}_\parallel', \vec{\kappa}_\parallel - \vec{q}_\parallel') - 2\omega}\Bigg] j_{h,lv}(z'''; 2\vec{\kappa}_\parallel + \vec{q}_\parallel''' - 2\vec{q}_\parallel')$$

$$\times j_{k,vn}(z''; 2\vec{\kappa}_\parallel + 2\vec{q}_\parallel''' + \vec{q}_\parallel'' - 2\vec{q}_\parallel') j_{j,ml}(z'; 2\vec{\kappa}_\parallel - \vec{q}_\parallel')\Big\}$$

$$\times j_{i,nm}(z; 2\vec{\kappa}_\parallel + \vec{q}_\parallel''' + \vec{q}_\parallel'' - \vec{q}_\parallel')\delta(\vec{q}_\parallel''' + \vec{q}_\parallel'' - \vec{q}_\parallel' - \vec{q}_\parallel)d^2\kappa_\parallel, \tag{A.37}$$

where we have omitted the now superfluous index m from the surface states $\vec{\kappa}_\parallel$. As was the case with parts A–F, we are particularly interested in finding the PCDFWM response tensor, and thus we insert the DFWM pump fields given by Eqs. (A.12) and (A.13) into Eq. (A.36). This allows us to carry out the integrals over $q_\parallel'''$ and $q_\parallel''$, consequentally followed by solution to the integral over $q_\parallel'$. The resulting expression is then split according to Eq. (8.8), and the PCDFWM conductivity tensor part G appear as Eq. (8.23).

Appendix B

In this appendix we discuss the analytic solution to the integrals over $\vec{\kappa}_{\|}$ appearing in the linear and nonlinear conductivity tensor. The discussion is limited to cover the low temperature limit, and it is presented as a principal solution to all integrals over $\vec{\kappa}_{\|}$ appearing in Eqs. (8.15)–(8.23).

B.1 General type of integrals

Every integral over $\vec{\kappa}_{\|}$ in both the linear conductivity tensor, Eqs. (8.15) and (8.16), and the nonlinear conductivity tensor, Eqs. (8.17)–(8.23), can when scattering takes place in the x-z-plane be expressed as a sum over terms of the general type

$$\mathcal{F}_{pq}^{\beta}(n,\{a\},\{b\},s) = \int\int \frac{\kappa_x^p \kappa_y^q f_n(\vec{\kappa}_{\|}+s\vec{e}_x)}{\prod_{k=1}^{\beta}[a_k\kappa_x+b_k]}d\kappa_x d\kappa_y, \tag{B.1}$$

where p,k,β are nonnegative integers, and q is an even nonnegative integer. The functions in general depends on (i) the quantum number n, which is a positive nonzero integer, (ii) a set of real quantities, $\{a\} \equiv \{a_1,\dots,a_{\beta}\}$ appearing in front of the integration variable κ_x in the denominator, (iii) a set of complex nonzero quantities, $\{b\} \equiv \{b_1,\dots,b_{\beta}\}$ apearing as the other quantity in each term of the denominator, and (iv) the real quantity s representing the displacement of the center of the Fermi-Dirac distribution function from $(\kappa_x,\kappa_y)=(0,0)$. The quantity s together with each element in the set $\{a\}$ is in general a function of the parallel components of the probe and pump wavevectors, $\vec{q}_{\|}$ and $\vec{k}_{\|}$. Each element in the set $\{b\}$ is furthermore a function of τ, the relaxation time.

In the low temperature limit the Fermi-Dirac distribution function is zero outside the Fermi sphere and equal to one inside, and it is therefore advantageous to shift κ_x by $-s$, followed by a one-to-one mapping of the x-y-plane into polar coordinates (r-θ-plane). Using in this way $\kappa_x = r\cos\theta$, $\kappa_y = r\sin\theta$, and thus $d\kappa_x d\kappa_y = rd\theta dr$, the indefinite integral in Eq. (B.1) is turned into the definite integral

$$\mathcal{F}_{pq}^{\beta}(n,\{a\},\{b\},s) = \int_0^{\alpha(n)} \int_0^{2\pi} \frac{r(r\cos\theta - s)^p (r\sin\theta)^q}{\prod_{k=1}^{\beta}[a_k(r\cos\theta - s)+b_k]}d\theta dr. \tag{B.2}$$

$$
[xxkh] \quad\quad\quad [xykh] \quad\quad\quad [xzkh]
$$

$$
\begin{bmatrix} \triangledown & \cdot & \oplus \\ \cdot & \times & \cdot \\ \oplus & \cdot & \bullet \end{bmatrix}
\begin{bmatrix} \cdot & \times & \cdot \\ \times & \cdot & \circ \\ \cdot & \circ & \cdot \end{bmatrix}
\begin{bmatrix} \oplus & \cdot & \bullet \\ \cdot & \circ & \cdot \\ \bullet & \cdot & + \end{bmatrix}
$$

$$
[yxkh] \quad\quad\quad [yykh] \quad\quad\quad [yzkh]
$$

$$
\begin{bmatrix} \cdot & \times & \cdot \\ \times & \cdot & \circ \\ \cdot & \circ & \cdot \end{bmatrix}
\begin{bmatrix} \times & \cdot & \circ \\ \cdot & \star & \cdot \\ \circ & \cdot & \otimes \end{bmatrix}
\begin{bmatrix} \cdot & \circ & \cdot \\ \circ & \cdot & \otimes \\ \cdot & \otimes & \cdot \end{bmatrix}
$$

$$
[zxkh] \quad\quad\quad [zykh] \quad\quad\quad [zzkh]
$$

$$
\begin{bmatrix} \oplus & \cdot & \bullet \\ \cdot & \circ & \cdot \\ \bullet & \cdot & + \end{bmatrix}
\begin{bmatrix} \cdot & \circ & \cdot \\ \circ & \cdot & \otimes \\ \cdot & \otimes & \cdot \end{bmatrix}
\begin{bmatrix} \bullet & \cdot & + \\ \cdot & \otimes & \cdot \\ + & \cdot & \triangle \end{bmatrix}
$$

Figure B.1: Distribution of the elements of the nonlinear conductivity tensor in terms of p and q. In one element ($\triangle$) the terms appear with $(p,q) = (0,0)$. In six elements ($\otimes$) the terms appear with $(p,q) = (0,2)$. In one element ($\star$) the terms appear with $(p,q) = (0,4)$. In four elements ($+$) the terms appear with $(p,q) \in \{(1,0),(0,0)\}$. In twelve elements ($\circ$) the terms appear with $(p,q) \in \{(1,2),(0,2)\}$. In six elements ($\bullet$) the terms appear with $(p,q) \in \{(2,0),(1,0),(0,0)\}$. In six elements ($\times$) the terms appear with $(p,q) \in \{(2,2),(1,2),(0,2)\}$. In four elements ($\oplus$) the terms appear with $(p,q) \in \{(3,0),(2,0),(1,0),(0,0)\}$. The final element ($\triangledown$) the terms appear with $(p,q)\{(4,0),(3,0),(2,0),(1,0),(0,0)\}$. Elements labelled with a '$\cdot$' are zero.

The quantity $\alpha(n) = \sqrt{k_F^2 - (\pi n/d)^2}$ is the radius of the (two-dimensional) Fermi circle for state n, given by Eq. (D.20). The Fermi wavenumber k_F obeys the relation $k_F > \pi n/d$, since the Fermi-Dirac distribution function is zero for $k_F < \pi n/d$, and thus in that case the integral would vanish.

B.2 Specific integrals to be solved

The necessary combinations of p and q in Eq. (B.2) to be calculated in order to solve the integrals over $\vec{\kappa}_{\parallel}$ in the nonlinear conductivity tensor are summarized in Fig. B.1. From Fig. B.1 we observe that a total of nine different combinations of p and q need to be calculated, namely when (p,q) takes the values $(0,0)$, $(0,2)$, $(0,4)$, $(1,0)$, $(1,2)$, $(2,0)$, $(2,2)$, $(3,0)$, or $(4,0)$, and it is seen from Eqs. (8.15)–(8.23) that β can take the values $\beta \in \{1,2,3\}$. However, the complexity of the total solution can be reduced, since functions with $\beta = 2$ can be expressed in terms of functions with $\beta = 1$ in the following

way

$$\mathcal{F}^2_{pq}(n,a_1,a_2,b_1,b_2,s) = \frac{a_1\,\mathcal{F}^1_{pq}(n,a_1,b_1,s) - a_2\,\mathcal{F}^1_{pq}(n,a_2,b_2,s)}{a_1b_2 - a_2b_1}, \tag{B.3}$$

$a_k \neq 0, k \in \{1,2\}$. In a similar fashion, the functions with $\beta = 3$ can be written in terms of functions with $\beta = 1$, namely

$$\mathcal{F}^3_{pq}(n,a_1,a_2,a_3,b_1,b_2,b_3,s) = \frac{a_1^2\,\mathcal{F}^1_{pq}(n,a_1,b_1,s)}{(a_2b_1 - b_2a_1)(a_3b_1 - b_3a_1)}$$
$$+ \frac{a_2^2\,\mathcal{F}^1_{pq}(n,a_2,b_2,s)}{(a_2b_1 - b_2a_1)(a_3b_2 - b_3a_2)} + \frac{a_3^2\,\mathcal{F}^1_{pq}(n,a_3,b_3,s)}{(a_3b_1 - b_3a_1)(a_3b_2 - b_3a_2)}, \tag{B.4}$$

provided $a_k \neq 0$, $k \in \{1,2,3\}$. If any a_k, for instance a_1, becomes zero, we observe from Eq. (B.2) that the order of the denominator becomes smaller by one. This implies in Eq. (B.3) that $\mathcal{F}^2_{pq}(n,0,a_2,b_1,b_2,s) = \mathcal{F}^1_{pq}(n,a_2,b_2,s)/b_1$. The similar conclusion with respect to Eq. (B.4) is $\mathcal{F}^3_{pq}(n,0,a_2,a_3,b_1,b_2,b_3,s) = \mathcal{F}^2_{pq}(n,a_2,a_3,b_2,b_3,s)/b_1$. A corresponding reduction applies for any other $a_k = 0$ in Eqs. (B.3) and (B.4).

As a consequence of Eqs. (B.3) and (B.4), the integrals appearing in Eqs. (8.15)–(8.23) can now be written in terms of functions of the type

$$\mathcal{F}^1_{pq}(n,a,b,s) = \int_0^{\alpha(n)} \int_0^{2\pi} \frac{r(r\cos\theta - s)^p (r\sin\theta)^q}{b - as + ar\cos\theta} d\theta dr, \tag{B.5}$$

dropping the now superfluous index on a and b. Since the following treatment is a formal solution of Eq. (B.5), we will also drop the reference to n for brevity, letting $\alpha \equiv \alpha(n)$.

B.3 Solution when $a = 0$

Before carrying on with the solution to Eq. (B.5) in the appropriate cases, we take a look at it in the case where $a = 0$ (as would be the case in the local limit, for example). Then the only term left in the denominator is b, which is constant with respect to the integration variables. The solution to the remaining thus becomes trivial, with the results

$$\mathcal{F}^1_{00}(n,0,b,s) = \frac{2}{b}\int_0^\alpha \int_0^\pi r\,d\theta dr = \frac{\pi\alpha^2}{b}, \tag{B.6}$$

$$\mathcal{F}^1_{02}(n,0,b,s) = \frac{2}{b}\int_0^\alpha \int_0^\pi r^3 \sin^2\theta\, d\theta dr = \frac{\pi\alpha^4}{4b}, \tag{B.7}$$

$$\mathcal{F}^1_{04}(n,0,b,s) = \frac{2}{b}\int_0^\alpha \int_0^\pi r^5 \sin^4\theta\, d\theta dr = \frac{\pi\alpha^6}{8b}, \tag{B.8}$$

$$\mathcal{F}^1_{10}(n,0,b,s) = \frac{2}{b}\int_0^\alpha \int_0^\pi \left[r^2\cos\theta - rs\right] d\theta dr = -\frac{\pi s\alpha^2}{b}, \tag{B.9}$$

$$\mathcal{F}^1_{12}(n,0,b,s) = \frac{2}{b}\int_0^\alpha \int_0^\pi \left[r^4\cos\theta\sin^2\theta - r^3 s\sin^2\theta\right] d\theta dr = -\frac{\pi s\alpha^4}{4b}, \tag{B.10}$$

$$\mathcal{F}_{20}^1(n,0,b,s) = \frac{2}{b} \int_0^\alpha \int_0^\pi \left[r^3 \cos^2\theta + rs^2 - 2sr^2 \cos\theta \right] d\theta dr = \frac{\pi\alpha^4}{4b} + \frac{\pi s^2 \alpha^2}{b}, \quad \text{(B.11)}$$

$$\mathcal{F}_{22}^1(n,0,b,s) = \frac{2}{b} \int_0^\alpha \int_0^\pi \left[r^5 \cos^2\theta \sin^2\theta + r^3 s^2 \sin^2\theta - 2r^4 s \cos\theta \sin^2\theta \right] d\theta dr$$

$$= \frac{\pi\alpha^6}{24b} + \frac{\pi s^2 \alpha^4}{4b}, \tag{B.12}$$

$$\mathcal{F}_{30}^1(n,0,b,s) = \frac{2}{b} \int_0^\alpha \int_0^\pi \left[r^4 \cos^3\theta - 3r^3 s \cos^2\theta + 3r^2 s^2 \cos\theta - rs^3 \right] d\theta dr$$

$$= -\frac{3\pi s\alpha^4}{4b} - \frac{\pi s^3 \alpha^2}{b}, \tag{B.13}$$

$$\mathcal{F}_{40}^1(n,0,b,s) = \frac{2}{b} \int_0^\alpha \int_0^\pi \left[r^5 \cos^4\theta - 4r^4 s \cos^3\theta + 6r^3 s^2 \cos^2\theta - 4r^2 s^3 \cos\theta \right.$$

$$\left. + rs^4 \right] d\theta dr = \frac{\pi\alpha^6}{8b} + \frac{3\pi s^2 \alpha^4}{2b} + \frac{\pi s^4 \alpha^2}{b}, \tag{B.14}$$

where we have made use of the facts that (i) q is an even integer, and (ii) $\cos\theta$ and $\sin^2\theta$ are symmetric around $\theta = \pi$ in solving the angular integrals.

B.4 General solution

When $a \neq 0$, we have to consider the full solution to Eq. (B.5) for the nine different combinations of p and q we need. To solve Eq. (B.5), let us make the substitutions

$$\eta \equiv \frac{b - as}{a\alpha}, \quad r \equiv \alpha u, \tag{B.15}$$

giving $dr = \alpha du$. Thereby Eq. (B.5) is turned into the nine functions

$$\mathcal{F}_{00}^1(n,a,b,s) = \frac{\alpha}{a} \int_0^1 \int_0^{2\pi} \frac{u}{\eta + u\cos\theta} d\theta du, \tag{B.16}$$

$$\mathcal{F}_{02}^1(n,a,b,s) = \frac{\alpha^3}{a} \int_0^1 \int_0^{2\pi} \left[\frac{u^3}{\eta + u\cos\theta} - \frac{u^3 \cos^2\theta}{\eta + u\cos\theta} \right] d\theta du, \tag{B.17}$$

$$\mathcal{F}_{04}^1(n,a,b,s) = \frac{\alpha^5}{a} \int_0^1 \int_0^{2\pi} \left[\frac{u^5}{\eta + u\cos\theta} - \frac{2u^5 \cos^2\theta}{\eta + u\cos\theta} + \frac{u^5 \cos^4\theta}{\eta + u\cos\theta} \right] d\theta du, \tag{B.18}$$

$$\mathcal{F}_{10}^1(n,a,b,s) = \frac{\alpha^2}{a} \int_0^1 \int_0^{2\pi} \left[\frac{u^2 \cos\theta}{\eta + u\cos\theta} - \frac{s}{\alpha} \frac{u}{\eta + u\cos\theta} \right] d\theta du, \tag{B.19}$$

$$\mathcal{F}_{12}^1(n,a,b,s) = \frac{\alpha^4}{a} \int_0^1 \int_0^{2\pi} \left[\frac{u^4 \cos\theta}{\eta + u\cos\theta} - \frac{u^4 \cos^3\theta}{\eta + u\cos\theta} - \frac{s}{\alpha} \frac{u^3}{\eta + u\cos\theta} \right.$$

$$\left. + \frac{s}{\alpha} \frac{u^3 \cos^2\theta}{\eta + u\cos\theta} \right] d\theta du, \tag{B.20}$$

$$\mathcal{F}_{20}^1(n,a,b,s) = \frac{\alpha^3}{a} \int_0^1 \int_0^{2\pi} \left[\frac{u^3 \cos^2\theta}{\eta + u\cos\theta} - \frac{2s}{\alpha} \frac{u^2 \cos\theta}{\eta + u\cos\theta} + \frac{s^2}{\alpha^2} \frac{u}{\eta + u\cos\theta} \right] d\theta du,$$

$$\mathcal{F}_{22}^1(n,a,b,s) = \frac{\alpha^5}{a}\int_0^1\int_0^{2\pi}\left[\frac{u^5\cos^2\theta}{\eta+u\cos\theta} - \frac{u^5\cos^4\theta}{\eta+u\cos\theta} - \frac{2s}{\alpha}\frac{u^4\cos\theta}{\eta+u\cos\theta}\right.$$

$$\left. + \frac{2s}{\alpha}\frac{u^4\cos^3\theta}{\eta+u\cos\theta} + \frac{s^2}{\alpha^2}\frac{u^3}{\eta+u\cos\theta} - \frac{s^2}{\alpha^2}\frac{u^3\cos^2\theta}{\eta+u\cos\theta}\right]d\theta du, \tag{B.22}$$

$$\mathcal{F}_{30}^1(n,a,b,s) = \frac{\alpha^4}{a}\int_0^1\int_0^{2\pi}\left[\frac{u^4\cos^3\theta}{\eta+u\cos\theta} - \frac{3s}{\alpha}\frac{u^3\cos^2\theta}{\eta+u\cos\theta} + \frac{3s^2}{\alpha^2}\frac{u^2\cos\theta}{\eta+u\cos\theta}\right.$$

$$\left. - \frac{s^3}{\alpha^3}\frac{u}{\eta+u\cos\theta}\right]d\theta du, \tag{B.23}$$

$$\mathcal{F}_{40}^1(n,a,b,s) = \frac{\alpha^5}{a}\int_0^1\int_0^{2\pi}\left[\frac{u^5\cos^4\theta}{\eta+u\cos\theta} - \frac{4s}{\alpha}\frac{u^4\cos^3\theta}{\eta+u\cos\theta} + \frac{6s^2}{\alpha^2}\frac{u^3\cos^2\theta}{\eta+u\cos\theta}\right.$$

$$\left. - \frac{4s^3}{\alpha^3}\frac{u^2\cos\theta}{\eta+u\cos\theta} + \frac{s^4}{\alpha^4}\frac{u}{\eta+u\cos\theta}\right]d\theta du, \tag{B.24}$$

where we have made use of the relations

$$\sin^2\theta = 1 - \cos^2\theta, \tag{B.25}$$

$$\cos\theta\sin^2\theta = \cos\theta - \cos^3\theta, \tag{B.26}$$

$$\cos^2\theta\sin^2\theta = \cos^2\theta - \cos^4\theta, \tag{B.27}$$

$$\sin^4\theta = 1 - 2\cos^2\theta + \cos^4\theta. \tag{B.28}$$

B.4.1 Solution to the angular integrals

Next, to carry out the angular integrals, we put

$$t = e^{i\theta} \tag{B.29}$$

so that these integrals become

$$\int_0^{2\pi}\frac{\cos^h\theta}{\eta+u\cos\theta}d\theta = \frac{1}{2^h iu}\oint\frac{(1+t^2)^h}{t^h(t-t_+)(t-t_-)}dt, \tag{B.30}$$

where $h \in \{0,1,2,3,4\}$. In Eq. (B.30), the poles at $t_{\pm}$ in the t-plane are located at

$$t_{\pm} = -\frac{\eta}{u} \pm \sqrt{\left(\frac{\eta}{u}\right)^2 - 1}, \tag{B.31}$$

and the integration runs along the unit circle. Since we have $t_+ t_- = 1$, one of these poles is inside the unit circle while the other is outside. When $h > 0$ there are an additional pole of order h at $t = 0$. Using the unit circles shown in Fig. B.2 as the integration paths,
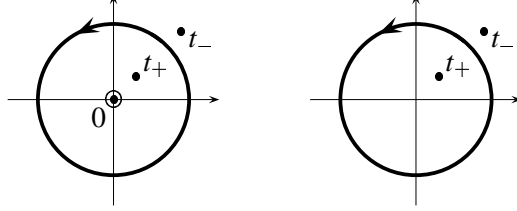
Figure B.2: The poles appearing in the complex t-plane in Eq. (B.30) are of order 1 at $t_\pm$ and of order h at $t = 0$, as shown to the left. To the right is shown the special case where $h = 0$ and the pole at $t = 0$ vanishes. The closed contour shown in each diagram is the integration path used.

we find by a residue calculation

$$\int_0^{2\pi} \frac{1}{\eta + u\cos\theta} d\theta = \frac{2\pi}{\sqrt{\eta^2 - u^2}}, \tag{B.32}$$

$$\int_0^{2\pi} \frac{\cos\theta}{\eta + u\cos\theta} d\theta = \frac{2\pi}{u}\left[1 - \frac{\eta}{\sqrt{\eta^2 - u^2}}\right], \tag{B.33}$$

$$\int_0^{2\pi} \frac{\cos^2\theta}{\eta + u\cos\theta} d\theta = \frac{2\pi\eta}{u^2}\left[\frac{\eta}{\sqrt{\eta^2 - u^2}} - 1\right], \tag{B.34}$$

$$\int_0^{2\pi} \frac{\cos^3\theta}{\eta + u\cos\theta} d\theta = \frac{\pi}{u} + \frac{2\pi\eta^2}{u^3}\left[1 - \frac{\eta}{\sqrt{\eta^2 - u^2}}\right], \tag{B.35}$$

$$\int_0^{2\pi} \frac{\cos^4\theta}{\eta + u\cos\theta} d\theta = \frac{2\pi\eta^3}{u^4}\left[\frac{\eta}{\sqrt{\eta^2 - u^2}} - 1\right] - \frac{\pi\eta}{u^2}. \tag{B.36}$$

Inserting these results into Eqs. (B.16)–(B.17), we get

$$\mathcal{F}_{00}^1(n,a,b,s) = \frac{2\pi\alpha}{a}\int_0^1 \frac{u}{\sqrt{\eta^2 - u^2}} du, \tag{B.37}$$

$$\mathcal{F}_{02}^1(n,a,b,s) = \frac{2\pi\alpha^3}{a}\int_0^1 \left[\frac{u^3}{\sqrt{\eta^2 - u^2}} - \frac{\eta^2 u}{\sqrt{\eta^2 - u^2}} + \eta u\right] du, \tag{B.38}$$

$$\mathcal{F}_{04}^1(n,a,b,s) = \frac{\pi\alpha^5}{a}\int_0^1 \left[\frac{2u^5}{\sqrt{\eta^2 - u^2}} - \frac{4\eta^2 u^3}{\sqrt{\eta^2 - u^2}} + \frac{2\eta^4 u}{\sqrt{\eta^2 - u^2}} + 3\eta u^3 - 2\eta^3 u\right] du, \tag{B.39}$$

$$\mathcal{F}_{10}^1(n,a,b,s) = \frac{2\pi\alpha^2}{a}\int_0^1 \left[u - \left(\eta + \frac{s}{\alpha}\right)\frac{u}{\sqrt{\eta^2 - u^2}}\right] du, \tag{B.40}$$

$$\mathcal{F}_{12}^1(n,a,b,s) = \frac{\pi\alpha^4}{a}\int_0^1 \left[u^3 - \left(2\eta^2 + \frac{2s\eta}{\alpha}\right)u - \left(2\eta + \frac{2s}{\alpha}\right)\frac{u^3}{\sqrt{\eta^2 - u^2}}\right]$$

$$+ \left(2\eta^3 + \frac{2s\eta^2}{\alpha}\right) \frac{u}{\sqrt{\eta^2 - u^2}}\right] du, \tag{B.41}$$

$$\mathcal{F}_{20}^1(n,a,b,s) = \frac{2\pi\alpha^3}{a} \int_0^1 \left[\left(\eta^2 + \frac{2s\eta}{\alpha} + \frac{s^2}{\alpha^2}\right) \frac{u}{\sqrt{\eta^2 - u^2}} - \left(\eta + \frac{2s}{\alpha}\right) u\right] du, \tag{B.42}$$

$$\mathcal{F}_{22}^1(n,a,b,s) = \frac{\pi\alpha^5}{a} \int_0^1 \left[\left(2\eta^2 + \frac{4\eta s}{\alpha} + \frac{2s^2}{\alpha^2}\right) \frac{u^3}{\sqrt{\eta^2 - u^2}} - \left(\eta + \frac{2s}{\alpha}\right) u^3\right.$$

$$\left. - \left(2\eta^4 + \frac{4\eta^3 s}{\alpha} + \frac{2\eta^2 s^2}{\alpha^2}\right) \frac{u}{\sqrt{\eta^2 - u^2}} + \left(2\eta^3 + \frac{4s\eta^2}{\alpha} + \frac{2s^2\eta}{\alpha^2}\right) u\right] du, \tag{B.43}$$

$$\mathcal{F}_{30}^1(n,a,b,s) = \frac{\pi\alpha^4}{a} \int_0^1 \left[u^3 + \left(2\eta^2 + \frac{6s\eta}{\alpha} + \frac{6s^2}{\alpha^2}\right) u\right.$$

$$\left. - \left(2\eta^3 + \frac{6s\eta^2}{\alpha} + \frac{6s^2\eta}{\alpha^2} + \frac{2s^3}{\alpha^3}\right) \frac{u}{\sqrt{\eta^2 - u^2}}\right] du, \tag{B.44}$$

$$\mathcal{F}_{40}^1(n,a,b,s) = \frac{\pi\alpha^5}{a} \int_0^1 \left[\left(2\eta^4 + \frac{8s\eta^3}{\alpha} + \frac{12s^2\eta^2}{\alpha^2} + \frac{8s^3\eta}{\alpha^3} + \frac{2s^4}{\alpha^4}\right) \frac{u}{\sqrt{\eta^2 - u^2}}\right.$$

$$\left. - \left(\eta + \frac{4s}{\alpha}\right) u^3 - \left(2\eta^3 + \frac{8s\eta^2}{\alpha} + \frac{12s^2\eta}{\alpha^2} + \frac{8s^3}{\alpha^3}\right) u\right] du. \tag{B.45}$$

B.4.2 Solution to the radial integrals

This result leaves us with radial integrals of the type

$$\int_0^1 \frac{u^h}{\sqrt{\eta^2 - u^2}} du, \qquad h \in \{1,3,5\}, \tag{B.46}$$

apart from the trivial u^n-type of integrals. The three integrals in Eq. (B.46) can be found for example in Gradshteyn and Ryzhik (1994) as Eqs. (2.271.7), (2.272.7), and (2.273.8), which by insertion of u and η becomes

$$\int \frac{u}{\sqrt{\eta^2 - u^2}} du = -\sqrt{\eta^2 - u^2}, \tag{B.47}$$

$$\int \frac{u^3}{\sqrt{\eta^2 - u^2}} du = -\frac{1}{3}\left[u^2 + 2\eta^2\right]\sqrt{\eta^2 - u^2}, \tag{B.48}$$

$$\int \frac{u^5}{\sqrt{\eta^2 - u^2}} du = -\frac{1}{15}\left[3u^4 + 8\eta^4 + 4u^2\eta^2\right]\sqrt{\eta^2 - u^2}, \tag{B.49}$$

in that order, verified by differentiation, and after correction of the misprint appearing in Eq. (2.273.8). By insertion of the limits we get

$$\int_0^1 \frac{u}{\sqrt{\eta^2 - u^2}} du = \eta - \sqrt{\eta^2 - 1}, \tag{B.50}$$

$$\int_0^1 \frac{u^3}{\sqrt{\eta^2 - u^2}} du = \frac{2\eta^3}{3} - \frac{1 + 2\eta^2}{3}\sqrt{\eta^2 - 1}, \tag{B.51}$$

$$\int_0^1 \frac{u^5}{\sqrt{\eta^2 - u^2}} du = \frac{8}{15}\eta^5 - \frac{1}{15}\left[3 + 8\eta^4 + 4\eta^2\right]\sqrt{\eta^2 - 1}. \tag{B.52}$$

By insertion of Eqs. (B.50)–(B.52) into Eqs. (B.37)–(B.45) and solving the trivial u^n-type of integrals, the resulting expressions for the nine different cases of Eq. (B.5) thus become

$$\mathcal{F}_{00}^1(n,a,b,s) = \frac{2\pi\alpha}{a}\left[\eta - \sqrt{\eta^2 - 1}\right], \tag{B.53}$$

$$\mathcal{F}_{02}^1(n,a,b,s) = \frac{2\pi\alpha^3}{a}\left[\frac{\eta^2 - 1}{3}\sqrt{\eta^2 - 1} - \frac{\eta^3}{3} + \frac{\eta}{2}\right], \tag{B.54}$$

$$\mathcal{F}_{04}^1(n,a,b,s) = \frac{\pi\alpha^5}{a}\left[\left(\frac{4}{5}\eta^2 - \frac{2}{5}\eta^4 - \frac{2}{5}\right)\sqrt{\eta^2 - 1} + \frac{2}{5}\eta^5 - \eta^3 + \frac{3}{4}\eta\right] \tag{B.55}$$

$$\mathcal{F}_{10}^1(n,a,b,s) = \frac{2\pi\alpha^2}{a}\left[\frac{1}{2} - \left(\eta + \frac{s}{\alpha}\right)\left(\eta - \sqrt{\eta^2 - 1}\right)\right], \tag{B.56}$$

$$\mathcal{F}_{12}^1(n,a,b,s) = \frac{\pi\alpha^4}{a}\left[\left(\frac{2s}{3\alpha} + \frac{2}{3}\eta - \frac{2s}{3\alpha}\eta^2 - \frac{2}{3}\eta^3\right)\sqrt{\eta^2 - 1} + \frac{2}{3}\eta^4 + \frac{2s}{3\alpha}\eta^3\right.$$
$$\left. - \eta^2 - \frac{s}{\alpha}\eta + \frac{1}{4}\right], \tag{B.57}$$

$$\mathcal{F}_{20}^1(n,a,b,s) = \frac{2\pi\alpha^3}{a}\left[\left(\eta^2 + \frac{2s\eta}{\alpha} + \frac{s^2}{\alpha^2}\right)\left(\eta - \sqrt{\eta^2 - 1}\right) - \frac{1}{2}\left(\eta + \frac{2s}{\alpha}\right)\right], \tag{B.58}$$

$$\mathcal{F}_{22}^1(n,a,b,s) = \frac{\pi\alpha^5}{a}\left[\left(\frac{2}{3}\eta^4 + \frac{4s}{3\alpha}\eta^3 + \left(\frac{2s^2}{3\alpha^2} - \frac{2}{3}\right)\eta^2 - \frac{4s}{3\alpha}\eta - \frac{2s^2}{3\alpha^2}\right)\sqrt{\eta^2 - 1}\right.$$
$$\left. - \frac{2}{3}\eta^5 - \frac{4s}{3\alpha}\eta^4 + \left(1 - \frac{2s^2}{3\alpha^2}\right)\eta^3 + \frac{2s}{\alpha}\eta^2 + \left(\frac{s^2}{\alpha^2} - \frac{1}{4}\right)\eta - \frac{s}{2\alpha}\right], \tag{B.59}$$

$$\mathcal{F}_{30}^1(n,a,b,s) = \frac{\pi\alpha^4}{a}\left[\frac{1}{4} + \frac{1}{2}\left(2\eta^2 + \frac{6s\eta}{\alpha} + \frac{6s^2}{\alpha^2}\right)\right.$$
$$\left. - \left(2\eta^3 + \frac{6s\eta^2}{\alpha} + \frac{6s^2\eta}{\alpha^2} + \frac{2s^3}{\alpha^3}\right)\left(\eta - \sqrt{\eta^2 - 1}\right)\right], \tag{B.60}$$

$$\mathcal{F}_{40}^1(n,a,b,s) = \frac{\pi\alpha^5}{a}\left[\left(2\eta^4 + \frac{8s\eta^3}{\alpha} + \frac{12s^2\eta^2}{\alpha^2} + \frac{8s^3\eta}{\alpha^3} + \frac{2s^4}{\alpha^4}\right)\left(\eta - \sqrt{\eta^2 - 1}\right)\right.$$
$$\left. - \frac{1}{4}\left(\eta + \frac{4s}{\alpha}\right) - \frac{1}{2}\left(2\eta^3 + \frac{8s\eta^2}{\alpha} + \frac{12s^2\eta}{\alpha^2} + \frac{8s^3}{\alpha^3}\right)\right]. \tag{B.61}$$

B.5 Verification

In order to verify the result, we take the limit where $a \to 0$, we use the binomial series expansion

$$
\sqrt{\eta^2 - 1} = \eta - \frac{1}{2\eta} - \sum_{n=2}^{\infty} \frac{(2n-3)!!}{(2n)!!\eta^{2n-1}}
$$

$$
= \eta - \frac{1}{2\eta} - \frac{1}{8\eta^3} - \frac{1}{16\eta^5} - \frac{5}{128\eta^7} - \frac{7}{256\eta^9} - \frac{21}{1024\eta^{11}} - \frac{33}{2048\eta^{13}}
$$

$$
- \frac{429}{32768\eta^{15}} - \frac{715}{65536\eta^{17}} - \cdots, \tag{B.62}
$$

where '$x!!$' is the 'double factorial' operator taken for the integer x, given by $x!! \equiv x(x-2)(x-4)\cdots(x-k)$ for $x > k$. Thus by insertion of Eq. (B.62) into Eqs. (B.53)–(B.61) we get for small values of a

$$
\mathcal{F}_{00}^1(n,a,b,s) = \frac{2\pi\alpha}{a} \left[\frac{1}{2\eta} + \frac{1}{8\eta^3} + \frac{1}{16\eta^5} + \frac{5}{128\eta^7} + \cdots \right], \tag{B.63}
$$

$$
\mathcal{F}_{02}^1(n,a,b,s) = \frac{2\pi\alpha^3}{a} \left[\frac{1}{8\eta} + \frac{1}{48\eta^3} + \frac{3}{384\eta^5} + \frac{3}{768\eta^7} + \cdots \right], \tag{B.64}
$$

$$
\mathcal{F}_{04}^1(n,a,b,s) = \frac{\pi\alpha^5}{a} \left[\frac{1}{8\eta} + \frac{1}{320\eta^3} + \frac{19}{640\eta^5} + \frac{21}{2560\eta^7} + \cdots \right] \tag{B.65}
$$

$$
\mathcal{F}_{10}^1(n,a,b,s) = -\frac{2\pi\alpha^2}{a} \left[\frac{s}{2\alpha\eta} + \frac{1}{8\eta^2} + \frac{s}{8\alpha\eta^3} + \frac{1}{16\eta^4} + \cdots \right], \tag{B.66}
$$

$$
\mathcal{F}_{12}^1(n,a,b,s) = -\frac{\pi\alpha^4}{a} \left[\frac{s}{4\alpha\eta} + \frac{1}{24\eta^2} + \frac{s}{24\alpha\eta^3} + \frac{3}{192\eta^4} + \cdots \right], \tag{B.67}
$$

$$
\mathcal{F}_{20}^1(n,a,b,s) = \frac{2\pi\alpha^3}{a} \left[\left(\frac{s^2}{2\alpha^2} + \frac{1}{8} \right) \frac{1}{\eta} + \frac{s}{4\alpha\eta^2} + \left(\frac{s^2}{8\alpha^2} + \frac{1}{16} \right) \frac{1}{\eta^3} + \frac{s}{8\alpha\eta^4} + \cdots \right], \tag{B.68}
$$

$$
\mathcal{F}_{22}^1(n,a,b,s) = \frac{\pi\alpha^5}{a} \left[\left(\frac{s^2}{4\alpha^2} + \frac{1}{24} \right) \frac{1}{\eta} + \frac{s}{12\alpha\eta^2} + \left(\frac{s^2}{24\alpha^2} + \frac{7}{192} \right) \frac{1}{\eta^3} + \frac{7s}{96\alpha\eta^4} + \cdots \right], \tag{B.69}
$$

$$
\mathcal{F}_{30}^1(n,a,b,s) = -\frac{\pi\alpha^4}{a} \left[\left(\frac{s^3}{\alpha^3} + \frac{3s}{4\alpha} \right) \frac{1}{\eta} + \left(\frac{3s^2}{4\alpha^2} + \frac{1}{8} \right) \frac{1}{\eta^2} + \left(\frac{s^3}{4\alpha^3} + \frac{3s}{8\alpha} \right) \frac{1}{\eta^3} \right.
$$

$$
\left. + \left(\frac{3s^2}{8\alpha^2} + \frac{5}{64} \right) \frac{1}{\eta^4} + \cdots \right], \tag{B.70}
$$

$$
\mathcal{F}_{40}^1(n,a,b,s) = \frac{\pi\alpha^5}{a} \left[\left(\frac{s^4}{\alpha^4} + \frac{3s^2}{2\alpha^2} + \frac{1}{8} \right) \frac{1}{\eta} + \left(\frac{s^3}{\alpha^3} + \frac{s}{2\alpha} \right) \frac{1}{\eta^2} \right.
$$

$$
\left. + \left(\frac{s^4}{4\alpha^4} + \frac{3s^2}{4\alpha^2} + \frac{5}{64} \right) \frac{1}{\eta^3} + \left(\frac{s^3}{2\alpha^3} + \frac{5s}{16\alpha} \right) \frac{1}{\eta^4} + \cdots \right], \tag{B.71}
$$

which by insertion of $\eta = (b - as)/(a\alpha)$ and subsequently letting $a = 0$ reduces to the results of Eqs. (B.6)–(B.14).

B.6 Result

In terms of the original a and b quantities, the resulting expressions for the specific integrals are:

$$\mathcal{F}_{00}^{1}(n,a,b,s) = \frac{2\pi}{a^2}\left[b - as - \sqrt{(b-as)^2 - a^2\alpha^2}\,\right],\tag{B.72}$$

$$\mathcal{F}_{02}^{1}(n,a,b,s) = \frac{2\pi}{3a^4}\left[\left((b-as)^2 - \alpha^2 a^2\right)^{\frac{3}{2}} - (b-as)^3 + \frac{3}{2}\alpha^2 a^2(b-as)\right].\tag{B.73}$$

$$\mathcal{F}_{04}^{1}(n,a,b,s) = \frac{2\pi}{5a^6}\left[(b-as)^5 - \frac{5}{2}a^2\alpha^2(b-as)^3 + \frac{15}{8}a^4\alpha^4(b-as)\right.$$
$$\left. - \left((b-as)^2 - a^2\alpha^2\right)^{\frac{5}{2}}\right]\tag{B.74}$$

$$\mathcal{F}_{10}^{1}(n,a,b,s) = \frac{2\pi\alpha^2}{a}\left[\frac{1}{2} - \frac{b}{a^2\alpha^2}\left(b - as - \sqrt{(b-as)^2 - a^2\alpha^2}\right)\right],\tag{B.75}$$

$$\mathcal{F}_{12}^{1}(n,a,b,s) = \frac{\pi}{a^5}\left[\frac{1}{4}a^4\alpha^4 - b\left(a^2\alpha^2(b-as) - 2(b-as)^2\right)\right.$$
$$\left. - \frac{2b}{3}\left((b-as)^2 - a^2\alpha^2\right)^{\frac{3}{2}}\right]\tag{B.76}$$

$$\mathcal{F}_{20}^{1}(n,a,b,s) = \frac{2\pi}{a^4}\left[b^2\left(b - as - \sqrt{(b-as)^2 - a^2\alpha^2}\right) - \frac{1}{2}a^2\alpha^2(b+as)\right],\tag{B.77}$$

$$\mathcal{F}_{22}^{1}(n,a,b,s) = \frac{2\pi}{3a^6}\left[b^2\left(6a^2\alpha^2(b-as) - 4a\alpha(b-as)^3 + \left((b-as)^2 - a^2\alpha^2\right)^{\frac{3}{2}}\right)\right.$$
$$\left. - \frac{3}{8}a^4\alpha^4(b+as)\right]\tag{B.78}$$

$$\mathcal{F}_{30}^{1}(n,a,b,s) = \frac{\pi\alpha^4}{a}\left[\frac{1}{4} + \frac{(b+as)^2}{a^2\alpha^2} - \frac{2b^3}{a^4\alpha^4}\left(b - as - \sqrt{(b-as)^2 - a^2\alpha^2}\right)\right],\tag{B.79}$$

$$\mathcal{F}_{40}^{1}(n,a,b,s) = \frac{\pi\alpha^5}{a}\left[\frac{2b^4}{a^5\alpha^5}\left(b - as - \sqrt{(b-as)^2 - a^2\alpha^2}\right) - \frac{b}{4a\alpha} - \frac{b^3}{a^3\alpha^3}\right.$$
$$\left. - \frac{s}{\alpha}\left(\frac{3}{4} + \frac{(b+as)^2}{a^2\alpha^2}\right)\right].\tag{B.80}$$

Using Eqs. (B.72)–(B.80) together with Eqs. (B.3) and (B.4) when they are needed, the solution to the integrals appearing in Eqs. (8.15)–(8.23), (10.5), (10.6), (10.13), and (14.11)–(14.14) are obtained in a straightforward manner. They can be found on detailed form in Appendix C.

Appendix C

Analytic solution to the integrals over $\vec{\kappa}_\parallel$ appearing in the conductivity tensors when scattering takes place in the x-z-plane

Taking a close look at the expressions for the different nonlinear conductivity tensor parts in Eqs. (8.17)–(8.23) we observe by insertion of the transition current density given by Eq. (8.14) that they can be separated into two independent parts. One of these parts depends solely on $\vec{\kappa}_\parallel$ and the other part depends only on z. In the remaining of this Appendix they will be denoted by ξ and $\mathcal{Z}$, respectively. The quantity ξ can be solved according to the solution scheme given in Appendix B, and the explicit solution will therefore in the following be given in terms of the functions solved in Appendix B. Furthermore it is possible to split the z-dependent part into independent functions of each z-coordinate. Since the z-dependence involves only the wave functions, we define the following three new quantities

$$\mathcal{Z}^x_{nm}(z) = \mathcal{Z}^y_{nm}(z) = \psi^*_m(z)\psi_n(z), \tag{C.1}$$

$$\mathcal{Z}^z_{nm}(z) = \psi^*_m(z)\frac{\partial \psi_n(z)}{\partial z} - \psi_n(z)\frac{\partial \psi^*_m(z)}{\partial z}, \tag{C.2}$$

in order to reduce the expressions in the following.

As the first step in preparing the solutions to the integrals over $\vec{\kappa}_\parallel$ we identify the transition frequencies occuring in the nonlinear conductivity tensor parts. Each of these transition frequencies can on general form be written

$$\omega_{nm}(\vec{\kappa}_\parallel + \vec{\beta}, \vec{\kappa}_\parallel + \vec{\gamma}) = \frac{1}{\hbar}\left[\varepsilon_n - \varepsilon_m + \frac{\hbar^2}{2m_e}\left(2\kappa_x(\beta_x - \gamma_x) + \beta_x^2 - \gamma_x^2\right)\right]. \tag{C.3}$$

Looking at Eqs. (8.17)–(8.23), we observe that the following transition frequencies appear in the nonlinear conductivity tensor:

$$\omega_{nm}(\vec{\kappa}_\parallel, \vec{\kappa}_\parallel) = \omega_{nm}(\vec{\kappa}_\parallel + \vec{q}_\parallel, \vec{\kappa}_\parallel + \vec{q}_\parallel) = \frac{1}{\hbar}\left[\varepsilon_n - \varepsilon_m\right], \tag{C.4}$$

$$\omega_{nm}(\vec{\kappa}_\parallel + \vec{k}_\parallel, \vec{\kappa}_\parallel) = \frac{1}{\hbar}\left[\varepsilon_n - \varepsilon_m + \frac{\hbar^2 k_x}{2m_e}\left(2\kappa_x + k_x\right)\right], \tag{C.5}$$

$$\omega_{nm}(\vec{\kappa}_\parallel, \vec{\kappa}_\parallel + \vec{k}_\parallel) = \frac{1}{\hbar}\left[\varepsilon_n - \varepsilon_m - \frac{\hbar^2 k_x}{2m_e}\left(2\kappa_x + k_x\right)\right], \tag{C.6}$$

$$\omega_{nm}(\vec{\kappa}_\parallel - \vec{k}_\parallel, \vec{\kappa}_\parallel) = \frac{1}{\hbar}\left[\varepsilon_n - \varepsilon_m + \frac{\hbar^2 k_x}{2m_e}\left(k_x - 2\kappa_x\right)\right], \tag{C.7}$$

$$\omega_{nm}(\vec{\kappa}_\parallel, \vec{\kappa}_\parallel - \vec{k}_\parallel) = \frac{1}{\hbar}\left[\varepsilon_n - \varepsilon_m + \frac{\hbar^2 k_x}{2m_e}\left(2\kappa_x - k_x\right)\right],\tag{C.8}$$

$$\omega_{nm}(\vec{\kappa}_\parallel + \vec{q}_\parallel, \vec{\kappa}_\parallel) = \frac{1}{\hbar}\left[\varepsilon_n - \varepsilon_m + \frac{\hbar^2 q_x}{2m_e}\left(2\kappa_x + q_x\right)\right],\tag{C.9}$$

$$\omega_{nm}(\vec{\kappa}_\parallel + \vec{q}_\parallel, \vec{\kappa}_\parallel + \vec{k}_\parallel) = \frac{1}{\hbar}\left[\varepsilon_n - \varepsilon_m + \frac{\hbar^2}{2m_e}\left(2\kappa_x(q_x - k_x) + q_x^2 - k_x^2\right)\right],\tag{C.10}$$

$$\omega_{nm}(\vec{\kappa}_\parallel + \vec{q}_\parallel, \vec{\kappa}_\parallel - \vec{k}_\parallel) = \frac{1}{\hbar}\left[\varepsilon_n - \varepsilon_m + \frac{\hbar^2}{2m_e}\left(2\kappa_x(q_x + k_x) + q_x^2 - k_x^2\right)\right],\tag{C.11}$$

$$\omega_{nm}(\vec{\kappa}_\parallel - \vec{k}_\parallel + \vec{q}_\parallel, \vec{\kappa}_\parallel) = \frac{1}{\hbar}\left[\varepsilon_n - \varepsilon_m + \frac{\hbar^2}{2m_e}(q_x - k_x)\left(2\kappa_x + (q_x - k_x)\right)\right],\tag{C.12}$$

$$\omega_{nm}(\vec{\kappa}_\parallel + \vec{k}_\parallel + \vec{q}_\parallel, \vec{\kappa}_\parallel) = \frac{1}{\hbar}\left[\varepsilon_n - \varepsilon_m + \frac{\hbar^2}{2m_e}(q_x + k_x)\left(2\kappa_x + (q_x + k_x)\right)\right],\tag{C.13}$$

$$\omega_{nm}(\vec{\kappa}_\parallel + \vec{k}_\parallel + \vec{q}_\parallel, \vec{\kappa}_\parallel + \vec{k}_\parallel) = \frac{1}{\hbar}\left[\varepsilon_n - \varepsilon_m + \frac{\hbar^2 q_x}{2m_e}\left(2\kappa_x + q_x + 2k_x\right)\right],\tag{C.14}$$

$$\omega_{nm}(\vec{\kappa}_\parallel + \vec{k}_\parallel + \vec{q}_\parallel, \vec{\kappa}_\parallel + \vec{q}_\parallel) = \frac{1}{\hbar}\left[\varepsilon_n - \varepsilon_m + \frac{\hbar^2 k_x}{2m_e}\left(2\kappa_x + k_x + 2q_x\right)\right],\tag{C.15}$$

$$\omega_{nm}(\vec{\kappa}_\parallel + \vec{q}_\parallel, \vec{\kappa}_\parallel - \vec{k}_\parallel + \vec{q}_\parallel) = \frac{1}{\hbar}\left[\varepsilon_n - \varepsilon_m + \frac{\hbar^2 k_x}{2m_e}\left(2\kappa_x + 2q_x - k_x\right)\right],\tag{C.16}$$

$$\omega_{nm}(\vec{\kappa}_\parallel - \vec{k}_\parallel + \vec{q}_\parallel, \vec{\kappa}_\parallel - \vec{k}_\parallel) = \frac{1}{\hbar}\left[\varepsilon_n - \varepsilon_m + \frac{\hbar^2 q_x}{2m_e}\left(2\kappa_x + q_x - 2k_x\right)\right],\tag{C.17}$$

$$\omega_{nm}(\vec{\kappa}_\parallel - \vec{k}_\parallel + \vec{q}_\parallel, \vec{\kappa}_\parallel + \vec{q}_\parallel) = \frac{1}{\hbar}\left[\varepsilon_n - \varepsilon_m + \frac{\hbar^2 k_x}{2m_e}\left(k_x - 2q_x - 2\kappa_x\right)\right].\tag{C.18}$$

We observe from Eqs. (8.17)–(8.23) that these transition frequencies gives rise to a number of different a and b coefficients, which we will use in the later sections of this Appendix. It turns out that there are a total of four different a's and thirteen different b's. To present an overview and for the sake of easy reference they are all listed together below, viz.

$$a_1 = \frac{\hbar k_x}{m_e},\tag{C.19}$$

$$a_2 = \frac{\hbar q_x}{m_e},\tag{C.20}$$

$$a_3 = \frac{\hbar}{m_e}(q_x + k_x),\tag{C.21}$$

$$a_4 = \frac{\hbar}{m_e}(q_x - k_x),\tag{C.22}$$

$$b_{nm}^1 = \frac{1}{\hbar}(\varepsilon_n - \varepsilon_m) + \frac{\hbar k_x^2}{2m_e} - \omega - i\tau_{nm}^{-1},\tag{C.23}$$

$$b_{nm}^2 = \frac{1}{\hbar}(\varepsilon_n - \varepsilon_m) - \frac{\hbar k_x^2}{2m_e} - \omega - i\tau_{nm}^{-1},\tag{C.24}$$

$$b_{nm}^3 = \frac{1}{\hbar}(\varepsilon_n - \varepsilon_m) + \frac{\hbar q_x^2}{2m_e} + \omega - i\tau_{nm}^{-1},$$

(C.25)

$$b_{nm}^4 = \frac{1}{\hbar}(\varepsilon_n - \varepsilon_m) + \frac{\hbar q_x^2}{2m_e} - \omega - i\tau_{nm}^{-1},$$

(C.26)

$$b_{nm}^5 = \frac{1}{\hbar}(\varepsilon_n - \varepsilon_m) + \frac{\hbar}{2m_e}(q_x - k_x)^2 - i\tau_{nm}^{-1},$$

(C.27)

$$b_{nm}^6 = \frac{1}{\hbar}(\varepsilon_n - \varepsilon_m) - \frac{\hbar}{2m_e}(q_x - k_x)^2 - i\tau_{nm}^{-1},$$

(C.28)

$$b_{nm}^7 = \frac{1}{\hbar}(\varepsilon_n - \varepsilon_m) + \frac{\hbar}{2m_e}(q_x + k_x)^2 - i\tau_{nm}^{-1},$$

(C.29)

$$b_{nm}^8 = \frac{1}{\hbar}(\varepsilon_n - \varepsilon_m) + \frac{\hbar}{2m_e}(q_x^2 - k_x^2) - i\tau_{nm}^{-1},$$

(C.30)

$$b_{nm}^9 = \frac{1}{\hbar}(\varepsilon_n - \varepsilon_m) + \frac{\hbar q_x}{2m_e}(q_x + 2k_x) + \omega - i\tau_{nm}^{-1},$$

(C.31)

$$b_{nm}^{10} = \frac{1}{\hbar}(\varepsilon_n - \varepsilon_m) + \frac{\hbar k_x}{2m_e}(k_x + 2q_x) - \omega - i\tau_{nm}^{-1},$$

(C.32)

$$b_{nm}^{11} = \frac{1}{\hbar}(\varepsilon_n - \varepsilon_m) + \frac{\hbar q_x}{2m_e}(q_x - 2k_x) + \omega - i\tau_{nm}^{-1},$$

(C.33)

$$b_{nm}^{12} = \frac{1}{\hbar}(\varepsilon_n - \varepsilon_m) + \frac{\hbar k_x}{2m_e}(2q_x - k_x) - \omega - i\tau_{nm}^{-1},$$

(C.34)

$$b_{nm}^{13} = \frac{1}{\hbar}(\varepsilon_n - \varepsilon_m) + \frac{\hbar k_x}{2m_e}(k_x - 2q_x) - \omega - i\tau_{nm}^{-1}.$$

(C.35)

C.1 Nonlinear process A

Starting with the pure interband term in Eq. (8.17) we separate the z-dependent and the $\vec{\kappa}_\parallel$-dependent parts in the following way:

$$\Xi_{xxxx}^A(z, z', z'', z'''; \vec{q}_\parallel, \vec{k}_\parallel) = \frac{2}{(i\omega)^3} \sum_{nm} Z_{nm}^A(z, z', z'', z''') \xi_{nm}^A,$$

(C.36)

where the indices on the quantities Z and ξ follows the indices of the quantum numbers in the sum. The z-dependent part above is

$$Z_{nm}^A(z, z', z'', z''') = Z_{mn}^x(z'') Z_{nm}^x(z) \delta(z - z') \delta(z'' - z'''),$$

(C.37)

and the solution to the integral over $\vec{\kappa}_\parallel$ in the low-temperature limit

$$\xi_{nm}^A = -\frac{e^4}{32\pi m_e^2 \hbar} \frac{\alpha_n^2 - \alpha_m^2}{(\varepsilon_n - \varepsilon_m)/\hbar - 2\omega - i\tau_{nm}^{-1}}$$

(C.38)

readily appears by use of Eq. (C.178), since only the Fermi-Dirac distribution functions depend on $\vec{\kappa}_\parallel$.

C.2 Nonlinear process B

In order to solve the integral over $\kappa_\parallel$ in Eq. (8.18), we rewrite it into

$$\Xi^B_{xxkh}(z,z',z'',z''';\vec{q}_\parallel,\vec{k}_\parallel) = \frac{2}{(i\omega)^3}\left(\frac{e\hbar}{2m_e}\right)^2 \sum_{nmv} Z^B_{kh,nmv}(z,z',z'',z''')\xi^B_{kh,nmv}(\vec{q}_\parallel,\vec{k}_\parallel),$$

(C.39)

in which both quantities Z and ξ are indexed according to their dependence on the two Cartesian indices of Ξ and the quantum numbers in the sum. Above, the z-dependent part in general is given by

$$Z^B_{kh,nmv}(z,z',z'',z''') = Z^h_{vn}(z''')Z^k_{mv}(z'')\delta(z-z')Z^x_{nm}(z),$$

(C.40)

in terms of Eqs. (C.1) and (C.2). Of these, the two with Cartesian indices *xx* and *yy* are equal. The solution to the other quantity above, $\xi^B_{kh,nmv}(\vec{q}_\parallel,\vec{k}_\parallel)$, in terms of the *a*'s and *b*'s and the functions solved in Appendix B, is written

$$\xi^B_{kh,nmv}(\vec{q}_\parallel,\vec{k}_\parallel) = -\frac{e^2}{4m_e\hbar^2}\frac{1}{(2\pi)^2}\frac{1}{(\varepsilon_n-\varepsilon_m)/\hbar-2\omega-i\tau^{-1}_{nm}}\left\{\mathcal{F}^B_{kh}(m,a_1,b^1_{vm},0)\right.$$
$$\left.-\mathcal{F}^B_{kh}(v,a_1,b^1_{vm},k_x)+\mathcal{F}^B_{kh}(n,-a_1,b^2_{nv},0)-\mathcal{F}^B_{kh}(v,-a_1,b^2_{nv},k_x)\right\},$$

(C.41)

which is written in terms of a set of functions $\mathcal{F}$ that vary from element to element. These functions are of the order $\beta = 1$ because only one transition frequency appears inside each integral. They are determined from the $\vec{\kappa}_\parallel$-dependent parts of the microscopic current densities, and they become

$$\mathcal{F}^B_{zz} = \mathcal{F}^1_{00},$$

(C.42)

$$\mathcal{F}^B_{yy} = 4\mathcal{F}^1_{02},$$

(C.43)

$$\mathcal{F}^B_{xz} = \mathcal{F}^B_{zx} = 2\mathcal{F}^1_{10,n} + k_x\mathcal{F}^1_{00},$$

(C.44)

$$\mathcal{F}^B_{xx} = 4\mathcal{F}^1_{20} + 4k_x\mathcal{F}^1_{10} + k^2_x\mathcal{F}^1_{00},$$

(C.45)

in short notation, since the functions at the right side of these equations take the same arguments as the functions to the left.

C.3 Nonlinear process C

Separating Eq. (8.19) into its z-dependent and $\vec{\kappa}_\parallel$-dependent parts, we write

$$\Xi^C_{xxxx}(z,z',z'',z''';\vec{q}_\parallel,\vec{k}_\parallel) = \frac{2}{(i\omega)^3}\sum_{nm} Z^C_{nm}(z,z',z'',z''')\xi^C_{nm}(\vec{q}_\parallel,\vec{k}_\parallel)$$

(C.46)

where the indices on the new quantities follows the quantum numbers in the sum. The z-independent part in this part of the conductivity tensor is

$$Z^C_{nm}(z,z',z'',z''') = Z^x_{mn}(z')Z^x_{nm}(z)\delta(z'-z''')\delta(z-z''),$$

(C.47)

in terms of Eq. (C.1). The solution to the quantity $\xi^C_{nm}(\vec{q}_{\parallel}, \vec{k}_{\parallel})$ then appears as

$$\xi^C_{nm}(\vec{q}_{\parallel}, \vec{k}_{\parallel}) = -\frac{e^4}{16\pi^2 m_e^2 \hbar} \left\{ \mathcal{F}^1_{00}(n, a_4, b^5_{nm}, q_x - k_x) - \mathcal{F}^1_{00}(m, a_4, b^5_{nm}, 0) \right\} \tag{C.48}$$

in terms of the a's and b's and the functions solved in Appendix B.

C.4 Nonlinear process D

Performing an adequate separation of variables in Eq. (8.20), it is written

$$\Xi^D_{xjkx}(z, z', z'', z'''; \vec{q}_{\parallel}, \vec{k}_{\parallel}) = \frac{2}{(i\omega)^3} \left(\frac{e\hbar}{2m_e}\right)^2 \sum_{nmv} \left\{ Z^{Da}_{jk,nmv}(z, z', z'', z''') \xi^{Da}_{jk,nmv}(\vec{q}_{\parallel}, \vec{k}_{\parallel}) \right.$$
$$\left. + Z^{Db}_{jk,nmv}(z, z', z'', z''') \xi^{Db}_{jk,nmv}(\vec{q}_{\parallel}, \vec{k}_{\parallel}) \right\}, \tag{C.49}$$

where the four new quantities are indexed according to the varying Cartesian coordinates of Ξ and the quantum numbers in the sum. The z-dependent terms in Eq. (C.49) are

$$Z^{Da}_{jk,nmv}(z, z', z'', z''') = \delta(z - z''') Z^k_{mv}(z'') Z^j_{vn}(z') Z^x_{nm}(z), \tag{C.50}$$
$$Z^{Db}_{jk,nmv}(z, z', z'', z''') = \delta(z - z''') Z^k_{vn}(z'') Z^j_{mv}(z') Z^x_{nm}(z) \tag{C.51}$$

in terms of Eqs. (C.1) and (C.2). In both equations above, the xx and yy permutations are the same. The solution to the ξ quantities we write in terms of the a's, b's, and the functions solved in Appendix B, the result being

$$\xi^{Da}_{jk,nmv}(\vec{q}_{\parallel}, \vec{k}_{\parallel}) = -\frac{e^2}{16\pi^2 m_e \hbar^2} \left\{ \mathcal{F}^{Da}_{jk}(m, \{a_3, a_1\}, \{b^7_{nm}, b^1_{vm}\}, 0) \right.$$
$$- \mathcal{F}^{Da}_{jk}(v, \{a_3, a_1\}, \{b^7_{nm}, b^1_{vm}\}, k_x) + \mathcal{F}^{Da}_{jk}(n, \{a_3, a_2\}, \{b^7_{nm}, b^9_{nv}\}, q_x + k_x)$$
$$\left. - \mathcal{F}^{Da}_{jk}(v, \{a_3, a_2\}, \{b^7_{nm}, b^9_{nv}\}, k_x) \right\}, \tag{C.52}$$

$$\xi^{Db}_{jk,nmv}(\vec{q}_{\parallel}, \vec{k}_{\parallel}) = -\frac{e^2}{16\pi^2 m_e \hbar^2} \left\{ \mathcal{F}^{Db}_{jk}(m, \{a_3, a_2\}, \{b^7_{nm}, b^3_{vm}\}, 0) \right.$$
$$- \mathcal{F}^{Db}_{jk}(v, \{a_3, a_2\}, \{b^7_{nm}, b^3_{vm}\}, q_x) + \mathcal{F}^{Db}_{jk}(n, \{a_3, a_1\}, \{b^7_{nm}, b^{10}_{nv}\}, q_x + k_x)$$
$$\left. - \mathcal{F}^{Db}_{jk}(v, \{a_3, a_1\}, \{b^7_{nm}, b^{10}_{nv}\}, q_x) \right\}, \tag{C.53}$$

which have been written in terms of a set of functions $\mathcal{F}$ that vary from element to element. These functions are again determined from the $\vec{\kappa}_{\parallel}$-dependent part of the microscopic current densities appearing in $\Xi^D_{xjkx}(z, z', z'', z'''; \vec{q}_{\parallel}, \vec{k}_{\parallel})$. They are

$$\mathcal{F}^{Da}_{zz} = \mathcal{F}^{Db}_{zz} = \mathcal{F}^2_{00}, \tag{C.54}$$
$$\mathcal{F}^{Da}_{yy} = \mathcal{F}^{Db}_{yy} = 4\mathcal{F}^2_{02}, \tag{C.55}$$
$$\mathcal{F}^{Da}_{xz} = 2\mathcal{F}^2_{10} + (2k_x + q_x)\mathcal{F}^2_{00,n}, \tag{C.56}$$
$$\mathcal{F}^{Db}_{xz} = 2\mathcal{F}^2_{10} + q_x \mathcal{F}^2_{00}, \tag{C.57}$$

$$\mathcal{F}_{zx}^{\mathrm{Da}} = 2\mathcal{F}_{10}^2 + k_x \mathcal{F}_{00}^2, \tag{C.58}$$

$$\mathcal{F}_{zx}^{\mathrm{Db}} = 2\mathcal{F}_{10}^2 + (k_x + 2q_x)\mathcal{F}_{00}^2, \tag{C.59}$$

$$\mathcal{F}_{xx}^{\mathrm{Da}} = 4\mathcal{F}_{20}^2 + 2(q_x + 3k_x)\mathcal{F}_{10}^2 + (2k_x^2 + q_x k_x)\mathcal{F}_{00}^2, \tag{C.60}$$

$$\mathcal{F}_{xx}^{\mathrm{Db}} = 4\mathcal{F}_{20}^2 + 2(3q_x + k_x)\mathcal{F}_{10}^2 + (2q_x^2 + q_x k_x)\mathcal{F}_{00}^2, \tag{C.61}$$

again in short notation, and for the same reason as before.

C.5 Nonlinear process E

Separation of the z-dependent part and the $\vec{\kappa}_{\parallel}$-dependent part in Eq. (8.21) yields

$$\Xi_{ijxx}^{\mathrm{E}}(z,z',z'',z''';\vec{q}_{\parallel},\vec{k}_{\parallel}) = \frac{2}{(\mathrm{i}\omega)^3}\left(\frac{e\hbar}{2m_e}\right)^2 \sum_{nmv}\Big\{ Z_{ij,nmv}^{\mathrm{Ea}}(z,z',z'',z''')\xi_{ij,nmv}^{\mathrm{Ea}}(\vec{q}_{\parallel},\vec{k}_{\parallel})$$

$$+ Z_{ij,nmv}^{\mathrm{Eb}}(z,z',z'',z''')\xi_{ij,nmv}^{\mathrm{Eb}}(\vec{q}_{\parallel},\vec{k}_{\parallel})\Big\}, \tag{C.62}$$

the new quantities being indexed according to their dependence on the varying Cartesian coordinates in $\Xi_{ijxx}^{\mathrm{E}}(z,z',z'',z''';\vec{q}_{\parallel},\vec{k}_{\parallel})$ and the quantum numbers in the sum. The z-dependent quantities are again written in terms of Eqs. (C.1)–(C.2), with the result

$$Z_{ij,nmv}^{\mathrm{Ea}}(z,z',z'',z''') = \delta(z''-z''')Z_{mv}^x(z'')Z_{vn}^j(z')Z_{nm}^i(z), \tag{C.63}$$

$$Z_{ij,nmv}^{\mathrm{Eb}}(z,z',z'',z''') = \delta(z''-z''')Z_{vn}^x(z'')Z_{mv}^j(z')Z_{nm}^i(z), \tag{C.64}$$

and again it appears, the quantities with Cartesian indices xx and yy are equal in each of the above equations. The solutions to the two ξ quantities are obtained in terms of the a's and b's and the functions solved in Appendix B, and they become

$$\xi_{ij,nmv}^{\mathrm{Ea}}(\vec{q}_{\parallel},\vec{k}_{\parallel}) = -\frac{e^2}{2^6\pi^2 m_e\hbar^2}\left\{ \frac{\mathcal{F}_{ij}^{\mathrm{E1}}(m,a_2,b_{nm}^4,0) - \mathcal{F}_{ij}^{\mathrm{E1}}(v,a_2,b_{nm}^4,0)}{(\varepsilon_v-\varepsilon_m)/\hbar - 2\omega - \mathrm{i}\tau_{vm}^{-1}}\right.$$

$$\left. + \mathcal{F}_{ij}^{\mathrm{E2}}(n,\{a_2,a_2\},\{b_{nm}^4,b_{nv}^3\},q_x) - \mathcal{F}_{ij}^{\mathrm{E2}}(v,\{a_2,a_2\},\{b_{nm}^4,b_{nv}^3\},0)\right\}, \tag{C.65}$$

$$\xi_{ij,nmv}^{\mathrm{Eb}}(\vec{q}_{\parallel},\vec{k}_{\parallel}) = -\frac{e^2}{2^6\pi^2 m_e\hbar^2}\left\{ \frac{\mathcal{F}_{ij}^{\mathrm{E1}}(n,a_2,b_{nm}^4,q_x) - \mathcal{F}_{ij}^{\mathrm{E1}}(v,a_2,b_{nm}^4,q_x)}{(\varepsilon_n-\varepsilon_v)/\hbar - 2\omega - \mathrm{i}\tau_{nv}^{-1}}\right.$$

$$\left. + \mathcal{F}_{ij}^{\mathrm{E2}}(m,\{a_2,a_2\},\{b_{nm}^4,b_{vm}^3\},0) - \mathcal{F}_{ij}^{\mathrm{E2}}(v,\{a_2,a_2\},\{b_{nm}^4,b_{vm}^3\},q_x)\right\}, \tag{C.66}$$

which is written in terms of a set of functions $\mathcal{F}$ that vary from element to element. Their structure is as before determined from the $\vec{\kappa}_{\parallel}$-dependent parts of the transition current densities, and we find for the pure interband transitions functions of order $\beta = 1$, since only one transition frequency occurs in each integral. They are

$$\mathcal{F}_{zz}^{\mathrm{E1}} = \mathcal{F}_{00}^1, \tag{C.67}$$

$$\mathcal{F}_{yy}^{\mathrm{E1}} = 4\mathcal{F}_{02}^1, \tag{C.68}$$

$$\mathcal{F}_{xz}^{\mathrm{E1}} = \mathcal{F}_{zx}^{\mathrm{E1}} = 2\mathcal{F}_{10}^1 + q_x\mathcal{F}_{00}^1, \tag{C.69}$$

$$\mathcal{F}_{xx}^{\mathrm{E1}} = 4\mathcal{F}_{20}^1 + 2q_x\mathcal{F}_{10}^1 + 2q_x^2\mathcal{F}_{00}^1, \tag{C.70}$$

in short notation, and for the mixed interband/intraband transitions functions of order $\beta = 2$ because two transition frequencies occur in each integral. They are

$$\mathcal{F}_{zz}^{E2} = \mathcal{F}_{00}^2, \tag{C.71}$$

$$\mathcal{F}_{yy}^{E2} = 4\mathcal{F}_{02}^2, \tag{C.72}$$

$$\mathcal{F}_{xz}^{E2} = \mathcal{F}_{zx}^{E2} = 2\mathcal{F}_{10}^2 + q_x\mathcal{F}_{00}^2, \tag{C.73}$$

$$\mathcal{F}_{xx}^{E2} = 4\mathcal{F}_{20}^2 + 2q_x\mathcal{F}_{10}^2 + 2q_x^2\mathcal{F}_{00}^2, \tag{C.74}$$

again in short notation, since all arguments to the functions are of the same type.

C.6 Nonlinear process F

The separation of variables of Eq. (8.22) into z-independent and $\vec{\kappa}_\parallel$-independent terms gives

$$\Xi_{ixxh}^{F}(z,z',z'',z''';\vec{q}_\parallel,\vec{k}_\parallel) = \frac{2}{(i\omega)^3}\left(\frac{e\hbar}{2m_e}\right)^2 \sum_{nmv}\left\{ Z_{ih,nmv}^{Fa}(z,z',z'',z''')\xi_{ih,nmv}^{Fa}(\vec{q}_\parallel,\vec{k}_\parallel) \right.$$
$$\left. + Z_{ih,nmv}^{Fb}(z,z',z'',z''')\xi_{ih,nmv}^{Fb}(\vec{q}_\parallel,\vec{k}_\parallel) \right\}, \tag{C.75}$$

where the new quantities have been indexed according to their dependence on the Cartesian indices of Ξ and the quantum numbers in the sum. In Eq. (C.75) above, the $\vec{\kappa}_\parallel$-independent terms are

$$Z_{ih,nmv}^{Fa}(z,z',z'',z''') = \delta(z'-z''')Z_{vn}^h(z'')Z_{mv}^x(z')Z_{nm}^i(z), \tag{C.76}$$

$$Z_{ih,nmv}^{Fb}(z,z',z'',z''') = \delta(z'-z''')Z_{mv}^h(z'')Z_{vn}^x(z')Z_{nm}^i(z). \tag{C.77}$$

in terms of the three quantities defined in Eqs. (C.1)–(C.2), and again the xx and yy elements in each of the two above quantities are equal. The solutions to the z-independent terms appear in terms of the a's and b's and the functions solved in Appendix B as

$$\xi_{ih,nmv}^{Fa}(\vec{q}_\parallel,\vec{k}_\parallel) = -\frac{e^2}{2^5\pi^2 m_e\hbar^2}\left\{ \mathcal{F}_{ih}^{Fa}(m,\{a_2,a_4\},\{b_{nm}^4,b_{vm}^5\},0) \right.$$
$$- \mathcal{F}_{ih}^{Fa}(v,\{a_2,a_4\},\{b_{nm}^4,b_{vm}^5\},q_x-k_x) + \mathcal{F}_{ih}^{Fa}(n,\{a_2,a_1\},\{b_{nm}^4,b_{nv}^{12}\},q_x)$$
$$\left. - \mathcal{F}_{ih}^{Fa}(v,\{a_2,a_1\},\{b_{nm}^4,b_{nv}^{12}\},q_x-k_x) \right\}, \tag{C.78}$$

$$\xi_{ih,nmv}^{Fb}(\vec{q}_\parallel,\vec{k}_\parallel) = -\frac{e^2}{2^5\pi^2 m_e\hbar^2}\left\{ \mathcal{F}_{ih}^{Fb}(m,\{a_2,a_1\},\{b_{nm}^4,b_{vm}^1\},0) \right.$$
$$- \mathcal{F}_{ih}^{Fb}(v,\{a_2,a_1\},\{b_{nm}^4,b_{vm}^1\},k_x) + \mathcal{F}_{ih}^{Fb}(n,\{a_2,a_4\},\{b_{nm}^4,b_{nv}^8\},q_x)$$
$$\left. - \mathcal{F}_{ih}^{Fb}(v,\{a_2,a_4\},\{b_{nm}^4,b_{nv}^8\},k_x) \right\}, \tag{C.79}$$

which are written in terms of a set of functions $\mathcal{F}$ that vary from element to element. They are again determined from the $\vec{\kappa}_\parallel$-dependent parts of the transition current densities

appearing, and thus they become

$$\mathcal{F}_{zz}^{\text{Fa}} = \mathcal{F}_{zz}^{\text{Fb}} = \mathcal{F}_{00}^2, \tag{C.80}$$

$$\mathcal{F}_{yy}^{\text{Fa}} = \mathcal{F}_{yy}^{\text{Fb}} = 4\mathcal{F}_{02}^2, \tag{C.81}$$

$$\mathcal{F}_{xz}^{\text{Fa}} = \mathcal{F}_{xz}^{\text{Fb}} = 2\mathcal{F}_{00}^2 + q_x \mathcal{F}_{00}^2, \tag{C.82}$$

$$\mathcal{F}_{zx}^{\text{Fa}} = 2\mathcal{F}_{10}^2 + (q_x - k_x)\mathcal{F}_{00}^2, \tag{C.83}$$

$$\mathcal{F}_{zx}^{\text{Fb}} = 2\mathcal{F}_{10}^2 + k_x\mathcal{F}_{00}^2, \tag{C.84}$$

$$\mathcal{F}_{xx}^{\text{Fa}} = 4\mathcal{F}_{20}^2 + 2(2q_x - k_x)\mathcal{F}_{00}^2 + (2q_x^2 - q_x k_x)\mathcal{F}_{00}^2, \tag{C.85}$$

$$\mathcal{F}_{xx}^{\text{Fb}} = 4\mathcal{F}_{20}^2 + 2(q_x + k_x)\mathcal{F}_{10}^2 + q_x k_x \mathcal{F}_{00}^2, \tag{C.86}$$

again in the abbreviated notation, where the functions in general take arguments of the type $(n, \{a_1, a_2\}, \{b_1, b_2\}, s)$.

C.7 Nonlinear process G

Finally, Eq. (8.23) becomes in terms of z-independent and $\vec{\kappa}_\parallel$-independent terms

$$\Xi_{ijkh}^{\text{G}}(z, z', z'', z'''; \vec{q}_\parallel, \vec{k}_\parallel) = \frac{2}{(\mathrm{i}\omega)^3}\left(\frac{e\hbar}{2m_e}\right)^4 \sum_{nmvl}\left\{ Z_{ijkh,nmvl}^{\text{Ga}}(z, z', z'', z''')\xi_{ijkh,nmvl}^{\text{Ga}}(\vec{q}_\parallel, \vec{k}_\parallel)\right.$$

$$\left. + Z_{ijkh,nmvl}^{\text{Gb}}(z, z', z'', z''')\xi_{ijkh,nmvl}^{\text{Gb}}(\vec{q}_\parallel, \vec{k}_\parallel) + Z_{ijkh,nmvl}^{\text{Gc}}(z, z', z'', z''')\xi_{ijkh,nmvl}^{\text{Gc}}(\vec{q}_\parallel, \vec{k}_\parallel)\right\}, \tag{C.87}$$

where again the new quantities have been indexed according to their dependence on the various Cartesian indices of Ξ and the quantum numbers of the sum. The z-dependent terms in Eq. (C.87) are on general form

$$Z_{ijkh,nmvl}^{\text{Ga}}(z, z', z'', z''') = Z_{ml}^h(z''') Z_{lv}^k(z'') Z_{vn}^j(z') Z_{nm}^i(z), \tag{C.88}$$

$$Z_{ijkh,nmvl}^{\text{Gb}}(z, z', z'', z''') = Z_{ml}^h(z''') Z_{vn}^k(z'') Z_{lv}^j(z') Z_{nm}^i(z), \tag{C.89}$$

$$Z_{ijkh,nmvl}^{\text{Gc}}(z, z', z'', z''') = Z_{lv}^h(z''') Z_{vn}^k(z'') Z_{ml}^j(z') Z_{nm}^i(z), \tag{C.90}$$

in terms of the quantities defined in Eqs. (C.1)–(C.2), and as in the previous cases we may observe that any element with a Cartesian index x is equal to the element with the Cartesian index y on the same place, the other Cartesian indices unchanged. The z-independent terms we write using the a's and b's and the functions solved in Appendix B, as before. They finally become

$$\xi_{ijkh,nmvl}^{\text{Ga}}(\vec{q}_\parallel, \vec{k}_\parallel) = -\frac{1}{8\hbar^3}\frac{1}{(2\pi)^2}\left\{\frac{1}{(\varepsilon_v - \varepsilon_m)/\hbar - 2\omega - \mathrm{i}\tau_{vm}^{-1}}\right.$$

$$\times\left[\mathcal{F}_{ijkh}^{\text{Ga1}}\left(l, \{a_2, -a_1\}, \{b_{nm}^4, b_{lm}^1\}, -k_x\right) - \mathcal{F}_{ijkh}^{\text{Ga1}}\left(m, \{a_2, -a_1\}, \{b_{nm}^4, b_{lm}^1\}, 0\right)\right.$$

$$\left.+\mathcal{F}_{ijkh}^{\text{Ga1}}\left(l, \{a_2, a_1\}, \{b_{nm}^4, b_{vl}^2\}, -k_x\right) - \mathcal{F}_{ijkh}^{\text{Ga1}}\left(v, \{a_2, a_1\}, \{b_{nm}^4, b_{vl}^2\}, 0\right)\right]$$

$$+ \mathcal{F}_{ijkh}^{\text{Ga2}} \left(l, \{a_2, a_1, a_3\}, \{b_{nm}^4, b_{vl}^2, b_{nl}^8\}, -k_x \right)$$

$$- \mathcal{F}_{ijkh}^{\text{Ga2}} \left(v, \{a_2, a_1, a_3\}, \{b_{nm}^4, b_{vl}^2, b_{nl}^8\}, 0 \right)$$

$$+ \mathcal{F}_{ijkh}^{\text{Ga2}} \left(n, \{a_2, a_2, a_3\}, \{b_{nm}^4, b_{nv}^3, b_{nl}^8\}, q_x \right)$$

$$- \mathcal{F}_{ijkh}^{\text{Ga2}} \left(v, \{a_2, a_2, a_3\}, \{b_{nm}^4, b_{nv}^3, b_{nl}^8\}, 0 \right) \Big\} \tag{C.91}$$

$$\xi_{ijkh,nmvl}^{\text{Gb}}(\vec{q}_\parallel, \vec{k}_\parallel) = -\frac{1}{8\hbar^3} \frac{1}{(2\pi)^2} \Big\{ \mathcal{F}_{ijkh}^{\text{Gb}} \left(l, \{a_2, -a_1, a_4\}, \{b_{nm}^4, b_{lm}^1, b_{vm}^5\}, -k_x \right)$$

$$- \mathcal{F}_{ijkh}^{\text{Gb}} \left(m, \{a_2, -a_1, a_4\}, \{b_{nm}^4, b_{lm}^1, b_{vm}^5\}, 0 \right)$$

$$+ \mathcal{F}_{ijkh}^{\text{Gb}} \left(l, \{a_2, a_2, a_4\}, \{b_{nm}^4, b_{vl}^{11}, b_{vm}^5\}, -k_x \right)$$

$$- \mathcal{F}_{ijkh}^{\text{Gb}} \left(v, \{a_2, a_2, a_4\}, \{b_{nm}^4, b_{vl}^{11}, b_{vm}^5\}, q_x - k_x \right)$$

$$+ \mathcal{F}_{ijkh}^{\text{Gb}} \left(l, \{a_2, a_2, a_3\}, \{b_{nm}^4, b_{vl}^{11}, b_{nl}^8\}, -k_x \right)$$

$$- \mathcal{F}_{ijkh}^{\text{Gb}} \left(v, \{a_2, a_2, a_3\}, \{b_{nm}^4, b_{vl}^{11}, b_{nl}^8\}, q_x - k_x \right)$$

$$+ \mathcal{F}_{ijkh}^{\text{Gb}} \left(n, \{a_2, a_1, a_3\}, \{b_{nm}^4, b_{nv}^{12}, b_{nl}^8\}, q_x \right)$$

$$- \mathcal{F}_{ijkh}^{\text{Gb}} \left(v, \{a_2, a_1, a_3\}, \{b_{nm}^4, b_{nv}^{12}, b_{nl}^8\}, q_x - k_x \right) \Big\} \tag{C.92}$$

$$\xi_{ijkh,nmvl}^{\text{Gc}}(\vec{q}_\parallel, \vec{k}_\parallel) = -\frac{1}{8\hbar^3} \frac{1}{(2\pi)^2} \Big\{ \mathcal{F}_{ijkh}^{\text{Gc1}} \left(l, \{a_2, a_2, a_4\}, \{b_{nm}^4, b_{lm}^3, b_{vm}^5\}, q_x \right)$$

$$- \mathcal{F}_{ijkh}^{\text{Gc1}} \left(m, \{a_2, a_2, a_4\}, \{b_{nm}^4, b_{lm}^3, b_{vm}^5\}, 0 \right)$$

$$+ \mathcal{F}_{ijkh}^{\text{Gc1}} \left(l, \{a_2, -a_1, a_4\}, \{b_{nm}^4, b_{vl}^{13}, b_{vm}^5\}, q_x \right)$$

$$- \mathcal{F}_{ijkh}^{\text{Gc1}} \left(v, \{a_2, -a_1, a_4\}, \{b_{nm}^4, b_{vl}^{13}, b_{vm}^5\}, q_x - k_x \right) + \frac{1}{(\varepsilon_n - \varepsilon_l)/\hbar - 2\omega - i\tau_{nl}^{-1}}$$

$$\times \Big[\mathcal{F}_{ijkh}^{\text{Gc2}} \left(l, \{a_2, -a_1\}, \{b_{nm}^4, b_{vl}^{13}\}, q_x \right) - \mathcal{F}_{ijkh}^{\text{Gc2}} \left(v, \{a_2, -a_1\}, \{b_{nm}^4, b_{vl}^{13}\}, q_x - k_x \right)$$

$$+ \mathcal{F}_{ijkh}^{\text{Gc2}} \left(n, \{a_2, a_1\}, \{b_{nm}^4, b_{nv}^{12}\}, q_x \right) - \mathcal{F}_{ijkh}^{\text{Gc2}} \left(v, \{a_2, a_1\}, \{b_{nm}^4, b_{nv}^{12}\}, q_x - k_x \right) \Big] \Big\},$$

$$\tag{C.93}$$

and again they are written in terms of a set of functions $\mathcal{F}$ that vary from element to element. As was the case in the previous sections, these functions are determined from the z-independent parts of the transition current densities appearing in Ξ.

In passing we should notice that parts $(Ga1)$ and $(Gc2)$ has $\beta = 2$ because of the pure interband transition appearing in one of their denominators, while parts $(Ga2)$, (Gb), and $(Gc1)$ has $\beta = 3$ since all their transitions are mixed interband/intraband transitions, we observe that a lot of $\mathcal{F}$ functions are equal. In the simplest case, we observe

$$\mathcal{F}_{zzzz}^{\text{Ga1}} = \mathcal{F}_{zzzz}^{\text{Gc2}} = \mathcal{F}_{00}^2 \tag{C.94}$$

$$\mathcal{F}_{zzzz}^{\text{Gb}} = \mathcal{F}_{zzzz}^{\text{Gc1}} = \mathcal{F}_{zzzz}^{\text{Ga2}} = \mathcal{F}_{00}^3. \tag{C.95}$$

At the second level of complexity we find

$$\mathcal{F}_{yyzz}^{\text{Ga1}} = \mathcal{F}_{yyzz}^{\text{Gc2}} = \mathcal{F}_{yzyz}^{\text{Ga1}} = \mathcal{F}_{yzyz}^{\text{Gc2}} = \mathcal{F}_{yzzy}^{\text{Ga1}} = \mathcal{F}_{yzzy}^{\text{Gc2}} = \mathcal{F}_{zyyz}^{\text{Ga1}} = \mathcal{F}_{zyyz}^{\text{Gc2}} = \mathcal{F}_{zyzy}^{\text{Ga1}} = \mathcal{F}_{zyzy}^{\text{Gc2}} =$$

$$\mathcal{F}_{zzyy}^{\text{Ga1}} = \mathcal{F}_{zzyy}^{\text{Gc2}} = 4\mathcal{F}_{02}^2, \tag{C.96}$$

$$\mathcal{F}_{yyzz}^{\text{Gb}} = \mathcal{F}_{yyzz}^{\text{Gc1}} = \mathcal{F}_{yyzz}^{\text{Ga2}} = \mathcal{F}_{yzyz}^{\text{Gb}} = \mathcal{F}_{yzyz}^{\text{Gc1}} = \mathcal{F}_{yzyz}^{\text{Ga2}} = \mathcal{F}_{yzzy}^{\text{Gb}} = \mathcal{F}_{yzzy}^{\text{Gc1}} = \mathcal{F}_{yzzy}^{\text{Ga2}} = \mathcal{F}_{zyyz}^{\text{Gb}} =$$

$$\mathcal{F}_{zyyz}^{\text{Gc1}} = \mathcal{F}_{zyyz}^{\text{Ga2}} = \mathcal{F}_{zyzy}^{\text{Gb}} = \mathcal{F}_{zyzy}^{\text{Gc1}} = \mathcal{F}_{zyzy}^{\text{Ga2}} = \mathcal{F}_{zzyy}^{\text{Gb}} = \mathcal{F}_{zzyy}^{\text{Gc1}} = \mathcal{F}_{zzyy}^{\text{Ga2}} = 4\mathcal{F}_{02}^3. \tag{C.97}$$

The third level of complexity gives

$$\mathcal{F}_{yyyy}^{\text{Ga1}} = \mathcal{F}_{yyyy}^{\text{Gc2}} = 16\mathcal{F}_{04}^2, \tag{C.98}$$

$$\mathcal{F}_{yyyy}^{\text{Gb}} = \mathcal{F}_{yyyy}^{\text{Gc1}} = \mathcal{F}_{yyyy}^{\text{Ga2}} = 16\mathcal{F}_{04}^3. \tag{C.99}$$

At the fourth level of complexity we observe

$$\mathcal{F}_{xzzz}^{\text{Ga1}} = \mathcal{F}_{xzzz}^{\text{Gc2}} = \mathcal{F}_{zxzz}^{\text{Ga1}} = \mathcal{F}_{zxzz}^{\text{Gc2}} = 2\mathrm{i}\mathcal{F}_{10}^2 + 2\mathrm{i}q_x\mathcal{F}_{00}^2, \tag{C.100}$$

$$\mathcal{F}_{xzzz}^{\text{Gb}} = \mathcal{F}_{xzzz}^{\text{Gc1}} = \mathcal{F}_{xzzz}^{\text{Ga2}} = \mathcal{F}_{zxzz}^{\text{Gc1}} = \mathcal{F}_{zxzz}^{\text{Ga2}} = 2\mathrm{i}\mathcal{F}_{10}^3 + 2\mathrm{i}q_x\mathcal{F}_{00}^3, \tag{C.101}$$

$$\mathcal{F}_{zzxz}^{\text{Ga1}} = \mathcal{F}_{zzzx}^{\text{Ga1}} = 2\mathrm{i}\mathcal{F}_{10}^2 - 2\mathrm{i}k_x\mathcal{F}_{00}^2, \tag{C.102}$$

$$\mathcal{F}_{zzxz}^{\text{Ga2}} = \mathcal{F}_{zzzx}^{\text{Gb}} = \mathcal{F}_{zzzx}^{\text{Ga2}} = 2\mathrm{i}\mathcal{F}_{10}^3 - \mathrm{i}k_x\mathcal{F}_{00}^3, \tag{C.103}$$

$$\mathcal{F}_{zzxz}^{\text{Gc2}} = \mathcal{F}_{zzzx}^{\text{Gc2}} = 2\mathrm{i}\mathcal{F}_{10}^2 + \mathrm{i}(2q_x - k_x)\mathcal{F}_{00}^2, \tag{C.104}$$

$$\mathcal{F}_{zzxz}^{\text{Gb}} = \mathcal{F}_{zzxz}^{\text{Gc1}} = \mathcal{F}_{zzzx}^{\text{Gc1}} = 2\mathrm{i}\mathcal{F}_{10}^3 + \mathrm{i}(2q_x - k_x)\mathcal{F}_{00}^3, \tag{C.105}$$

and the independent element

$$\mathcal{F}_{zxzz}^{\text{Gb}} = 2\mathrm{i}\mathcal{F}_{10}^3 + 2\mathrm{i}(q_x - 2k_x)\mathcal{F}_{00}^3. \tag{C.106}$$

In the fifth case we find

$$\mathcal{F}_{xyyz}^{\text{Ga1}} = \mathcal{F}_{xyyz}^{\text{Gc2}} = \mathcal{F}_{xyzy}^{\text{Ga1}} = \mathcal{F}_{xyzy}^{\text{Gc2}} = \mathcal{F}_{xzyy}^{\text{Ga1}} = \mathcal{F}_{xzyy}^{\text{Gc2}} = \mathcal{F}_{yxyz}^{\text{Ga1}} = \mathcal{F}_{yxyz}^{\text{Gc2}} = \mathcal{F}_{yxzy}^{\text{Ga1}} = \mathcal{F}_{yxzy}^{\text{Gc2}} =$$

$$\mathcal{F}_{zxyy}^{\text{Ga1}} = \mathcal{F}_{zxyy}^{\text{Gc2}} = -8\mathrm{i}\mathcal{F}_{12}^2 - 4\mathrm{i}q_x\mathcal{F}_{02}^2, \tag{C.107}$$

$$\mathcal{F}_{xyyz}^{\text{Gb}} = \mathcal{F}_{xyyz}^{\text{Gc1}} = \mathcal{F}_{xyyz}^{\text{Ga2}} = \mathcal{F}_{xyzy}^{\text{Gb}} = \mathcal{F}_{xyzy}^{\text{Gc1}} = \mathcal{F}_{xyzy}^{\text{Ga2}} = \mathcal{F}_{xzyy}^{\text{Gb}} = \mathcal{F}_{xzyy}^{\text{Gc1}} = \mathcal{F}_{xzyy}^{\text{Ga2}} = \mathcal{F}_{yxyz}^{\text{Gc1}} =$$

$$\mathcal{F}_{yxyz}^{\text{Ga2}} = \mathcal{F}_{yxzy}^{\text{Gc1}} = \mathcal{F}_{yxzy}^{\text{Ga2}} = \mathcal{F}_{zxyy}^{\text{Gc1}} = \mathcal{F}_{zxyy}^{\text{Ga2}} = -8\mathrm{i}\mathcal{F}_{12}^3 - 4\mathrm{i}q_x\mathcal{F}_{02}^3, \tag{C.108}$$

$$\mathcal{F}_{yxyz}^{\text{Gb}} = \mathcal{F}_{yxzy}^{\text{Gb}} = \mathcal{F}_{zxyy}^{\text{Gb}} = -8\mathrm{i}\mathcal{F}_{12}^3 - 4\mathrm{i}(q_x - 2k_x)\mathcal{F}_{02}^3, \tag{C.109}$$

$$\mathcal{F}_{yyxz}^{\text{Ga1}} = \mathcal{F}_{yzxy}^{\text{Ga1}} = \mathcal{F}_{zyxy}^{\text{Ga1}} = \mathcal{F}_{yyzx}^{\text{Ga1}} = \mathcal{F}_{yzyx}^{\text{Ga1}} = \mathcal{F}_{zyyx}^{\text{Ga1}} = -8\mathrm{i}\mathcal{F}_{12}^2 + 4\mathrm{i}k_x\mathcal{F}_{02}^2, \tag{C.110}$$

$$\mathcal{F}_{yyxz}^{\text{Ga2}} = \mathcal{F}_{yzxy}^{\text{Ga2}} = \mathcal{F}_{zyxy}^{\text{Ga2}} = \mathcal{F}_{yyzx}^{\text{Gb}} = \mathcal{F}_{yyzx}^{\text{Ga2}} = \mathcal{F}_{yzyx}^{\text{Gb}} = \mathcal{F}_{yzyx}^{\text{Ga2}} = \mathcal{F}_{zyyx}^{\text{Gb}} = \mathcal{F}_{zyyx}^{\text{Ga2}} =$$

$$-8\mathrm{i}\mathcal{F}_{12}^3 + 4\mathrm{i}k_x\mathcal{F}_{02}^3, \tag{C.111}$$

$$\mathcal{F}_{yyxz}^{\text{Gc2}} = \mathcal{F}_{yzxy}^{\text{Gc2}} = \mathcal{F}_{zyxy}^{\text{Gc2}} = \mathcal{F}_{yyzx}^{\text{Gc2}} = \mathcal{F}_{yzyx}^{\text{Gc2}} = \mathcal{F}_{zyyx}^{\text{Gc2}} = -8\mathrm{i}\mathcal{F}_{12}^2 + 4\mathrm{i}(k_x - 2q_x)\mathcal{F}_{02}^2, \tag{C.112}$$

$$\mathcal{F}_{yyxz}^{\text{Gb}} = \mathcal{F}_{yyxz}^{\text{Gc1}} = \mathcal{F}_{yzxy}^{\text{Gb}} = \mathcal{F}_{yzxy}^{\text{Gc1}} = \mathcal{F}_{zyxy}^{\text{Gb}} = \mathcal{F}_{zyxy}^{\text{Gc1}} = \mathcal{F}_{yyzx}^{\text{Gc1}} = \mathcal{F}_{yzyx}^{\text{Gc1}} = \mathcal{F}_{zyyx}^{\text{Gc1}} =$$

$$-8\mathrm{i}\mathcal{F}_{12}^3 + 4\mathrm{i}(k_x - 2q_x)\mathcal{F}_{02}^3, \tag{C.113}$$

In the sixth case we observe the related functions

$$\mathcal{F}_{xxzz}^{\text{Ga1}} = \mathcal{F}_{xxzz}^{\text{Gc2}} = -4\mathcal{F}_{20}^2 - 4q_x\mathcal{F}_{10}^2 - q_x^2\mathcal{F}_{00}^2, \tag{C.114}$$

$$\mathcal{F}_{xxzz}^{\text{Gc1}} = \mathcal{F}_{xxzz}^{\text{Ga2}} = -4\mathcal{F}_{20}^3 - 4q_x\mathcal{F}_{10}^3 - q_x^2\mathcal{F}_{00}^3, \tag{C.115}$$

$$\mathcal{F}_{xzxz}^{\text{Ga1}} = \mathcal{F}_{xzzx}^{\text{Ga1}} = \mathcal{F}_{zxxz}^{\text{Ga1}} = \mathcal{F}_{zxzx}^{\text{Ga1}} = -4\mathcal{F}_{20}^2 - 2(q_x - k_x)\mathcal{F}_{10}^2 + q_x k_x\mathcal{F}_{00}^2, \tag{C.116}$$

$$\mathcal{F}^{\text{Ga2}}_{xzxz} = \mathcal{F}^{\text{Gb}}_{xzzx} = \mathcal{F}^{\text{Ga2}}_{xzzx} = \mathcal{F}^{\text{Ga2}}_{zxxz} = \mathcal{F}^{\text{Ga2}}_{zxzx} = -4\mathcal{F}^3_{20} - 4(q_x - k_x)\mathcal{F}^3_{10} + q_x k_x \mathcal{F}^3_{00}, \quad \text{(C.117)}$$

$$\mathcal{F}^{\text{Gb}}_{xzxz} = \mathcal{F}^{\text{Gc1}}_{xzxz} = \mathcal{F}^{\text{Gc1}}_{xzzx} = \mathcal{F}^{\text{Gc1}}_{zxxz} = \mathcal{F}^{\text{Gc1}}_{zxzx} =$$
$$-4\mathcal{F}^3_{20} - 2(3q_x - k_x)\mathcal{F}^3_{10} - q_x(2q_x - k_x)\mathcal{F}^3_{00}, \quad \text{(C.118)}$$

$$\mathcal{F}^{\text{Gc2}}_{xzxz} = \mathcal{F}^{\text{Gc2}}_{xzzx} = \mathcal{F}^{\text{Gc2}}_{zxxz} = \mathcal{F}^{\text{Gc2}}_{zxzx} = -4\mathcal{F}^2_{20} - 2(3q_x - k_x)\mathcal{F}^2_{10} - q_x(2q_x - k_x)\mathcal{F}^2_{00}, \quad \text{(C.119)}$$

and the eight independent functions

$$\mathcal{F}^{\text{Gb}}_{xxzz} = -4\mathcal{F}^3_{20} - 4(q_x - k_x)\mathcal{F}^3_{10} - q_x(q_x - 2k_x)\mathcal{F}^3_{00}, \quad \text{(C.120)}$$

$$\mathcal{F}^{\text{Gb}}_{zxxz} = -4\mathcal{F}^3_{20} - 6(q_x - k_x)\mathcal{F}^3_{10} - (2q_x^2 + 2k_x^2 - 5q_x k_x)\mathcal{F}^3_{00}, \quad \text{(C.121)}$$

$$\mathcal{F}^{\text{Gb}}_{zxzx} = -4\mathcal{F}^3_{20} - 2(q_x - 3k_x)\mathcal{F}^3_{10} - k_x(2k_x - q_x)\mathcal{F}^3_{00}, \quad \text{(C.122)}$$

$$\mathcal{F}^{\text{Ga1}}_{zzxx} = -4\mathcal{F}^2_{20} + 4k_x\mathcal{F}^2_{10} - k_x^2\mathcal{F}^2_{00}, \quad \text{(C.123)}$$

$$\mathcal{F}^{\text{Ga2}}_{zzxx} = -4\mathcal{F}^3_{20} + 4k_x\mathcal{F}^3_{10} - k_x^2\mathcal{F}^3_{00}, \quad \text{(C.124)}$$

$$\mathcal{F}^{\text{Gb}}_{zzxx} = -4\mathcal{F}^3_{20} - 4(q_x - k_x)\mathcal{F}^3_{10} - k_x(k_x - 2q_x)\mathcal{F}^3_{00}, \quad \text{(C.125)}$$

$$\mathcal{F}^{\text{Gc1}}_{zzxx} = -4\mathcal{F}^3_{20} - 2(2q_x - k_x)\mathcal{F}^3_{10} - (2q_x - k_x)^2\mathcal{F}^3_{00}, \quad \text{(C.126)}$$

$$\mathcal{F}^{\text{Gc2}}_{zzxx} = -4\mathcal{F}^2_{20} - 2(2q_x - k_x)\mathcal{F}^2_{10} - (2q_x - k_x)^2\mathcal{F}^2_{00}. \quad \text{(C.127)}$$

The seventh case has the following related functions

$$\mathcal{F}^{\text{Ga1}}_{xxyy} = \mathcal{F}^{\text{Gc2}}_{xxyy} = 16\mathcal{F}^2_{22} + 16q_x\mathcal{F}^2_{12} + 4q_x^2\mathcal{F}^2_{02}, \quad \text{(C.128)}$$

$$\mathcal{F}^{\text{Gc1}}_{xxyy} = \mathcal{F}^{\text{Ga2}}_{xxyy} = 16\mathcal{F}^3_{22} + 16q_x\mathcal{F}^3_{12} + 4q_x^2\mathcal{F}^3_{02}, \quad \text{(C.129)}$$

$$\mathcal{F}^{\text{Ga1}}_{xyxy} = \mathcal{F}^{\text{Ga1}}_{xyyx} = \mathcal{F}^{\text{Ga1}}_{yxxy} = \mathcal{F}^{\text{Ga1}}_{yxyx} = 16\mathcal{F}^2_{22} + 8(q_x - k_x)\mathcal{F}^2_{12} - 4q_x k_x \mathcal{F}^2_{02}, \quad \text{(C.130)}$$

$$\mathcal{F}^{\text{Ga2}}_{xyxy} = \mathcal{F}^{\text{Gb}}_{xyyx} = \mathcal{F}^{\text{Ga2}}_{xyyx} = \mathcal{F}^{\text{Ga2}}_{yxxy} = \mathcal{F}^{\text{Ga2}}_{yxyx} = 16\mathcal{F}^3_{22} + 8(q_x - k_x)\mathcal{F}^3_{12} - 4q_x k_x \mathcal{F}^3_{02}, \quad \text{(C.131)}$$

$$\mathcal{F}^{\text{Gb}}_{xyxy} = \mathcal{F}^{\text{Gc1}}_{xyxy} = \mathcal{F}^{\text{Gc1}}_{xyyx} = \mathcal{F}^{\text{Gc1}}_{yxxy} = \mathcal{F}^{\text{Gc1}}_{yxyx} =$$
$$16\mathcal{F}^3_{22} + 8(3q_x - k_x)\mathcal{F}^3_{12} + 4q_x(2q_x - k_x)\mathcal{F}^3_{02}, \quad \text{(C.132)}$$

$$\mathcal{F}^{\text{Gc2}}_{xyxy} = \mathcal{F}^{\text{Gc2}}_{xyyx} = \mathcal{F}^{\text{Gc2}}_{yxxy} = \mathcal{F}^{\text{Gc2}}_{yxyx} = 16\mathcal{F}^2_{22} + 8(3q_x - k_x)\mathcal{F}^2_{12} + 4q_x(2q_x - k_x)\mathcal{F}^2_{02}, \quad \text{(C.133)}$$

and the eight independent functions

$$\mathcal{F}^{\text{Gb}}_{xxyy} = 16\mathcal{F}^3_{22} + 16(q_x - k_x)\mathcal{F}^3_{12} + 4q_x(q_x - 2k_x)\mathcal{F}^3_{02}, \quad \text{(C.134)}$$

$$\mathcal{F}^{\text{Gb}}_{yxxy} = 16\mathcal{F}^3_{22} + 24(q_x - k_x)\mathcal{F}^3_{12} + 4(2q_x^2 + 2k_x^2 - 5q_x k_x)\mathcal{F}^3_{02}, \quad \text{(C.135)}$$

$$\mathcal{F}^{\text{Gb}}_{yxyx} = 16\mathcal{F}^3_{22} + 8(q_x - 3k_x)\mathcal{F}^3_{12} + 4k_x(2k_x - q_x)\mathcal{F}^3_{02}, \quad \text{(C.136)}$$

$$\mathcal{F}^{\text{Ga1}}_{yyxx} = 16\mathcal{F}^2_{22} - 16k_x\mathcal{F}^2_{12} + 4k_x^2\mathcal{F}^2_{02}, \quad \text{(C.137)}$$

$$\mathcal{F}^{\text{Ga2}}_{yyxx} = 16\mathcal{F}^3_{22} - 16k_x\mathcal{F}^3_{12} + 4k_x^2\mathcal{F}^3_{02}, \quad \text{(C.138)}$$

$$\mathcal{F}^{\text{Gb}}_{yyxx} = 16\mathcal{F}^3_{22} + 16(q_x - k_x)\mathcal{F}^3_{12} + 4k_x(k_x - 2q_x)\mathcal{F}^3_{02}, \quad \text{(C.139)}$$

$$\mathcal{F}^{\text{Gc1}}_{yyxx} = 16\mathcal{F}^3_{22} + 16(2q_x - k_x)\mathcal{F}^3_{12} + 4(2q_x - k_x)^2\mathcal{F}^3_{02}, \quad \text{(C.140)}$$

$$\mathcal{F}^{\text{Gc2}}_{yyxx} = 16\mathcal{F}^2_{22} + 16(2q_x - k_x)\mathcal{F}^2_{12} + 4(2q_x - k_x)^2\mathcal{F}^2_{02}. \quad \text{(C.141)}$$

The eighth case gives

$$\mathcal{F}^{\text{Ga1}}_{xxxz} = \mathcal{F}^{\text{Ga1}}_{xxzx} = -8i\mathcal{F}^2_{30} - 4i(2q_x - k_x)\mathcal{F}^2_{20} - 2iq_x(q_x - 2k_x)\mathcal{F}^2_{10} + iq_x^2 k_x \mathcal{F}^2_{00}, \quad \text{(C.142)}$$

$$\mathcal{F}_{xxxz}^{Ga2} = \mathcal{F}_{xxzx}^{Ga2} = -8i\mathcal{F}_{30}^3 - 4i(2q_x - k_x)\mathcal{F}_{20}^3 - 2iq_x(q_x - 2k_x)\mathcal{F}_{10}^3 + iq_x^2 k_x \mathcal{F}_{00}^3, \quad \text{(C.143)}$$

$$\mathcal{F}_{xxxz}^{Gc1} = \mathcal{F}_{xxzx}^{Gc1} = -8i\mathcal{F}_{30}^3 - 4i(4q_x - k_x)\mathcal{F}_{20}^3 - 2iq_x(5q_x - 2k_x)\mathcal{F}_{10}^3$$
$$-iq_x^2(2q_x - k_x)\mathcal{F}_{00}^3, \quad \text{(C.144)}$$

$$\mathcal{F}_{xxxz}^{Gc2} = \mathcal{F}_{xxzx}^{Gc2} = -8i\mathcal{F}_{30}^2 - 4i(4q_x - k_x)\mathcal{F}_{20}^2 - 2iq_x(5q_x - 2k_x)\mathcal{F}_{10}^2$$
$$-iq_x^2(2q_x - k_x)\mathcal{F}_{00}^2, \quad \text{(C.145)}$$

$$\mathcal{F}_{xzxx}^{Ga1} = \mathcal{F}_{zxxx}^{Ga1} = -8i\mathcal{F}_{30}^2 - 4i(q_x - 2k_x)\mathcal{F}_{20}^2 - 2ik_x(k_x - 2q_x)\mathcal{F}_{10}^2 - iq_x k_x^2 \mathcal{F}_{00}^2, \quad \text{(C.146)}$$

$$\mathcal{F}_{xzxx}^{Ga2} = \mathcal{F}_{zxxx}^{Ga2} = -8i\mathcal{F}_{30}^3 - 4i(q_x - 2k_x)\mathcal{F}_{20}^3 - 2ik_x(k_x - 2q_x)\mathcal{F}_{10}^3 - iq_x k_x^2 \mathcal{F}_{00}^3, \quad \text{(C.147)}$$

$$\mathcal{F}_{xzxx}^{Gc1} = \mathcal{F}_{zxxx}^{Gc1} = -8i\mathcal{F}_{30}^3 - 4i(5q_x - 2k_x)\mathcal{F}_{20}^3 - 2i(2q_x - k_x)(4q_x - k_x)\mathcal{F}_{10}^3$$
$$-iq_x(2q_x - k_x)^2\mathcal{F}_{00}^3, \quad \text{(C.148)}$$

$$\mathcal{F}_{xzxx}^{Gc2} = \mathcal{F}_{zxxx}^{Gc2} = -8i\mathcal{F}_{30}^2 - 4i(5q_x - 2k_x)\mathcal{F}_{20}^2 - 2i(2q_x - k_x)(4q_x - k_x)\mathcal{F}_{10}^2$$
$$-iq_x(2q_x - k_x)^2\mathcal{F}_{00}^2, \quad \text{(C.149)}$$

and the four independent elements

$$\mathcal{F}_{xxxz}^{Gb} = -8i\mathcal{F}_{30}^3 - 4i(4q_x - 3k_x)\mathcal{F}_{20}^3 - 2i(5q_x^2 + 2k_x^2 - 8q_x k_x)\mathcal{F}_{10}^3$$
$$-iq_x(2q_x^2 + 2k_x^2 - 5q_x k_x)\mathcal{F}_{00}^3, \quad \text{(C.150)}$$

$$\mathcal{F}_{xxzx}^{Gb} = -8i\mathcal{F}_{30}^3 - 4i(2q_x - 3k_x)\mathcal{F}_{20}^3 - 2i(q_x^2 + 2k_x^2 - 4q_x k_x)\mathcal{F}_{10}^3$$
$$+iq_x k_x(q_x - 2k_x)\mathcal{F}_{00}^3, \quad \text{(C.151)}$$

$$\mathcal{F}_{xzxx}^{Gb} = -8i\mathcal{F}_{30}^3 - 4i(3q_x - 2k_x)\mathcal{F}_{20}^3 - 2i(2q_x^2 + k_x^2 - 4q_x k_x)\mathcal{F}_{10}^3$$
$$+iq_x k_x(2q_x - k_x)\mathcal{F}_{00}^3, \quad \text{(C.152)}$$

$$\mathcal{F}_{zxxx}^{Gb} = -8i\mathcal{F}_{30}^3 - 4i(3q_x - 4k_x)\mathcal{F}_{20}^3 - 2i(2q_x^2 + 5k_x^2 - 8q_x k_x)\mathcal{F}_{10}^3$$
$$+ik_x(2q_x^2 + 2k_x^2 - 5q_x k_x)\mathcal{F}_{00}^3. \quad \text{(C.153)}$$

The most complex solution group of Cartesian indices gives the five independent functions

$$\mathcal{F}_{xxxx}^{Ga1} = 16\mathcal{F}_{40}^2 + 16(q_x - k_x)\mathcal{F}_{30}^2 + 4(q_x^2 + k_x^2 - 4q_x k_x)\mathcal{F}_{20}^2 + 4q_x k_x(k_x - q_x)\mathcal{F}_{10}^2$$
$$+(q_x k_x)^2\mathcal{F}_{00}^2, \quad \text{(C.154)}$$

$$\mathcal{F}_{xxxx}^{Ga2} = 16\mathcal{F}_{40}^3 + 16(q_x - k_x)\mathcal{F}_{30}^3 + 4(q_x^2 + k_x^2 - 4q_x k_x)\mathcal{F}_{20}^3 + 4q_x k_x(k_x - q_x)\mathcal{F}_{10}^3$$
$$+(q_x k_x)^2\mathcal{F}_{00}^3, \quad \text{(C.155)}$$

$$\mathcal{F}_{xxxx}^{Gb} = 16\mathcal{F}_{40}^3 + 32(q_x - k_x)\mathcal{F}_{30}^3 + 4(5q_x^2 + 5k_x^2 - 12q_x k_x)\mathcal{F}_{20}^3$$
$$+2(q_x - k_x)(2q_x^2 + 2k_x^2 - 8q_x k_x)\mathcal{F}_{10}^3 - q_x k_x(2q_x^2 + 2k_x^2 - 5q_x k_x)\mathcal{F}_{00}^3, \quad \text{(C.156)}$$

$$\mathcal{F}_{xxxx}^{Gc1} = 16\mathcal{F}_{40}^3 + 16(3q_x - k_x)\mathcal{F}_{30}^3 + 4((2q_x - k_x)^2 + q_x(9q_x - 4k_x))\mathcal{F}_{20}^3$$
$$+4q_x(2q_x - k_x)(3q_x - k_x)\mathcal{F}_{10}^3 + q_x^2(2q_x - k_x)^2\mathcal{F}_{00}^3, \quad \text{(C.157)}$$

$$\mathcal{F}_{xxxx}^{Gc2} = 16\mathcal{F}_{40}^2 + 16(3q_x - k_x)\mathcal{F}_{30}^2 + 4((2q_x - k_x)^2 + q_x(9q_x - 4k_x))\mathcal{F}_{20}^2$$
$$+4q_x(2q_x - k_x)(3q_x - k_x)\mathcal{F}_{10}^2 + q_x^2(2q_x - k_x)^2\mathcal{F}_{00}^2. \quad \text{(C.158)}$$

The immediate conclusion of these observations is that only 65 of the original 246 possible functions are independent.

C.8 The $\mathcal{Z}$ coefficients with uniform pump field amplitudes

If the pump fields have uniform amplitudes along the z-axis, we take the local limit in the two coordinates z''' and z'' in the $\mathcal{Z}$ coefficients, such that in general we may write,

$$\mathcal{Z}(z,z') = \iint \mathcal{Z}(z,z',z'',z''')dz'''dz'', \tag{C.159}$$

and thus

$$\bar{\bar{\Xi}}(z,z';\vec{q}_\parallel,\vec{k}_\parallel) = \iint \bar{\bar{\Xi}}(z,z',z'',z''';\vec{q}_\parallel,\vec{k}_\parallel)dz'''dz''. \tag{C.160}$$

Using an orthogonal set of wave functions, parity teaches that the integrals over x- and y-components gives

$$\int \mathcal{Z}_{nm}^x(z)dz = \int \mathcal{Z}_{nm}^y(z)dz = \delta_{nm}, \tag{C.161}$$

where δ_{nm} is the Kronecker delta. The only question left is the z-components, which may be determined as soon as the wave functions for the system is known. Then part A of the nonlinear conductivity tensor does not contribute to the phase conjugated response because of the result of integration over z''. For the same reason, part E vanish, since the pure interband terms vanish by themselves, and the rest of part Ea becomes equal in magnitude to the rest of part Eb, but with the opposite sign. All other terms still contribute to the response.

C.8.1 Infinite barrier quantum well

If we choose a quantum well within the infinite barrier model with boundaries at 0 and $-d$ as the source, then we find

$$\mathcal{Z}(z,z') = \int_{-d}^{0}\int_{-d}^{0} \mathcal{Z}(z,z',z'',z''')dz'''dz'', \tag{C.162}$$

and thus

$$\bar{\bar{\Xi}}(z,z';\vec{q}_\parallel,\vec{k}_\parallel) = \int_{-d}^{0}\int_{-d}^{0} \bar{\bar{\Xi}}(z,z',z'',z''';\vec{q}_\parallel,\vec{k}_\parallel)dz'''dz'', \tag{C.163}$$

in general. Since the individual $\mathcal{Z}_{nm}^{x,y,z}(z)$ are independent, the result is written as a product of these in the coordinates z, z', z'', and z'''. Then the integrals over z-components gives

$$\int_{-d}^{0} \mathcal{Z}_{nm}^z(z)dz = \frac{4nm[1-(-1)^{n+m}]}{(n^2-m^2)d}. \tag{C.164}$$

C.8.2 Probe with a single wavevector

If we take the probe field as $\vec{E}(z';\vec{q}_\parallel) = \vec{E}e^{iq_\perp z'}$ and thus $\vec{E}^*(z';\vec{q}_\parallel) = \vec{E}^*e^{-iq_\perp z'}$, then we may further reduce the z-dependence, if we define

$$\mathfrak{Z}(z) = \int_{-d}^{0} \mathcal{Z}(z,z')e^{-iq_\perp z'}dz', \tag{C.165}$$

where we have indicated the modification before integration of the $\mathcal{Z}(z,z')$ quantity by shifting the symbol from calligraphic style to fraktur. Then, from the two integrals

$$\int_{-d}^{0} \mathcal{Z}_{nm}^{x}(z)e^{\pm iq_\perp z}dz = \int_{-d}^{0} \mathcal{Z}_{nm}^{y}(z)e^{\pm iq_\perp z}dz =$$
$$\mp \frac{4\pi^2 nm iq_\perp d[e^{\mp iq_\perp d}(-1)^{n+m}-1]}{[(iq_\perp d)^2 + \pi^2(n+m)^2][(iq_\perp d)^2 + \pi^2(n-m)^2]}, \tag{C.166}$$

$$\int_{-d}^{0} \mathcal{Z}_{nm}^{z}(z)e^{\pm iq_\perp z}dz = \frac{4\pi^4(n^2-m^2)nm[e^{\mp iq_\perp d}(-1)^{n+m}-1]}{d[(iq_\perp d)^2 + \pi^2(n+m)^2][(iq_\perp d)^2 + \pi^2(n-m)^2]}, \tag{C.167}$$

we may deduce the reduced quantities.

C.8.3 Combining $\mathfrak{Z}$ with Ω

If we combine the $\mathfrak{Z}$-quantities with the two different exponentials appearing in the Ω-quantities, we get new quantities that are independent of z. Defining

$$\mathfrak{Z}^{\pm} = \int_{-d}^{0} \mathfrak{Z}(z)e^{\pm iq_\perp z}dz, \tag{C.168}$$

we may now deduce the z-independent quantities that will finally appear in the expressions for the Ω-quantities. Even though we have modified the $\mathfrak{Z}$ coefficients again before integration, we keep the symbol, since the main purpose of selecting another symbol is to indicate that it is modified from the original $\mathcal{Z}$ quantities.

C.9 The nonlinear conductivity tensor in the Ω coefficients

If we concatenate the definitions made in this compliment until now, we may define the new quantity to be considered in the Ω coefficients [Eqs. (14.44)–(14.46)]

$$\vec{\vec{\mathfrak{X}}}^{\pm}(\vec{q}_\parallel,\vec{k}_\parallel) = \int_{-d}^{0}\int_{-d}^{0}\int_{-d}^{0}\int_{-d}^{0} \vec{\vec{\Xi}}(z,z',z'',z''';\vec{q}_\parallel,\vec{k}_\parallel)e^{-iq_\perp z'}e^{\pm iq_\perp z}dz'''dz''dz'dz. \tag{C.169}$$

As we did with the $\mathcal{Z}$ coefficients, the modification before integration have led us to define the new quantity in fraktur rather as Ξ.

Then the nonlinear conductivity tensors combined with the z-dependent parts of the probe and the Ω coefficient can be written

$$\mathfrak{X}^{A\pm}_{xxxx}(\vec{q}_\parallel, \vec{k}_\parallel) = \frac{2}{(i\omega)^3} \sum_{nm} \mathfrak{Z}^{A\pm}_{nm} \varsigma^A_{nm}, \tag{C.170}$$

$$\mathfrak{X}^{B\pm}_{xxkh}(\vec{q}_\parallel, \vec{k}_\parallel) = \frac{2}{(i\omega)^3} \left(\frac{e\hbar}{2m_e}\right)^2 \sum_{nmv} \mathfrak{Z}^{B\pm}_{kh,nmv} \varsigma^B_{kh,nmv}(\vec{q}_\parallel, \vec{k}_\parallel), \tag{C.171}$$

$$\mathfrak{X}^{C\pm}_{xxxx}(\vec{q}_\parallel, \vec{k}_\parallel) = \frac{2}{(i\omega)^3} \sum_{nm} \mathfrak{Z}^{C\pm}_{nm} \varsigma^C_{nm}(\vec{q}_\parallel, \vec{k}_\parallel), \tag{C.172}$$

$$\mathfrak{X}^{D\pm}_{xjkx}(\vec{q}_\parallel, \vec{k}_\parallel) = \frac{2}{(i\omega)^3} \left(\frac{e\hbar}{2m_e}\right)^2 \sum_{nmv} \left\{ \mathfrak{Z}^{Da\pm}_{jk,nmv} \varsigma^{Da}_{jk,nmv}(\vec{q}_\parallel, \vec{k}_\parallel) + \mathfrak{Z}^{Db\pm}_{jk,nmv} \varsigma^{Db}_{jk,nmv}(\vec{q}_\parallel, \vec{k}_\parallel) \right\}, \tag{C.173}$$

$$\mathfrak{X}^{E\pm}_{ijxx}(\vec{q}_\parallel, \vec{k}_\parallel) = \frac{2}{(i\omega)^3} \left(\frac{e\hbar}{2m_e}\right)^2 \sum_{nmv} \left\{ \mathfrak{Z}^{Ea\pm}_{ij,nmv} \varsigma^{Ea}_{ij,nmv}(\vec{q}_\parallel, \vec{k}_\parallel) + \mathfrak{Z}^{Eb\pm}_{ij,nmv} \varsigma^{Eb}_{ij,nmv}(\vec{q}_\parallel, \vec{k}_\parallel) \right\}, \tag{C.174}$$

$$\mathfrak{X}^{F\pm}_{ixxh}(\vec{q}_\parallel, \vec{k}_\parallel) = \frac{2}{(i\omega)^3} \left(\frac{e\hbar}{2m_e}\right)^2 \sum_{nmv} \left\{ \mathfrak{Z}^{Fa\pm}_{ih,nmv} \varsigma^{Fa}_{ih,nmv}(\vec{q}_\parallel, \vec{k}_\parallel) + \mathfrak{Z}^{Fb\pm}_{ih,nmv} \varsigma^{Fb}_{ih,nmv}(\vec{q}_\parallel, \vec{k}_\parallel) \right\}, \tag{C.175}$$

$$\mathfrak{X}^{G\pm}_{ijkh}(\vec{q}_\parallel, \vec{k}_\parallel) = \frac{2}{(i\omega)^3} \left(\frac{e\hbar}{2m_e}\right)^4 \sum_{nmvl} \left\{ \mathfrak{Z}^{Ga\pm}_{ijkh,nmvl} \varsigma^{Ga}_{ijkh,nmvl}(\vec{q}_\parallel, \vec{k}_\parallel) \right.$$
$$\left. + \mathfrak{Z}^{Gb\pm}_{ijkh,nmvl} \varsigma^{Gb}_{ijkh,nmvl}(\vec{q}_\parallel, \vec{k}_\parallel) + \mathfrak{Z}^{Gc\pm}_{ijkh,nmvl} \varsigma^{Gc}_{ijkh,nmvl}(\vec{q}_\parallel, \vec{k}_\parallel) \right\}, \tag{C.176}$$

in terms of the $\mathfrak{Z}$ coefficients just calculated.

C.10 The local limit in three coordinates

In the local limit, the vector potentials (and electric fields) are independent of their z-coordinate, and thus the nonlinear conductivity tensor alone has to be integrated over the z''', z'', and z' coordinates, viz.

$$\bar{\bar{\Xi}}(z; \vec{q}_\parallel, \vec{k}_\parallel) = \iiint \bar{\bar{\Xi}}(z, z', z'', z'''; \vec{q}_\parallel, \vec{k}_\parallel) dz''' dz'' dz'. \tag{C.177}$$

C.11 Analytical expressions for C, $\mathcal{D}$, and $\mathcal{N}$

In the quantity $C(q_\parallel - k_\parallel)$, given by Eq. (10.5), $\beta = 1$ in Eq. (B.1) and $p = 0$, and in the quantity $\mathcal{D}(q_\parallel, k_\parallel)$ [Eq. (10.6)], $\beta = p = 2$. In the quantity $\mathcal{N}$ [Eq. (10.13)], $p = a_k = 0$ and $b_k = 1$, and it can be solved immediately, with the result

$$\mathcal{N} = \frac{4}{(2\pi)^2} \int_0^\alpha \int_0^\pi r d\theta dr = \frac{\alpha^2}{2\pi}. \tag{C.178}$$

Using the analysis in Appendix B, the quantities $C(q_\parallel \pm k_\parallel)$ and $\mathcal{D}(q_\parallel, k_\parallel)$ can be expressed as

$$C(q_\parallel \pm k_\parallel) = 2\left[\mathcal{F}_0^1(a_1, b_1, q_\parallel \pm k_\parallel) - \mathcal{F}_0^1(a_1, b_1, 0)\right], \tag{C.179}$$

and

$$
\begin{aligned}
\mathcal{D}(q_\parallel, k_\parallel) = 2\big[&\mathcal{F}_2^2(a_2, a_3, b_2, b_3, 0) - \mathcal{F}_2^2(a_2, a_3, b_2, b_3, k_\parallel) \\
&+\mathcal{F}_2^2(a_2, a_4, b_2, b_4, k_\parallel + q_\parallel) - \mathcal{F}_2^2(a_2, a_4, b_2, b_4, k_\parallel) \\
&+\mathcal{F}_2^2(a_2, a_4, b_2, b_5, 0) - \mathcal{F}_2^2(a_2, a_4, b_2, b_5, q_\parallel) \\
&+\mathcal{F}_2^2(a_2, a_3, b_2, b_6, k_\parallel + q_\parallel) - \mathcal{F}_2^2(a_2, a_3, b_2, b_6, q_\parallel)\big],
\end{aligned}
\tag{C.180}
$$

where

$$a_1 = \hbar(q_\parallel - k_\parallel)/m_e, \tag{C.181}$$
$$a_2 = \hbar(q_\parallel + k_\parallel)/m_e, \tag{C.182}$$
$$a_3 = \hbar k_\parallel/m_e, \tag{C.183}$$
$$a_4 = \hbar q_\parallel/m_e, \tag{C.184}$$
$$b_1 = \hbar(q_\parallel - k_\parallel)^2/(2m_e) - i/\tau, \tag{C.185}$$
$$b_2 = \hbar(q_\parallel + k_\parallel)^2/(2m_e) - i/\tau, \tag{C.186}$$
$$b_3 = \hbar k_\parallel^2/(2m_e) - i/\tau - \omega, \tag{C.187}$$
$$b_4 = \hbar q_\parallel(q_\parallel + 2k_\parallel)/(2m_e) - i/\tau + \omega, \tag{C.188}$$
$$b_5 = \hbar q_\parallel^2/(2m_e) - i/\tau + \omega, \tag{C.189}$$
$$b_6 = \hbar k_\parallel(k_\parallel + 2q_\parallel)/(2m_e) - i/\tau - \omega. \tag{C.190}$$

C.12 Analytic expressions for the Q quantities

Let us finish this appendix by giving the solutions to Eqs. (14.11)–(14.14). They are

$$
\begin{aligned}
Q_{nm}^{xx}(\vec{q}_\parallel, \omega) = \frac{2i\hbar}{(2\pi)^2}\left(\frac{e\hbar}{2m_e}\right)^2 \\
\times \big[&4\mathcal{F}_{20,n}^2(a_1, a_2, b_{1,nm}, b_{2,nm}, q_x) + 4q_x\mathcal{F}_{10,n}^2(a_1, a_2, b_{1,nm}, b_{2,nm}, q_x) \\
&+q_x^2\mathcal{F}_{00,n}^2(a_1, a_2, b_{1,nm}, b_{2,nm}, q_x) - 4\mathcal{F}_{20,m}^2(a_1, a_2, b_{1,nm}, b_{2,nm}, 0) \\
&-4q_x\mathcal{F}_{10,m}^2(a_1, a_2, b_{1,nm}, b_{2,nm}, 0) - q_x^2\mathcal{F}_{00,m}^2(a_1, a_2, b_{1,nm}, b_{2,nm}, 0)\big],
\end{aligned}
\tag{C.191}
$$

$$
\begin{aligned}
Q_{nm}^{xz}(\vec{q}_\parallel, \omega) = \frac{2i\hbar}{(2\pi)^2}\left(\frac{e\hbar}{2m_e}\right)^2 \\
\times \big[&2\mathcal{F}_{10,n}^2(a_1, a_2, b_{1,nm}, b_{2,nm}, q_x) + q_x\mathcal{F}_{00,n}^2(a_1, a_2, b_{1,nm}, b_{2,nm}, q_x)
\end{aligned}
$$

$$-2\,\mathcal{F}_{10,m}^2(a_1,a_2,b_{1,nm},b_{2,nm},0) - q_x\,\mathcal{F}_{00,m}^2(a_1,a_2,b_{1,nm},b_{2,nm},0)\big]\,, \tag{C.192}$$

$$Q_{nm}^{yy}(\vec{q}_{\parallel},\omega) = \frac{2i\hbar}{(2\pi)^2}\left(\frac{e\hbar}{2m_e}\right)^2$$
$$\times 4\left[\mathcal{F}_{02,n}^2(a_1,a_2,b_{1,nm},b_{2,nm},q_x) - \mathcal{F}_{02,m}^2(a_1,a_2,b_{1,nm},b_{2,nm},0)\right]\,, \tag{C.193}$$

$$Q_{nm}^{zz}(\vec{q}_{\parallel},\omega) = \frac{2i\hbar}{(2\pi)^2}\left(\frac{e\hbar}{2m_e}\right)^2$$
$$\times\left[\mathcal{F}_{00,n}^2(a_1,a_2,b_{1,nm},b_{2,nm},q_x) - \mathcal{F}_{00,m}^2(a_1,a_2,b_{1,nm},b_{2,nm},0)\right]\,, \tag{C.194}$$

according to the treatment of these types of integrals given in Complement B. Above we have used

$$a_1 = a_2 = \frac{\hbar q_x}{m_e}, \tag{C.195}$$

$$b_{1,nm} = \varepsilon_n - \varepsilon_m + \frac{\hbar q_x^2}{2m_e} - \frac{i\hbar}{\tau_{nm}}, \tag{C.196}$$

$$b_{2,nm} = \varepsilon_n - \varepsilon_m + \frac{\hbar q_x^2}{2m_e} - \frac{i\hbar}{\tau_{nm}} - \hbar\omega. \tag{C.197}$$

Appendix D

Fermi energy, quantum well thickness, and $\alpha(n)$

The number of electrons $n(\vec{r})$ in a system where the spin energies are degenerate can be written

$$n(\vec{r}) = 2\sum_N |\Psi_N(\vec{r})|^2 f_N, \tag{D.1}$$

where the number 2 represents the degeneracy of the spin energies, and the sum runs over all electron states in the system multiplied by the probability of finding an electron in that state. This probability is given as a Fermi-Dirac distribution

$$f_N = \frac{1}{1 + \exp((\mathcal{E}_N - \mu)/(k_B T))}, \tag{D.2}$$

where $\mathcal{E}_N$ is the energy of the electron in state N, μ is the chemical potential, k_B is Boltzmann's constant and T is the absolute temperature.

We will now look at the case where we have two-dimensional translational invariance along the x-y-plane. In this case the wave function gives plane-wave solutions in the direction of the plane,

$$\Psi_N(\vec{r}) = \frac{1}{2\pi}\psi_n(z)e^{i\vec{\kappa}_\parallel \cdot \vec{r}} \tag{D.3}$$

and the corresponding energy is

$$\mathcal{E}_N = \varepsilon_n + \frac{\hbar^2 \kappa_\parallel^2}{2m_e}, \tag{D.4}$$

where $\kappa_\parallel = |\kappa_\parallel|$. By insertion into Eq. (D.1), it is converted into

$$n(z) = 2\sum_n |\psi_n(z)|^2 \int_{-\infty}^{\infty} \left(1 + \exp\left[\frac{\varepsilon_n + (\hbar^2 \kappa_\parallel^2)/(2m_e) - \mu}{k_B T}\right]\right)^{-1} \frac{d^2\kappa_\parallel}{(2\pi)^2}, \tag{D.5}$$

taking into account that the sum over the plane-wave expansion parallel to the surface can be converted into an integral, and the notation $n(z) \equiv n(\vec{r})$ is introduced for consistency. Solving the integral, we get

$$n(z) = \frac{2m}{\hbar^2}\sum_n G_n |\psi_n(z)|^2, \tag{D.6}$$

165

with

$$G_n = \frac{k_B T}{2\pi} \ln \left[1 + \exp \left(\frac{\mu - \varepsilon_n}{k_B T} \right) \right]$$ (D.7)

as the number of electrons in the quantum well for any temperature T.

D.1 Fermi energy in the low temperature limit

In the low temperature limit, the chemical potential obeys,

$$\lim_{T \to 0} \mu = \mathcal{E}_F,$$ (D.8)

where $\mathcal{E}_F$ is the Fermi energy. Then

$$G_n = \begin{cases} 0 & \text{for } \varepsilon_n > \mathcal{E}_F, \\ (\mathcal{E}_F - \varepsilon_n)/(2\pi) & \text{for } \varepsilon_n < \mathcal{E}_F, \end{cases}$$ (D.9)

for $T \to 0$, and thus

$$n(z)|_{T \to 0} = \frac{m}{\pi \hbar^2} \sum_n (\mathcal{E}_F - \varepsilon_n) \Theta(\mathcal{E}_F - \varepsilon_n) |\psi_n(z)|^2$$ (D.10)

is the number of electrons (negative charges) in the system.

Additionally, the global neutrality condition teaches that if the net electric charge should be zero, the number of positive charges should be equal to the number of negative charges, that is

$$\begin{aligned} ZN_+ d &= \int n(z) dz \\ &= \frac{m}{\pi \hbar^2} \sum_n (\mathcal{E}_F - \varepsilon_n) \Theta(\mathcal{E}_F - \varepsilon_n) \int |\psi_n(z)|^2 dz \\ &= \frac{m}{\pi \hbar^2} \sum_n (\mathcal{E}_F - \varepsilon_n) \Theta(\mathcal{E}_F - \varepsilon_n) \end{aligned}$$ (D.11)

where N_+ is the number of positive ions per unit volume and Z is the valence of each of these ions.

Defining the quantity N_F as the index of the highest occupied level, this may be rewritten into

$$ZN_+ d = \frac{m}{\pi \hbar^2} \sum_{n=1}^{N_F} (\mathcal{E}_F - \varepsilon_n),$$ (D.12)

from which the Fermi energy easily is extracted as

$$\mathcal{E}_F = \frac{1}{N_F} \left[\frac{\pi \hbar^2}{m_e} ZN_+ d + \sum_{n=1}^{N_F} \varepsilon_n \right].$$ (D.13)

D.2 Infinite barrier quantum well

In the infinite barrier model for a quantum well extending from 0 to $-d$ in the z-direction and infinitely in the x-y-plane, we have

$$\varepsilon_n = \frac{\pi^2 \hbar^2 n^2}{2m_e d^2}, \tag{D.14}$$

which inserted into Eq. (D.13) gives

$$\mathcal{E}_F = \frac{1}{N_F} \left[\frac{\pi \hbar^2}{m_e} ZN_+ d + \frac{\pi^2 \hbar^2}{2m_e d^2} \sum_{n=1}^{N_F} n^2 \right]$$
$$= \frac{\pi \hbar^2}{N_F m_e} \left[ZN_+ d + \frac{\pi}{2d^2} \frac{N_F(N_F + 1)(2N_F + 1)}{6} \right]. \tag{D.15}$$

From this equation, the limits on the thickness of the quantum well can be determined if we know the number of bound states we want below the Fermi level, the minimal thickness for the quantum well to have n levels being determined from the simple relation $\mathcal{E}_F = \varepsilon_n$, and thus the maximal thickness can be determined from $\mathcal{E}_F = \varepsilon_{n+1}$, since it has the same limit value as the minimal thickness to obtain $n+1$ bound states. Thus, for n bound states below the Fermi level,

$$\frac{\pi \hbar^2}{nm_e} \left[ZN_+ d + \frac{\pi}{2d^2} \frac{n(n+1)(2n+1)}{6} \right] = \frac{\pi^2 \hbar^2 n^2}{2m_e d^2}, \tag{D.16}$$

which gives the related minimal and maximal thicknesses to have these n bound states

$$d_{\min}^n = \sqrt[3]{\frac{\pi n}{2ZN_+} \left[n^2 - \frac{(n+1)(2n+1)}{6} \right]},$$
$$d_{\max}^n = \sqrt[3]{\frac{\pi(n+1)}{2ZN_+} \left[(n+1)^2 - \frac{(n+2)(2n+3)}{6} \right]}. \tag{D.17}$$

For a quantum well with only a single bound state we thus get

$$d_{\min}^{(1)} = 0,$$
$$d_{\max}^{(1)} = \sqrt[3]{3\pi/2ZN_+}, \tag{D.18}$$

for two bound states

$$d_{\min}^{(2)} = \sqrt[3]{3\pi/2ZN_+},$$
$$d_{\max}^{(2)} = \sqrt[3]{39\pi/6ZN_+}, \tag{D.19}$$

and so on.

Since $\hbar^2 k_F^2 = 2m_e \mathcal{E}_F$, the radius of the two-dimensional Fermi circle for state n, $\alpha(n)$, used as integration boundary in Appendix B can be found using Eq. (D.15). It is

$$\alpha(n) = \sqrt{\frac{\pi ZN_+ d}{N_F} + \frac{\pi^2}{2d} \frac{(N_F + 1)(2N_F + 1)}{6} - \frac{n^2 \pi^2}{d^2}}. \tag{D.20}$$

Appendix E

Solution to integrals over z in Chapter 14

In this appendix we give some intermediate steps of the solution to integrals in the quantity $\vec{\vec{K}}(\vec{q}_\parallel, \omega)$ appering in the description of the multilevel quantum well in Chapter 14.

Inserting the expressions for the different F quantities [Eqs. (14.18)–(14.22)] into Eqs. (14.26)–(14.30), we get

$$K_{xx,mn}^{vl}(\vec{q}_\parallel, \omega) = -i\mu_0\omega\left\{ Q_{lv}^{xx}(\vec{q}_\parallel, \omega) \iint \mathcal{Z}_{mn}^x(z) G_{xx}(z, z''; \vec{q}_\parallel, \omega) \mathcal{Z}_{lv}^x(z'') dz'' dz \right.$$

$$\left. -iQ_{lv}^{xz}(\vec{q}_\parallel, \omega) \iint \mathcal{Z}_{mn}^x(z) G_{xz}(z, z''; \vec{q}_\parallel, \omega) \mathcal{Z}_{lv}^z(z'') dz'' dz \right\}, \tag{E.1}$$

$$K_{xz,mn}^{vl}(\vec{q}_\parallel, \omega) = i\mu_0\omega\left\{ iQ_{lv}^{xz}(\vec{q}_\parallel, \omega) \iint \mathcal{Z}_{mn}^x(z) G_{xx}(z, z''; \vec{q}_\parallel, \omega) \mathcal{Z}_{lv}^x(z'') dz'' dz \right.$$

$$\left. +Q_{lv}^{zz}(\vec{q}_\parallel, \omega) \iint \mathcal{Z}_{mn}^x(z) G_{xz}(z, z''; \vec{q}_\parallel, \omega) \mathcal{Z}_{lv}^z(z'') dz'' dz \right\}, \tag{E.2}$$

$$K_{yy,mn}^{vl}(\vec{q}_\parallel, \omega) = -i\mu_0\omega Q_{lv}^{yy}(\vec{q}_\parallel, \omega) \iint \mathcal{Z}_{mn}^x(z) G_{yy}(z, z''; \vec{q}_\parallel, \omega) \mathcal{Z}_{lv}^x(z'') dz'' dz, \tag{E.3}$$

$$K_{zx,mn}^{vl}(\vec{q}_\parallel, \omega) = -i\mu_0\omega\left\{ Q_{lv}^{xx}(\vec{q}_\parallel, \omega) \frac{q_\parallel}{q_\perp} \iint \mathcal{Z}_{mn}^z(z) G_{xx}(z, z''; \vec{q}_\parallel, \omega) \mathcal{Z}_{lv}^x(z'') dz'' dz \right.$$

$$\left. -iQ_{lv}^{xz}(\vec{q}_\parallel, \omega) \frac{q_\parallel}{q_\perp} \iint \mathcal{Z}_{mn}^z(z) G_{xz}(z, z''; \vec{q}_\parallel, \omega) \mathcal{Z}_{lv}^z(z'') dz'' dz \right\}, \tag{E.4}$$

$$K_{zz,mn}^{vl}(\vec{q}_\parallel, \omega) = i\mu_0\omega\left\{ iQ_{lv}^{xz}(\vec{q}_\parallel, \omega) \frac{q_\parallel}{q_\perp} \iint \mathcal{Z}_{mn}^z(z) G_{xx}(z, z''; \vec{q}_\parallel, \omega) \mathcal{Z}_{lv}^x(z'') dz'' dz \right.$$

$$\left. +Q_{lv}^{zz}(\vec{q}_\parallel, \omega) \frac{q_\parallel}{q_\perp} \iint \mathcal{Z}_{mn}^z(z) G_{xz}(z, z''; \vec{q}_\parallel, \omega) \mathcal{Z}_{lv}^z(z'') dz'' dz \right\}. \tag{E.5}$$

Using an infinite barrier potential along the z-direction of the quantum well, the $\mathcal{Z}(z)$ quantities are described in Eqs. (14.34) and (14.35). Then by use of Gradshteyn and Ryzhik (1994), Eqs. 2.663.1 and 2.663.3,

$$\int e^{ax}\sin(bx)dx = \frac{e^{ax}[a\sin(bx) - b\cos(bx)]}{a^2 + b^2}, \tag{E.6}$$

$$\int e^{ax}\cos(bx)dx = \frac{e^{ax}[a\cos(bx) + b\sin(bx)]}{a^2 + b^2}, \tag{E.7}$$

we find that integrals over the source region takes the form

$$\int_{-d}^{0} e^{ax} \sin\left(\frac{b\pi x}{d}\right) dx = \frac{\pi b d[e^{-ad}(-1)^b - 1]}{a^2 d^2 + \pi^2 b^2},$$

(E.8)

$$\int_{-d}^{0} e^{ax} \cos\left(\frac{b\pi x}{d}\right) dx = \frac{ad^2[1 - e^{-ad}(-1)^b]}{a^2 d^2 + \pi^2 b^2},$$

(E.9)

in which b is an integer. This result leads to

$$\int G_{xx}(z,z';\vec{q}_{\parallel},\omega) \mathscr{Z}_{nm}^x(z') dz' =$$
$$\frac{2\pi^2 nm c_0^2 q_\perp^2 d \left[1 + r^p - \left(e^{-iq_\perp d} + r^p e^{iq_\perp d}\right)(-1)^{n+m}\right]}{\omega^2[(iq_\perp d)^2 + \pi^2(n-m)^2][(iq_\perp d)^2 + \pi^2(n+m)^2]} e^{-iq_\perp z},$$

(E.10)

$$\int G_{xz}(z,z';\vec{q}_{\parallel},\omega) \mathscr{Z}_{nm}^x(z') dz' =$$
$$\frac{2\pi^2 nm c_0^2 q_\parallel q_\perp d \left[1 - r^p - \left(e^{-iq_\perp d} - r^p e^{iq_\perp d}\right)(-1)^{n+m}\right]}{\omega^2[(iq_\perp d)^2 + \pi^2(n-m)^2][(iq_\perp d)^2 + \pi^2(n+m)^2]} e^{-iq_\perp z},$$

(E.11)

$$\int G_{yy}(z,z';\vec{q}_{\parallel},\omega) \mathscr{Z}_{nm}^x(z') dz' =$$
$$\frac{2\pi^2 nmd \left[1 - r^s - \left(e^{-iq_\perp d} - r^s e^{iq_\perp d}\right)(-1)^{n+m}\right]}{[(iq_\perp d)^2 + \pi^2(n-m)^2][(iq_\perp d)^2 + \pi^2(n+m)^2]} e^{-iq_\perp z},$$

(E.12)

$$\int G_{xz}(z,z';\vec{q}_{\parallel},\omega) \mathscr{Z}_{nm}^z(z') dz' =$$
$$\frac{2\pi^4 nm(n^2 - m^2) c_0^2 q_\parallel [(e^{-iq_\perp d} + r^p e^{iq_\perp d})(-1)^{n+m} - 1 - r^p]}{i\omega^2 d[(iq_\perp d)^2 + \pi^2(n-m)^2][(iq_\perp d)^2 + \pi^2(n+m)^2]} e^{-iq_\perp z},$$

(E.13)

and

$$\int \mathscr{Z}_{mn}^x(z) e^{-iq_\perp z} dz = \frac{4\pi^2 nm i q_\perp d[e^{iq_\perp d}(-1)^{n+m} - 1]}{[(iq_\perp d)^2 + \pi^2(n-m)^2][(iq_\perp d)^2 + \pi^2(n+m)^2]},$$

(E.14)

$$\int \mathscr{Z}_{mn}^z(z) e^{-iq_\perp z} dz = \frac{4\pi^4 nm(n^2 - m^2)[e^{iq_\perp d}(-1)^{n+m} - 1]}{d[(iq_\perp d)^2 + \pi^2(n-m)^2][(iq_\perp d)^2 + \pi^2(n+m)^2]},$$

(E.15)

since $(-1)^{n-m} = (-1)^{n+m}$ for n and m integers. Then

$$F_{nm}^{xx}(z;\vec{q}_{\parallel},\omega) = -\frac{2\pi^2 inm}{\varepsilon_0 \omega} e^{-iq_\perp z} \left\{ Q_{nm}^{xx}(\vec{q}_{\parallel},\omega) q_\perp^2 d + Q_{nm}^{xz}(\vec{q}_{\parallel},\omega) \frac{\pi^2(n^2 - m^2)q_\parallel}{d} \right\}$$
$$\times \frac{1 + r^p - \left(e^{-iq_\perp d} + r^p e^{iq_\perp d}\right)(-1)^{n+m}}{[(iq_\perp d)^2 + \pi^2(n-m)^2][(iq_\perp d)^2 + \pi^2(n+m)^2]}$$

(E.16)

$$F_{nm}^{xz}(z;\vec{q}_{\parallel},\omega) = \frac{2\pi^2 inm}{\varepsilon_0 \omega} e^{-iq_\perp z} \left\{ iQ_{nm}^{xz}(\vec{q}_{\parallel},\omega) q_\perp^2 d - Q_{nm}^{zz}(\vec{q}_{\parallel},\omega) \frac{\pi^2(n^2 - m^2)q_\parallel}{id} \right\}$$
$$\times \frac{1 + r^p - \left(e^{-iq_\perp d} + r^p e^{iq_\perp d}\right)(-1)^{n+m}}{[(iq_\perp d)^2 + \pi^2(n-m)^2][(iq_\perp d)^2 + \pi^2(n+m)^2]},$$

(E.17)

$$F_{nm}^{yy}(z; \vec{q}_{\parallel}, \omega) = -2\pi^2 i\mu_0 \omega nmd e^{-iq_{\perp}z} Q_{nm}^{yy}(\vec{q}_{\parallel}, \omega)$$

$$\times \frac{1 - r^s - \left(e^{-iq_{\perp}d} - r^s e^{iq_{\perp}d}\right)(-1)^{n+m}}{[(iq_{\perp}d)^2 + \pi^2(n-m)^2][(iq_{\perp}d)^2 + \pi^2(n+m)^2]}, \tag{E.18}$$

If we now insert Eqs. (E.16)–(E.18), (14.21) and (14.22) into Eqs. (E.1)–(E.5) and perform the remaining integration, we get Eqs. (14.26)–(14.30).

Bibliography

Abbe, E. (1873). Beiträge zur Theorie des Mikroskops und der Mikroskopischen Wahrnehmung. *Archiv f. Mikroskop. Anat. 9*, 413–468.

Ackerhalt, J. R. and P. W. Milonni (1984). Interaction Hamiltonian of quantum optics. *J. Opt. Soc. Amer. B 1*, 116–120.

Agarwal, G. S. and S. D. Gupta (1995). Evanescent coupling of a dipole to a phase conjugate mirror. *Opt. Commun. 119*, 591–596.

Agarwal, G. S. (1982). Dipole Radiation in the Presence of a Phase Conjugate Mirror *Opt. Commun. 42*, 205–207.

Aktsipetrov, O. A., A. A. Fedyanin, and M. C. Downer (1996). Dc-Electric-Field Induced Second-Harmonic Generation Studies of Surfaces and Buried Interfaces of Column IV Semiconductors. In O. Keller (Ed.), *Notions and Perspectives of Nonlinear Optics*, pp. 301–338. Singapore: World Scientific. ISBN 981-02-2627-6.

Aktsipetrov, O. A., A. V. Melnikov, T. V. Murzina, A. A. Nikulin, and A. N. Rubtsov (1995). DC-electric-field-induced optical second harmonic generation at the smooth metal-electrolyte interface. *Surf. Sci. 336*, 225.

Andersen, T. and O. Keller (1998). Local-field theory for optical phase conjugation by degenerate four wave mixing in mesoscopic interaction volumes of condensed media. *Phys. Scripta 58*. In press.

Arnoldus, H. F. and T. F. George (1995). Theory of optical phase conjugation in Kerr media. *Phys. Rev. A 51*, 4250–4263.

Arutyunyan, G. V. and G. P. Dzhotyan (1987). Phase conjugation in a field of surface reference waves. *Opt. Spektrosk. 63*, 575–578. [English translation (1987): *Opt. Spectrosc. (USSR) 63*, 338–339].

Ash, E. A. and G. Nichols (1972). Super-resolution aperture scanning microscope. *Nature 237*, 510–513.

Ashcroft, N. W. and N. D. Mermin (1976). *Solid State Physics*. New York: Holt, Rinehart and Winston. ISBN 0-03-083993-9.

Bagchi, A., R. G. Barrera, and A. K. Rajagopal (1979). Perturbative approach to the calculation of the electric field near a metal surface. *Phys. Rev. B 20*, 4824–4838.

Bavli, R. and Y. B. Band (1991). Sum and difference frequency generation in a two-level system with permanent dipole moments. *Phys. Rev. A 43*, 5044–5048.

Bethe, H. A. (1944). Theory of Diffraction by Small Holes. *Phys. Rev. 66*, 163–182.

Bloembergen, N. (1965). *Nonlinear Optics*. Reading, Massachusetts: W.A. Benjamin. ISBN 0-8053-0938-1.

Bloembergen, N., H. Lotem, and R. T. Lynch Jr. (1978). Lineshapes in Coherent Resonant Raman Scattering. *Indian J. Pure & Appl. Phys. 16*, 151–158.

Bloom, D. M. and G. C. Bjorklund (1977). Conjugate wave-front generation and image reconstruction by four-wave mixing. *Appl. Phys. Lett. 31*, 592–594.

Bohm, D. (1951). *Quantum Theory*. New York: Prentice-Hall.

Born, M. and E. Wolf (1980). *Principles of Optics, Sixth edition*. Oxford: Pergamon Press. ISBN 0-08-026481-6.

Bouwkamp, C. J. (1950a). On Bethe's theory of diffraction by small holes. *Philips Research Reports 5*, 321–332.

Bouwkamp, C. J. (1950b). On the diffraction of electromagnetic waves by small circular disks and holes. *Philips Research Reports 5*, 401–422.

Boyd, R. W. (1992). *Nonlinear Optics*. San Diego: Academic Press. ISBN 0-12-121680-2.

Bozhevolnyi, S. I. (1997). *Subwavelength Apertureless Light Confinement: Near-Field Phase Conjugation, Holography and Surface Polariton Localization*. Aalborg: Institute of Physics, Aalborg University. ISBN 87-89195-14-0.

Bozhevolnyi, S. I., E. A. Bozhevolnaya, and S. Berntsen (1995). Theoretical model for phase conjugation of optical near fields. *J. Opt. Soc. Amer. A 12*, 2645–2654.

Bozhevolnyi, S. I., O. Keller, and I. I. Smolyaninov (1994). Phase conjugation of an optical near field. *Opt. Lett. 19*, 1601–1603.

Bozhevolnyi, S. I., O. Keller, and I. I. Smolyaninov (1995). Scattered light enhancement near a phase conjugating mirror. *Opt. Commun. 115*, 115–120.

Bozhevolnyi, S. I. and I. I. Smolyaninov (1995). Characterization of phase-conjugated near-field light spots. *J. Opt. Soc. Amer. B 12*, 1617–1620.

Bozhevolnyi, S. I. and B. Vohnsen (1997). Phase conjugation of optical near fields by a surface hologram. *Opt. Commun. 135*, 19–23.

Bragg, W. L. (1950). Microscopy by Reconstructed Wave-fronts. *Nature 166*, 399–400.

Brueck, S. R. J. (Ed.) (1989). *Special Issue on Nonlinear Optical Phase Conjugation*. New York: Institute of Elelctric and Electronics Engineers. [*IEEE J. Quantum Electronics 25*, No. 3].

Chen, X. and O. Keller (1997). Photon drag in single and multiple two-level quantum wells. *Phys. Rev. B 55*, 15706–15719.

Cohen-Tannoudji, C., B. Diu, and F. Laloë (1977). *Quantum Mechanics*. Paris: Hermann and Wiley. ISBN 0-471-16433-X (Vol. I) 0-471-16435-X (Vol. II).

den Dekker, A. J. and A. van den Bos (1997). Resolution: a survey. *J. Opt. Soc. Amer. A 14*, 547–557.

Ducloy, M. and D. Bloch (1984). Polarization properties of phase-conjugate mirrors: angular dependence and disorienting collision effects in resonant backward four-wave mixing for Doppler-broadened degenerate transitions. *Phys. Rev. A 30*, 3107–3122.

Einstein, A. (1916). Zur Quantentheorie der Strahlung. *Mitt. d. phys. Ges. Zürich 18*, 47–62.

Einstein, A. (1917). Zur Quantentheorie der Strahlung. *Phys. Z. 18*, 121–128. [Same content as Einstein (1916)].

Farzad, M. H. and M. T. Tavassoly (1997). Degenerate four-wave mixing without slowly varying amplitude approximation. *J. Opt. Soc. Amer. B 14*, 1707–1715.

Fauster, T. and W. Steinmann (1995). Two-photon photoemission spectroscopy of image states. In P. Halevi (Ed.), *Photonic Probes of Surfaces*, pp. 347–411. Amsterdam: North-Holland. ISBN 0-444-82198-8.

Feibelman, P. J. (1975). Microscopic calculation of electromagnetic fields in refraction at a jellium-vacuum interface. *Phys. Rev. B 12*, 1319–1336.

Feibelman, P. J. (1982). Surface electromagnetic fields. *Prog. Surf. Sci. 12*, 287–408.

Fischer, U. C. (1985). Optical characteristics of 0.1μm circular apertures in a metal film as light sources for scanning ultramicroscopy. *J. Vac. Sci. Technol. 83*, 386–390.

Fischer, U. C. and D. W. Pohl (1989). Observation of Single-Particle Plasmons by Near-Field Optical Microscopy. *Phys. Rev. Lett. 62*, 458–461.

Fisher, R. A. (Ed.) (1983). *Optical Phase Conjugation.* New York: Academic Press. ISBN 0-12-257740-X.

Franken, P. A., A. E. Hill, C. W. Peters, and G. Weinrich (1961). Generation of optical harmonics. *Phys. Rev. Lett. 7*, 118–119.

Fukui, M., J. E. Sipe, V. C. Y. So, and G. I. Stegeman (1978). Nonlinear mixing of oppositely travelling surface plasmons. *Solid State Commun. 27*, 1265–1267.

Gabor, D. (1948). A new microscopic principle. *Nature 161*, 777–778.

Gabor, D. (1949). Microscopy by reconstructed wave-fronts. *Proc. Roy. Soc. A 197*, 454–486.

Garcia-Vidal, F. J. and J. B. Pentry (1996). Collective Theory for Surface Enhanced Raman Scattering. *Phys. Rev. Lett. 77*, 1163.

Gavrila, M. (Ed.) (1992). *Atoms in Intense Laser Fields*. Boston: Academic Press. ISBN 0-12-003901-X.

Georges, A. T. (1995). Theory of the multiphoton photoelectric effect: A stepwise excitation process. *Phys. Rev. B 51*, 13735–13738.

Gerritsen, H. J. (1967). Nonlinear effects in image formation. *Appl. Phys. Lett. 10*, 239–241.

Goldstein, E. V., K. Plättner, and P. Meystre (1995). Atomic phase conjugation. *J. Eur. Opt. Soc. B 7*, 743–749.

Goodman, J. W. (Ed.) (1983). *Optical Phase Conjugation.* New York: Optical Society of America. [*J. Opt. Soc. Amer. 73*, No. 5].

Goossens, M., F. Mittelbach, and A. Samarin (1994). *The LaTeX Companion.* Reading, Massachusetts: Addison-Wesley. ISBN 0-201-54199-8.

Goossens, M., S. Rahtz, and F. Mittelbach (1997). *The LATEX Graphics Companion.* Reading, Massachusetts: Addison-Wesley. ISBN 0-201-85469-4.

Gordon, J. P., H. J. Zeiger, and C. H. Townes (1954). Molecular Microwave Oscillator and New Hyperfine Structure in the Microwave Spectrum of NH_3. *Phys. Rev. 95*, 282–284.

Gordon, J. P., H. J. Zeiger, and C. H. Townes (1955). The Maser—New Type of Microwave Amplifier, Frequency Standard, and Spectrometer. *Phys. Rev. 99*, 1264–1274.

Gower, M. and D. Proch (Eds.) (1994). *Optical Phase Conjugation.* Berlin: Springer-Verlag. ISBN 3-540-56703-8.

Gradshteyn, I. S. and I. M. Ryzhik (1994). *Table of Integrals, Series, and Products.* London: Academic Press. ISBN 0-12-294755-X.

Haight, R. (1995). Electron dynamics at surfaces. *Surf. Sci. Rep. 21*, 275–325.

Heinz, T. F. (1991). Second-Order Nonlinear Optical Effects at Surfaces and Interfaces. In H.-E. Ponath and G. I. Stegeman (Eds.), *Nonlinear Surface Electromagnetic Phenomena*, pp. 353–416. Amsterdam: Elsevier. ISBN 0-444-88359-2.

Hellwarth, R. (1977). Third-order optical susceptibilities of liquids and solids. *Prog. Quantum Electron. 5*, 1–68.

Hellwarth, R. W. (1982). Optical beam phase conjugation by stimulated backscattering. *Optical Engineering 21*, No. 2, 257–262.

Hendriks, B. H. W. and G. Nienhuis (1989). Atomic dipole in front of a phase-conjugate mirror. *Phys. Rev. A 40*, 1892–1898.

van Hulst, N. and A. Lewis (Eds.) (1998). *Near-field Optics and Related Techniques.* Amsterdam: North-Holland. *Ultramicroscopy 71*, Nos. 1–4, 1–398.

Isaacson, M. (Ed.) (1995). *Near-Field Optics.* Amsterdam: North-Holland. *Ultramicroscopy 57*, Nos. 2/3, 113–322.

Jalochowski, M., M. Stróżak, and R. Zdyb (1997). Optical reflectivity of ultrathin Pb layers and the quantum size effect. *Private communication.*

Javan, A., W. R. B. Jr., and D. R. Herriot (1961). Population inversion and continous optical maser oscillation in a gas discharge containing a He-Ne mixture. *Phys. Rev. Lett. 6*, 106–110.

Keller, O. (1992). Nonlocal electrodynamics of an atom in front of a normal or phaseconjugating mirror. *J. Quantum Nonlin. Phenom. 1*, 139–163.

Keller, O. (1993). Photon drag in a single-level metallic quantum well. *Phys. Rev. B 48*, 4786–4798.

Keller, O. (1995). Electromagnetic Self-Action in a BCS-Paired Superconductor: Third-Order Response Function. *J. Quantum Nonlin. Phenom. 2*, 51–70.

Keller, O. (1996a). Local Fields in the Electrodynamics of Mesoscopic Media. *Phys. Rep. 268*, 85–262.

Keller, O. (1996b). Photon Drag in Non-Simply Connected Mesoscopic Media and Quantum Confinement of Light. In O. Keller (Ed.), *Notions and Perspectives of Nonlinear Optics*, pp. 140–233. Singapore: World Scientific. ISBN 981-02-2627-6.

Keller, O. (1996c). Quantum dots of light. *J. Nonl. Opt. Phys. Mat. 5*, 109–132.

Keller, O. (1997a). Aspects of Local-Field Electrodynamics in Condensed Matter. In T. Hakioğlu and A. S. Shumovsky (Eds.), *Quantum Optics and the Spectroscopy of Solids*, pp. 1–44. Dordrecht: Kluwer. ISBN 0-7923-4414-6.

Keller, O. (1997b). Local Fields in Linear and Nonlinear Optics of Mesoscopic Systems. In E. Wolf (Ed.), *Progress in Optics XXXVII*. Amsterdam: Elsevier. ISBN 0-444-82796-X.

Keller, O. (1998). Electromagnetic Propagators in Micro- and Mesoscopic Optics. In D. A. Jelski and T. F. George (Eds.), *Computational Studies of New Materials*. Singapore: World Scientific. ISBN 981-02-3325-6. In press.

Keller, O. and G. Wang (1997). Angular-momentum photon-drag current in a mesoscopic metallic cylinder shell. *Phys. Rev. B 56*, 12327–12338.

Knight, J. C., N. Dubreuil, V. Sandoghdar, J. Hare, V. Lefèvre-Seguin, J. M. Raimond, and S. Haroche (1995). Mapping whispering-gallery modes in microspheres with a near-field probe. *Opt. Lett. 20*, 1515–1517.

Knoester, J. and S. Mukamel (1991). Transient gratings, four-wave mixing and polariton effects in nonlinear optics. *Phys. Rep. 205*, 1–58.

Knuth, D. E. (1984). *The TEXbook*. Reading, Massachusetts: Addison-Wesley. ISBN 0-201-13448-9.

Kogelnik, H. (1965). Holographic Image Projection through Inhomogeneous Media. *Bell System Technical J. 44*, 2451–2455.

Kretschmann, E. and H. Raether (1968). Radiative Decay of Non Radiative Surface Plasmons Excited by Light. *Z. Naturforsch. 23a*, 2135–2136.

Leith, E. N. and J. Upatnieks (1962). Reconstructed Wavefronts and Communication Theory. *J. Opt. Soc. Amer. 52*, 1123–1130.

Leith, E. N. and J. Upatnieks (1964). Wavefront Reconstruction with Diffused Illumination and Three-Dimensional Objects. *J. Opt. Soc. Amer. 54*, 1295–1301.

Lenz, G., P. Meystre, and E. M. Wright (1993). Nonlinear Atom Optics. *Phys. Rev. Lett. 71*, 3271–3274.

Lenz, G., P. Meystre, and E. M. Wright (1994). Nonlinear atom optics: General formalism and atomic solitons. *Phys. Rev. A 50*, 1681–1691.

Lewis, A., M. Isaacson, A. Harootunian, and A. Murray (1984). *Ultramicroscopy 13*, 227–231.

Liebsch, A. (1995). Electronic excitations at metal surfaces. In P. Halevi (Ed.), *Photonic Probes of Surfaces*, pp. 479–532. Amsterdam: North-Holland. ISBN 0-444-82198-8.

von der Linde, D. (1996). Harmonic Generation in Femtosecond Laser-Produced Plasmas. In O. Keller (Ed.), *Notions and Perspectives of Nonlinear Optics*, pp. 234–271. Singapore: World Scientific. ISBN 981-02-2627-6.

Liu, A. and O. Keller (1995). Nonlocal Theory of the Intersubband Optical Kerr Effect in a Semiconductor Quantum Well. *Phys. Scripta 52*, 116–125.

Maiman, T. H. (1960). Stimulated Optical Radiation in Ruby. *Nature 187*, 493–494.

Mamaev, A. V., N. A. Mel'nikov, N. F. Pilipetskiĭ, A. N. Sudarkin, and V. V. Shkunov (1984). Wave-front reversal on a semiconductor surface during plasma reflection. *Zh. Eksp. Teor. Fiz. 86*, 232. [English translation (1984): *Sov. Phys. JETP 59*, 132–137].

Mandel, L. and E. Wolf (1995). *Optical Coherence and Quantum Optics*. Cambridge: Cambridge University Press. ISBN 0-521-41711-2.

Marburger, J. H. (1983). Improvements upon the Simple Theory of Degenerate Four-Wave Mixing. In R. A. Fisher (Ed.), *Optical Phase Conjugation*, pp. 99–125. London: Academic Press. ISBN 0-12-257740-X.

Maxwell, J. C. (1864). On Faraday's Lines of Force. *Trans. Camb. Phil. Soc. X*, 27–83.

Maxwell, J. C. (1891). *A Treatise on Electricity and Magnetism* (third ed.). Clarendon Press. Reprinted by Dover in two volumes, 1954. ISBN 0-486-60636-8 (Vol. I) 0-486-60637-6 (Vol. II).

Metcalf, M. and J. Reid (1996). *Fortran 90/95 explained.* Oxford: Oxford University Press. ISBN 0-19-851888-9.

Milonni, P. W., R. J. Cook, and J. R. Ackerhalt (1989). Natural line shapes. *Phys. Rev. A 40*, 3764–3768.

Mishchenko, E. Z. and L. A. Fal'kovskii (1995). Long-wavelength optical phonons: damping, surface oscillations, and Raman scattering. *Sov. Phys. JETP 80*, 531.

Montemezzani, G. and P. Günter (1996). Inorganic and Organic Photorefractive Materials. In O. Keller (Ed.), *Notions and Perspectives of Nonlinear Optics*, pp. 370–427. Singapore: World Scientific. ISBN 981-02-2627-6.

Mukamel, S. (1995). *Principles of Nonlinear Optical Spectroscopy.* New York: Oxford University Press. ISBN 0-19-509278-3.

Mukhin, Y. V., N. F. Pilipetskiĭ, A. N. Sudarkin, and K. N. Ushakov (1985). Four-wave mixing of surface polaritons. *Dokl. Akad. Nauk SSSR 285*, 874–877. [English translation (1985): *Sov. Phys. Dokl. 30*, 1041–1043].

von Neumann, J. (1932). *Mathematische Grundlagen der Quantenmechanik.* Berlin: Julius Springer. [English translation (1955): *Mathematical Foundations of Quantum Mechanics.* New Jersey: Princeton. ISBN 0-691-08003-8].

Nieto-Vesperinas, M. and N. García (Eds.) (1996). *Optics at the Nanometer Scale: Imaging and Storing with Photonic Near Fields*. Dordrecht: Kluwer. ISBN 0-7923-4020-5.

Nkoma, J. S. (1989). Theory of Raman scattering by surface polaritons in a four-media system. *J. Phys. Cond. Matt. 1*, 9623–9636.

Nosach, O. Y., V. I. Popovichev, V. V. Ragul'skii, and F. S. Faizullov (1972). Cancellation of phase distortions in an amplifying medium with a "Brillouin mirror". *ZhETF Pis. Red. 16*, 617–621.

Nunzi, J. M. and D. Ricard (1984). Optical Phase Conjugation and Related Experiments with Surface Plasma Waves. *Appl. Phys. B 35*, 209–216.

O'Keefe, J. A. (1956). Resolving Power of Visible Light. *J. Opt. Soc. Amer. 46*, 359.

Otto, A. (1968). Excitation of Nonradiative Surface Plasma Waves in Silver by the Method of Frustrated Total reflection. *Z. Phys. 216*, 398.

Otto, A. (1976). Spectroscopy of surface polaritons by attenuated total reflection. In B. O. Seraphin (Ed.), *Optical Properties of Solids – New Developments*, pp. 677–729. Amsterdam: North-Holland. ISBN 0-7204-0363-4.

Paesler, M. and N. van Hulst (Eds.) (1995). *Near-field Optics and Related Techniques*. Amsterdam: North-Holland. *Ultramicroscopy 61*, Nos. 1–4, 1–304.

Paesler, M. A. and P. J. Moyer (1996). *Near-Field Optics: Theory, Instrumentation, and Applications*. New York: Wiley. ISBN 0-471-04311-7.

Pedersen, K. (1995). Second-harmonic generation from surfaces of centrosymmetric media. In O. Keller (Ed.), *Studies in Classical and Quantum Nonlinear Phenomena*, pp. 385–418. New York: Nova Science. ISBN 1-56072-168-5.

Pepper, D. M. (1982). Nonlinear optical phase conjugation. *Optical Engineering 21*, No. 2, 156–186.

Pepper, D. M. (1985). Nonlinear Optical Phase Conjugation. In M. L. Stitch and M. Bass (Eds.), *Laser Handbook, Volume 4*, pp. 333–485. Amsterdam: North-Holland. ISBN 0-444-86927-1.

Pilipetskiĭ, N. F., A. N. Sudarkin, and K. N. Ushakov (1987). Phase conjugation by four-wave mixing of electromagnetic surface waves. *Zh. Eksp. Teor. Fiz. 93*, 118–126. [English translation (1987): *Sov. Phys. JETP 66*, 66–70].

Pohl, D. W. and D. Courjon (Eds.) (1993). *Near Field Optics*. Dordrecht: Kluwer. ISBN 0-7923-2394-7.

Pohl, D. W., W. Denk, and M. Lanz (1984). Optical stethoscopy: Image recording with resolution $\lambda/20$. *Appl. Phys. Lett. 44*, 651–653.

Press, W. H., S. A. Teukolsky, W. T. Vetterling, and B. P. Flannery (1992). *Numerical Recipes in FORTRAN: The Art of Scientific Computing* (2nd ed.). Cambridge: Cambridge University Press. ISBN 0-521-43064-X.

Press, W. H., S. A. Teukolsky, W. T. Vetterling, and B. P. Flannery (1996b). *Numerical Recipes Code CDROM*. Cambridge: Cambridge University Press. ISBN 0-521-57607-5.

Press, W. H., S. A. Teukolsky, W. T. Vetterling, and B. P. Flannery (1996a). *Numerical Recipes in FORTRAN 90: The Art of Parallel Scientific Computing*. Cambridge: Cambridge University Press. ISBN 0-521-57439-0.

Pustogowa, U., W. Hübner, and K. H. Bennemann (1994). Theory for the nonlinear magneto-optical Kerr effect at ferromagnetic transition metal surfaces. *Surf. Sci. 307–309*, A1129–A1133.

Raether, H. (1988). *Surface Plasmons on Smooth and Rough Surfaces and Gratings*. Berlin: Springer-Verlag. ISBN 3-540-17363-3.

Rasing, T. (1996). Nonlinear Optics of Thin Magnetic Films. In O. Keller (Ed.), *Notions and Perspectives of Nonlinear Optics*, pp. 339–369. Singapore: World Scientific. ISBN 981-02-2627-6.

Rasing, T. and M. G. Goerkamp (1995). Giant nonlinear magneto-optic Kerr effect. *Proc. SPIE 2801*, 96–107.

lord Rayleigh (1896). On the Theory of Optical Images, with Spetial Reference to the Microscope. *Phil. Mag. 42*, 167–195.

Reider, G. A. and T. F. Heinz (1995). Second-order nonlinear optical effects at surfaces and interfaces: Recent advances. In P. Halevi (Ed.), *Photonic Probes of Surfaces*, pp. 413–478. Amsterdam: North-Holland. ISBN 0-444-82198-8.

Richmond, G. L., J. M. Robinson, and V. L. Shannon (1988). Second harmonic generation studies of interfacial structure and dynamics. *Prog. Surf. Sci. 28*, 1–70.

Ronchi, V. (1961). Resolving power of calculated and detected images. *J. Opt. Soc. Amer. 51*, 458–460.

Sakai, J.-I. (1992). *Phase Conjugate Optics*. New York: McGraw-Hill. ISBN 0-07-054315-1.

Schawlow, A. L. and C. H. Townes (1958). Infrared and Optical Masers. *Phys. Rev. 112*, 1940–1949.

Schrödinger, E. (1926a). Quantisierung als Eigenwertproblem. *Ann. d. Phys. (IV). 79*, 361–376 (Erste Mitteilung), 489–527 (Zweite Mitteilung), *80*, 437–490 (Dritte Mitteilung: Störungstheorie, mit Anwendung auf den Starkeffekt der Balmerlinien), *81*, 109–139 (Vierte Mitteilung).

Schrödinger, E. (1926b). Über das Verhältnis der Hiesenberg-Born-Jordanschen Quantenmechanik zu der meinen. *Ann. d. Phys. (IV) 79*, 734–756.

Schubert, M. and B. Wilhelmi (1986). *Nonlinear Optics and Quantum Electronics*. New York: Wiley. ISBN 0-471-08807-2.

Shalaev, V. M., C. Douketis, T. Haslett, T. Stuckless, and M. Moskovits (1996). Two-photon electron emission from smooth and rough metal films in the threshold region. *Phys. Rev. B 53*, 11193–11206.

Shen, Y. R. (1984). *The Principles of Nonlinear Optics*. New York: Wiley. ISBN 0-471-88998-9.

Sipe, J. E. and G. I. Stegeman (1982). Nonlinear Optical Response of Metal Surfaces. In V. M. Agranovich and D. L. Mills (Eds.), *Surface Polaritons*, pp. 661–701. Amsterdam: North-Holland. ISBN 0-444-86165-3.

Stegeman, G. I. and C. Karaguleff (1983). Degenerate four wave mixing with long range surface plasmons in attenuated total reflection geometries. *J. Appl. Phys. 54*, 4853–4855.

Syed, K. S., G. J. Crofts, R. P. M. Green, and M. J. Damzen (1996). Vectorial phase conjugation via four-wave mixing in isotropic saturable-gain media. *J. Opt. Soc. Amer. B 14*, 2067–2078.

Synge, E. H. (1928). A Suggested Method for extending Microscopic Resolution into the Ultra-Microscopic Region. *Phil. Mag. 6*, 356–362.

Synge, E. H. (1932). An Application of Piezo-Electricity to Microscopy. *Phil. Mag. 13*, 297–300.

Tergiman, Y. S., K. Warda, C. Girardeau-Montaut, and J.-P. Girardeau-Montaut (1997). Metal surface photoelectric effect: dependence on the dynamic electron distribution function. *Opt. Commun. 142*, 126–134.

Ujihara, K. (1982a). Four-Wave Mixing and Two-Dimensional Phase Conjugation of Surface Plasmons. *Opt. Commun. 42*, 1–4.

Ujihara, K. (1982b). Phase conjugation of surface plasmon waves by the third order nonlinearity of a free electron gas. *Opt. Commun. 43*, 225–228.

Ujihara, K. (1983). Phase conjugation of a bulk wave by surface plasmons. *J. Opt. Soc. Amer. 73*, 610–616.

Vasko, F. T. (1996). Photon drag effect in tunnel-coupled quantum wells. *Phys. Rev. B 53*, 9576–9578.

Vohnsen, B. (1997). *Phase Conjugation of Optical Near Fields*. Aalborg: Institute of Physics, Aalborg University. ISBN 87-89195-13-2.

Wang, G. (1997). *Circulating photon-drag currents in mesoscopic metallic media*. Aalborg: Institute of Physics, Aalborg University. ISBN 87-89195-12-4.

Weisbuch, C. and B. Vinter (1991). *Quantum Semiconductor Structures: Fundamentals and Applications*. San Diego: Academic Press. ISBN 0-12-742680-9.

Whittaker, E. T. (1951). *A History of the Theories of Aether and Electricity I. The Classical Theories*. London: Nelson.

Whittaker, E. T. (1953). *A History of the Theories of Aether and Electricity II. The Modern Theories*. London: Nelson.

Wolf, E. and W. H. Carter (1982). Comments on the theory of phase-conjugated waves. *Opt. Commun. 40*, 397–400.

Yariv, A. (1978). Phase Conjugate Optics and Real-Time Holography. *IEEE J. Quantum Electronics 14*, 650–660.

Yariv, A. (1982). Reply to the paper "Comments on the theory of phase-conjugated waves", by E. Wolf and W. H. Carter. *Opt. Commun. 40*, 401.

Yariv, A. and R. A. Fisher (1983). Introduction. In R. A. Fisher (Ed.), *Optical Phase Conjugation*, pp. 1–22. New York: Academic Press. ISBN 0-12-257740-X.

Yariv, A. and D. M. Pepper (1977). Amplified reflection, phase conjugation, and oscillation in degenerate four-wave mixing. *Opt. Lett. 1*, 16–18.

Yariv, A. and P. Yeh (1984). *Optical Waves in Crystals*. New York: Wiley. ISBN 0-471-09142-1.

Zel'dovich, B. Y., N. F. Pilipetskii, A. N. Sudarkin, and V. V. Shkunov (1980). Wavefront reversal by an interface. *Dokl. Akad. Nauk SSSR 252*, 92–95. [English translation (1980): *Sov. Phys. Dokl. 25*, 377–379].

Zel'dovich, B. Y., N. F. Pilipetsky, and V. V. Shkunov (1985). *Principles of Phase Conjugation*. Berlin: Springer-Verlag. ISBN 3-540-13458-1.

Zel'dovich, B. Y., V. I. Popovichev, V. V. Ragul'skii, and F. S. Faizullov (1972). Connection between the wave fronts of the reflected and exciting light in stimulated Mandel'shtam-Brillouin scattering. *Zh. Eksp. Teor. Fiz. Pis. Red. 15*, 160–164. [English translation (1972): *Sov. Phys. JETP 15*, 109–112].

Dansk resumé

For at studere den mulige fasekonjugation af optiske nærfelter er det nødvendigt at gå ud over den langsomtvarierende indhyldningskurve approksimation samt den elektriske dipoltilnærmelse, der normalt anvendes i fasekonjugationsstudier hvor rumligt udæmpede (eller i det mindste svagt dæmpede) svingninger blandes. I den foreliggende afhandling præsenteres en vilkårlig-fase tilnærmet beregning af den ulineære og ikke-lokale optiske responstensor der beskriver den ulinerære strømtæthed af tredie orden, som genereres af firebølgeblanding i en uensartet elektrongas. Beskrivelsen er baseret på en halvklassisk model, hvori det elektromagnetiske felt antages at være en klassisk størrelse og udgangspunktet er bevægelsesligningen for tæthedsmatrix-operatoren. Vekselvirknings Hamilton-operatoren anvendes i dens minimale koblingsform, og den indeholder det led i strømtæthedsoperatoren, der er proportionalt med det påtrykte vektorpotential. Ved brug af denne formalisme er den rumlige struktur af systemets optiske respons beskrevet ved hjælp af mikroskopiske overgangsstrømtætheder. Beregningen inkluderer derfor både bidrag fra $\vec{p} \cdot \vec{A}$ og $\vec{A} \cdot \vec{A}$ leddene i vekselvirknings-Hamilton-operatoren. Det er vist at der introduceres nogle vigtige fænomener, som er begrebsmæssigt forskellige fra de der har deres oprindelse i $\vec{p} \cdot \vec{A}$-leddet, ved at inkludere $\vec{A} \cdot \vec{A}$ leddet i vekselvirknings Hamilton-operatoren. For at fremhæve den fysiske mening af de forskellige processer er koblingerne mellem observationspunkter for feltet og strømtætheden præsenteret i form af diagrammer. Resultatet af en analyse af tensorsymmetrierne, der er tilknyttet $\vec{p} \cdot \vec{A}$ og $\vec{A} \cdot \vec{A}$ vekselvirkningerne er summeret i form af symmetriskemaer for fasekonjugationsprocessen. Den teoretiske model efterfølges af en beregning af det fasekonjugerede respons fra en et-niveau metallisk kvantebrønd. Et-niveau kvantebrønden repræsenterer den simplest mulige konfiguration en kvantebrønds-fasekonjugator kan have. Ydermere er den et interessant objekt, idet dens optiske respons ikke indeholder noget dipol-led. Diskussionen af responset er baseret på stimulering af processen ved brug af lys, der er polariseret enten i spredningsplanet eller vinkelret på spredningsplanet. Det vises, at fasekonjugationsprocessen er ekstremt effektiv i det dæmpede område af bølgevektor-spektret. Dernæst anskues problemet med at generere plane bølger til excitation i den høje ende af det dæmpede spektrum, og vi diskuterer brugen af en bredbåndskilde (i vinkelspektret) til at stimulere processen. En sådan bredbåndskilde kan være en kvantetråd, og det fasekonjugerede vinkelspektrum fra en kvantetråd præsenteres og diskuteres. Kvantetrådens subbølgelængde størrelse gør den en mulig kandidat til en diskussion af den mulige rumlige komprimering af lys, og rumlig begrænsning af lys foran en et-niveau metallisk kvantebrøndsfasekonjugator er diskuteret i to dimensioner. Det retfærdiggøres at man ved et passende valg af strømtæthedens orientering i kvantetråden kan opnå en feltkomprimering, der er væsentligt på den anden side af Rayleighs grænseværdi. Afhandlingen afsluttes med en kort beskrivelse af det mere generelle tilfælde, hvor kvantebrønden tillades at have mere end en energi-egentilstand. Numeriske resultater, der viser responset hvis en to-niveau kvantebrønd anvendes som fasekonjugerende medium, er præsenteret og diskuteret.

In order to study the possible phase conjugation of optical near-fields, it is necessary to go beyond the slowly varying envelope- and electric dipole approximations that are normally applied in phase conjugation studies where spatially non-decaying (or at least slowly decaying) modes are mixed. In the present dissertation a random-phase-approximation calculation of the nonlocal nonlinear optical response tensor describing the third order nonlinear current density generated by degenerate four-wave mixing in an inhomogeneous electron gas is established. The description is based on a semi-classical approach, in which the electromagnetic field is considered as a classical quantity, and the starting point is the equation of motion for the density matrix operator. The interaction Hamiltonian is taken in its minimal coupling form, and it includes the term in the current density operator which is proportional to the prevailing vector potential. Using this formalism the spatial structure of the optical response of the system is described in terms of the microscopic transition current densities. The calculation thus includes contributions originating from both the $\vec{p} \cdot \vec{A}$ and $\vec{A} \cdot \vec{A}$ terms in the interaction Hamiltonian. It is demonstrated that inclusion of the $\vec{A} \cdot \vec{A}$ term in the interaction Hamiltonian introduces some important phenomena that are conceptually different from those originating in the $\vec{p} \cdot \vec{A}$ part. To emphasize the physical meaning of the various processes, the couplings between observation points for the field and the current density is presented in a diagrammatic form. The result of an analysis of the tensor symmetries associated with the $\vec{p} \cdot \vec{A}$ and $\vec{A} \cdot \vec{A}$ interactions are summarized in terms of symmetry schemes for the phase conjugation process. The theoretical model is followed by a calculation of the phase conjugated response from a single-level metallic quantum well. The single-level quantum well represents the simplest possible configuration of a quantum-well phase conjugator. Furthermore, it is an interesting object, since its optical response contains no dipole terms. The discussion of the response is based on the use of light that is polarized either in the scattering plane or perpendicular to the scattering plane to excite the process. It is demonstrated that the phase conjugation process is extremely efficient in the evanescent regime of the wavevector spectrum. We address the problem of plane-wave excitation in the high wavenumber end of the evanescent regime and discuss the use of a broadband source to excite the process. One possible broad angular band source is a quantum wire, and the phase conjugated angular spectrum from a quantum wire is presented and discussed. The subwavelength size of the quantum wire makes it a possible candidate for discussion of confinement of light, and the confinement of light in two dimensions in front of a single-level metallic quantum-well phase conjugator is discussed. It is justified that by a proper choice of orientation of the current in the quantum wire a field compression substantially beyond the Rayleigh limit is obtained. The thesis is concluded with a short description of the more general case where the quantum well is allowed to have more than one energy eigenstate, and numerical results showing the response from a two-level quantum well as the phase conjugating medium are presented and discussed.